School of Civil and Mechanical Engineering

Electrospun Silk Nanofibre Mats and Their Potential as Tissue Scaffolds

Soheila Mohammadzadehmoghadam

This thesis is presented for the Degree of

Doctor of Philosophy of

Curtin University

December 2018

Declaration

To the best of my knowledge and belief this thesis contains no material previously published by any other person except where due acknowledgment has been made. This thesis contains no material which has been accepted for the award of any other degree or diploma in any university.

Signature: ***Soheila Mohammadzadehmoghadam***

Date: 18th December 2018

Abstract

Tissue engineering (TE) uses an interdisciplinary approach involving integrating the science and technology of cells, biomaterials and biologically active molecules to create, repair and/or replace tissues and organs. Generally, TE uses biomaterials for the manufacturing of scaffolds which provide structural support for cell attachment, cell growth, and cell differentiation. The generation of scaffolds with tailored, biomimetic geometries, mimicking the extracellular matrix (ECM), underpins the success of TE. Electrospinning is a versatile technique for producing nano/microscale fibres and it has great potential for producing scaffolds that imitate the microenvironment of native ECM. Variety of materials have been electrospun for the purpose of TE. Silk fibroin (SF) from the *Bombyx mori* silkworm is increasingly being recognised as a promising biomaterial due to its good biocompatibility, adaptable biodegradability and good oxygen/water vapour permeability. However, for some tissues the strength of scaffolds composed only of SF is not sufficient, and for others the biocompatibility of SF scaffolds could be further improved. There is, therefore, a requirement to improve the bioactivity of SF-based materials which will facilitate better tissue regeneration and as a consequence broaden the biomedical applications for which SF-based biomaterials can be used. This study aims to develop new electrospun SF based nanocomposites and evaluate their material and cyto-compatible characteristics as a way of determining their potential for use in TE applications.

Halloysite nanotubes (HNT) are natural inorganic nanoparticles that have been widely incorporated into polymer matrices to obtain nanocomposites with improved mechanical, drug-loading, and cell attachment properties. In **Chapter IV**, SF/HNT nanocomposites with various HNT loadings were fabricated. The addition of a low amount of HNT (*e.g.* 1 wt%) enhanced the hydrophilicity and increased the water uptake capacity (WUC) of the composite nanofibre scaffolds above those fabricated from plain SF. Furthermore the Young's modulus and tensile strength of scaffolds containing 3 wt% HNT was also higher than that of plain SF. However, HNT loadings higher than 3 wt% had a detrimental effect on these properties due to HNT agglomeration. Interestingly, composite scaffolds containing 1 wt% HNT better supported the viability and spreading of 3T3 fibroblasts, and the ordered differentiation of C2C12 myoblasts to produce aligned myotubes was similarly enhanced on this scaffold.

Gelatin, is an inexpensive, natural material which can promote cell functions. In **Chapter V**, the effects of incorporating gelatin into SF matrix on material and biological properties of these scaffolds were investigated. It was found that when the gelatin content was increased, the degree of crosslinking also increased as a result of glutaraldehyde fixation of the composites. This enhanced crosslinking appeared to directly affect the mechanical, porosity, and WUC properties of the scaffolds. Furthermore, proliferation assays using 3T3 fibroblasts revealed that SF/gelatin nanofibre scaffolds at the blend ratio of 70/30 had the lowest 3T3 fibroblast proliferation rates and the deposition of ECM proteins was also the lowest on these scaffolds.

Collagen type I (Col I), is a natural protein and the main component of many tissue ECMs. It contains abundant binding sites for cell adhesion molecules including those of the integrin family and this gives rise to the favourable cell adhesion and cell proliferation, and hence tissue regeneration characteristics attributed to this protein. In **Chapter VI**, the functionality of SF/Col I constructs as tissue scaffolds was assessed. Coating SF with Col I hydrogel was found to reduce the proliferation rate of 3T3 fibroblasts relative to that seen on plain SF nanofibres. Moreover, immunofluorescent images revealed that incorporation of Col I hydrogels into the SF scaffolds down regulated fibroblast derived ECM protein deposition, and this was particularly apparent for fibronectin.

Decellularised ECMs derived from cultured cells are attracting attention as scaffold materials for TE because it is increasingly being recognised that a cell's ECM contains a complex, dynamic network of glycoproteins and growth factors that can direct cell fate. In **Chapter VI**, the functionalities of deposited 3T3 fibroblast- and human dermal fibroblast (HDF)-derived ECMs on scaffolds developed in previous Chapters and selected for their favourable characteristics, (*i.e.* SF and SF/HNT 1wt%) were explored for their ability to support keratinocyte expansion. It was found that SF and SF/HNT 1wt% scaffolds supported keratinocyte growth, but that coating with either 3T3 cell or HDF ECM further enhanced keratinocyte expansion. Interestingly, keratinocytes grown on scaffolds coated with HDF-ECM appeared to be less committed to terminal differentiation. Keratinocytes cultured on SF/HNT 1wt%-HDF ECM proliferated more and more keratinocytes were undifferentiated, as indicated by the lower involucrin expression. In general SF/HNT 1wt%-HDF ECM was a superior substrate

for the growth of primary human keratinocytes *in vitro* compared to SF scaffolds coated with 3T3 ECM or uncoated scaffolds.

The goal of this project was to develop new electrospun SF based scaffolds which would broaden the application of SF biomaterials in TE. Data obtained from this study have shown the potential of SF/HNT nanocomposites as scaffolds. In addition, the novel SF/HNT 1wt%-HDF ECM scaffolds developed in this project may serve as substrates for the *in vitro* expansion of undifferentiated keratinocytes for clinical applications.

Publications and Awards

Journal Papers:

- **Soheila Mohammadzadehmoghadam**, Yu Dong. "Fabrication and Characterization of Electrospun Silk Fibroin/Gelatin Scaffolds Crosslinked with Glutaraldehyde Vapor", *Frontiers in Materials,* 2019, 6, 91.
- **Soheila Mohammadzadehmoghadam**, Yu Dong, Ian Jeffery Davies. "Modeling Electrospun Nanofibers: An Overview from Theoretical, Empirical, and Numerical Approaches", *International Journal of Polymeric Materials and Polymeric Biomaterials,* 2016, 65, 901-915.
- **Soheila Mohammadzadehmoghadam,** Yu Dong, Ian Jeffery Davies. "Recent Progress in Electrospun Nanofibres: Reinforcement Effect and Mechanical Performance", *Journal of Polymer Science, Part B: Polymer Physics*, 2015, 53, 1171-1212.
- Yu Dong, Jordan Marshall, Hazim J. Haroosh, **Soheila Mohammadzadehmoghadam**, Dongyan Liu, Xiaowen Qi , Kin-Tak Lau. "Polylactic acid (PLA)/halloysite Nanotube (HNT) Composite Mats: Influence of HNT Content and Modification", *Composites Part A*, 2015, 76, 28–36.

Book Chapter:

- **Soheila Mohammadzadehmoghadam**, Yu Dong, Salim Barbhuiya, Linjun Guo, Dongyan Liu, Rehan Umer, Xiaowen Qi. "Electrospinning: Current status and future trends" In book: Nano-size Polymers: Preparation, Properties, Applications, Edition: 1st, Chapter: 4, Publisher: Springer, Editors: Stoyko Fakirov, 2016, pp.89-154.

Conference Paper:

- **Soheila Mohammadzadehmoghadam**, Yu Dong, Electrospinning and Characterisation of Silk fibroin/gelatin Nanofibre Mats. ICFNNNM 2018, September 17-18, 2018, Rome, Italy (Oral presentation).

Awards

- Best Paper Award conferred at “20th International Conference on Frontiers of Nanomaterials, Nanoparticles and Nanocomposite Materials” (ICFNNNM) 2018, Rome, Italy, September 17-18, 2018.
- Curtin University Thesis Completion Scholarship, 2018.
- Curtin International Postgraduate Research Scholarship, (2015-2018).

Acknowledgment

First and foremost, I would like to thank my primary supervisor Dr. Yu Dong for providing me with the opportunity to conduct this research. I am truly grateful for his mentorship and his continued guidance and support throughout this research journey.

I would like to express my deepest gratitude to my co-supervisor, Professor Deirdre Coombe for her invaluable advice; her passion for science has been a real inspiration. She guided me to the right direction whenever I am heading towards the wrong path in my research. The door to her office was always open whenever I faced a trouble or had a problem on my research. She is not only a good supervisor but as a good friend as well.

I extend my sincere gratitude to my co-supervisor, Associate Professor Ian J. Davies for his valuable advice and supports during my study.

I am greatly indebted to Ms Bev Kinnear, lab member of the Molecular Immunology Group, who taught me everything I now know about cell culture and biological assay techniques. Without her continued guidance and direction I would have been lost. A big “thank you” to Dr Wong Chee Wai for sharing his valuable knowledge in culturing Keratinocytes. He always tried his best to help me by providing any possible assistance.

I greatly appreciate and acknowledge the support received from the technical staff at School of Civil and Mechanical Engineering, Dr Ray Mahidasht, Mr Graeme Watson and Mr David Parker for their support and valuable instructions.

I would also like to gratefully acknowledge the staff at Curtin University’s Microscopy and Microanalysis Facility especially Ms Elaine Miller and Ms Veronica Avery who were very generous with their time and knowledge.

Lastly, I must express my profound gratitude to thank my parents and brothers for all their love and encouragement. My partner Mohammadreza who has persistently encouraged, supported and had faith in me every step of the way. Your love, unconditional support and absolute belief in me has made this journey possible.

Table of Contents

List of Figures

List of Tables

List of Abbreviations

The following abbreviations are used throughout this thesis:

3D	3-dimensional
α-SMA	Alpha-Smooth Muscle Actin
Bombyx mori	*B.mori*
BSA	Bovine Serum Albumin
CNTs	Carbon Nanotubes
Col I	Type I Collagen
ddH_2O	Double Distilled Water
dECM	Decellularised Extracellular Matrix
DKSFM	Defined Keratinocyte Serum Free Media
DMEM	Dulbecco's Modified Eagle's Medium
DMSO	Dimethyl Sufoxide
DSC	Differential Scanning Calorimetry
DTG	Differential Thermal Gravimetric
ECM	Extracellular Matrix
Eq	Equation
F-actin	Filamentous actin
FBS	Fetal Bovine Serum
FTIR	Fourier Transform Infrared Spectroscopy
GAGs	Glycosaminoglycans
GC	D,L-glyceraldehyde
GTA	Glutaraldehyde
HEPES	N-2-hydroxyethylpiperazine-N-2-ethane sulfonic acid
HNT	Halloysite nanotube
IgG	Immunoglobulin Superfamily
K10	Cytokeratin 10
K14	Cytokeratin 14
LiBr	Lithium Bromide
MCDM	Macromolecular Crowding ECM Deposition Media
$MgCl_2$	Magnesium Chloride
MMC	Macromolecular Crowding

MSCs	Mesenchymal Stem Cells
MWCNTs	Multi-walled Carbon Nanotubes
M_W	Molecular weight
NDM	Normal ECM Deposition Media
P value	Probability value
PBS	Phosphate Buffered Saline
PCL	Polycaprolactone
PEO	Poly-(ethylene oxide)
PGA	Polyglycolic acid
PLGA	Poly-l-lactic-co-glycolic acid
PLA_2	Phospholipase A_2
PLA	Polylactic acid
PLLA	Poly-l-lactic acid
P(L(LA-CL))	Poly(L-lactic acid-co-ϵ-caprolactone)
PP	Poly(propylene)
PU	Polyurethane
PVA	Polyvinyl alcohol
RGD	Arginyl-glycyl-aspartic acid
RT	Room Temperature
SDS	Sodium Dodecyl Sulfate
SEM	Scanning electron microscopic
SF	Silk Fibroin
SD	Standard Deviation
SWCNTs	Single Wall Carbon Nanotube
T_{d1}	Maximum degradation rate for degradation peaks 1
T_{d2}	Maximum degradation rate for degradation peaks 2
T_{d3}	Maximum degradation rate for degradation peaks 3
T_c	Crystallisation temperature
T_g	Glass transition temperature
T_m	Melting temperature
TE	Tissue Engineering
TGA	Thermogravimetric analysis
TNBS	2,4,6-trinitro-benzene-sulfonic acid

Tris	Tris (Hydroxymethyl) Aminomethane
U	Unit of Enzyme
UV	Ultra Violet radiation
WUC	Water Uptake Capacity
XRD	X-ray Diffraction

Chapter I: Introduction

1.1 Background

Every day, thousands of surgical procedures are performed to repair/replace damaged or lost tissue caused by disease, injury or trauma. Tissue engineering (TE) is an emerging multidisciplinary field which aims to develop technologies that allow damaged organs to be substituted with tissues generated *in vitro*. Ultimately TE approaches could solve issues associated with conventional allograft transplantation, like the scarcity of donor organs, the complexity of surgery, and the complicated postoperative care [1, 2]. In most cases, TE requires a porous biomaterial to provide structural support for the cells. In the body the extracellular matrix (ECM) which is secreted by cells performs the scaffold role of the biomaterial in TE. Ideally, the artificial, biomaterial scaffold used TE should be degraded and replaced by the natural ECM of the intended tissue. The success of an implantable tissue engineered graft is enhanced if the biomaterial scaffold resembles the ECM structure of the tissue it is emulating; generally this means the scaffold should be composed of three-dimensional (3D) networks of nanoscaled fibrous proteins embedded in a glycosaminoglycan hydrogel [3-6].

The process of electrospinning has attracted enormous attention in TE. Electrospinning produces nanofibres with diameters ranging from several micrometres to nanometres, resembling natural ECMs in tissue with approximate diameter range of 50–500 nm. The simplicity and cost-effectiveness as well as the versatility in the materials that can be used are advantages of electrospinning. Moreover, the nanofibres can be tuned to produce large surface areas, high porosities and interconnected pores, which facilitate cell adhesion, proliferation, migration, and differentiation [7]. The simplicity and cost-effectiveness as well as the versatility in the materials that can be used are advantages of electrospinning. Electrospinning also allows the chemical and mechanical properties of the nanofibres to be modified by the incorporation of bioactive species, or the blending of the base materials with other polymers or nanoparticles. These features make electrospun nanofibres well suited as scaffolds for TE. Over the last few years, there has been unprecedented advances in the manufacturing of electrospun fibres and their corresponding functions for TE, including the regeneration of skin, bone, muscle, cartilage, and blood vessels [7-9].

Choosing an appropriate biomaterial is a critical for any cell scaffold. Amongst the variety of materials tested, silk fibroin (SF) has attracted attention due to its excellent mechanical properties, good biocompatibility for wound healing, very low immunogenicity and biodegradability. Generally SF for biomaterials is extracted from cocoons of the silkworm *Bombyx mori (B. mori).* SF from this species has been used clinically in surgical sutures since the end of the 19th century, and is still being used in dissolvable sutures. SF has been shown to be a promising scaffolding material for repairing skin, bone, cartilage, ligament and tendon, as well as vascular, neural, tracheal and bladder tissues [10, 11]. It has major advantages over many proteins derived from tissues of allogeneic or xenogeneic origins, such as a lower risk of infection, and easier isolation and purification procedures. Furthermore, the large-scale processing infrastructure already in place for traditional silk textile industries provide economic advantages for also using SF from *B. mori* for biomedical applications [12].

1.2 Research Significance and Objectives

1.2.1 Research Significance

In spite of the aforementioned advantages of SF as a biomaterial for TE scaffolds, there are aspects of SF-based scaffolds that could be improved. For example, for some tissues the strength of scaffolds composed only of SF is not sufficient, and the biocompatibility of SF scaffolds could be further improved [13-16]. SF from *B. mori* does not have the amino acid motif, arginine-glycine-aspartic acid (RGD), that is recognised by many cell surface integrins and integrin engagement via this motif is important for promoting cell attachment and growth for many cell types. Hence, promoting better cell attachment to SF biomaterials is one of the challenges in TE [17-19]. Recent developments have improved the effectiveness of SF in tissue scaffolds, such as blending the SF with other polymers, incorporating growth factors or bioactive proteins in the SF scaffolds and so forth [11, 20]. However, other strategies could further improve the bioactivity of SF-based materials for better tissue regeneration and as a consequence broaden biomedical applications for which SF-based biomaterials can be used. This study aims to develop new electrospun SF based nanocomposites and evaluate their material characteristics as well as their potential for TE applications.

I. Halloysite nanotubes (HNT) are natural inorganic nanomaterials that have been widely incorporated into polymer matrices to obtain nanocomposites with improved mechanical properties, drug-loading properties, cell attachment and hemostatic performance. HNTs have many virtues as nanofillers including their abundance naturally, good dispersion ability, low toxicity and low cost. Other tubular nanoparticles, such as carbon nanotubes (CNTs), have been successfully used as functional fillers for nanocomposites for TE use. Nonetheless, there is evidence that CNTs may cause chronic inflammation and granuloma development [21, 22]. In contrast, phagocytes can effectively phagocytose HNT, thereby reducing their potential to induce inflammation [23]. In addition, the cheaper price of HNT is a further advantage. HNT can easily be dispersed into a range of different polymers where they have shown good reinforcing abilities, giving rise to composites with improved mechanical properties. Accordingly, HNTs have been introduced as a reinforcing agent into polyvinyl alcohol (PVA) [24], chitosan [25], gelatin [26] and alginate [27]. HNT can be also used as either a carrier for drugs, or as a substrate for protein adsorption because of their hollow tubular nanostructure [28]. In the latter case, HNT functionalised with the adhesion protein selectin were shown to preferentially bind leukaemic cells, an attribute that could assist in cancer treatment.

Electrospun scaffolds prepared for TE that contain HNTs have also been reported. These include scaffolds of electrospun polymeric nanofibres, including polylactic acid (PLA) [29], poly(l-lactide) acid (PLLA) [30], PVA [24], polycaprolactone (PCL) [31], poly (lactic-co-glycolic acid) (PLGA) [32] or alginate [27]. There are reports suggesting scaffolds that contain HNTs have potential for accelerating wound healing because the presence of HNTs supports cell adhesion and proliferation as well as enhancing the tensile strength and Young's modulus of the scaffold [33-35]. For example, HNT significantly improved the compression properties of chitosan scaffolds, whilst the cell attachment and skin repairing properties of the chitosan were also increased [25]. The addition of HNT to PLLA polymer matrices in a composite system was found to enhance their tensile strength and Young's modulus, which may have contributed to the improved adhesion and proliferation of the murine osteoblastic cells that was observed [34]. The presence of HNT allowed higher protein adsorption and

improved the mineralisation of PCL/HNT nanocomposite relative to pristine PCL [31]. Furthermore higher osteoblast differentiation was observed, suggesting the potential of PCL/HNT scaffolds for bone TE. It was reported that HNT-"doped" PLGA nanofibres not only demonstrated significantly higher mechanical properties compared to their "not doped" counterparts, but they were also able to better promote cell attachment and proliferation [32]. A study conducted on electrospun PLGA/HNT nanofibrous mats demonstrated that the nanocomposite exhibited an excellent biocompatibility [36]. Moreover, fibroblasts cultured on the nanocomposite scaffolds displayed a phenotypic shape, implying that the cells could penetrate and migrate within the scaffolds similar to native ECM. Consequently from these examples it can be deduced that polymer/HNT nanocomposites exhibit great potential for TE applications.

However, to our knowledge, there is no scientific report on developing SF/HNT nanocomposites. Accordingly, the properties of HNTs inspired us to explore the benefits of ST blended with HNTs as a novel scaffold material for TE applications.

II. Decellularised ECM derived from cultured cells are attracting attention as scaffold materials for TE because it is increasingly recognised that a cell's ECM contains a complex, cell/tissue-specific, dynamic network of glycoproteins and growth factors that are capable of directing cell fate. Nonetheless, major challenges for these scaffolds are their fragility and their integrity loss upon cell adhesion and cell generated tension [37]. In recent years, a new strategy has been developed based on incorporating native ECM into polymeric biomaterials. As such, polymeric scaffolds provide structural support, and ECM provides biological cues to regulate cell phenotype and function [38]. Some studies have demonstrated the efficacy of ECM/polymer scaffolds for the regeneration of various tissues including bone [39, 40], cartilage [38] and nerves [41]. For instance, chitosan/SF scaffolds coated with schwann cell derived-ECM proteins demonstrated superior regenerative outcomes in the repair of a 10 mm gap in the sciatic nerve of rat, over the scaffold only group [41]. Harvestine *et al.* [39] similarly reported that the addition of a mesenchymal stem cell secreted ECM coating to bioactive glass /poly(lactide-co-glycolide)

scaffolds potentiated the efficacy of this substrate by promoting cell survival and function *in vitro* and *in vivo*.

However, this type of polymer/ECM scaffold, has not been fully studied. In particular, to our knowledge, there are no reported studies on the applicability for TE of electrospun SF scaffolds with an ECM coating. Hence, we developed SF based scaffolds with fibroblast derived ECM and evaluated their functionality as tissue scaffolds. In addition, two proteins were chosen to be added to SF to improve its bioactivity. The rationale for this choice is given below:

a) Gelatin, is an inexpensive, natural material obtained from the hydrolysis of the ECM component, type I collagen. Gelatin promotes cell adhesion, proliferation and migration, in part because it contains the amino acid motif, RGD, which facilitates cell adhesion via certain members of the integrin family of cell adhesion molecules [42, 43]. Improvements in scaffold hydrophilicity and cell viability were demonstrated upon adding gelatin to the following polymers such as PLLA [44], PCL [45] , PLGA [46] and polyurethane [47]. In relation to SF scaffolds, their lack of bioactivity and their slow degradation rates may, depending on their use, induce certain concerns. It was reported that blending SF with gelatin can improve cell adhesion and cell proliferation on SF based scaffolds and these scaffolds also degraded more quickly than similarly prepared scaffolds composed on SF only [48].

b) Collagen type I, is a natural protein and the main component of many tissue ECMs. It contains the amino acid motif, GFOGER, which is recognised by a sub-set of cell surface integrins particularly during wound healing [49]. In addition, a number of proteins that contain the RGD integrin-binding motif bind to collagen, and so give rise to indirect cell-collagen interactions that cell adhesion and cell proliferation, and hence tissue regeneration [50]. Collagen was used with PLGA and it was found that the presence of collagen contributed to enhancing the distribution of skin fibroblasts as well as promoting the formation of an epithelium in 2–4 weeks [51]. The presence of collagen within PCL scaffolds markedly elevated cell

migration through activation of β1-integrins [52]. Many other studies have shown that incorporation of collagen type I with other polymers promoted the biocompatibility of those polymers while retaining their mechanical strength [53, 54]. Therefore, SF functionalisation with collagen could enhance cell adhesion and result in more ECM deposition.

1.2.2 Research Objectives

A range of different SF based electrospun nanofibres have been produced by others as scaffolds for tissue engineering, but to our best knowledge the incorporation of HNTs into electrospun SF mats is novel and has not previously been examined. Similarly, functionalising the SF mats with human dermal fibroblast extracellular matrices, as a way to better support primary human keratinocyte expansion is also novel. Hence, the main goal of this study was to produce electrospun SF scaffolds to support the proliferation of primary human keratinocytes. Accordingly, three different SF based scaffolds were prepared and analysed. These were achieved by: (1) incorporating HNT into the SF solution, (2) blending SF with gelatin and (3) coating SF electrospun scaffolds with collagen type I. Based on material and biological characterisations, an optimum scaffold was chosen and further functionalised with the deposition of fibroblast ECM. The efficiency of this SF based/ECM hybrid scaffold for keratinocyte expansion was investigated. The detailed steps are given as follows:

- Manufacture SF/HNT nanocomposite scaffolds at different HNT contents (*i.e.,* 1, 3, 5 and 7 wt %).
- Characterise SF/HNT nanocomposites. Examine material properties and investigate fibroblasts cell proliferation, C2C12 myoblast cell differentiation and cell morphology to find the optimum HNT content for a tissue scaffold.
- Fabricate SF/gelatin blended nanofibres with different blend ratios (*i.e.,* SF/gelatin 100/0, 90/10 and 70/30).
- Investigate the effect of SF/gelatin blend ratio on SF fibres using both material characterisation techniques and biological tests including fibroblast cell proliferation and fibroblast derived ECM deposition assays to find the optimum SF/gelatin blend ratio for a tissue scaffold.

- Prepare SF scaffold coated with type I collagen and study their material and biological properties.

- Deposit ECM from 3T3 fibroblasts and primary human dermal fibroblasts (HDFs) on optimised SF based scaffolds and evaluate the potential of these scaffolds for keratinocyte expansion as a way of assessing if they could be useful for repairing skin wounds.

1.3 Thesis Outline

The thesis is structured into seven chapters as summarised below and Figure 1.1:

Chapter I presents a brief background about the tissue engineering, SF based scaffolds as well as electrospinning and explains the research objectives of the project.

Chapter II is an extensive literature review describing current findings and knowledge gaps in tissue engineering, electrospinning, silk fibroin and tissue scaffolds.

Chapter III describes the research methodology including the preparation of the SF based spinning solution, electrospinning setup, post treatments as well as material and biological characterisation methods.

Chapter IV describes SF/HNT nanocomposite fabrication with various HNT contents. The resulting nanocomposites were subjected to different material characterisation techniques including scanning electron microscopy (SEM), X-ray diffraction (XRD), Fourier transform infrared spectroscopy (FTIR), tensile tests, thermal analysis, water uptake and water contact angle measurements. The potential of SF/HNT scaffolds for TE applications were evaluated by conducting cell proliferation assays, cell differentiation assays and fluorescent imaging of cells on scaffolds. Based on these results, a scaffold with optimum HNT content in terms of both material properties and biological characterisation was reported.

Chapter V describes the detailed fabrication of SF/gelatin scaffolds with different gelatin weight ratios. Prepared scaffolds were analysed by SEM, FTIR, XRD, porosity measurement, tensile tests, water uptake and water contact angle measurements. Cell proliferation assays and fibroblast derived ECM deposition studies were performed to assess scaffold functionality.

Chapter VI explains the preparation of SF nanofibre/collagen hydrogel composites and the evaluation of their morphology using SEM technique. Their hydrophilic properties are also described. The functionality of SF/collagen constructs as a tissue scaffold was investigated by examining the proliferation of cells plated on these surfaces and the extent of ECM deposition. Thereafter scaffolds chosen from results obtained and described in ***Chapter IV*** and ***Chapter V*** were functionalised by fibroblast derived ECM and used as a substrate for growing keratinocytes. The effects of ECM deposition on the functionality of scaffolds for growing keratinocytes were assessed and reported.

Chapter VII summarises main conclusions and presents a number of recommendations for future work.

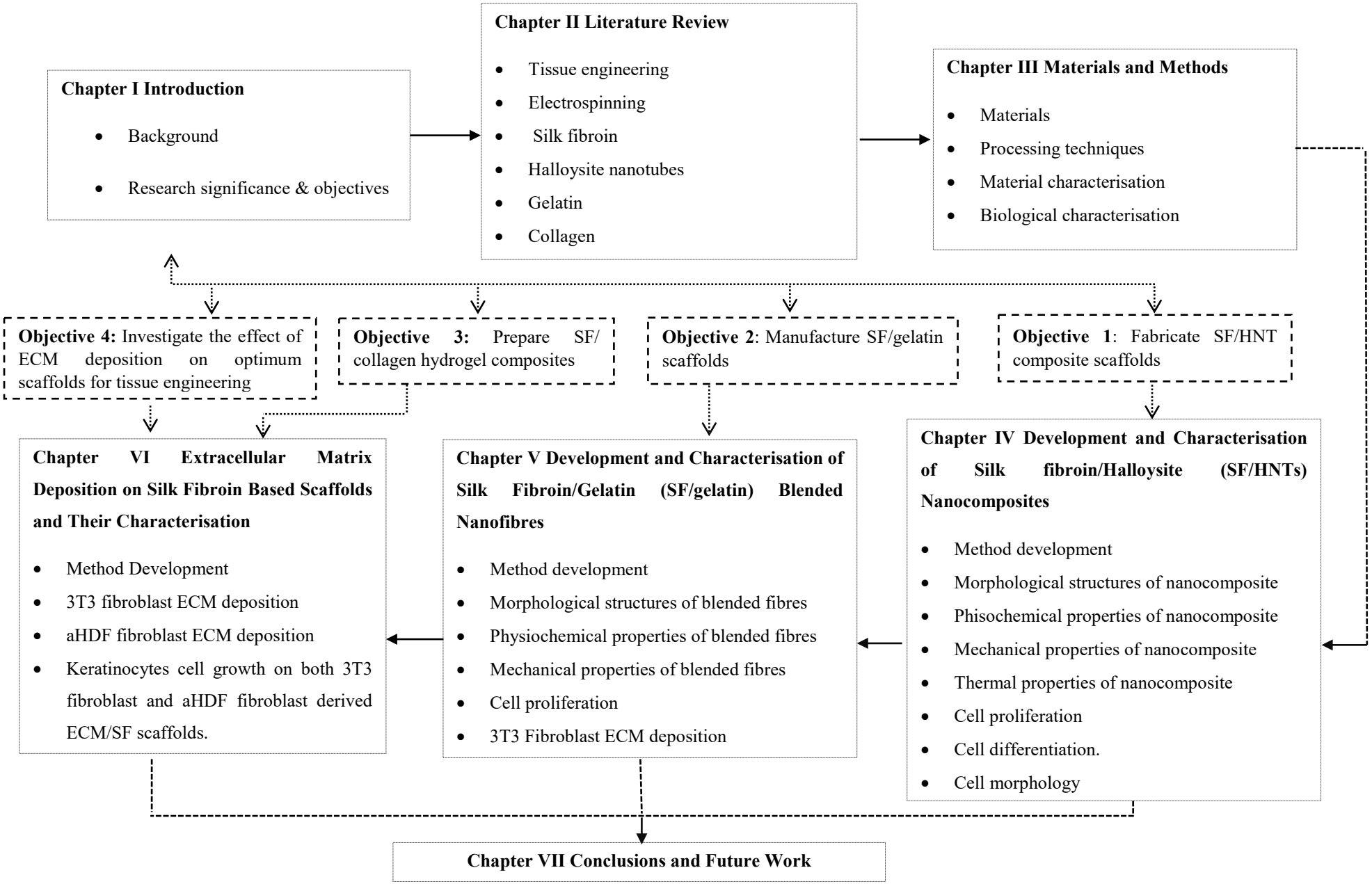

Figure 1.1 Thesis outline flowchart.

Chapter II: Literature Review

2.1 Tissue Engineering

Disease, injury and trauma can lead to damage and degeneration of tissues in human body. Traditionally, transplanting tissue from one site to another in the same patient (an autograft) or from one individual to another (a transplant or allograft) have been the bedrock to replace damaged and diseased parts of the body. Both approaches, however, have limitations. Harvesting autografts have serious constraints including lack of available donor tissue and donor site morbidity. Transplantation is limited by donor shortage, risk of infection, tumour development and requires life-long immunosuppression regimes [1, 55, 56]. To address the aforementioned shortages, tissue engineering (TE) has emerged as an alternative approach with the potential to provide a cost-effective and long-term solution. The term TE was coined by Fung in October 1987 at a National Science Foundation Workshop in Washington, USA. Although tissue engineering may be recognised as a relatively new approach, the idea of replacing tissue with another dates back to the 16th century when Italian surgeon Gaspare Tagliacozzi (1546–99) developed a technique using grafted skin taken from the patient's arm for reconstructing of the nose [57]. TE requires an interdisciplinary approach which combines the principles of engineering and life sciences towards the development of biological substitutes for regenerating, repairing or replacing diseased tissues. Its principle is to create tissues and organs that can mimic the structure and physiochemical characteristics of its natural counterparts through combination of the patient's own cells and polymeric scaffolds, and ultimately transplanted into a patient by injection or surgery [55, 58-60]. Figure 2.1 illustrates the classic tissue engineering strategy.

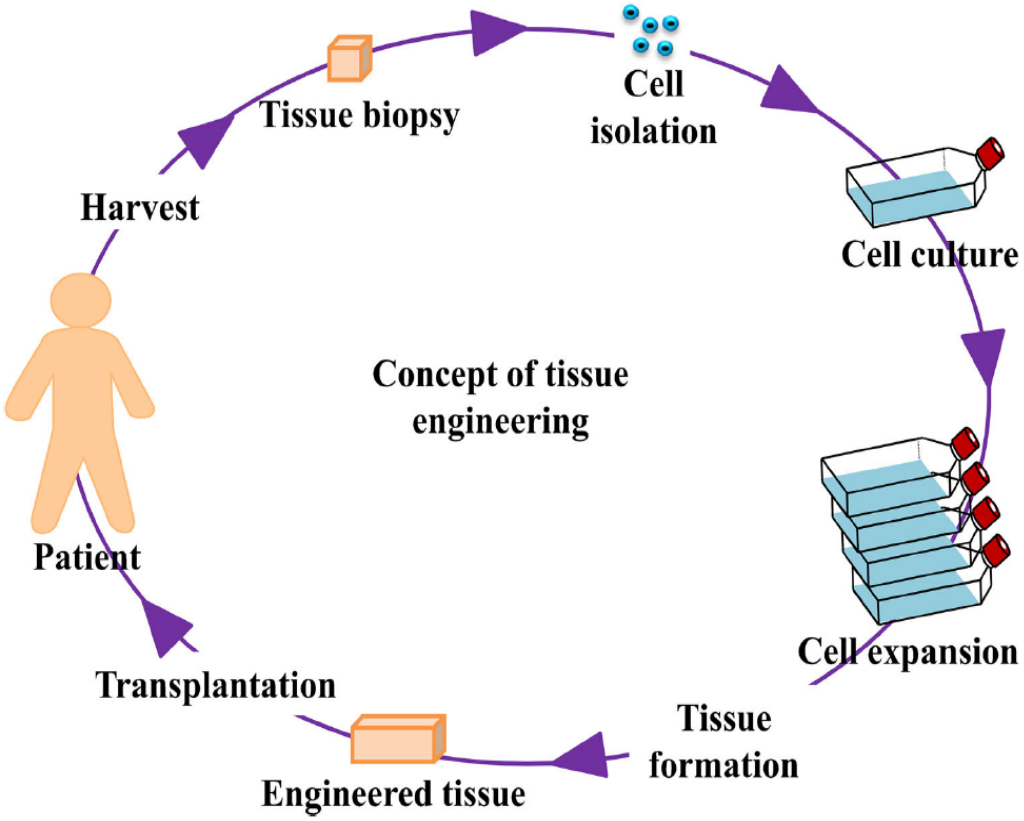

Figure 2.1 Classic concept of tissue engineering [59].

2.2 Scaffolds

One of the main objective in TE is to design and create a 3-dimensional (3D) template to simulate the structures and biological functions of the natural extracellular matrix (ECM) and to support cell growth, differentiation and spreading for the regeneration of new tissues. Regardless of the tissue type, key criteria should be considered for designing a scaffold as follows:

i. **Biocompatibility**: This term refers to the ability of a biomaterial to perform its desired function with respect to a medical therapy, without eliciting any undesirable local or systemic effects in the recipient or beneficiary of that therapy, but generating the most appropriate beneficial cellular or tissue response in that specific situation, and optimising the clinically relevant performance of that therapy [61]. Scaffolds should provide a microenvironment to support cell adhesion, proliferation and differentiation either *in vitro* culture or *in vivo* implantation. Biocompatibility is a necessity for biomaterials in order

to minimise inflammatory response, cytotoxicity and immunological reactions from the body [57, 62].

ii. **Biodegradability**: Principally the scaffold degradation time should be matched with that of tissue regeneration, and additionally the degraded by-products must be non-toxic, metabolised safely and exit the host body without any interference with other organs [63, 64].

iii. **Scaffold geometry**: Scaffolds act as temporary templates and should resemble the structure of the native ECM in terms of architecture. Therefore a 3D construct with interconnected pore structure and a suitable pore distribution are required for cellular penetration, diffusion of nutrients and waste exchange, vascularisation and new tissue formation. Furthermore, scaffold topographical features can influence cell behaviour by providing contact guidance for cells, which in turn have an effect on the cytoskeletal arrangement and cell adhesion [3, 65].

iv. **Mechanical properties**: Biomaterials should possess mechanical properties comparable to the host tissue with shape stability and retain structural integrity. Moreover, critical cell functions such as differentiation, cytoskeletal organisation and process extension are influenced by the scaffold mechanical properties [66, 67]. Such a mechanosensitivity has been shown for the differentiation of mesenchymal stem cells (MSCs). As such, depending on substrate stiffness, they can differentiate to neuronal cells or support osteogenic differentiation, indicating the role of substrate stiffness on the differentiation of stem cells towards specific lineages [68].

Hence it can be inferred that choosing the proper type of biomaterials and methods of scaffold fabrication are critical for producing a clinically and commercially viable tissue-engineered construct.

2.2.1 Scaffold Approaches in Tissue Engineering

During the previous decade there has been growing interest in creating scaffolds for tissue engineering with four major scaffolding strategies being evolved (Figure 2.2): (i) cell encapsulation in self-assembled hydrogel matrix, (ii) cell sheets with self-

secreted ECM, (iii) pre-made porous scaffolds for cell seeding and (iv) decellularised ECM (dECM) for cell seeding. In the following subsection, each method is briefly discussed.

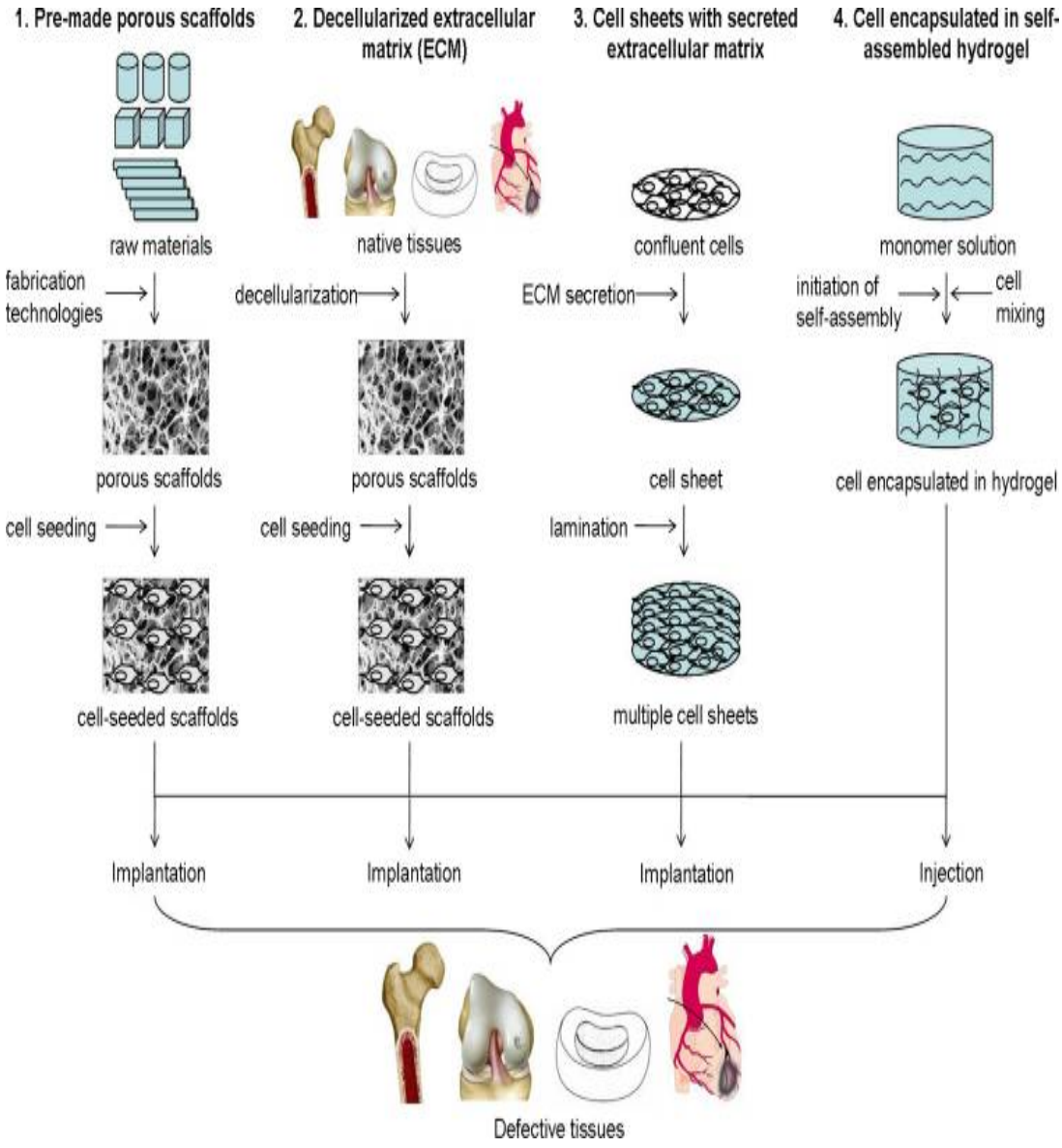

Figure 2.2 Schematic diagram of various methods for scaffold preparation in tissue engineering [62].

2.2.1.1 Cell Encapsulation in Self-assembled Hydrogel Matrix

In this approach, living cells were entrapped within a semi-permeable membrane or within a homogenous solid mass. The common materials for encapsulation are hydrogels, which are formed by covalent or physical crosslinking of water-soluble

polymers [69, 70]. This method is a simple one-step procedure and featured as an injectable system whereby cells suspended in a liquid precursor solution were delivered *in vivo* to the site of interest. However, this approach has been rarely employed for hard tissue applications, mainly due to the weak mechanical properties of hydrogels [62].

2.2.1.2 Cell Sheets with Self-secreted ECM

The concept of this approach is based on cells secreting their own ECM upon confluency to create sheet-like structures for tissue reconstruction. Hence the cells were cultured on thermo-responsive culture surfaces until confluency, followed by detaching cell sheets by thermally adjusting the hydrophobicity of polymer coatings without enzymatic treatment. This method can be repeated to laminate multiple single cell layers and form a thicker matrix [62, 71]. The main advantage of this technique is rapid neovascularisation. Nonetheless, it is difficult to prepare thick scaffolds since the thickness of each layer is typically 30 μm [72, 73].

2.2.1.3 Pre-made Porous Scaffolds for Cell Seeding

This is the most common and well-established method for scaffold fabrication. Essentially it involves fabricating scaffolds using natural or synthetic polymers, which is followed by seeding therapeutic cells and implantation. Many studies have been conducted to develop techniques for shaping polymers into unique geometries to direct tissue regeneration, which are reproducible and can mimic the ECM structure. This scaffolding approach is associated with advantages such as a board choice of biomaterials as well as the capability to design scaffolds with tuneable architectures and microstructures [74, 75]. Nevertheless, due to the limited penetration of cells into scaffolds the post cell-seeding process is time-consuming, thus leading to an inhomogeneous distribution of cells within the scaffolds resulting in the presence of heterogeneous features within the engineered tissue [62].

2.2.1.3.1 Scaffold Fabrication

It is crucial to develop scalable fabrication processes which are cost effective with good reproducibility. In this respect, scaffold manufacturing technology is an intensive research area and numerous methods have been developed, which can be divided into two main categories, namely conventional and advanced techniques [76]. Scaffold

fabrication by conventional methods includes solvent casting or particulate leaching [77], phase separation [78], gas foaming [79], melt moulding and combinations of these techniques [76, 80]. Advanced manufacturing techniques include electrospinning and rapid prototyping (*i.e.*, solid free-form) with examples of this prototyping technique including selective laser sintering, 3D printing and lithography [81, 82]. Depending on the material bulk and surface properties and required scaffold functions, fabrication techniques must be selected so that scaffolds in the form of meshes, fibres, sponges, hydrogel, foams, *etc.*, can be fabricated. In most fabrication techniques, polymers either undergo a heat and/or pressure treatment or else are dissolved in organic solvents to mould the materials into the appropriate shape [75]. However, each method is associated with different merits and limitations as summarised in Table 2.1.

Solvent Casting and Particulate Leaching: Porous scaffolds could be generated by mixing polymeric solutions with porogens such as salt particles or organic compounds by casting them into a mould. Following this the solvent can be evaporated and the resulting membranes immersed in water or solvent in order to leach out porogens for producing a porous construct [77].

Gas Foaming: In this technique**,** moulded polymers were exposed to a high pressure foaming agent such as carbon dioxide, nitrogen or fluoroform up to saturation [83]. Due to kinetic instability of the polymeric foam, the dispersed gas phase (*i.e.* discontinuous phase) tended to move upwards to form a scaffold composed of a nonporous bottom layer with a highly porous top surface [79, 84, 85].

Phase Separation: This method used thermal energy to induce phase separation leading to a polymer-rich phase and a polymer-lean phase. The polymer-rich phase solidifies and the polymer poor phase is removed, leaving a highly porous polymer network [86]. This generally takes place either by quenching the solution temperature below a binodal solubility curve or else exposing the solution to another immiscible solvent. The polymer-lean phase is eliminated by a subsequent freeze-drying or freeze-extraction process resulting in porous polymeric scaffolds [78, 87].

Melt Moulding: This technique involved mixing polymer powders (poly lactic-co-glycolic acid (PLGA), poly(l-lactic acid) (PLLA), poly (glycolic acid) (PGA)) and porogen components (*e.g.*, salt or polymer microspheres), which was followed by

pouring into the mould and heating the mould above the glass transition temperature of polymer [88]. The leachable components are then removed by immersing the composite in water or solvents with a porous scaffolds to conform to the mould shape [89].

Fibre Bonding: Originally this method was developed by Mikos *et al*. [90] and the composite formation was based on non-bonded fibres embedded within a matrix, followed by thermal treatment and the selective dissolution of the matrix. For example, PLLA can be dissolved in chloroform as a matrix and cast over PGA non-woven meshed fibres and dried. Solvent removal is carried out by evaporation following heat treatment and fibre bonding [91].

Self-assembly: The self-assembly process is based on spontaneous organisation of components into an ordered structure, which is induced by van der Waals interactions, hydrogen bonds, ionic bonds, water-mediated hydrogen bonds and hydrophobic interactions. Self-assembled matrices can be produced using natural or synthetic molecules such as peptide motifs and synthetic proteins [92-94].

Electrospinning: Synthetic and/or natural polymeric solution or melt are fabricated into fibrous scaffolds with diameters in a nanometer range. In this process, a high voltage is applied to a polymer solution in a defined distance between a capillary and collecting substrate. As a result, polymer jet is ejected from the charged capillary and solvents are evaporated, which allows for the production of continuous micro- to nanoscale polymeric fibres collected on the collecting substrates [7, 95].

Rapid Prototyping (RP): RP is also called solid free-form fabrication (SFF) or additive manufacturing (AM), which is a group of advanced manufacturing processes in which 3D architectures with controllable structures can be built layer by layer in an additive manner using computer-aided design (CAD)/computer-assisted manufacturing (CAM) software [76, 82]. Briefly, 3D computer models can be created and cut into two-dimensional (2D) patterns that represent the cross-section of 3D structures used for manufacturing complex objects in a layer-by-layer fashion. The layers can be produced through different methods such as the solidification of melts, stereolithography or bonding of particles using either laser beam induced sintering (*i.e.*, selective laser sintering) or special binders (3D printing®) [81, 96].

Table 2.1 Advantages and disadvantages for scaffold fabrication methods.

Fabrication Technique	Advantages	Disadvantages	Reference
Solvent Casting/Particulate Leaching	• Simple • Inexpensive • Highly porous scaffold	• Toxic solvent, • Time consuming • Thin membrane • Hard to control pores interconnectivity	77, 84
Gas Foaming	• Solvent-free process • Control porosity and pore size	• Non-porous external surface • Low level of interconnectivity	97, 98
Phase Separation	• Easily combined with other fabrication technologies to design 3D structures with control of pore morphology • High porosity	• Limited material selection • Long process	87, 99-101
Melt Moulding	• Non-solvent fabrication process • Control of morphology and shape	• High processing temperatures • Possibility of residual porogen	88, 102
Fibre Bonding	• Large surface area • High porosity	• Poor control of porosity and pore size • Lack of availability of suitable solvents • Required appropriate melting temperatures of polymers	86, 91
Self-Assembly	• Integration of bioactive molecules	• Time-consuming • Lab based • Low yield • Poor mechanical properties • High cost	86, 93, 94

Repaid Prototyping	• High reproducibility • Excellent control over • geometry, porosity • No supporting material required	• Expensive • Limited polymer type	76, 81
Electrospinning	• High surface area • Quick and simple process • Cost effective • Continuous nanofibres	• Hard to generate complex structure • No control over 3D pore structures • Large nanometer to micron scaled fibres	86, 93

2.2.1.3.2 Scaffold Material

To fulfil the diverse demands in tissue engineering, various materials have been exploited as scaffolds for tissue regeneration. The choice of biomaterials, from which the scaffold should be fabricated, plays a critical role in this technology, and has a direct impact on selecting the fabrication method. Accordingly, material chemistry, molecular weight, solubility, shape and structure, hydrophilicity, lubricity, surface energy, water absorption and degradation are all important characteristics for biomaterials when applied to tissue engineering. Based on structural, chemical, and biological features, biomaterials used for tissue engineering can be categorised into various types such as ceramics, glasses, polymers and so forth. Biomaterials used in tissue engineering are typically divided into three groups including ceramics, synthetic polymers and natural polymers [57, 75, 103].

Ceramics: Bioceramics such as hydroxyapatite (HA) and tri-calcium phosphate (TCP), and certain compositions of silicate and phosphate glasses (bioactive glasses) and glass-ceramics (such as apatite-wollastonite) react with physiological fluids and form strong bonds through the cellular activity to hard tissues, and in some cases for soft tissue engineering as well [75, 104]. Due to their high mechanical stiffness and trivial tissue reactions, they have been favourable for bone implant applications although low elasticity, hard brittle surface and the difficulty of shaping for implantation restrict their potential use in clinical situations [57, 105].

Synthetic Polymers: Numerous synthetic polymers have been used for tissue engineering. Among the big list of synthetic polymers PGA, PLGA, polyanhydride,

poly(propylene fumarate), polylactic acid (PLA), polycaprolactone (PCL), polyethylene glycol (PEG), and polyurethane (PU) are the most commonly used [103]. They offer distinct advantages such as the ability to tailor their properties for specific applications, availability in large uniform quantities, long shelf time, and predictable and reproducible mechanical and physical properties [75, 106, 107]. However, their lack in bioactivity increases the risk of rejection within the body. To modify their biocompatibility, different procedures have been developed such as surface laser engineering [108] and coating with natural biomaterials [109]. Moreover, in some cases the by-products of degraded synthetic based scaffolds such as PLLA and PGA can cause cell and tissue necrosis [57].

Natural Polymers: Natural polymers can be categorised as proteins (*e.g.*, silk, collagen, gelatin, fibrinogen, elastin, keratin, actin, and myosin), polysaccharides (*e.g.*, cellulose, amylose, dextran, chitin, and glycosaminoglycans (GAGs)), or polynucleotides (*e.g.*, DNA and RNA) [75, 103, 110]. Unlike synthetic polymers, they offer bioactive properties, thereby increasing cell attachment and viability. However, poor mechanical properties, in addition to potential immunogenicity due to their allogenic or xenogenic sources, are major concerns when natural polymer is used [57]. To tackle these issues, technologies for reinforcing natural biomaterials and reducing the immunogenicity, such as the removal of telopeptides in procollagen, have been proposed [62, 111].

It should be noted that polymers in their pure form (*i.e.,* single component) cannot accommodate all the requirements for various tissue engineering applications. Therefore, by incorporating other components, multiple types of biomaterials with distinct properties can be fabricated to fulfil a specific application [112].

2.2.1.4 Decellularised ECM for Cell Seeding

Despite the growing knowledge and development in tissue engineering, synthetic scaffolds have failed to simulate the molecular complexity and organisation of native ECM. Moreover, each tissue has a specific ECM composition. Thereby, fabricating appropriate ECM mimicry may be beyond the means of any current engineering technique [62, 113]. Decellularised extracellular matrices have been considered as one of the most promising alternatives, offering the advantage of preserving the structure proteins such as GAGs, glycoproteins and bioactive cues of their respective tissues

and organs [114-116]. Essentially, this scaffolding method relies on eliminating the allogenic or xenogenic cellular antigens through physical, chemical, and biochemical methods while maintaining the natural composition of the basic structural and functional ECM proteins and GAGs [117-119]. This method was first reported in 1973 as a technique to retain tissues to be used as a barrier for burn patients. However, ECM was first produced through the decellularisation of a source tissue for subsequent use as a bioscaffold for tissue regeneration in 1995, in which small intestinal submucosa (SIS) were used for vascular applications [120-122]. In the last decade, the number of studies employing cell-derived ECM (CDM) have increased remarkably to process various types of tissues, including skeletal muscle, brain, urinary bladder, small intestinal submucosa, liver, skin/adipose tissue, blood vessels, heart valves and tendons [119, 121, 123-125]. Moreover, there are decellularised scaffolds available commercially with Food and Drug Administration (FDA) approval to be used in humans such as dermis tissue (Alloderm®; LifeCell), porcine heart valves (Synergraft®; Cryolife) and porcine urinary bladder (Urinary bladder matrix; ACell) [114, 125].

The main merit of this approach is to generate scaffolds with the most natural-simulating structures with high biocompatibility. However, cell residues may elicit pro-inflammatory and immune reactions upon implantation. In addition to this, it is very challenging to remove all the antigens from the construct without jeopardising the ECM integrity [62, 114]. The creation of CDM requires three major considerations comprising cell source, culture condition and decellularisation methods [118].

2.2.1.4.1 Extra Cellular Matrix: Composition and Function

ECM represents the secreted products of resident cells of each tissue and organ, which not only act as a physical scaffold for cellular constituents, but also provide contextual information engaged in the regulation of various processes of any cell type. ECM can be defined as non-cellular tissue components, which are composed of either structural or non-structural (also known as glycoproteins) proteins. The main structural ECM proteins include collagens, laminins, fibronectin, and elastin that are organised into multimolecular nets to warrant the stiffness of tissue and meanwhile serve as ligands of cellular membrane receptors. Other important constituents of ECM are proteoglycans, growth factors and proteolytic enzymes, which are responsible for the

dissolution of the ECM [126-129]. In fact, the ratios of ECM proteins as well as the topological, and biochemical composition of ECM are tissue-specific and markedly heterogeneous [130]. Furthermore, ECM is a highly dynamic structure that can continuously undergo controlled remodelling usually in an enzymatical or non-enzymatical manner, and its molecular compositions are exposed to a myriad of post-translational modifications [129].

ECM has a profound influence on cell signalling and tissue homeostasis (*i.e.*, regulating cell behaviour by conveying information to cells). ECM conduct multiple functions, which in turn determines cell on cell migration, cell cycle progression, and cell fate decision. Firstly, it can serve as an anchorage site which is pivotal in the cell-division process of stem cells. In addition, ECM's physical properties can either support or inhibit cell migration by functioning as a barrier, anchorage site, or movement pathway.

Moreover, biochemical features of the ECM allow cells to interrelate with their environment through various signal transduction cascades, emanating from the cell surface to the nucleus leading to gene expression or other changes of cell behaviour. The ECM limits the diffusive range, accessibility, and signalling direction of ligands to their cognate receptors. Moreover, the ECM can also directly initiate signalling events, particularly by functioning as a precursor of biologically active signalling fragments [131, 132]. Collectively, through these functions, ECM generates physical and biochemical cues that are critical for cell regrowth and tissue repair, and thus provides a natural microenvironment niche, support to preserve and enhance site appropriate cell phenotypes, and hence benefits tissue regeneration [132-134]. Therefore it can be postulated that the presence of ECM is essential for tissue engineering procedures. Consequently, numerous studies have attempted to recapitulate the ECM's function using synthetic or isolated ECM components such as collagen, fibrin or hyaluronan [135-137]. In spite of many advantages in the use of engineered scaffolds made of non-native materials, particularly the ease of tailoring mechanical and chemical properties and rate of degradation, they have failed to reproduce the molecular complexity or organisation of native tissue ECM [118, 138]. This has driven the use of native ECM itself as a biomaterial source, which is mainly grouped into tissue-derived ECM and cell-derived ECM. Both products have been granted FDA approval and have been utilised in pre-clinical and clinical applications. In particular, promising results were

manifested by using CDM for preparing off-the-shelf tissue engineered vascular grafts and heart valves, and novel cell culture substrates by mimicking specific niche microenvironments [118, 139].

2.2.1.4.2 Cell Source

The primary determinant of CDM composition is the cell source as the ECM expression patterns differ based on cell types [118, 125]. Various cell types have been studied as an ECM source such as chondrocytes [140, 141], MSCs [142, 143] and fibroblasts. Fibroblasts are referred as a main cell type in connective tissues with their well-recognised potential to produce a collage-rich ECM [118]. Cell type has a great impact on inducing specific cell functions within the resulting CDM matrices [139]. For example, using CDM with different cell sources (*e.g.*, chondrocytes, MSCs and fibroblasts) is known to affect the chondrocyte function [144]. Relative to MSC or fibroblasts, chondrocytes cultured on ECM derived from chondrocytes, displayed higher chondrocyte adhesion along with lower proliferation.

2.2.1.4.3 Culture Conditions: Macromolecular Crowding

Culture condition has a predominant role in cell deposition and their organisation into the ECM. Cells within an *in vivo* tissue microenvironment are typically surrounded by dense macromolecules that regulate the molecular assembly of the ECM. However, under the standard culture setting, the physiological crowding of molecules failed to be replicated leading to the formation of unstructured ECM with a lack of critical components [145-147]. In other words, despite the feasibility of creating an acellular ECM *in vitro,* standard culture conditions were regarded as an inefficient process and thereby resulted in the failure of CDM to copy the *in vivo* microenvironment of the tissue where the cells were obtained. The concept of adding macromolecular crowding (MMC) including inert synthetic or natural macromolecules into *in vitro* cultures becomes increasingly important for cell culture applications wishing to more accurately mimic the *in vivo* state [148, 149]. It has been well documented that the addition of MMC promotes the deposition and formation of a more structured ECM [145, 150-153].

2.2.1.4.4 Decellularisation Techniques

The main objective of decellularisation is to balance the trade-off between elimination of cell associated antigens and retention of molecular composition, bioactivity and

structural integrity of the matrix itself. Decellularisation methods have been classified as physical, chemical, biological/enzymatic methods or a combination of these approaches [114, 118]. A brief overview of common methods along with their influence on ECM structures is presented in Table 2.2.

Chemical Methods: Chemical methods can include treatment with alkaline and acidic compounds, non-ionic, ionic or zwitterionic detergents [154]. Chemical reagents are very efficient in removing both cellular cytoplasmic components and nucleic acids, such as RNA and DNA. Nevertheless, chemicals such as hydrochloric acid, ammonium hydroxide and acidic compounds may damage important molecules (*e.g.* GAGs) and further disrupt ECM structures [114, 119, 154].

Physical Methods: Physical decellularisation typically involves snap-freezing [155], hydrostatic pressure [156], non-thermal irreversible electroporation [157], sonication [158] and agitation [159] to disrupt cell membranes and promote cell lysis. In all these methods, the speed of treatment, volume of reagent and mechanical agitation time should be modulated corresponding to composition, volume and density of the tissue. Physical methods can be adjusted to minimise the ECM disruption since they can be set to only break cellular membranes. However, other enzymatic or chemical treatments should be added in order to remove cellular debris [114, 154].

Biological/Enzymatic Methods: This method includes two types of agents: (i) enzymatic-like nucleases [160], proteases [161], esterases [162], and (ii) non-enzymatic such as chelating agents (*i.e.*, ethylenediaminetetraacetic acid (EDTA) and ethylene glycol tetraacetic acid (EGTA)) [163]. Although enzymatic treatments can provide the effective removal of cell residues or undesirable ECM constituents, the risk of ECM disruption as well as the adverse impact of enzyme remanent on recellularisation or *in vivo* immune response is considerable [37, 119, 154, 164].

Table 2.2 Used methods for decellularisation of tissues/organs [114, 115, 119].

Method	Mode of action	Effect on ECM
Chemical		
Alkaline; acid	Solubilise cytoplasmic components of cells and disrupt nucleic acid	Possibility of collagen, GAG and growth factors loss
Non-ionic detergents: Triton X-100	Disrupts DNA–protein, lipid–lipid and lipid–protein interactions	Efficiency depends on tissue (effective for thin tissues)
Ionic detergents: Sodium dodecyl sulfate (SDS)	—	Remove nuclear residues and cytoplasmic proteins from dense tissue; tend to disrupt native tissue structures
Sodium deoxycholate	Solubilise cells and nuclear cellular membranes	Mixed results depend on tissue structures, more disruptive to tissue structures relative to SDS
Triton X-200	—	Yield efficient cell removal when used with zwitterionic detergents
Zwitterionic detergents: CHAPS	Possess properties of non-ionic and ionic detergents	Remove cells with ECM disruption similar to that of Triton X-100
Physical		

Snap freezing	Intracellular ice crystals disrupt cell membrane	ECM disruption or fraction fractured during rapid freezing
Mechanical force	Pressure rapture cells	ECM can be damaged by applied mechanical forces
Mechanical agitation	Cause cell lysis, but more commonly used to facilitate chemical exposure and cellular material removal	Aggressive agitation or sonication can disrupt ECM as the cellular material is removed
Electroporation	Micropore formation in cell membrane due to electrical potential destabilisation causes cell lysis	Electric field oscillation can disrupt ECM
Biological		
Trypsin	Cleaves peptide bonds on the C-side of Arg and Lys	Prolonged exposure can disrupt ECM
Endonucleases	Catalyse the hydrolysis of the interior bonds of RNA and DNA	Difficult to remove from the tissues
Exonucleases	Catalyse the hydrolysis of terminal bonds of RNA and DNA	__

2.3 Electrospinning

In recent years, electrospinning, also known as electrostatic spinning, has gained enormous attention due to its potential for generating fibrous scaffold similar to the structure and function of ECM. Electrospinning is a versatile technique with a relatively low-cost and simple setup to produce continuous fibres from natural, recombinant proteins and synthetic precursors with a diameter from nanometres to a few micrometres. Fibrous structures offer large specific surface area, high porosity and good inter-pore connectivity with a smooth surface, thus making electrospinning a popular choice for a board range of tissue engineering applications from neural and skin grafts, drug delivery devices to scaffold fabrication [165, 166].[1] Figure 2.3 shows the popularity of electrospinning and its applications for tissue scaffolds, both of which are evidenced from a significantly increasing number of publications.

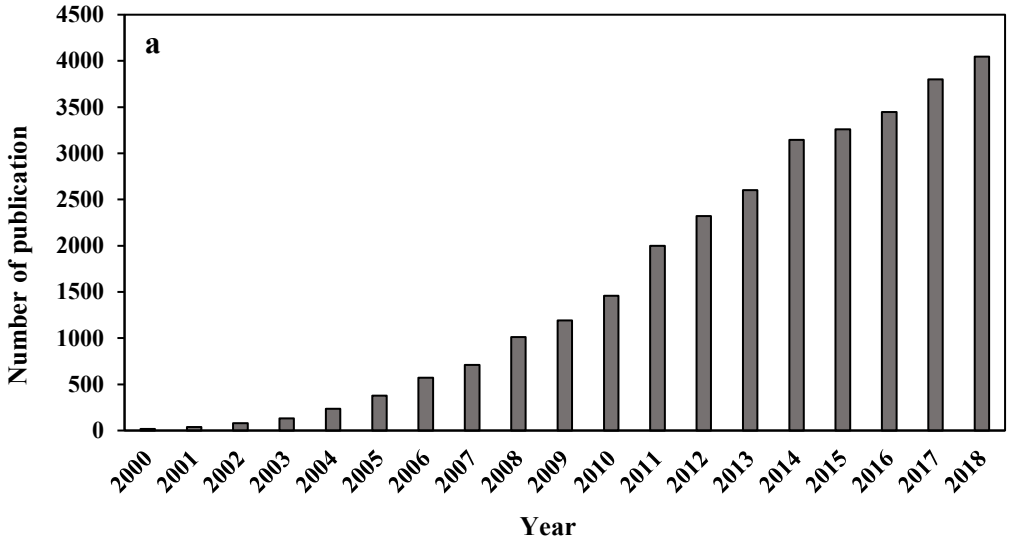

[1] This section is captured and reorganized from the paper "Recent Progress in Electrospun Nanofibers: Reinforcement Effect and Mechanical Performance". The authors' attribution on this paper are given in Appendix C.

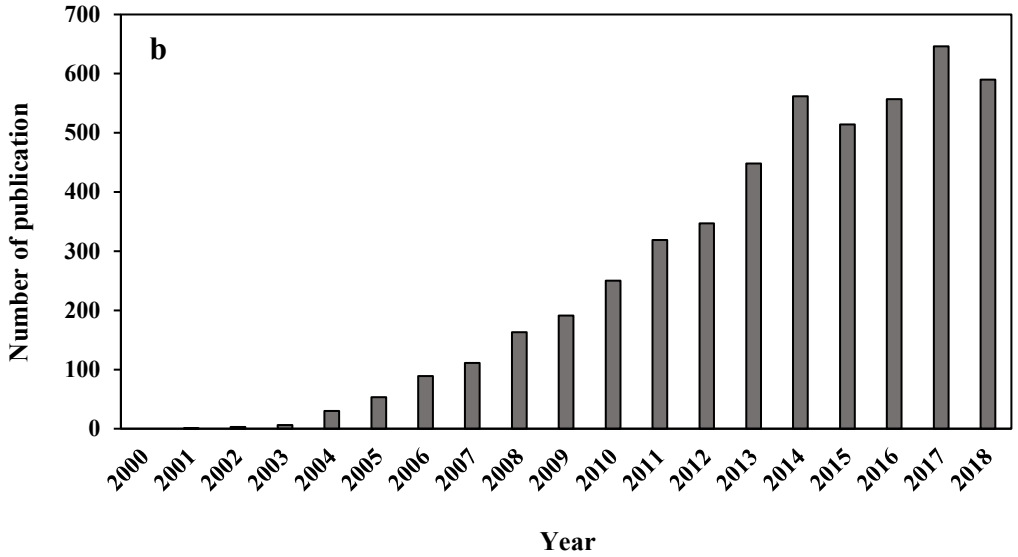

Figure 2.3 (a) Overview of the number of papers published with regard to electrospinning in the last 18 years (sourced from Scopus database). (b) Overview of the number of papers published with regard to electropun nanofibres for tissue scaffolds in the last 18 years (sourced from Scopus database).

Electrospinning has been expanded from the original electrospraying technique when Morton and Cooley patented a method to disperse fluids using electrostatic forces in 1902 [167]. The method was further developed by Formhals who patented the fabrication of polymer filaments by electrospinning [168]. In 1969, Taylor investigated the electrospinning process through mathematical modelling of the conical shape of fluid droplets formed under electrostatic forces, which has since then been referred to as the "Taylor cone" [169]. Later in 1981, further improvements in the method were accomplished by Larrondo and Manley who reported the electrospinning of polymer melts [170]. The potential of electrospinning for fabricating nanofibres was not well-recognised until the early 1990s. However, since then extensive research have been carried out in this field and generated fibres have provided desirable features for a wide range of applications including nanofiltration, nanosensors, protective clothing, composite reinforcement, drug delivery and tissue engineering [165].

The necessary criteria for polymer solution or melt to be electrospinable is being electrically conductive and possessing sufficient viscosity to be stretched without breaking into droplets. A basic set up of electrospinning apparatus consists of a high voltage supplier, spinneret system and collector (Figure 2.4). Polymer solution or melt is pushed into a capillary tube with a controlled flow rate. Upon applying a high electric force (10-50 kV) the pendant droplets at the end of the needle are distorted from a hemispherical shape into a cone shape (*i.e.*, Taylor cone). When the electric

forces exceed the surface tension force of the Taylor cone, the charged jet travels toward a collector and, simultaneously, dries out or solidifies to leave ultra-fine fibres on the collector. Based on the jet trajectory direction, two electrospinning configurations, known as vertical and horizontal configurations, are generally used [165, 166].

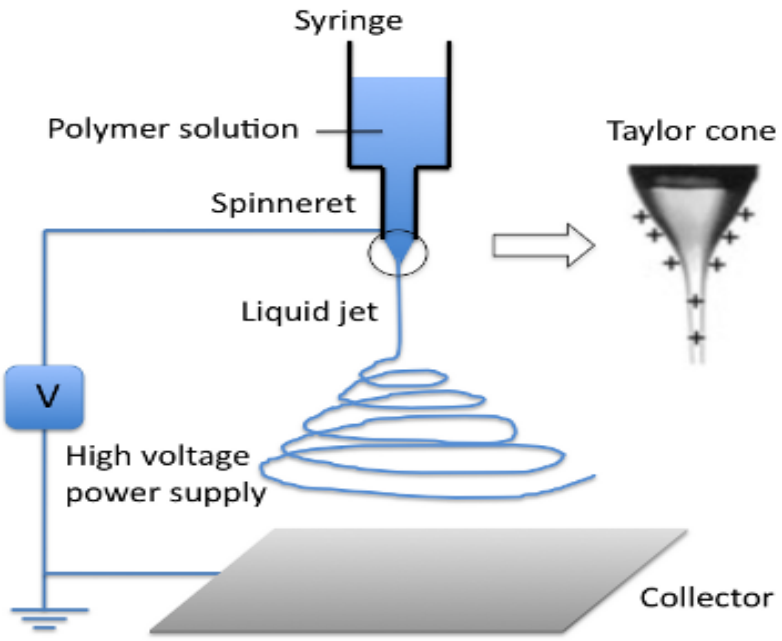

Figure 2.4 Schematic diagram of electrospinning [171].

Typical electrospun nanofibres usually demonstrate monolithic, circular-shaped morphology with randomly oriented nonwoven structures and smooth surfaces. However, following recent developments, different nanofibres with specific structures such as core/shell, porous, hollow, necklace -like ribbon and multichannel tubular structures can also be fabricated [172]. In order to manufacture well-aligned fibres, collectors have been amended into various forms such as rotating drum collector, rotating disk collector, frame collector, and auxiliary electrode/electrical field [173]. Despite substantial attempts, electrospinning is subjected to some drawbacks including low productivity (up to 300 mg/hr) and the use of toxic solvents. Hence to overcome these issues tremendous efforts have been made leading to the incorporation of various developed electrospinning systems such as coaxial electrospinning, co-

electrospinning, multi-jet and multi-hole electrospinning, emulsion electrospinning, side-by-side electrospinning, near field electrospinning (NFES) and electroblowing [166]. Currently, a few companies are engaged in commercial industrial-scale electrospinning such as Inovenso Ltd., Elmarco Co, Stellenbosch Nanofiber Company, SNS NanoFiber Technology and others[174].

2.3.1 Effects of Various Parameters on Electrospun Nanofibres Morphology

Fibre diameter and structural morphology are the most prominent features of electrospun nanofibres that directly determine their performance in targeted functional applications. Interestingly, these features can be tuned through the proper manipulation of different parameters that can be divided into three groups as follow: (i) solution parameters (*i.e.*, solution viscosity, concentration, molecular weight, surface tension, electrical conductivity, dielectric strength and solvent volatility), (ii) operational parameters (*i.e.*, flow rate, electric field strength, tip-to-collector distance, needle shape, collector type and geometry) and (iii) ambient parameters (temperature, humidity and air flow) [166, 175, 176]. The relationship between these parameters and fibre properties has been investigated extensively and the summarised results are presented in Table 2.3.

Table 2.3 Effect of different electrospinning parameter on fibres morphology.

Parameter		Effect on fibre morphology	Reference
Solution parameter	Concentration ↑	Diameter ↑, pore size ↑ Beaded fibres forms below the optimum range	175, 177
	Molecular weight↑	Diameter ↑	166
	Electrical conductivity↑	Diameter ↓, pore size ↓ Formation of micro-sized beads and dense net for excessive high conductivity	178, 179
	Surface tension↓	Diameter ↓, pore size ↓	180, 181
Processing parameter	Flow rate↑	Diameter ↑ , pore size ↑ beaded morphologies occur if the flow rate is too high	179, 182
	Applied voltage↑	Diameter ↓ initially, then ↑ (not monotonic)	166, 179

	Tip to collector distance↑	Diameter ↓ Beads tend to form when the distance is too short or too long.	183, 184
Ambient parameter	Humidity↓	Diameter ↓, pore size ↓	166, 179, 185
	Temperature↑	Diameter ↓	179, 182, 186

2.3.2 Applications for Electrospun Nanofibres

Due to distinctive features of electrospun nanofibres such as high surface area and interconnected fibrous networks, they have received significant attention for diverse applications. A schematic diagram of electrospinning applications in various fields is shown in Figure 2.5.

2.3.2.1 Composite Reinforcement

Electrospun nanofibres have been considered as an ideal candidate for composite reinforcements due to their high aspect ratio, high specific surface area, good mechanical properties and low density. The pioneering work in this field was conducted by Kim and Reneker [187] in 1999 when they tried to reinforce butadiene rubber (SBR) matrix with electrospun polybenzimidazole (PBI) nanofibres. Compared to pure SBR, an increase in Young's modulus of ten times was achieved for the composite system. Following this, researchers investigated the effect of various factors such as fibre content, diameter, alignment, structure, surface treatment and so forth on their reinforcement efficiency to fully exploit nanofibres potential in this regard with more details being found elsewhere [165].

2.3.2.2 Tissue Engineering

Tremendous efforts have been made for the manufacturing of scaffolds mimicking ECM structures to assist in the formation of new tissue. The potential of electrospinning techniques to fabricate fibrous constructs as building blocks for tissue engineering scaffolds is well-recognised [177, 188, 189]. Electrospinning offers the flexibility in material selection as well as the ability to control scaffold structure and properties. As a result of this, electrospun nanofibres have been widely used for different tissue engineering applications such as skin, bone, liver, neural, vascular and

cartilage [189, 190]. In addition to this, nanofibre mats have been applied as drug carriers in drug delivery systems with the capability to control drug release and enhance the efficiency towards the sustained discharge of drug rather than a burst release. Drugs can be loaded into nanofibres by blending them with polymer solution, immobilised by physical or chemical procedures or indirectly loaded onto nanofibres. In addition, using electrospun nanofibres as a drug vehicle provides the opportunity to deliver drugs into desired target areas of the body. Furthermore, drug release kinetics can be regulated by changing fibre diameter, porosity, geometry, and morphology or by selecting different polymers. The incorporation of various drugs and molecules including antibiotics, anticancer agents, anti-inflammatory agents, proteins, DNA and RNA into nanofibres by electrospinning technique has been reported [177, 191] .

2.3.2.3 Filtration

Electrospun nanofibre structures provide necessary requisites for filtration purposes including high porosity and interconnected open-pore structures, submicron pore sizes, and large surface area to volume ratio. A thin layer of electropsun nanofibre over a metal mesh membrane displayed an extremely effective removal of more than 95% of PM2.5 (*i.e.*, particulate matter of size 2.5 μm) in a polluted city environment [192]. There are reports showing the feasibility to tune nanofibre filtration efficiency by changing the diameter, membrane thickness or physical and thermal post modifications [193-195].

2.3.2.4 Sensor

Electropsun nanofibres provide solutions to the challenge of highly sensitive and fast acting sensors mainly due to the provision of fabrication of more efficient interfaces with large surface areas, tailored pore structures, large stacking dimensions and easy surface modification. The sensitivity of materials in form of electrospun fibres are often higher than their cast film counterparts [196]. Electrospun nanofibres have been utilised for acoustic wave, resistive, photoelectric, optical, and amperometric sensors [196, 197].

2.3.2.5 Catalyst

The surge of interest in using electrospun nanfibres for applications where chemical reactions are involved has been raised. Unlike nanoparticles, fibrous membranes are self-supporting and their porous structures provide abundant exposed reaction sites

without any further concerns relating to agglomeration [198]. Electrospun nanofibres can be used to form a catalytic material by electrospinning catalytic substances [199] or inclusion of catalytic nanoparticles or substances into nanofibres [200] or else serving as a template in which catalytic substances are coated over it [201].

2.3.2.6 Protective Clothing

Electrospun nanofibres can be easily incorporated into the design of protective clothing in possession of good mechanical properties, high penetration resistance of particles, and good breathability by eliminating costly manufacturing steps due to the possibility of their direct applications to garment systems [202, 203]. The filtration efficiency of electrospun nylon 6 nanofibres over nylon/cotton woven fabrics for protective clothing was evaluated using NaCl particles (particle size= 300 nm) [204]. The efficiency of more than 99.5% without losing the air permeability and pressure drop was attained. Besides, the incorporation of electrospun nanofibres not only enhanced the barrier performance of the filter significantly, but also their air permeability was much higher than that of most materials currently used for protective clothing [205].

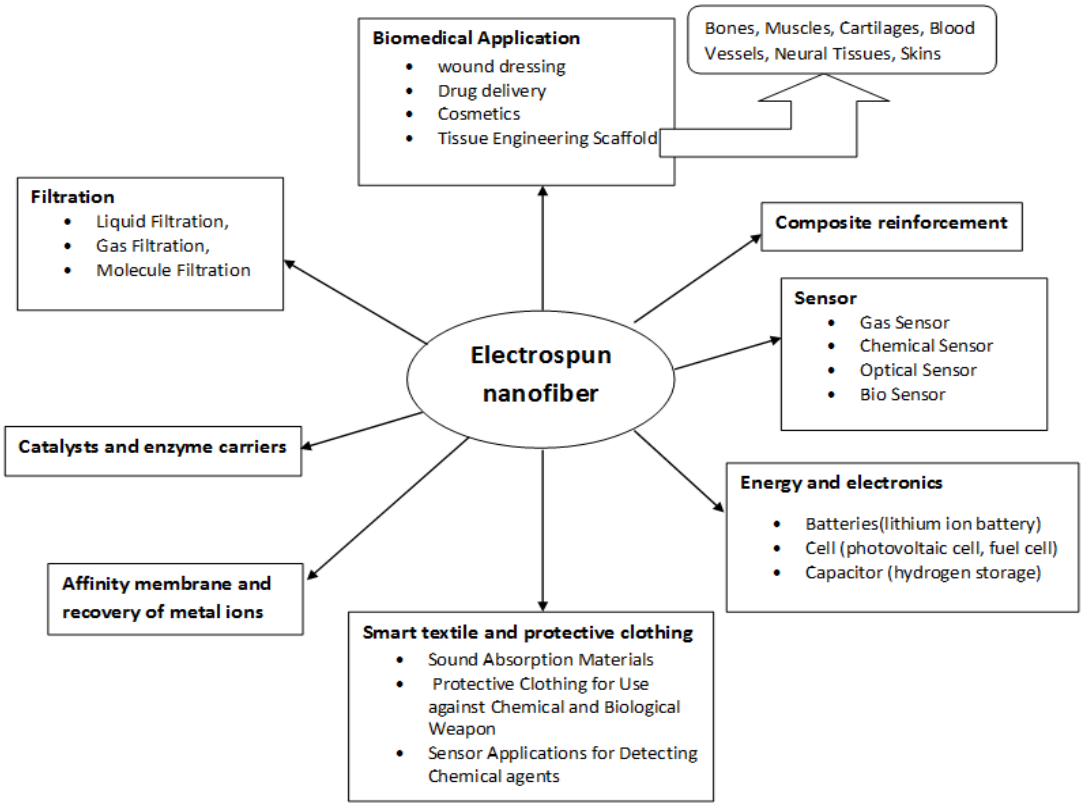

Figure 2.5 Electrospun nanofibres application [165].

2.4 Silk

Silk is the only natural filament fibre which has been used for thousands of years. Silk fibres from silkworms have been used in textiles for nearly 5000 years and in the form of sutures for centuries[206, 207]. It is a protein-based polymer presenting in the glands of silk producing arthropods including silkworms, spiders, scorpions, mites and bees. Therefore a board diversity in the sequence, structural features and properties among the different species may be observed [11, 20, 208-211]. For example it has been shown that relative to the African wild silk moth, *Bombyx mori* (*B.mori*) silk demonstrates a considerable higher amount of polar amino acids resulting in different cell attachment and also changes the chemical reactivity for side chain modification [212]. It is also revealed that silk originating from spiders has superior strength and elasticity though, due to the cannibalistic nature of spiders, the commercial production of spider silk is restricted [11, 20]. Silk fibres obtained from silkworm cocoons (*e.g. B.mori*) are one of the best characterised alongside with its ease of domesticating and cultivation [11]. Silk

can be processed easily into a variety of structures including powders, films, sponges, mats, gels, fibres, tubes and microspheres [213].

2.4.1 Silk Structure

B.mori silk is composed of two classes of proteins, fibroin (fibrous protein) and sericin (globular protein). Sericins, with a molecular weight between 10 to 300 kDa, are the glue-like proteins which coats fibroin. Sericin constitutes 25–30% of the total silkworm cocoon mass, which due to its hydrophilic nature can be easily removed by a thermochemical process, known as 'degumming'. It has been reported that sericin elicits an allergic reaction, and is therefore limited in its application in tissue engineering. However, recent studies have shown that the natively combined fibroin/sericin structures stimulate an immune response in the host and neither fibroin nor sericin by itself is associated with the immune response [214, 215]. Some studies investigated the potential of sericin for biomedical applications, but thus far silk fibroin (SF) has been the most commonly used form of silk for biomedical applications [20].

SF fibres produced from the gland located in the posterior region of *B.mori*, are about 10–25 mm in diameter. SF protein consist of a light chain (Mw= ~26 kDa) and a heavy chain (Mw= ~390 kDa) which are present in a 1:1 ratio and attached together via a disulfide bond, as well as a glycoprotein (P25), which is non-covalently linked to these chains. The light chains are composed of a non-repetitive and more hydrophilic sequence, whilst a repetitive sequence of hydrophilic and hydrophobic blocks is present in the heavy chain. The hydrophobic domains of heavy chains are responsible for the crystalline structures of fibroin, and contain Gly-Ala-Gly-Ala-Gly-Ser, which is accordingly associated with extensive hydrogen and hydrophobic interactions within protein chains leading to homogeneous secondary structures. These highly crystalline regions yield high mechanical strength and toughness to the protein-based materials [208, 211, 213, 216]. The three common crystalline structures of fibroin are silk I, II, and air/ water assembled interfacial silk (silk III, with a helical structure). The alteration in silk conformation strongly influences its physiochemical and mechanical properties as well as solubility, thermal and enzymatic degradation [208, 217]. The α-silk or silk I is the metastable structure that is obtained from spinning dope. There are different methods to convert silk I to a more stable structure (silk II) as a result of its β-sheet conformation. The most common approach to evoke β-sheets conformation, and

therefore induce water stability, is methanol treatment [218-220]. Alternative methods include heat exposure, water vapour treatment, shear-force and the use of salts. In order to induce a reduction in β-sheet structures and sustain its elasticity, annealing with water is more promising relative to methanol treatment. The silk II structure is characterised by β-sheet capacity and is insoluble in mild acid and alkaline conditions. The β-sheet structures are asymmetrical featuring hydrogen side chains from glycine on one side and methyl side chains from alanine on the other, forming hydrophobic domains [217].

2.4.2 Mechanical Properties

Silk native fibres possess a favourable balance of modulus, breaking strength, and elongation. Silk toughness is higher than Kevlar which is referred to as a benchmark for high-performance fibres. Furthermore, in contrast to collagen that suffer from a lack of sufficient tensile strength (0.9–7.4 MPa) leading to the limitation of applications, *B. mori* silk fibres demonstrate high tensile strength (740 MPa) owing to its robust β-sheet conformation. It is worth mentioning that materials developed from silk fibroin solution display poor mechanical properties and brittleness, which is partly related to the loss of secondary structures in processed silk [208, 213]. Different approaches have been implemented to tailor the mechanical properties of electrospun SF fibres. The most common strategies focus on inducing β-sheet structures using organic solvents or cross linking agents. Moreover, the fabrication of SF composites by adding agents into spinning dope, such as carbon nanotubes (CNTs) [221, 222], poly(L-lactic acid-co-Ɛ-caprolactone) (P(LLA-CL)) [223], and native silk fibril [224] or depositing or growing ceramics [225] have been employed as an effective reinforcing method. Another approach is to improve the orientation degree of the fibres by using different collectors, although the resulting structures exhibit limited length or else are arranged parallel to one direction [226, 227]. Jiang *et al.* [228] applied a straightforward method to construct the SF scaffolds with a grill-like structure which was found to be efficient for improving tensile properties. Ha *et al.* [229] mimicked the condition provided by insect such as using acidic dope solutions and the subsequent post-spin fibre drawing, which in turn increased the tensile properties. Fan *et al.* [230] reported additional enhancements in mechanical properties of SF scaffolds in the drawing direction relative to the transverse direction. The post-treatment of electrospun SF results in different mechanical properties. For instance, methanol-treatment causes higher yield stress and tensile

modulus, whereas water-vapour annealing yields better elastic properties [231]. Overall these promising methods provide opportunities to fabricate SF scaffolds with mechanical properties corresponding to required target tissue applications.

2.4.3 Biocompatibility

Silk has been used as medical sutures for decades, indicating its biocompability. In 1993 the FDA approved SF as a biomaterial and its potential was verified by the attachment and growth of fibroblast cells on *B. mori* SF matrices later in 1995. Various silk based medical devices have received their regulatory approvals such as the long-term bioresorbable surgical mesh Seriscaffold® and a SF based ligament graft SeriACLTM [211]. The potential of SF for supporting various cell type adhesion and growth including keratinocytes, osteoblasts mesenchymal stem cells, endothelial cells, epithelial cells, schwann cells, *etc.*, has been well documented [208, 232-234]. For tissue restoration it is crucial that the implanted scaffold causes no or minimal immune reaction from the recipient. Hence the evaluation of the biodegradation rate of material employing both *in vitro* trials and *in vivo* animal tests has gained increasing interest. It is well known that SF does not trigger the activation of an immune response and its subsequent foreign body response has been noted to be analogous or even less than the common materials in use today as biomaterials [235, 236]. The biocompatibility of SF electropun scaffold was assessed by its implantation in rats on both sides of back and hip muscles for 8 weeks [237]. A well-tolerated response by the host animals was observed and the scaffold degraded completely *in vivo* after 8 weeks. However, phagocytes and lymphocytes were found to have invaded the materials. Electrospun SF tube was used by Cotto *et al.* [238] as a vascular graft and based on *in vivo* evaluation a mild host reaction was observed. In another study where SF scaffold was implanted beneath the dorsal skin of rats, it was found that the biodegradation of the scaffold was inflammation-mediated to a certain level and that the biodegradation rate in the subcutaneous implantation model can be controlled by scaffold pore size [239]. *In vivo* studies for ligament regeneration using MSCs cells seeded SF scaffold in a pig model demonstrated no record of malfunction after 24 weeks [240]. It was shown that the morphological, structural properties and extent of β-sheet crystallinity of SF resulting from its preparation process influenced the *in vivo* behaviour. Thus, it is possible to tailor a SF scaffold in order to accommodate the required functions, repair characteristics and rates [241]. In brief, the encouraging results confirm that SF based

products render good biocompatibility for wound healing and it is comparable to other biomaterials including collagen. Albeit there are reports implying moderate pro-inflammatory cytokine production associated with SF [242], as well as amyloidogenesis caused by the debris of degraded SF [243]. Furthermore, there exists concerns regarding the safety of silk biomaterials in the human body for a prolonged time period which need further investigations [208, 211].

2.4.4 Biodegradation

Biodegradation is a critical factor for tissue engineering, which has been well recognised with different definitions. It can be referred to as the degradability of material with biological elements by producing fragments, which can move away from the site by fluid transfer, but not necessarily from the body [244]. United States Pharmacopeia related the absorbable biomaterial to the loss of tensile strength within 60 days of post-implantation *in vivo* [208]. Generally an ideal tissue engineering scaffold in most cases should be a temporary ECM with a degradation profile matching the formation of new tissue. To elucidate how SF nanofibres degrade, researchers utilised various measures such as mass loss and morphology changes, analysis of degraded products *in vitro, in vivo* evaluation by structural integration examinations, as well as testing mechanical properties after specific time intervals. The rate and extent of degradation may be highly differing, according to solvent type, SF concentration and crystalline and pore structure induced during processing. Implanted aqueous-derived SF scaffolds in Lewis rats degraded at a faster rate compared to the counterpart prepared by 1,1,1,3,3,3 hexafluoro- 2-propanol (HFIP) solvent. The latter demonstrated the presence of residues after 12 months while the former's integrity was preserved for up to 6 months [245]. The higher concentration of SF lessens the degradability of the scaffolds, which may be considered as a consequence of the enhancement in mechanical strength of the scaffolds and extent of material that has to be hydrolysed [246]. Luo *et al.* [247] investigated the effect of porosity on the degradation of SF with the exposure of SF to collagenase IA for a duration ranging from 6 to 12 days. It was found that higher pore density SF degraded more slowly relative to the scaffold with lower pore density. Proteolytic enzymes such as protease XIV, alphachymotrypsin and collagenase IA are able to digest SF. However, the susceptibility of SF to protease XIV is more pronounced [248]. Furthermore, the degraded products of SF are soluble peptides and free amino acids, which are easily metabolised

by the body. A correlation was found between the β-sheet content and enzymatic degradation rate, where the presence of higher levels of crystalline structures resulted in reduced degradability rate [249, 250]. To modulate the degradation of electrospun SF, Kim *et al.* [251] used different ratios of ethanol/propanol mixtures. It was reported that the 50/50 mixture ratio degraded faster than 70/30 and 100/0, suggesting the possibility of controlling SF biodegradation by changing recrystallisation conditions. The incorporation of protease specific cleavage sites contributes to hinder the degradation of SF *in vitro* [252] . Based on these findings, SF can be regarded as a good candidate for tissue engineering applications with the potential to control its biodegradability.

2.4.5 SF Electrospinning

SF was first electrospun from HFIP as the solvent by Zarkoob *et al*. in 1998 and patented in 2000 [253]. Early research in SF electrospinning focused on the selection of a proper solvent and controlling the conformational transitions of fibroin during electrospinning. The former influences fibres biocompatibility of SF whilst the latter determines their mechanical properties. In the following subsections, a brief overview on SF electrospinning is provided.

2.4.5.1 SF Solvent

The fabrication of SF nanofibres with hexafluoroacetone-hydrate and formic acid as a spinning solvent has been reported [254-256]. Jin *et al*. [257] demonstrated the possibility of SF electrospinning with a lower concentration of aqueous silk fibroin when it was blended with poly-(ethylene oxide) (PEO). Uniform fibres with fibre diameters in the range of 800–1000 nm and predominantly random coil structures were obtained. However, the inclusion of water soluble PEO can sacrifice the structural integrity and stability of SF fibres. Jeong *et al*. [254] investigated the effect of different solvents including HFIP and formic acid on fibre diameter and structure. It was reported that solvents with a faster evaporation rate (HFIP) led to the formation of smaller fibres with a lower proportion of β-sheet structures. In order to eliminate the concerns relating to the effect of residual organic solvent due to their toxicity, Wang *et al*. [258] used the SF aqueous solution for electrospinning. Nevertheless, it was found that a concentrated SF aqueous solution (28 w/v%) was required for its spinnability. Mimicking the silkworm's spinning condition, Zhu *et al*. [259, 260] prepared weakly acidic aqueous SF spinning dope (pH=4.8) and their results showed that by reducing pH, both

spinnable solution concentration and consequently the average diameter of the electrospun silk fibres could be decreased. The dominant role of pH for electrospinning a SF aqueous solution at low concentrations was further emphasised by Kishimotoa *et al*. [261] and their findings indicated that a basic solution (pH= 10–11) was very important for electrospinning at the low concentration of 5 wt%. In another study, they compared the SF spinnability, morphology and structure using an aqueous solution and formic acid solution [262]. It was found that fibre diameters from formic acid solution were larger than that using aqueous solution. Nonetheless, no significant difference of the secondary structures was detected. Singah *el al*. [263] prepared concentrated aqueous SF solution by applying mild shearing under forced dehumidified air and generated SF non-woven mats using a free-liquid-surface electrospinning machine. The shear induced concentrating mechanism improved the electrospinning process by enhancing the viscosity and decreasing solution surface tension.

2.4.5.2 Effect of Electrospinning Parameter on SF Morphology

Sukigara *et al*. [255] investigated the SF morphology by varying electric field, solution concentration and tip-to-collector distance. The associated results indicated a dominant role of solution concentration in producing uniform SF. Meinel *et al*. [264] reported that at a relative humidity (RH) of 60%, uneven and beaded SF were obtained, whereas electrospinning below 30% RH led to the formation of uniform and bead-free fibres with fibre diameters of 530 ± 100 nm. Similar results were reported elsewhere [265] by examining the effects of RH and PEO concentration on SF prior to the PEO extraction. It was revealed that after PEO extraction, the average fibre diameter of SF decreased from 414 ± 73 to 290 ± 46 nm. Cao *et al*. [261] electrospun SF with controllable morphology and thickness, which was shown to depend primarily on the SF concentration and electrical conductivity of the solution. Under an optimal spinning condition, SF non-woven mat displayed satisfactory apparent stress and strain to failure with values being 11.1 ± 0.7 MPa and 10.2 ± 1.6%, respectively.

To gain a better insight and predict the optimal conditions for SF electrospinning, mathematical models were also used to develop a quantitative correlation between different electrospinning parameters and SF morphology and diameters. Sukigara *et al*. [266] employed response surface methodology (RSM) analysis and it was found that the effect of altering electric field on the fibre diameter of SF may be surprisingly small

or conversely unexpectedly significant depending on the SF concentration. This reflects possible interactions between spinning distance and fibre diameter on solution concentration and electric field. Amiralian *et al*. [267] evaluated the effect of concentration and applied voltage on the morphology and fibre diameter of SF via a RSM analysis. It was concluded that SF solution concentration was the most significant factor with a considerable influence on fibre diameter, whereas no significant effect was detected when applied voltage was varied. Recently, Chomachayi *et al*. [268] developed models based on a group method of data handling (GMDH) and artificial neural network to estimate the diameter of SF electrospun nanofibres. Both models provided relatively good accuracy. However, GMDH was reported as being more appropriate when the target was to predict SF diameter trends with the variation of electrospinning parameters.

SF electrospinning is highly sensitive to the preparation conditions of silk, solution age and storage conditions, which ultimately influences the solution properties and rheological properties. Ko *et al*. [269] evaluated the effects of degumming conditions on solution properties and electrospinning performance of silk. It was revealed that the viscosity of the silk solution increased significantly by a slight increase in the sericin content below 1% (or at the degumming ratio above 25%) resulted in the improvement of electrospinnability and increase in fibre diameter. Aznar-Cervantes *et al*. [270] studied the effect of SF aqueous solutions' preservation time at 4 °C on rheological properties and electrospinnability. The associated results demonstrated an increase in solution viscosity during the aging time for SF solutions up to 12 days in order to improve the electrospinnability. Furthermore, the light-chains of SF were influenced by the refrigeration time and its presence in the RSF solution decreased during storage, whereas in case of H-chains slight decrement in it's the molecular weight were observed over the experiment. The effect of formic acid on the degradation of SF during storage was evaluated by Kim *et al*. [271]. It was shown that the viscosity was nearly unchanged for 2 days, indicating that SF molecules were relatively stable in formic acid without any severe degradation. However, increasing the storage time demonstrated a detrimental effect on stability.

2.4.5.3 SF Electrospun Fibre Post Treatment

In general, compared to natural cocoon fibres, as spun SF electrospun nanofibre possess poor mechanical properties and stability. This is mainly ascribed to the conformation changes induced under a regeneration process, which results in a lower β sheet configuration. As a consequence, lower crystallinity and lower mechanical properties can take place [272, 273]. Organic solvents such as methanol and ethanol have been frequently used to convert random coil structures into the stable β-sheet conformation [274, 275]. Kim *et al*. [271] immersed electrospun SF in 50% (v/v) aqueous methanol solution by varying the duration from 10 to 60 min at room temperature (RT) and the relevant results implied a fast conformational transition within 10 min, as evidenced by solid-state attenuated total reflectance infrared spectroscopy (ATR-IR) and X-ray diffraction. However after methanol treatment for SF, a decrease in porosity from 76.1% to 68.1% was observed, which suggested that the shrinkage happened due to the dehydration effects of this solvent. Methanol treatment induced a high degree of crystallinity in SF leading to a brittle structure and loss of porous structures. Therefore, water vapour treatment was employed as an alternative effective approach resulting in less brittleness. However, a longer treatment time is required to complete such a transition, namely at least 1 h versus 10 min for methanol treatment. More interestingly, water vapour treatment can improve the elastic properties of SF, whereas methanol treatment tends to enhance yield stress and tensile modulus [276-278]. In a different approach, Silva *et al*. [279] successfully induced β-sheet structures by adding genipin into SF spinning dope without any post-treatment. Furthermore, this approach reduced the extent of swelling, and thereby led to thinner fibres when compared with silk fibroin nanofibres. Glutaraldehyde (GTA) has also been used as a chemical crosslinker in order to increase the stability of silk based nanofibres in SF [280].

2.4.5.4 SF Composite Electrospinning

To address the shortcomings of SF electrospun nanofibres in terms of strength, biodegradability, biocompatibility and also expand applications of materials with SF as their building blocks, various SF based electrospun composites have been developed. Table 2.4 lists some of typical polymers and nanoparticles that used with SF.

Table 2.4 Electrospun SF-based nanocomposites and their application.

Polymer	Research highlights	Application	Reference
PCL	• Core/shell structure • Enhance tensile strength	Drug delivery	281
	• Highly oriented conduit of electrospun biocomposite	Vascular tissue engineering	282
PLA	• Core/sell structure with nerve growth factor encapsulation manufactured • Plasma treated composites to improve surface hydrophilicity	Nerve tissue engineering	283
P(LLA-CL)	• Increase tensile strength and elongation at break • Increase contact angle	Vascular tissue engineering	223
	• Aligned electrospun composite fabricated by loading Vitamin B5	Nerve tissue regeneration	284
PLGA	• Improve mechanical properties and cell viability • Increase degradation rate	Nerve tissue Engineering	285
Keratin	• Enhance thermal stability • Decrease fibre diameter • Increase viscosity	Tissue engineering	286
	• Improve wettability • Decrease fibre diameter	Vascular tissue engineering	287
Collagen	• Increase fibre diameter and crystallinity with increasing collagen content • No significant difference in water uptake and tensile strength	Vascular tissue engineering	288
	• Collagen/SF hybrid nanofibrous matrix may be a better candidate than a collagen/SF blend nanofibrous matrix	Wound dressing	58
Gelatin	• Faster degradation rate by increasing gelatin ratio • Promote healing and elicit anti-scar effects on partial-thickness burn wound	Wound dressing	289
	• Improve spinnability • Increase b-sheet structure and consequently breaking tenacity • Improve biological properties	Blood vessel engineering	290
Chitin	• Improve ydrophilicity • two types of electrospun structures (*i.e.,* blend and hybrid scaffolds) • Phase-separated morphology for blend structures	Tissue engineering scaffold	

Chitosan	• Promote conformational transition in SF • Decrease fibre diameter	——	291
	• Chitosan enhances osteogenic differentiation and SF promotes proliferation in nanofibre	Bone tissue engineering	292
Sericin	• Improve thermal stability and mechanical properties	Tissue engineering	293
Single wall carbon nanotube (SWCNTs)	• Improve Young's modulus • Nucleating effect of SWNTs on the silk	——	221
Multi-walled carbon nanotubes (MWCNTs)	• Enhance mechanical properties	Wound dressing	222
	• Increase in diameter, crystallisation and electrical conduction with increasing MWCNT loading	Biomedical application	294
Graphene	• Increase contact angle, electrochemical conductivity and porosity with increasing of graphene content • Improve breaking strength and elongation	Peripheral nerve regeneration	295
	• Improve thermal stability with the addition of graphene • Enhance electroactivity and mechanical properties	Tissue engineering	296
Magnetite nanoparticles	• Decrease in crystallinity • Decrease in fibre diameter • Not cytotoxic regardless of particle concentration	Tissue engineering	297
Silver nanoparticle	• Antibacterial activity against P. aeruginosa even at low Ag content (*e.g.,* 0.1% Ag, w/v) • Secondary structure affects the release of Ag+	Drug delivery	280
Hydroxyapatite (HAp)	• Enhance mechanical properties • Uniform distribution of HAp as a result of using coupling agent	Bone tissue engineering	225

2.4.6 SF Electrospun Nanofibres and Their Tissue Engineering Applications

2.4.6.1 Bone Regeneration

In vitro studies show that SF naofibres can support human bone marrow stromal cell attachment, spreading and growth [298]. The effects of SF scaffolds on bone regeneration in a rabbit calvarial model were investigated. It was found that mouse preosteoblast (MC3T3-E1) cells maintained their phenotypic features, as evidenced by the production of ALPase and osteocalcin, and calcification. Furthermore, SF nanofibres provided enough space for selectively guiding bone cells into the wound space, yielding new bone tissue formation within 12 weeks [299]. Ki *et al*. [300] prepared 3D SF scaffolds by using a modified electrospinning method, and examined its potential for bone regeneration using a MC3T3-E1 cell line. Their findings confirmed the superiority of 3D SF structures over their 2D counterparts in terms of cell adhesion and proliferation, which was mainly ascribed to higher porosity. In spite of the osteogenic potential of electrospun SF biomaterials, it is preferable that nanofibrous structures of the scaffolds possess the reinforcement to render the mechanical properties required for bone formation. Therefore, SF composites have been developed by depositing or growing ceramics such as HAp on the surface of electrospun SF nanofibres [301, 302]. To achieve a uniform distribution of HAp and enhance interfacial bonding between SF and HAp, Kim *et al*. [225] modified HAp nanoparticles using γ-glycidoxypropyltrimethoxysilane. Their results demonstrated the reinforcing effect of HAp up to 20 wt.% and osteoblasts-cultured scaffolds confirmed the scaffold biocompatibility. The biomineralisation of HAp through a calcium phosphate alternate soaking method on SF electrospun nanofibres was also found to be an effective procedure to prevent the agglomeration of HAp nanoparticles and resulting composites can support the early stage of osteoblast adhesion with a considerable improvement on the differentiation stage [303]. To boost SF ability for bone repair, SF nanofibrous scaffolds were prepared with two-stage HAp incorporation in both the inner portions and outer surfaces of nanofibre structures. The scaffolds not only demonstrated an improvement of mechanical properties, but also were capable of providing a bone-specific physiological microenvironment [304].

Since bone is a complex connective tissue with a unique combination of organic and inorganic elements embedded in ECM, the convenience of incorporating various components as well as the feasibility of manufacturing different structures by an electrospinning process, makes it attractive for bone tissue engineering. Li *et al*. [184] assessed the bone formation from human bone marrow-derived mesenchymal stem cells (hMSCs) grown on SF nanofibres that were encapsulated with bone morphogenetic protein 2 and HAp nanoparticles alone or in combination. Based on the mineralisation and transcripts for genes involved in osteogenesis measurement, it was revealed that SF scaffolds containing both BMP-2 and HAp enhanced the bone formation significantly relative to plain SF. Recently, it was shown that the conjugation of recombinant human bone morphogenic protein-2 with SF scaffolds increased both water retention capacity and osteoinductivity of scaffolds [305]. Yuan *et al*. [306] manufactured SF/PCL aligned fibrous scaffolds and reported the cooperation of fibre alignment with guiding cell elongation in the fibre direction, thereby affecting the cell movement direction. Since chitosan is beneficial for osteogenic differentiation, Chen *et al*. [307] produced electrospun SF/chitosan composites, followed by a new developed chemical post treatment using ethanol/ammonia. The chemically treated scaffolds were reported to enhance the proliferation and osteogenic differentiation of human foetal osteoblastic cells.

2.4.6.2 Vascular Regeneration

Vascular grafts should be non-thrombogenic and vasoactive with appropriate mechanical properties in terms of compliance, burst pressure, strength and suture retention. SF electropsun scaffolds with tubular structures demonstrated sufficient burst strength to sustain arterial pressures. The combination of good mechanical properties and biological compatibility make SF a good candidate for vascular grafts [308]. Zhou *et al*. [309] fabricated vascular graft scaffold from aqueous solution of SF possessing seamless and porous (80% porosity) tubular structures. They also developed tubular constructs from SF/collagen using water as a solvent. By adding collagen, the fibre diameter and scaffold crystallinity increased, leading to a decrease in elongation ratio [288]. Marelli *et al*. [310] developed SF tubular scaffolds (Inner diameter (ID) = 6 mm) demonstrating a compliance value higher than Dacron® and Goretex® prostheses, but rather lower than human saphenous vein. Catto *et al*. [238] manufactured

SF tubes for vascular applications with ID=1.5 mm with estimated compliance, which was similar or higher than that of native rat aorta and Goretex® prosthesis.

SF has been electrospun with polymers such as PLGA [311], gelatin [312] and PU [313] to be used as vascular grafts. For example, thermoplastic PU were blended with SF and electropsun to provide elastomeric characteristics required for cardiovascular SF based patches and implanted into rat abdominal aorta [313]. The scaffold could induce the growth of a neo-artery composed of tissue present in native healthy artery. Yu *el al*. [314] developed a novel rotating collector and fabricated a continuous wavy–flat alternating SF/thermoplastic PU fibrous structure along the circumferential direction that provided a graft similar to natural elastic tissues. Vascular grafts of SF with a small diameter (ID = 3 mm) can be reinforced by coating with a silk sponge, leading to improvements in tensile strength and elastic modulus circumferentially and longitudinally as well as water permeation [315].

One of the major problem in vascular graft is failure in obtaining a confluent endothelium on the lumenal surface, which can be caused by the thrombus formation of loosely attached endothelial cells. Hence, Liu *et al*. [316] prepared sulfated SF nanofibrous scaffolds to improve scaffold antithrombogenicity and evaluated their anticoagulant activity and cytocompatibility. Results indicated that sulfated scaffolds with improved anticoagulant activity supported endothelial cells and smooth muscle cells (SMCs) adhesion and proliferation with a higher expression of some phenotype-related marker genes and proteins relative to plain SF.

2.4.6.3 Neural Regeneration

Peripheral nerve injury remains a common clinical problem. For the nerve gap shorter than 1–2 cm, the peripheral nervous system subjects to spontaneous nerve regeneration, whereas bridging methods are needed for longer nerve gap repair. With the development of tissue engineering, it is possible to fabricate implantable scaffolds for bridging disruption caused by peripheral nerve injury that will produce similar results to that of autografting. Electrospinning techniques have been applied to obtain SF-based neural scaffolds for repairing peripheral nerve injures [285, 317, 318]. SF electropsun scaffolds implanted as a nerve guidance conduit in a 10-mm defect of the sciatic nerve in rats promoted functional recovery by guiding regenerative axons and diminished neuropathic pain after nerve injury [319]. Wang *et al*. [320] manufactured

aligned SF/P(LLA-CL) scaffolds, and then reeled them into nerve guidance conduits to enhance peripheral nerve regeneration. The results have shown that blending SF with P(LLA-CL) could promote nerve regeneration considerably. Tian *et al*. [283] fabricated PLA/SF scaffold and encapsulated nerve growth factor (NGF) along with SF as a core of the scaffolds. The differentiated PC12 cells on plasma treated core/shell scaffolds showed elongated neurites with a length of 95 μm.

The functionalisation of SF based nerve guidance conduits with neurotrophin such as NGF and glial-derived nerve factor (GDNF) has been demonstrated to improve the functional recovery of injured peripheral nerves [321]. Liu *et al*. [322] loaded aligned electrospun SF scaffolds with dual factors of brain-derived neurotrophic factor and vascular endothelial growth factor for sustained released and implanted them in a mouse model to support nerve regeneration and angiogenesis *in vivo.* Compared to the control group, the dual-factor loaded SF scaffolds significantly promoted nerve regeneration and possessed a great potential in peripheral nerve repair. Madduri *et al*. [323] loaded aligned and non-aligned SF fibres with GDNF and nerve NGF, which demonstrated that the presence of a nanoscaled topography on membranes and in nerve conduits considerably improved the axonal elongation and the orientation of axons and associated glial cells.

Electrically active neural SF based implants incorporated with polyaniline [324], graphene [295], and SWCNTs [325] has shown to reduce the resistance of an electrically insulating material like SF, leading to make SF more appropriate for neural tissue engineering applications. The synergic effect of electrical stimulation and NGF on neuron growth was reported by the coaxial electrospinning of aligned P(LLA-CL)/SF loaded with NGF and polyaniline, which effectively supported PC12 neurite outgrowth and increased the percentage of neurite-bearing cells as well as the median neurite length [326].

2.4.6.4 Skin Tissue Engineering and Wound Dressing

Wound healing is a complex biological process and an ideal wound dressing should be biocompatible, prevent wound dehydration, protect the wound against dust and bacteria, and allow gas permeation [327]. SF is beneficial to simulate the skin microenvironment, eliminate scarring and mitigate atopic dermatitis; accordingly wound dressings based on SF have drawn great attention [328, 329]. Many researchers

tailored the structure [330] or surface of SF scaffolds [265] or else incorporated them with epidermal growth factor (EGF) [327], silver nanoparticles [331] and epidermal growth factor/silver sulfadiazine combinations [332] with the aim to enhance the wound healing process by increasing the cell proliferation (*i.e.*, granulation tissue formation), increase the rate of neovascularisation, reduce inflammation and prevent the risk of infection. Moreover, the inclusion of antioxidant components such as grape seed extract [328], curcumin [333] and vitamin C [334] with SF nanofibres have shown promising results for skin regeneration applications. Wound healing efficiency of SF nanofibres incorporated with fenugreek was investigated using full thickness excisional wounds in a rat model [335]. The relevant results indicated that the fenugreek inclusion not only enhanced mechanical, thermal, and antioxidant properties of scaffolds, but also the rates of wound healing and collagen deposition were improved. Manuka honey can modulate the moisture retention of SF scaffolds and *in vivo* wound healing assay indicated that the addition of Manuka honey improved the wound healing rate of SF fibrous matrices [336, 337]. The immobilisation of antimicrobial peptide motif (Cys-KR12) onto electrospun SF nanofibre membranes through a thiol-maleimide coupling procedure exhibited an antimicrobial activity against four pathogenic bacterial strains. Besides, it assisted the proliferation of keratinocytes and fibroblasts and improved the differentiation of keratinocytes with elevating cell-cell attachment [338].

To obviate the thickness limitation and small pore size of electrospun sheets, Ju *et al*. [330] employed a modified electrospinning approach integrated with progens (*i.e.*, sodium chloride crystal) to create 3D SF membrane with large pores. The wound healing efficiency was evaluated using a deep second-degree burn animal model in rats and it was found that the presence of 3D nanostructures facilitated the expression of growth factor gene in the burn wounds, yielding accelerated wound healing compared to a medical gauze control. Sheikh *et al*. [339] introduced a cold-plate electrospinning technique. The obtained SF construct exhibited high porosity with controlled thickness and an easy contouring of facial shape, making it a suitable scaffold for artificial skin reconstruction. Akturk *et al*. [340] employed wet electrospinning, which was followed by freeze drying to prepare 3D SF nanofibres and coated scaffolds with citrate-capped gold nanoparticles. Gold nanoparticles enhanced degradation profiles and mechanical properties significantly without a notable effect on the healing stage compare to SF scaffolds without nanoparticles, albeit they were

both better than an untreated skin control in terms of neovascularisation and granulation tissue formation. To optimise the architecture of SF scaffolds for enhancing their wound healing ability, Hodgkinson *et al*. [341] compared nano- to microscaled SF scaffolds and noted higher expressions of ECM genes, collagen types I and III as SF diameter decreased. Lee *et al*. [342] introduced a new approach to induce large pore size into SF scaffolds, thereby facilitating cell infiltration by dropping two different sizes of NaCl crystals above the rotating collector, and compared its wound healing effect for a full-thickness skin defect with Matriderm. The dermal regenerative effect was comparable for both scaffolds although the SF scaffold mostly degraded and did not cause wound contracture unlike Matriderm.

2.5 Halloysite Nanotube (HNT)

The name 'halloysite' was derived from Omalius d'Halloy who found the mineral in Angleur, Liége, Belgium and it was first described by Berthier in 1826. Halloysite nanotubes (HNT) with the chemical formula of $Al_2Si_2O_5(OH)_4 \cdot nH_2O$ are naturally occurring aluminosilicate tubule clays, formed by rolling kaolin sheets with an Al:Si ratio of 1:1 and are found deposited in soils worldwide [33, 343]. Based on the state of hydration, HNTs are generally categorised into two groups: hydrated HNTs (when $n = 2$) (*i.e.*, HNTs-10 Å), in which the "10 Å" designation indicates the d_{001} value of the layers. On the other hand, dehydrated structures (when $n = 0$) (*i.e.*, HNTs-7 Å) can be attained by the loss of interlayer water molecules under mild conditions [344]. The physical appearance and structure of HNTs is shown in Figure 2.6. Generally, HNTs are 0.2 to 2 μm in length with inner and outer diameters in the range of 10-40 and 40-70 nm, respectively. The internal lumen is mostly composed of (Al–OH) groups, while the external shell is covered by siloxane groups (Si–O–Si), and the edges of the sheet have a few silanols/aluminols [28]. This morphology and chemical structure results in HNT possessing internal and external surfaces with positive and negative charges, respectively. Generally, the HNTs surfaces have a negative charge in a wide pH range, facilitating the electrostatic interaction with cationic polymers. Both their site-dependent aluminosilicate chemistry and lumen structures are cooperative to achieve the feasibility of implementing various post-modifications on HNTs for targeted applications. In comparison with nanoclays and nanosilica, their lower content of hydroxyl groups make them less hydrophilic (*i.e.*, HNT contact angle in water is as low as $10 \pm 3°$) [28, 343, 345].

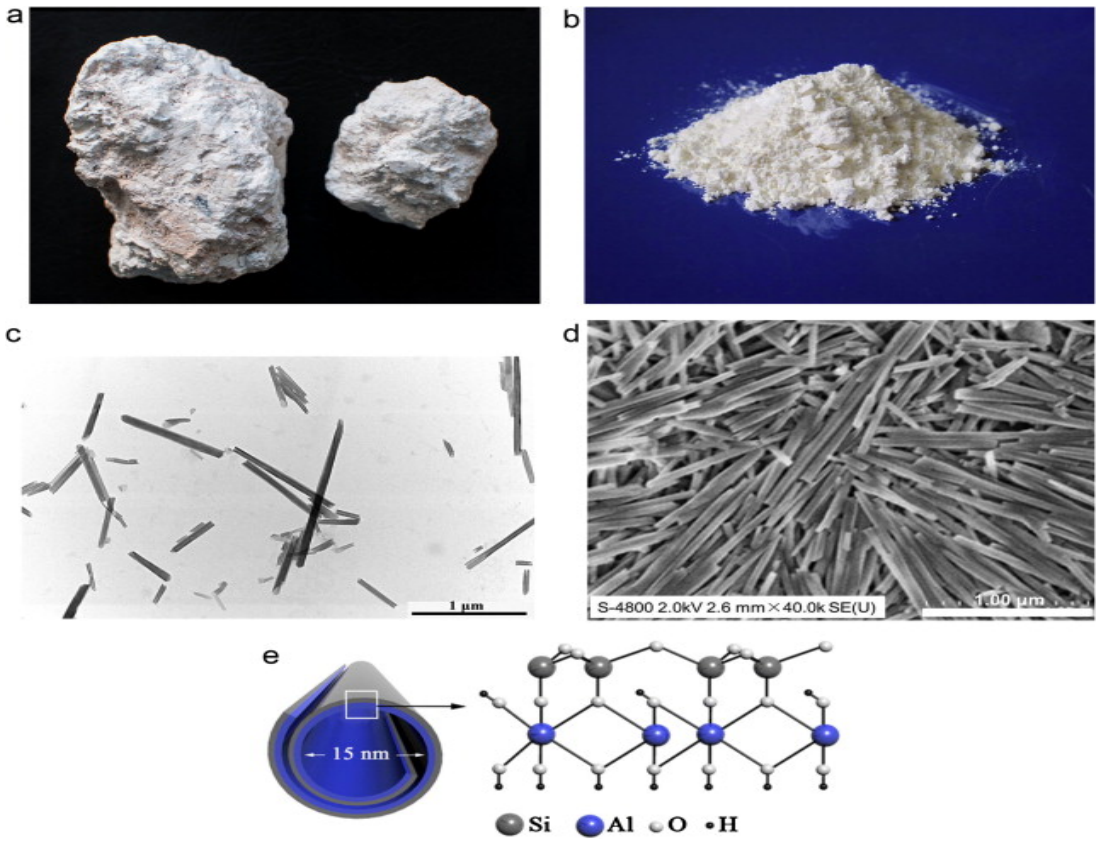

Figure 2.6 (a) Raw halloysite, (b) ground halloysite, (c) TEM and (d) SEM photos of HNT mined from Hunan Province, China, [28] and (e) schematic diagram of the crystalline structure of HNT [346].

HNTs are a green and cheap material (typically $4 per kg) and abundantly available from natural deposits with a global supply totalling several thousand tons per year, which facilitates their mass-scale industrial applications. This is unlike the gram-scale production of CNTs with a relatively high price ($500 per kg). Due to their tubular structures, HNTs possess high aspect ratios in a typical range of 10-50, which is beneficial for potentiating polymers by the optimisation of load transfer from polymer matrices to HNT in composite systems. Besides, their hollow structure yields a relatively low density (2.14–2.59 g/cm^3), which is similar to montmorillonite (MMT) and kaolinite and lower than fillers such as talc and calcite $CaCO_3$. Their low density is advantageous for preparing light-weight polymer composites. In terms of porosity, HNTs have one-dimensional tubular porous structures with rich mesoporous (2–50 nm) and even macroporous (> 50 nm) scales, which are larger than fillers such as CNTs. Thus their specific surface area and total pore volumes are relatively high although still lower than those of MMT. It should be noted that the morphology and structure of HNTs are highly altered and become dependent on the deposits [28, 343, 347].

Generally, a major challenge in using nanoparticles is to achieve uniform particle dispersion in solutions due to their high surface activities, which encourages nanoparticle agglomeration. For instance, the existence of strong intrinsic van der Waals attractions between CNTs impedes their uniform dispersion in common solutions [348]. Interestingly, the tube-like morphology of HNT, as well as the presence of a few hydroxyl groups and siloxane on their surface, diminishes the tube-tube interactions. As such, uniform HNT dispersion can be usually achieved, which is also beneficial to the industrialisation of polymer/HNT nanocomposites. It is worth mentioning that the high biocompatibility and low cytotoxicity of HNTs warrant their safe use in different fields [28, 33, 349].

HNTs can also act as free flame retardants in polymers by exerting a barrier effect toward both mass and heat transport. Furthermore, when compared to polymers, HNTs have a much higher thermal stability with an initial degradation taking place at approximately 400 °C. In addition, polymeric chains and degradation products can enter the lumens of HNTs, thus hindering mass transport and further promoting the thermal stability [343].

2.5.1 Applications of HNTs

The abundant nanosized tubular HNTs with tubular structure, good mechanical properties and low cytotoxicity are of increasing interest for the manufacture of advanced materials in diverse applications including nanoscaled carriers for storage and controlled release of guest molecules, drug delivery, tissue engineering, filler in polymers, adsorbent, energy storage devices, catalysts and biosensors [350, 351]. Here we focused on polymer/HNT nanocomposites and focus on electrospun HNT-based nanocomposites and their biomedical applications.

2.5.2 HNT Based Nanocomposites: Fabrication Methods, Properties and Biomedical Applications

HNT as a type of natural, environmentally inert and inorganic filler has been added into many polymers to improve mechanical properties, thermal stability, flame retardancy or even act as nucleating agents for the accelerated crystallinity of polymers. HNT nanocomposites can be fabricated through different methods such as

solution/melt casting [352], *in situ* polymerisation [353], layer-by-layer (LbL) techniques [354], electrophoretic deposition [355] and electrospinning [36]. A brief description of each manufacturing technique and corresponding examples of polymers that have been used are presented in Table 2.5.

Table 2.5 Fabrication approaches of HNT based nanocomposites.

Technique	Method description	Polymer	Reference
Solution Casting	HNTs and polymer were dispersed in proper solvent and composites formed by casting or precipitation.	PVA PEG	352 356
In situ Polymerisation	HNTs were dispersed in a liquid (monomer, solvent) followed by polymerization.	Polyaniline Polystyrene	357 353
LbL Technique	Layers of oppositely charged materials were deposited alternatively with washing steps in between.	Polyetherimide Chitosan	354 358
Electrophoretic Deposition	The method is based on electrophoretic motion of colloidal particles or polymer macromolecules under the influence of an electric field forming a deposit at the electrode surface.	Hyaluronic acid	359
Electrospinning	High-voltage was applied to a stream of polymer solution, forming continuous micro/ nanofibres.	PLA PCL PLGA	29 31 36

Due to their high aspect ratios and excellent mechanical properties (the elastic modulus of HNTs is 140 GPa), it is expected that HNTs can be promising nanofibres for reinforcing polymers [26, 28]. For instance, the inclusion of 2.3 wt% HNTs into epoxy improved the impact strength by 4 times without sacrificing flexural properties [360]. Handge *et al*. [361] reported a linear enhancement of elasticity and storage modulus of polyamide 6 with increasing HNT content, in which 90% improvement in Young's modulus was observed with the incorporation of 30 wt% HNTs. Liu *et al*. [362] revealed that HNTs enhanced tensile stress and Young's modulus of chitosan/HNT composites considerably by 134% and 65%, respectively, with increasing HNT content up to 7.5 wt.%.

The incorporation of HNTs into polymers can also increase thermal stability of nanocomposites, which is mainly ascribed to their lumen structure and high thermal stability. Such improvements in thermal stability and flame retardancy have been observed on polymers such as polyethylene [363], chitosan [364] and so forth. Du *et al*. [365] observed 60 °C and 74 °C increases in the temperature at 5% weight loss in nitrogen and the temperature at maximum weight loss rate in air, respectively, when modified HNTs were incorporated into poly(propylene) (PP). The flame-retardant effect of HNTs on polyamide 6 was investigated with the results suggesting that HNTs acted as a thermal insulation barrier at the composite surface during burning, and consequently improved the fire performance of the composites [366].

HNTs can also act as a heterogeneous nucleating agents and hence alter the crystallisation behaviour of semicrystalline polymers. Accordingly, an enhancement in crystallisation temperature and degree of crystallinity, together with a decrease in activation energy for the crystallisation, can be expected [28, 33]. HNTs play a heterogeneous nucleating agent role for polymers such as polyvinyl alcohol (PVA) [367], PLA [368] and PCL [369]. The addition of HNTs to PVA led to an increase in the crystallisation temperature of composites whilst the use of excessive amounts of HNTs tended to reduce the increasing trend in the crystallisation temperature due to the aggregation of HNTs in polymer matrix [367]. As reported by Ning *et al*. [370], well-dispersed HNTs in PP matrices act as nucleating agents resulting in an increase of overall crystallisation rate.

Due to hollow HNT lumen structures along with their cytocompatibility, non-toxic characteristics and natural abundancy, HNTs can be incorporated into polymers with the aim to develop biomedical applications. It has been shown that HNTs significantly enhanced the compression properties of chitosan scaffolds, whilst the cell attachment and skin repairing properties of the chitosan were also improved [25]. The incorporation of HNTs into alginate by solution-mixing and freeze-drying enhanced the attachment and proliferation of mouse fibroblast cells due to the biocompatibility of HNTs as well as an increase in surface roughness [27]. The feasibility of using HNTs as a drug carrier has been studied and there are many reports concerning drug release of nanocomposites based on HNTs embedded in various polymers such as PVA [371], alginate [372], gelatin [373] and so forth. The drug release rate could be further retarded by coating polymers onto drug-loaded HNTs. For example, coating HNTs with chitosan

demonstrated a drastic reduction in drug release compared to uncoated HNT counterparts due to the existence of an additional barrier through which the drug must diffuse [374]. Except for drugs, other active agents have also been encapsulated into HNTs for sustained release including antimicrobial agents [375], essential oils [376] and DNA [377]. Since pore size is a critical factor for drug delivery purposes, various techniques have been implemented to enlarge the lumen size and HNT porosity such as etching of alumina from the inside of the tubes or changing the pH of a water suspension containing HNTs [378, 379].

According to the above-mentioned advantages of HNTs, there are significant prospects for polymer/HNT composites. To fully profit from the incorporation of HNTs into nanocomposites, particle dispersion and interface interaction between HNTs and the polymer matrix must be regulated, otherwise they may have detrimental effects such as interfacial slippage and weak mechanical properties. Consequently, HNT functionalisation is a promising method to enhance particle dispersion and load transfer between HNTs and matrix. In this regard, two common methods have been employed, namely covalent functionalisation and non-covalent modifications, with more details being found elsewhere [28].

2.5.2.1 Electrospinning HNT Based Nanocomposites: Properties and Biomedical Applications

As mentioned in Section 2.5.2, electrospinning is one of material processing methods that has been employed to fabricate HNTs based nanocomposites. The first study on electrospun polymer reinforced with HNTs was conducted by Touny *et al*. [380] in which PLA/HNT composites were fabricated and the effects of various electrospinning parameters to obtain bead-free fibres were investigated. Final results indicated a decreasing trend in fibre diameter upon addition of HNT owing to an increase in electrical conductivity. Tao *et al*. [381] demonstrated that the addition of a small amount of HNTs (<5 wt%) into PGA induced chain orientation by hydrogen bonding between PGA carbonyl groups and silanol groups on HNT surfaces, whereas at higher loading disordered PGA chain orientation occurred, which was related to HNT aggregation and anisotropic alignment in PGA fibres. The characterisation of electrospun PLA:PCL/HNT composites showed a slight decrease in the crystallinity of nanocomposites, thereby decreasing the glass transition temperature of PCL, the

crystallisation temperature and melting temperature of PLA within composite materials [382]. Based on a systematic study evaluating the effect of HNT content on the properties of PLGA/HNT nanocomposites, the incorporation of a small amount of HNT (1 and 3% relative to PLGA) significantly increased strength and Young's modulus without sacrificing the biocompatibility of PLGA nanofibres [32].

Lue *at al*. [383] studied the impact of HNT surface modification with polydopamine layers on mechanical properties and cytocompatibility of electrospun PLLA/HNT composite scaffolds. The associated results revealed more uniform HNT dispersion under filler modification in the matrix. As a result, superior tensile strength as well as MC3T3-E1 cells adhesion and proliferation were detected relative to both PLLA and HNT/PLLA fibre membranes. Further investigations on evaluating the HNT modification effect on PLA/HNT nanocomposites implied that modification of HNTs contributed to better nanoparticle dispersion leading to the enhancement in both tensile modulus and strength [29]. To enhance drug absorption capacity of HNTs, it was shown that HNT modification by a coupling reaction with 3- aminopropyltriethoxysilane and maleic anhydride from hydroxyl groups of neat HNTs facilitated the drug loading of diclofenac sodium and diphenhydramine hydrochloride due to electrostatic interaction. Additionally, nanofibres containing modified HNTs displayed excellent mechanical properties and thermal stability relative to those with neat HNT, which was mainly attributed to homogeneous dispersion of modified HNTs and strong interfacial adhesion between HNTs and polymer matrix [384].

As evidenced by Nitya *et al*. [31], the presence of HNTs allowed for higher protein adsorption and improved the mineralisation of PCL/HNT nanocomposites when compared to pristine PCL. Furthermore, higher osteoblast differentiation was observed, suggesting the potential of PCL/HNT composite scaffolds for bone tissue engineering. Moreover, it was reported that the incorporation of HNTs into polydioxanone matrices by electrospinning formed a 3D scaffold prone to being used for regenerative endodontics [385]. According to proliferation results with human dental pulp-derived cells as a function of the HNT content, HNTs exhibited a high level of biocompatibility. However, a HNT loading of 10 wt% led to a significant increase in fibre diameter as well as a reduction in scaffold strength.

Qi *et al*. [36] reported a drug delivery system using HNTs as a carrier for loading a drug model, tetracycline hydrochloride, embedded within PLGA nanofibres to achieve a sustained release profile. Based on their findings, the inclusion of drug loaded PLGA/HNT nanocomposites not only considerably improved mechanical properties, but also reduced the drug burst release and prolonged the release rate. Further studies confirmed the cytocompatibility of composite based on *in vitro* viability results using mouse fibroblast cells cultured onto fibrous scaffolds [386]. Moreover, composite nanofibres were able to release the antibacterial drug TCH in a sustained manner for 42 days and displayed antimicrobial activity solely associated with the encapsulated TCH drug. Lee *et al*. [24] revealed that the crosslinking of PVA/HNT nanocomposites could alter the release pattern of encapsulated drugs, at which non-crosslinked nanofibres released the loaded drug more quickly than those that had been crosslinked. Another study demonstrated that the inclusion of 20 wt % HNTs in fibres, which allowed for 25 wt % metronidazole drug loading in PCL/gelatin microfibres, led to a 3-week sustained drug release relative to 4 days when directly admixed into the microfibres, which favoured to prevent the colonisation of anaerobic fusobacteria and potential use of such scaffolds as guided tissue regeneration membranes [387]. Unlike most studies that focused on single drug delivery systems, Zhang *et al*. [30] encapsulated two types of drugs, namely polymyxin B sulphate (antimicrobial) and dexamethasone (anti-inflammatory), into HNTs and embedded these into PLA via electrospinning. Based on the *in vivo* study of infected full-thickness burns, nanocomposite membranes were capable of co-delivering both drugs and improved wound healing significantly.

2.6 Gelatin

Gelatin is a natural biopolymer obtained from the hydrolysis of collagen and can be easily extracted from animal tissues such as skin, cartilage, and bone. The hydrolysis of collagen denatures the triple-helix conformation and gelatin, with a heterogeneous mixture of single or multi-stranded polypeptides, each with extended left-handed proline helix conformations and containing between 300–4000 amino acids, is obtained. The amino acid sequence of gelatin is similar to its parent protein and composed of 14% hydroxyproline, 16% proline and 26% glycine [388-390]. Gelatin can possess a structure with different physical properties and chemical heterogeneity features, depending on its collagen source (bovine, porcine or fish), type and age of animal as well as preparation technique. Generally, depending on the pre-treatment

procedure, two types of gelatin are commercially available, namely Type A (acid process) and Type B (alkaline process). The former type possesses a larger number of amino groups whilst the latter is obtained by converting glutamine and asparagine residues into glutamic and aspartic acid, leading to the higher content of carboxyl groups [391]. Due to the existence of both acid and basic functional groups, gelatin demonstrates an amphoteric behaviour. In other words, it can be negatively or positively charged in an alkaline or acidic environment, respectively. Moreover, the isoelectric point for gelatin depends on processing conditions and its value can vary in a pH range of 6–9.5 and 4.5–5.6 for type A and type B gelatin, respectively [389, 392]. Gelatin is water soluble and its aqueous formed gel is thermally reversible with a gel melting temperature less than 35 °C, which is below the body temperature and endowing unique organoleptic characteristics [388]. Rheological properties of gelatin have a crucial role in determining its quality for particular applications. Accordingly, the gel strength and thermal stability have been measured based on a standard protocol and the value referred to as 'bloom strength'. The term 'bloom strength' is indicative of the number of grams required for a 0.5 inch diameter probe to deflect a set gel by 4 mm, typically ranging from 30 to 300 g. The bloom strength and thermostability are dependent on the molecular properties of gelatin, specifically its amino acid composition and molecular weight distribution. Typically gelatin extracted from fish exhibits lower bloom strength relative to those from mammals [390, 393]. Additionally, mammalian gelatin is widely used as an excipient in pharmaceutical processing [42], as a stabiliser in vaccines [394], and as an agent in food processing for many years [391]. Based on target applications, gelatin can be manufactured into various forms such as films, nanofibres, micro- or nanoparticles, and dense or porous hydrogels [395].

2.6.1 Gelatin Electrospinning

Gleatin was first electrospun by Huang *et al*. [396] and it was shown that, despite the solubility of gelatin in water, electrospinning gelatin aqueous solution is not feasible mainly due to its instability and gel transition at RT. To make an electrospinnable gelatin solution, organic solvents such as 2,2,2-trifluoroethanol [397] or HFIP [398] have been successfully employed. Due to the highly corrosive nature of these solvents, alternative solvent systems such as using carboxylic acids (formic acid [399] or acetic acid [400]), solvent mixtures (acetic acid and ethyl acetate) [401], aqueous solutions of carboxylic acids [402], or use of gelatin aqueous solution at high temperature [403] have

been proposed. Many reports investigated gelatin electrospinning and optimisation of the resulting nanofibres in detail and gelatin fibres with small and large diameters were manufactured by changing electrospinning parameters such as solvent systems and concentration [392, 404, 405]. However, electrospun gelatin nanofibres are water soluble and mechanically weak which can further restrict their long-term application, especially for biomedical purposes. Therefore, different physical, enzymatic and chemical crosslinking methods have been applied in the literature [392]. Physical methods were based on using plasma, UV radiation, electron beam irradiation [406], and dehydrothermal treatment, which are nontoxic but generally less efficient, with a lack of control over the reaction kinetics of crosslinking [404, 407, 408]. So far, chemical crosslinking is the most common method to crosslink gelatin and many chemicals including formaldehyde [409], GTA [408] carbodiimide [410], dextran dialdehyde [411], diepoxy [412], glucose [400] and genipin [413] have been used. Amongst them, GTA has gained increasing attention due to its high efficiency, low price and availability. However, the residuals of GTA can impose cytotoxic effects on the cells [414]. The specific reaction mechanism of glutaraldehyde with amino acids in proteins is not clearly understood. Glutaraldehyde is presumed to cross-link in an inter- and intramolecular fashion by the formation of covalent bonds. This can occur in two ways: formation of Schiff bases by reaction of an aldehyde group with an amino group of lysine or hydroxylysine or an aldol condensation between two adjacent aldehydes. The Schiff base linkage is a very unstable bond, whereas the aldol condensation product is stable[415, 416]. Sisson *et al*. [417] explored the effect of different crosslinking methods on electrospun gelatin nanofibres such as vapour-phase GTA, aqueous phase genipin, and glyceraldehyde, as well as reactive oxygen species from a plasma cleaner. The final results showed the best results from glyceraldehyde and genipin due to their low toxicity and resistance toward degradation in cell culture medium at 37 °C. Cross-linking can also induce significant improvements on the mechanical performance of gelatin nanofibres. For instance, crosslinking gelatin nanofibres with genepin improved elastic modulus and strength at break up to values of approximately 990 and 21 MPa, respectively, when compared with 240 and 6 MPa for the non-crosslinked counterparts [418]. Similarly, Zhang *et al*. [419] reported a nearly 10-fold increase in both tensile strength and tensile modulus of gelatin naofibres after treatment using GTA. Furthermore, fibres preserved their morphology up to 6 days when subjected to immersion in warm water at a temperature of 37 °C. To develop a new and convenient crosslinking approach for gelatin

nanofibres, Zhan *et al*. [420] reported an *in situ* material process to produce crosslinked nanofibre membranes by incorporating GTA into electrospinning solutions before processing.

Gelatin has been blended with other polymers such as PCL [421, 422], PLGA [423], PLLA [398], PGA [424] and PU [425] to improve their stability and mechanical properties. In addition, gelatin possesses a fast degradation time and highly hydrophilic surfaces while the nature of other synthetic polymers such as PLCL, PCL, PLA, *etc.*, are hydrophobic with good mechanical performance. Hence electrospinning blended gelatin/synthetic polymers is an efficient way to combine these advantages and minimise their respective defects [392]. Li *et al*. [426] reported that adding polyaniline into gelatin reduced the average diameter and increased mechanical integrity. Gelatin has also been electrospun with PCL to create scaffolds in order to avoid the requirement for cross-linking. The incorporation of 30 and 40 wt% gelatin showed an optimum combination of hydrophilicity [427]. Similarly, the blending of gelatin into PCL with a blend ratio of 30:70 resulted in the formation of composites with high mechanical stability and excellent elastic properties of fibres with an improvement in their degradation rate [428].

Apart from synthetic polymers, some natural polymers are also electrospinnable with gelatin including chitosan [429], SF [289], zein [430], fibrinogen [431] and so forth. Interestingly, electrospinning gelatin with zein led to the formation of scaffolds with hydrophobic surfaces with a water contact angle of 118.0°, which is ascribed to homogenous dispersion of zein acting as cross-linkers with strong interactions in an aqueous phase to maintain 3D nanofibre structures [430]. Li *et al*. [432] reported that the incorporation of hyaluronic acid could improve the electrospinning processability of aqueous gelatin solutions. Blending gelatin with chitosan also rendered fibres with more uniform morphologies and enhanced elastic properties when compared to pure gelatin or chitosan nanofibres, implying the existence of intermolecular interactions within electrospun gelatin/chitosan nanofibres [429].

Compared to other natural polymers, there are more reports on electrospinning gelatin with SF and evaluating the resulting nanocomposite properties. The addition of gelatin into SF not only enhanced the spinnability of SF, but also improved mechanical properties because of the formation of intermolecular hydrogen bonds and the

increment of β-sheet structures in nanocomposites [290]. Chomachayi *et al*. [433] found that the incorporation of gelatin to SF enhanced nanofibre diameter, bulk hydrophilicity, surface wettability, and mass loss percentage. Nevertheless, a slight reduction in ultimate tensile strength and Young's modulus was also observed. Okhawilai *et al*. [434] investigated the effect of preparation conditions for electrospun fibre mats of Thai SF/type B gelatin, which reported a decrease in average fibre diameter by increasing the applied voltage and decreasing the SF content. Additionally, SF degradation was elevated and cell proliferation was enhanced by adding gelatin to SF scaffolds. Sasithorn *et al*. [435] fabricated SF/gelatin composite nanofibres by varying the weight ratios of SF to gelatin via needleless electrospinning and highlighted a positive role of gelatin weight ratio in increasing the diameter of the resulting nanofibres.

2.6.2 Gelatin-Based Electrospun Materials for Tissue Engineering

Electrospun gelatin fibre has evoked the interest of researchers for tissue engineering applications due to its similarities to collagen and other distinctive features including biological origin, excellent biocompatibility, antithrombogenicity, non-immunogenicity, biodegradability, and commercial availability. Gelatin has many integrin binding sites to facilitate the adhesion and differentiation of living cells. Additionally, their 3D fibrous structure simulates the ECM of human and organs very well, which can be potentially used in developing biomimicking artificial ECM for engineering tissues, wound healing dressings, and drug release [389, 392, 408].

2.6.2.1 Bone Regeneration

Meng *et al*. [46] studied the potential of gelatin/PLGA composites with aligned and randomly oriented morphologies as bone tissue engineering scaffolds. The addition of gelatin improved the hydrophilicity of scaffolds and increased their adhesion and proliferation of MC3T3-E1 cells. In addition, the aligned construct directed cell orientation in the longitudinal axis for guided bone regeneration. Blending gelatin with PCL also promoted the wettability and cell viability of scaffolds and their guided bone regeneration ability was apparent [397]. Rong *et al*. [45] embedded natural bone powders into electrospun PCL/gelatin scaffolds and studied their biocompatibility by seeding adipose-derived stem cells (ADSCs). The biocompability of gelatin with the mechanical strength of PCL, along with the rigidity of natural bone, were found to

combine to promote ADSCs cell growth, proliferation, and differentiation of prepared scaffolds. The inclusion of β-tricalcium phosphate into gelatin nanofibrous membranes promoted alkaline phosphatase activities, and osteogenic gene expression in rat bone marrow MSCs cells [436]. To obtain specific bioactivity towards bone applications, satisfactory results were reported by embedding calcium phosphates and bioactive glasses [389, 437]. Kim *et al*. [438] showed a significant improvement in bone-derived cellular activities with the inclusion of hydroxyapatite into gelatin nanofibres relative to pure gelatin. *In vivo* bone formation results indicated that biphasic calcium phosphate loaded gelatin/PVA composites increased bone formation within 2 and 4 weeks [439].

2.6.2.2 Neural Regeneration

Fibre orientation provides the informational cues to the cells and accordingly can influence neural outgrowth [392]. Aligned biocomposites based on PCL/gelatin nanofibrous scaffolds were studied for neural tissue regeneration. Gelatin blending ratio considerably influenced scaffold properties and the probability of fibre breakage increased with increasing the gelatin content. PCL/gelatin with a weight ratio of 70:30 was noted to possess the most balanced characteristics to match all the required specifications for nerve tissue. Furthermore, neonatal mouse cerebellum nerve cells were elongated parallel to the direction of fibres [440]. The same positive results were observed by Gupta *et al*. [441] when they seeded schwann cells for axonal regeneration on PCL/gelatin scaffolds. However, the affinity of cells toward nanofibres with random structures was more pronounced relative to aligned counterparts. Binan *et al*. [442] developed a non-woven material made of co-electrospun PLA/gelatin fibres loaded with instructive cues including retinoic acid and purmorphamine. The resultant scaffolds displayed a degradation rate and mechanical properties similar to those of peripheral nerve tissue and seeding neural stem-like cells on scaffolds resulted in rapid cell proliferation and differentiation into motor neurons.

2.6.2.3 Vascular Regeneration

Shalumon *et al*. [44] mixed gelatin with PLLA to increase the flexibility of PLLA and render a cell-friendly environment. Gelatin content directly influenced the hydrophilicity of scaffolds and increased the viability and proliferation of human umbilical vein endothelial cells (HUVECs) and SMCs cells proportional to the gelatin

content. The addition of PLLLA also improved the estimated burst pressure, which can be used to prepare more strengthened vessels [443]. Wang *et al*. [444] loaded heparin, an anticoagulant agent, into gelatin nanofibres as controlled delivery devices for vascular tissue engineering. The addition of heparin decreased fibre diameters considerably and the sustained release of heparin over 14 days was achieved. Blending gelatin with synthetic polymers such as PU can improve endothelial cell adhesion and proliferation relative to plain PU by providing a closer matching construct to native vessels [47]. Core-sheath configurations for vascular grafts were explored using PCL/gelatin mixture as the core and PU in the shell, leading to both favourable mechanical properties and binding sites for the cell attachment and proliferation [445]. Coimbra *et al*. [446] showed that the presence of gelatin in core-shell mats composed of a PCL core and a functionalised gelatin shell enhanced the hydrophilicity of scaffolds, and thus decreased the hemolytic and thrombogenic characteristics. The recent study conducted by Joy *et al*. [447] showed the benefits of *in situ* crosslinked blend of gelatin-oxidised carboxymethyl cellulose for vascular tissue engineering. The mechanical properties validated the physical eligibility for its prospective usage as a vascular graft and its non-toxicity and minimal immune response for implantation.

2.6.2.4 Corneal Regeneration

A desirable scaffold for corneal regeneration should have corneal ECM structures with a thickness of around 550 μm and providing sufficient refractive power. Corneal ECM can be considered as natural fibre reinforced hydrogel [389]. To mimic corneal ECM structures, gelatin nanofibres were used to reinforce alginate hydrogel and 15–16% weight fractions of electrospun gelatin fibres improved their elastic modulus from 78 kPa to 0.45–0.5 MPa, which was very close to the cornea's value [448]. Gao *et al*. [449] conducted a comparative study using aligned and randomly structured gelatin/PLLA scaffolds for guiding the aligned growth of corneal stroma cells. It was deduced that aligned nanocomposite scaffolds provided an external stimulus for the orderly arrangement of cells and enhanced cell viability more significantly.

2.6.2.5 Skin Regeneration and Wound Healing

Gelatin based scaffolds possess an inherent capability to promote *in vitro* adhesion and proliferation of fibroblasts and *in vivo* skin wound healing due to it being a collagen derivative which is a major ECM protein [392]. Powell and Boyce [450] fabricated dermal

substitutes by electrospinning gelatin and observed the key role of porosity and interfibre distance in tissue morphogenesis. Inter-fibre distances between 5 and 10 μm supported satisfactory dermal and epidermal layer formation including a continuous basal keratinocyte layer. Due to the moist and nutritious nature of wound environments, there is a high risk for bacterial infection which can hinder the healing process. The addition of silver nanoparticles into gelatin nanofibres exhibited the highest antibacterial activity against *Pseudomonas aeroginosa*, which was followed by *Staphylococcus aureus*, *Escherichia coli*, and methicillin-resistant *S. aureus*, respectively [451]. Gelatin fibres loaded with vitamin E and/or A impeded the growth of *Escherichia coli* and *S. aureus* significantly [452]. Moreover, fibres were also found to promote the adhesion and proliferation of L929 fibroblasts in the early stages of culture and elevated their collagen production. The incorporation of herbal extract with wound healing ability such as *Centella asiatica* into gelatin nanofibres were explored and an *in vivo* study in a rat model demonstrated their higher recovery rate compared with neat gelatin mats with reduced frequency of dressing change [453] Further studies on gelatin fibrous scaffolds loaded with extracts of grape seed polyphenols [454], *Lawsonia inermis* [455], thyme essential oil [433] and antibacterial agents such as ceftazidime [456] and gentamicin sulfate [457] were conducted resulting in the acceleration of wound healing processes. The feasibility of elecrospun cellulose acetate/gelatin as an effective simulator of the structure and composition of native skin was assessed by Vatankhah *et al*. [458]. It was shown that scaffold adherence to the wound could be tuned by altering the gelatin amount within the compositional blend. Interestingly, scaffolds with a blend ratio of 25:75 enhanced the skin regeneration of full-thickness-injured tissues while a ratio of 75:25 could act as a low-adherent wound dressing.

An ideal tissue skin graft and wound care should possess good mechanical properties along with ease of handling. Hence, researchers blended gelatin with other polymers such as PLLA [459], PU [460] and PCL [461] and so on to fulfil the required demands in fabricated nanofibrous scaffolds. Duan *et al*. [462] investigated the mechanical properties of electrospun gelatin/PCL fibres and reported that increasing the PCL content enhanced mechanical properties but reduced cell adhesion. Gelatin/PCL retained sufficient mechanical strength for handling after 1 week of culture time and further *in vivo* transplantation studies revealed the capability of nanocomposites to repair skin defects in the nude mouse. The efficiency of gelatin/PLLCL fibres for wound healing

was studied both *in vitro* and *in vivo* [463]. Gelatin/PLLCL (blend ratio: 60:40) fibres resulted in good mechanical strength in wet conditions. Furthermore, compared to controlled wounds, nanofibrous scaffold accelerated wound closure and regeneration to 10 days and promoted re-epithelisation. Nourozi *et al*. [464] encapsulated epidermal growth factor in PLGA/gelatin hybrid nanofibres for skin regeneration and associated results indicated the higher gene expression of collagen type I and III relative to plain gelatin with excellent hemostatic features. For smart wound dressing, shape memory polymer or a multifunctional polymer was blended with gelatin and promising results were observed. Tan *et al*. [465] noted that electrospinning blends of gelatin/chitosan/shape memory PU not only provided favourable water vapour transmission ratio, hydrophilicity, cytocompatibility antibacterial activity, but also that PU was found to possess good controllability on the tensile force under different strains, which could further ease material processing and shape recovery-assisted closure of cracked wounds. Dongargaonkar *et al*. [466] electrospun blends of covalently conjugated highly branched star-shaped polyamidoamine dendrimer to gelatin and converted such electrospun scaffolds into semi-interpenetrating networks with photoreactive polyethylene glycol diacrylate. This unique gelatin−dendrimer nanofibre construct allowed higher drug loading capacity accompanied with the remarkable flexibility for generating electrospun multifunctional dressing materials. In order to promote skin graft quality and reduce scarring, astragaloside IV (AS) was loaded to gelatin/SF scaffolds and applied topically on deep partial-thickness burn wounds [289]. AS-loaded SF/gelatin nanofibrous dressing was more effective for wound healing when compared with that of control samples without the nanofibrous dressing and triggered pro-angiogenesis of partial thickness burn wound whilst exerting anti-scar effects. Promising results were also observed when human dermal fibroblasts cultured on gelatin/GAGs nanofibres, in which cells were completely attached and populated on the fabricated scaffold surfaces.

2.7 Collagen

Collagen is regarded as the most abundant protein within the mammalian body, which imparts physical support and structural integrity to tissues. Collagen, containing molecular structures or fibrillar structure, is the predominant protein of most hard and soft tissues comprising about 25% of total dry weight of mammals. To date, 29 distinct collagen types have been identified. Based on their structure, chain bonding, and

position within the human body, it can be classified into eight families including fibril-forming, basement membrane, microfibrillar, anchoring fibrils, hexagonal network-forming, fibril-associated collagens with interrupted triple helix [FACIT], transmembrane, and multi-plexins [50, 467, 468]. Collagen types I, II and III are the most common collagens and referred to as classical fibril-forming collagens. Trimeric molecules of collagen have three polypeptide α chains assembled into triple helix structures leading to either homotrimers or heterotrimer formation. Each α chain consists of amino acids with -Gly-X-Y- sequences in which X and Y are mostly proline and 4-hydroxyproline, respectively [469-471].

Since collagen is a ubiquitous protein, it has various sources such as animals and vegetables. Common sources of collagen from animals are bovine, porcine, rat, human collagen, and marine organisms such as fish. It is preferably extracted from tissues rich in fibrous collagens including dermis, tendon and bone [50, 467]. However, due to the concerns about using animal-isolated collagen such as variability, allergic reactions and risk of disease transfection, synthetic sources have been developed. For example, artificial polymer commercially named as KOD is a synthetic protein made of 36 amino acids and it emulates native collagen structures and folding [472]. Moreover, producing recombinant human collagens by host cells is an alternative promising approach to obtain collagen whilst avoiding the risks of immune problems [473, 474].

One of the valuable aspect of collagen based material is their good biocompatibility and poor immunogenicity relative to other proteins. Furthermore, collagen possesses unique properties such as porous structure, permeability, good biodegradability and offers the ability to tune the morphology, adhesion, migration and differentiation of cells. All these characteristics are contributed to the widespread use of this material in many biomedical applications. Nonetheless, due to poor mechanical properties, as well as structural instability upon hydration, various approaches such as crosslinking or a structural modification agent or blending with other polymers have been applied [467, 468, 475].

2.7.1 Collagen-Based Scaffolds for Tissue Engineering

Owing to its high water affinity, low antigenicity, very good cell compatibility and the ability to promote tissue regeneration, collagen has been considered as a favourable material for tissue repair and reconstruction. Therefore, many studies have reported on

collagen fabrication and its widespread range of applications both *in vivo* and *in vitro* [392, 476, 477]. Collagen scaffold can be fabricated by electrospinning conferring structural and biological properties of the natural collagen ECM under optimised conditions. Intrinsic features of the electrospinning process make it possible to manufacture collagen fibres analogous to native collagen characteristics with an ability to improve cell growth and penetration capacity [53, 478, 479]. Another efficient technique to manufacture collagen scaffold is lyophilisation in which the mechanical properties of the resulting scaffolds depend on the collagen concentration in solution [480]. Collagen scaffolds in a mono-component system can be characterised by weak mechanical properties with limited applications. Hence, apart from crosslinking, blending with other polymers is a promising strategy to overcome its deficiencies [481]. Natural polymers such as chitosan [482], SF [35] and alginate [483] and synthetic polymer including PLA [484], [485] and PVA [486] were blended with collagen to modify collagen-based scaffolds with promising prospects in tissue engineering applications.

For instance, it was reported that the addition of silk into collagen scaffolds greatly improved the matrix stability against excessive fibre swelling and shape deformation in cell culture medium [487]. Moreover, the ultimate tensile strength and elasticity of collagen scaffolds increased monotonically with silk content, ranging from 40 to 182 MPa and from 0.58 to 4.45 GPa, respectively. Sionkowska *et al*. [488] noted that the use of hyaluronic acid to collagen/chitosan blends improved the scaffold elasticity along with its porosity.

Incorporating a low amount of PGA into collagen sponge not only enhanced the compressive modulus by a factor of six times, but also suppressed collagen shrinkage when submerged in simulated body fluid. Hence, a higher number of L929 cells were attached with deeper infiltration [489]. Baylan *et al*. [490] found that increasing the weight fraction of PCL nanofibres within collagen scaffolds displayed better size retention. In addition, inclusion of PCL resulted in accelerated mature osteoblast phenotype development. Mozdzen *et al*. [491] integrated arrays of PLA fibres into collagen scaffolds using 3D printing for the development of tendon bone junction repair. The results demonstrated the ability to tune the mechanical performance of fibre-scaffold composites at the bulk scale.

In the following subsection, several typical applications of collagen based scaffolds in tissue engineering are briefly introduced.

2.7.1.1 Bone/Cartilage Regeneration

The main components of bone tissues are collagen type I and hydroxyapatite with a small amount of type V. Therefore, collagen is an attractive polymer to prepare scaffolds emulating the native ECM of bone. It should be noted that various collagen based scaffolds were proposed with the aim of improving its mechanical properties so that it can be used as a hard tissue [468]. For example, the incorporation of inorganic bioceramic components such as calcium phosphate or β-tricalcium phosphate into collagen improved not only its mechanical properties, but also enhanced osteoconductivity and dimensional stability of the scaffolds. In addition, the surface area of the collagen scaffolds also increased, which yielded incremental cellular adhesion [492-494]. Apart from this, carbon based components such as CNTs possessed good bone-tissue compatibility and could support osteoblast proliferation and bone-forming functions [495]. There are many investigations reporting promising results when natural or synthetic polymers were blended with collagen for bone repair. Alhag *et al*. [496] found that collagen/GAGs scaffolds could provide a proper 3D microenvironment for the osteogenic differentiation of MSCs with the stimulating effect of osteogenic factors. The bone mimicking tri-component scaffolds, composed of PCL, collagen I, and HAp, promoted MSCs cell spreading and proliferation and simultaneously offered a good support for endogenous reparative cells that could be infiltrated into the implant sites [497].

Collagen-based biomaterials used for cartilage regeneration tend to be more flexible and are preferably made with type II collagen as opposed to most other collagen-based biomaterials, which are prepared using type I collagen [50]. Collagen gel as matrix scaffolds can be used for a clinically applicable treatment for focal defects of articular cartilage. However, its biomechanical property is still unsatisfactory [498]. Recently, a novel technology known as matrix-induced ACI has raised attention to promote cartilage repair. This method is based on the combination of autologous chondrocytes with tissue engineering scaffolds and artificial 3D collagen matrix [499].

2.7.1.2 Neural Regeneration

Collagen based scaffolds, either in the form of tubular conduits or aligned templates, were shown to be good substrates for nerve regeneration in several preclinical models, mainly due to the excellent biocompatibility and cell-adhesive nature of collagen [500]. Liu *et al*. [501] demonstrated the potential of electrospun collagen nanofibres for spinal cord injuries. It was noted that aligned collagen fibrous membranes resulted in elongated astrocytes. Cui *et al*. [502] manufactured functional collagen scaffolds by filling the collagen nerve conduit with linear ordered collagen scaffolds integrated with recombinant proteins to bridge a 35 mm long facial nerve gap in minipig models. The functional composite conduit exhibited favourable mechanical properties, as well as an acceleration in nerve reconstruction. Moreover, the addition of collagen into synthetic scaffolds such as PCL was shown to improve schwann cell migration, neurite orientation, and process formation of schwann cells, fibroblasts and olfactory ensheathing cells relative to plain PCL [503].

2.7.1.3 Vascular Regeneration

In 1986, collagen based scaffolds were employed for blood vessel reconstruction by Weinberg and Bell [504]. The scaffolds were composed of collagen multilayers integrated with a Dacron mesh to provide desirable tensile strengths. Further investigation by Lee *et al*. [505] indicated that collagen/PCL scaffolds could serve as an appropriate environment for vascular cell growth. Concurrently, it could resist high degrees of pressure and flow for a long time.

2.7.1.4 Skin and Wound Healing

Collagen is considered as the most clinically effective material that facilitates wound healing and has distinctive merits for skin tissue engineering since up to 70% to 80% of the dry weight of dermis is consisted of collagen type I [506]. Collagen-based wound dressings have long been used for burn coverage and ulcer treatment [507, 508]. They have been processed into various form of gel, sheet, fibre, or sponge and are commercially available (Promogram®, Johnson & Johnson and Puraply®, Royce Medical) [509]. Rho *et al*. [510] fabricated fibrous collagen scaffolds and evaluated their effects on human keratinocytes and skin tissue engineering. Based on *in vitro* observation, keratinocyte adhesion and spreading were promoted and open wound healing tests indicated the

proliferation of fibroblasts and young capillaries in the early stage of wound healing. Collagen can be blended with several bioactives and polymers that could act in a synergistic manner, which helped to accelerate the wound healing process. Previous work illustrated that freeze dried collagen/chitosan scaffolds seeded with fibroblasts and keratinocytes could promote rapid remodeling of ECM at a rate similar to that of the native dermis [511]. In addition, the authors also reported the organisation of elastin deposits in thin fibrils after 90 days, a process which normally took several years in humans. Ti *et al*.[512] fabricated collagen/chitosan spongy scaffolds loaded with thymosin beta 4 (Tβ4) to elevate a wound healing process in diabetic rats. Their results revealed the sustained release of Tβ4, which in turn caused the enhancement of both migratory and proliferative activities of high glucose-treated HUVECs cells, as well as angiogenesis improvement. To mimic the biological cues offered by the skin dermis, Rnjak-Kovacina *et al*. [513] prepared electrospun collagen/elastin scaffolds and found that crosslinked scaffold nanofibres supported human dermal fibroblast attachment, migration and proliferation. It was noted that adding elastin to collagen was beneficial to reduce wound contraction and improve skin regeneration. Many studied embedded silver nanoparticle into collagen scaffolds and reported good wound-healing efficacy owing to their intrinsic antibacterial, anti-inflammatory, controlled drug release profile, and hemostatic properties [514, 515]. PCL is a synthetic polymer frequently used with collagen for skin regeneration. The presence of collagen within PCL/collagen scaffolds facilitated cell migration through the activation of integrin-β1 [52]. In addition, the differentiation ability of keratinocytes can be promoted by immobilising epidermal growth factor on PCL/collagen fibres [516]. Apart from PCL, collagen was also used with PLGA and it was found that the presence of collagen contributed to skin fibroblast distribution enhancement as well as promoting the formation of an epithelium in 2–4 weeks [51, 517]. There have been many reports incorporating diverse organic/inorganic materials which have strengthened the properties of collagen scaffolds in the scientific research. Nonetheless, since July 2015, only a limited number of polymers including collagen, hyaluronic acid, PLLA, hyaluronic acid and non-biodegradable polymethylmethacrylate (PMMA) beads have been granted FDA approval as dermal fillers [468]. Hence, further research should be carried out to obtain the clinical requirements for therapeutic applications.

2.8 Summary

The injury of organ and/or tissues has an important impact on life quality and involves large social and economic costs. Using traditional medical and surgical treatments is constrained due to limitations including donor shortage, immunological problems and the risk of infection. In this context, tissue engineering has emerged to regenerate required tissues or organs for patients. With the evolution of scaffold design for tissue engineering, electrospinning has attracted enormous attention because of its ability to generate fibrous scaffolds resembling natural ECMs in tissue. Electrospinning is considered to be an inexpensive, versatile, scalable and straightforward technique, which offers continuous ultrafine fibre manufacturing from either synthetic or natural polymers. Physical, mechanical, and chemical properties of scaffold constructs produced by electrospinning processes can be modified to generate a variety of different matrices. Furthermore, the ability of electrospinning techniques to combine different types of materials leads to an unlimited material range of scaffolds with distinctive features [4, 518].

Amongst a variety of materials tested, SF has established a good reputation in various tissue engineering applications. SF-derived scaffolds have distinctive properties, such as good biocompatibility, biodegradability, minimal inflammatory response and ease of processability. Many studies have reported that electrospun SF scaffolds not only support cell adhesion, proliferation, and differentiation *in vitro*, but also enhance tissue repair *in vivo* [11, 217, 519]. However, slow degradation, and relatively weak mechanical properties are disadvantageous for clinical applications. In addition, when the SF nanofibre component is alone, it is difficult to regulate cell proliferation and differentiation. The previous findings demonstrate that SF properties could be improved by blending with other polymers [228, 290, 519]. Despite the significant progress made, the SF based scaffold application could be tremendously expanded by developing new SF composites and accordingly enhance specific properties of SF scaffolds for certain applications.

In addition, to date, great endeavour has been taken in creating scaffolds mimicking ECM. However, most approaches focus on incorporating one component of the ECM to polymeric scaffolds as opposed to the entire network. ECM-polymer composite scaffolds harness the naturally-occurring bioactive signals from a selected cell source

to improve the biological responses of subsequently seeded cell populations. For example, scaffolds containing human osteoblast-derived ECM have been demonstrated to promoted osteogenic differentiation of human embryonic stem cells [520, 521]. There is an unmet demand to develop ECM-polymer composite scaffolds and investigate their performance particularly for tissue engineering applications.

Chapter III: Materials and Methods

3.1 Silk Fibroin Extraction

Bombyx mori silk fibroin (SF, The Yarn Tree, Greenville, SC, USA) was extracted from silk cocoons, as described by Rockwood *et al*. [213]. 5 g of cocoons were cut and worms discarded. Cocoon pieces were boiled in a 0.02 M sodium carbonate (Na_2CO_3, ≥99%, Sigma Aldrich, NSW, Australia) aqueous solution for 30 min, and subsequently rinsed 3 times with ultrapure water for 20 min and subjected to gentle stirring on a stir plate to remove sericin proteins. The extracted SF was then dried at room temperature (RT) for 24 h, and dissolved in 9.3 M lithium bromide (LiBr, ≥99.9%, Sigma) solution at 60 °C. This solution was dialysed against ultrapure water at RT for 48 h using a dialysis membrane (MWCO 12400 Da, Sigma), followed by filtration (Pore size: 0.22 µm, Thermo Fisher Scientific). The solution was freeze-dried to produce regenerated SF. The preparation process is illustrated in Figure 3.1.

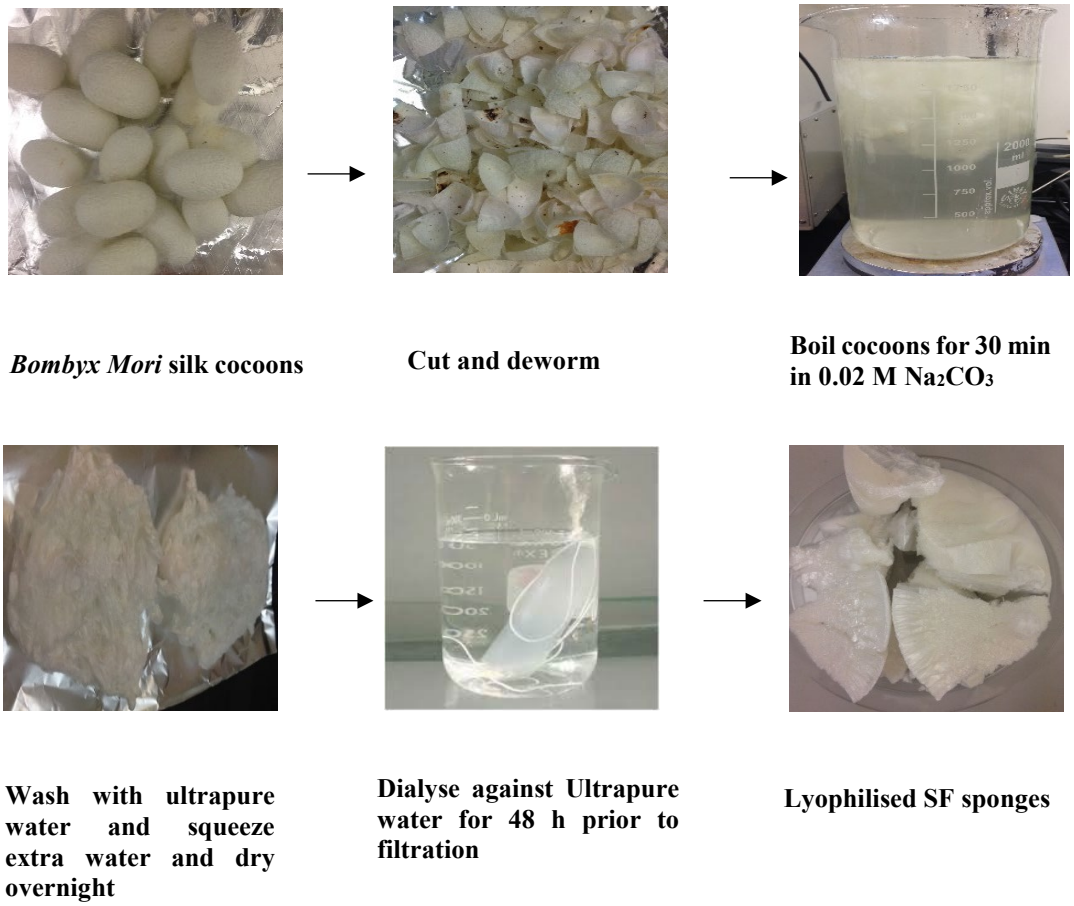

Figure 3.1 The preparation process of SF.

3.2 Electrospinning

3.2.1 SF/HNT Electrospinning

Halloysite nanotubes (HNTs), donated by Imerys Tableware Asia Ltd, New Zealand, contain 49.5% SiO_2, 35.5% Al_2O_3, 0.29% Fe_2O_3 and 0.09% TiO_2, with traces of CaO, MgO, K_2O and Na_2O. HNTs possess outer diameters in the range of 40-120 nm and lumen diameters of 15-100 nm. The HNT lengths vary ranging from 300–1500 nm. HNTs were first sieved through a 125 μm mesh to remove granules[522, 523]. HNTs were dried at 80 °C under vacuum for 12 h, and then HNTs at different loadings relative to SF (1, 3, 5 and 7 w/w%) were dispersed in formic acid (≥98%, Sigma) using a IKA T 25 digital ULTRA-TURRAX® dispenser (IKA, Staufen, Germany) with a rotor speed of 7000 rpm for 30 min prior to the ultrasonication (model ELMA Ti-H-5, Elma Schmidbauer GmbH, Singen Germany) at 25 kHz with a sweep mode and 100 % power intensity at 40 °C for 1 h. The lyophilised SF at the concentration of 13 w/v% was added to the HNT/formic acid solution and stirred for 3 h. The NaBond NEU commercial nanofibre electrospinning unit (NaBond Technologies Co., Ltd, Shenzhen, China) was used for electrospinning. Prepared SF/HNT solutions were loaded into a plastic syringe using an 18 gauge stainless steel needle at the tip. A voltage of 16 kV was applied to the blunt needle (inner diameter of 0.6 mm) and the flow rate was set at 0.3 mL/h using a syringe pump. The fibres were formed on a plate collector covered by aluminium foil with a needle-to-collector distance of 13 cm. The electrospinning process was carried out at RT and the setup is illustrated in Figure 3.2.

3.2.1.1 Post Treatment of Electrospun SF/HNT Scaffolds

To improve the stability of nanofibres, they were immersed in methanol (≥99.9%, Sigma Aldrich) for 15 min and then left in the fume hood overnight to dry.

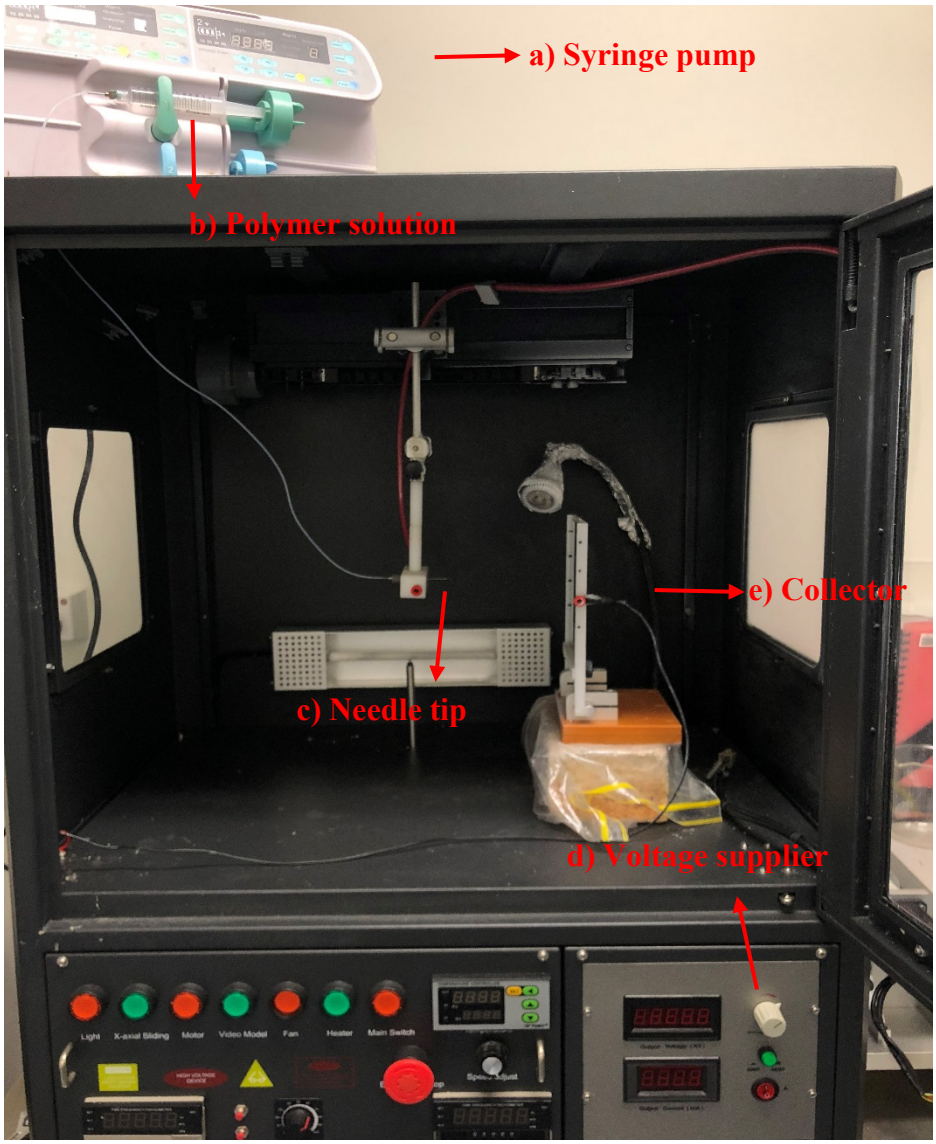

Figure 3.2 The electrospinning setup, (a) syringe pump, (b) polymer solution, (c) needle tip, (d) voltage supplier, (e) collector.

3.2.2 SF/gelatin Electrospinning

To prepare SF/gelatin blended solution, lyophilised SF were dissolved in formic acid and stirred for 1h. Subsequently, type A gelatin from porcine skin (300 bloom, Sigma) was added to the solution at the weight ratios given below, and this mixture was stirred for 2 h to obtain a homogeneous solution. The final concentration of spinning solution

was controlled at 13 w/v% and various blending ratios of SF/ gelatin by weight (*i.e.,* 100/0, 90/10 and 70/30) were prepared. For the electrospinning process, the prepared SF/ gelatin solution was placed in a 10 mL syringe equipped with a blunt needle (inner diameter: 0.6 mm). The flow rate was set at 0.3 mL/h using a syringe pump. The needle was connected with a high voltage power supplier set at 16 kV to stretch the droplets of the injected solution. The electrospun nanofibres were collected on a plate collector with a needle-to-collector distance of 13 cm. The collected fibre mats were left overnight under fume hood to dry. The electrospinning process was carried out at ambient conditions.

Gelatin nanofibres were also manufactured by dissolving gelatin in formic acid at solution concentration of 13 w/v% and similar electrospinning parameter as a benchmark.

3.2.2.1 Post Treatment of Electrospun SF/gelatin Scaffolds

To stabilise and control the degradation rate of the fabricated SF/gelatin nanofibres, three different crosslinking procedures were followed as below:

1. Methanol treatment: air dried SF/gelatin scaffolds were treated with methanol (99.9%, Sigma) for 15 min and left under fume cabinet to dry.

2. D,L-glyceraldehyde (GC) treatment: based on a material-processing protocol mentioned by Sisson *et al.*[417] SF/gelatin scaffolds were immersed in the following solution for 19 h at room temperature (RT): 0.5% w/w GC (≥90%), Sigma Aldrich) dissolved in 70% (v/v) ethanol/water.

3. Glutaraldehyde (GTA) treatment: 10 mL of aqueous GTA solution (20% v/v, Sigma Aldrich) in a petri dish was placed in a sealed desiccator. SF/ gelatin nanofibres together with a supporting aluminium foil were exposed to GTA vapour for 6 h at RT. Afterwards, crosslinked nanofibre scaffolds were immersed in a 0.1 M glycine (Sigma Aldrich) aqueous solution for 1 h to block unreacted aldehyde groups.

3.3 Material Characterisation

3.3.1 Viscosity Measurement

The viscosities of prepared solutions for electrospinning were measured using Modular Advanced Rheometer System (Haake MARS, Thermo Electron Corp., Germany) and associated data were extracted via HAAKE RheoWin Data Manager Software. The temperatures of the cone and plate were kept constant at 25 °C and shear rate was linearly increased from 10 to 100 s^{-1} at 25 °C. The test was conducted on three replicates from each group of solutions.

3.3.2 Scanning Electron Microscopy (SEM)

Morphological characterisation of electrospun nanofibres was investigated with scanning electron microscope (ZEISS EVO 40XVP, Carl Zeiss, Oberkochen, Germany), depicted in Figure 3.3 at an accelerating voltage of 15 kV. Nanofibre mat samples were mounted on SEM stubs with carbon tape and sputter coated with platinum. The average fibre diameter was determined by randomly measuring 100 fibres (*i.e.,* N=100) from each SEM image using ImageJ software, in expression of mean ± standard deviation (SD).

To identify the embedded HNT on the surfaces of SF nanofibres, elemental analysis was performed using an Oxford Instruments energy-dispersive X-ray spectrometer (EDS) at the accelerating voltage of 10 kV. The analysis of X-ray spectra was performed using Inca software (Oxford Instruments, Abingdon, UK). The relevant test was conducted on two replicates from each group of scaffolds.

Figure 3.3 SEM instrument.

3.3.3 Fourier Transform Infrared Spectroscopy (FTIR)

In order to observe structural and conformational changes of the proteins within the scaffolds, chemical characterisation was carried out by Spectrum 100 Optica FTIR Spectrometer (PerkinElmer Inc., Waltham, MA, USA). FTIR spectra were acquired in a transmission mode with the resolution of 4 cm^{-1} and a wave number range of 400–4000 cm^{-1} using an attenuated total reflectance (ATR) method [524]. Test was conducted on three replicates from each group of scaffolds.

3.3.4 X-ray Diffraction Analysis

The X-ray diffraction was conducted by an X-ray diffractometer D8 Advance (Bruker AXS, Germany), with a Cu Kα radiation source (wavelength λ= 0.1541 nm) at 40 kV and 40 mA using a LynxEye detector (Figure 3.4). XRD analysis was carried out on two replicates from each group of scaffolds. All XRD samples were scanned from the

diffraction angle 2θ = 5–40° at a scan rate of 0.015°/s. The d-spacing (d) for a specific scattering angle (θ) was determined from Bragg's law as follows:

$$n\lambda = 2dsin\theta \quad (1)$$

where n is an integer.

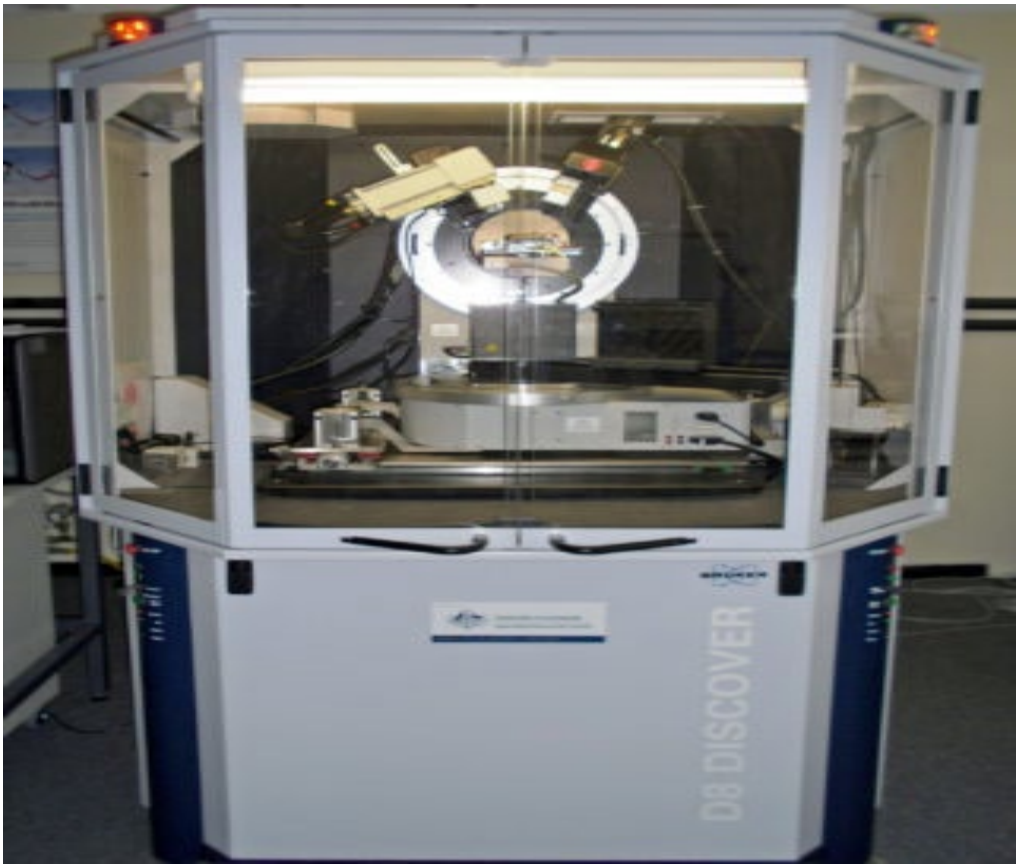

Figure 3.4 XRD instrument.

3.3.5 Contact Angle and Water Uptake Capacity

Fibre mat hydrophilicity was evaluated by measuring the water contact angles of the scaffolds using a CAM101 goniometer (KSV Instruments Ltd, Finland). The water droplet, approximately 5 µl, was deposited on scaffold surfaces and images of the droplet were automatically taken as a function of time. The contact angle was calculated by CASTTM2.0 software based on captured images. The average of 5 separate samples was calculated for the contact angle data.

To determine the water uptake capacity of scaffolds, samples were weighed and subsequently immersed in distilled water at RT for 24 h. Before measuring the weights

of wet samples, the excess of water on the surfaces was removed with filter paper. The water uptake capacity of scaffolds can be calculated as follows:

$$water\ uptake\ (\%) = \left(\frac{W - W_0}{W_0}\right) \times 100\% \quad (2)$$

Where W and W_0 represent the weights of the sample before and after soaking in water, respectively. The average of 5 samples was calculated.

3.3.6 Porosity Measurements

The Brunauer−Emmet−Teller (BET) surface area, pore volume, and pore width of SF/HNT scaffolds were characterised using a Tristar 3000 (Micromeritics, Norcross, GA, USA). The pore volume and the pore-size were computed by applying the Barrett–Joyner–Halenda (BJH) method in the relative pressure (P/P_0) range of 0.01 to 0.99. The samples were degassed in a vacuum at 40 °C overnight before the tests. Two samples for each material batch were used and representative data were reported.

The porosities of SF/gelatin scaffolds were determined using their apparent density ($\rho_{apparent}$) and bulk density (ρ_{bulk}), as shown in Eq. (3). In between, $\rho_{apparent}$ in the unit of g/cm^3 was estimated on the basis of scaffold mass $m_{scaffold}$ (g), scaffold thickness t (cm) and scaffold area A (cm^2) according to Eq. (4). As for the parameter of ρ_{bulk}, bulk densities of SF and gelatin (*i.e.,* ρ_{SF} and $\rho_{gelatin}$) were referred to as 1.25 and 1.35 g/cm^3, respectively [525, 526] in order to determine corresponding bulk density of SF/gelatin fibre mats. ρ_{bulk} was calculated in Eq. (5) where $w_{gelatin}$ and w_{SF} denoted the mass fractions of gelatin and SF, respectively. Five samples for each material batch were used with finally reported average data and standard deviations.

$$\text{Porosity} = \left(1 - \left[\frac{\rho_{apparent}}{\rho_{bulk}}\right]\right) \times 100\% \quad (3)$$

$$\rho_{apparent} = \frac{m_{scaffold}}{\text{t} \times \text{A}} \quad (4)$$

$$\frac{1}{\rho_{bulk}} = \frac{w_{gelatin}}{\rho_{gelatin}} + \frac{w_{SF}}{\rho_{SF}} \quad (5)$$

The thickness of scaffolds (t) was measured by using a micrometer at four different positions of fibre mats for obtaining their average measurements.

3.3.7 Degree of Crosslinking

The degree of crosslinking of SF/gelatin scaffolds were determined using 2,4,6-trinitro-benzene-sulfonic acid (TNBS, 5 % (w/v) in H_2O, Sigma) assay, as described by Bubnis et al.[527] Briefly, 1-3 mg of each scaffold was immersed in 1 ml of a 4% (w/v) $NaHCO_3$ (≥99.5%, Sigma) solution and 1 ml of a freshly prepared solution of 0.5% (w/v) TNBS. After the incubation for 2 h at 40 °C, 3 mL of 6 M hydrochloric acid (HCl, 37%, Sigma) was added and the solution was heated at 60 °C for 90 min. After cooling down to room temperature, the resulting solution was diluted with 5 ml of deionised water, and absorbance was measured at 345 nm with a UV/vis spectrometer (BioPhotometer plus, Eppendorf, Hamburg, Germany). The degree of crosslinking was calculated as follows:

$$\text{Degree of crosslinking}\ (\%) = \left(\frac{A_0 - A_C}{A_0}\right) \times 100\% \quad (6)$$

where A_0 and A_C are the absorbance of SF/gelatin nanofiber mats before and after crosslinking, respectively. The experiment was performed in triplicate under the same conditions.

3.3.8 Tensile Tests

Mechanical properties of the scaffolds were obtained from stress−strain curves using a Lloyds Universal Testing Machine (Lloyds EZ50, Ametek-Lloyd Instruments Inc., Fareham, UK) at the crosshead speed of 10 mm/min with the ambient temperature of 25 °C and humidity of 65%. Rectangular scaffold specimens with a dimension of 10 mm × 30 mm were prepared according to the method reported in the previous literature [528]. First, a cardboard frame was cut in a rectangular shape (10 × 50 mm^2). Then the scaffolds were cut in dimensions of 10 mm (width) × 30 mm (gauge length), glued onto the top and bottom areas of the frame, and further mounted on the tester. Subsequently, the frame edges of cardboard were cut prior to the tests. The specimen thickness was measured using a micrometer at five different positions of the scaffolds to record the average thickness in range of 200–530 μm. Sample preparation and tensile testing procedure are demonstrated in Figure 3.5. Ten samples from each material batch were used for measurements.

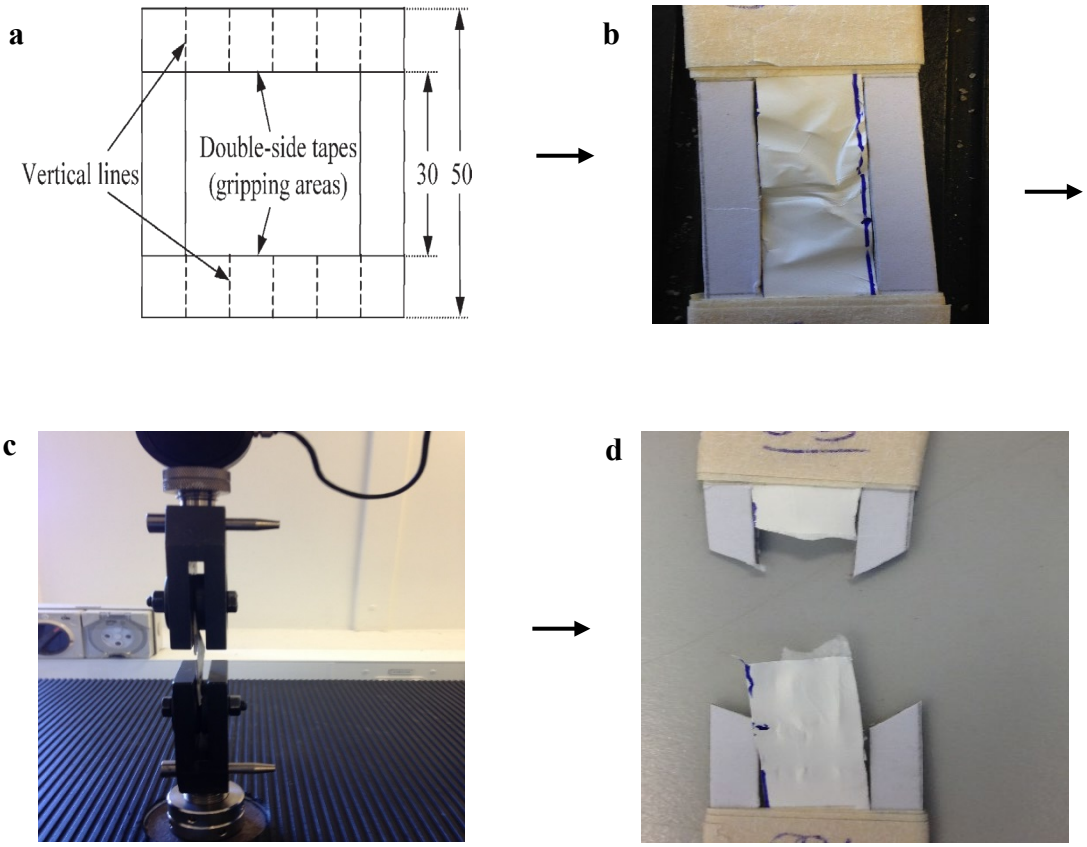

Figure 3.5 Tensile tests of scaffolds, a) paper template for preparing samples [396], b) a typical tensile test sample, c) tensile test operation and d) tested sample after fracture.

3.3.9 Thermal Analysis

Thermal properties of nanofibres were examined using a Mettler-Toledo TGA/DSC 1 STARe System thermogravimetric analyser and differential scanning calorimeter (Schwerzenbach, Switzerland) along with STARe software, as shown in Figure 3.6. Approximately 8 mg from each scaffold was weighed into alumina crucibles and heated from 30 °C to 800 °C at a rate of 10 °C /min under the flow of argon gas at flow rate of 20 mL/min. Thermal analysis were conducted on two replicates from each group of scaffolds and representative data were reported.

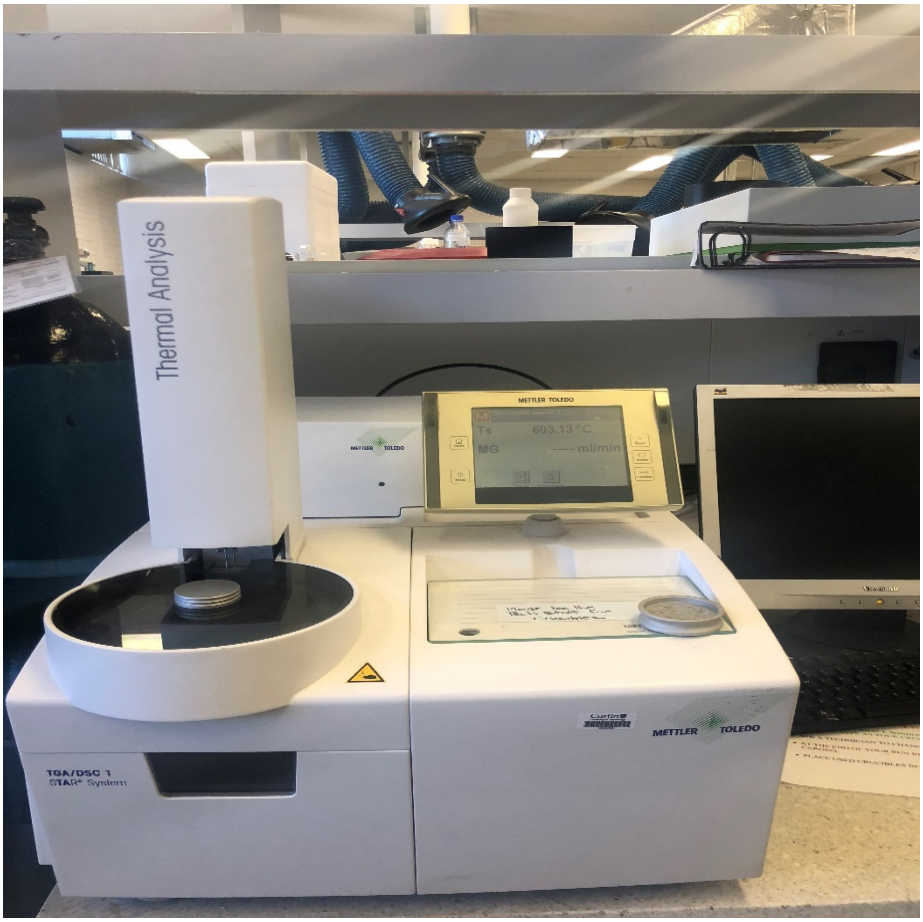

Figure 3.6 TGA/DSC instrument.

3.4 Biological Characterisation: Tissue Culture and Cell Based Assays

3.4.1 Cell Lines

3T3 Murine Fibroblasts

3T3 cells were purchased from European Collection of Cell Cultures, Porton Down,UK.

Primary human dermal fibroblasts (HDFs)

Primary human dermal fibroblasts (PCS-2-1-012) (HDFs) were purchased from American Type culture collection (ATCC, Manassas, VA).

C2C12 Murine Myoblast

C2C12 cell line was obtained from the American Type Culture Collection (ATCC, Manassas, VA, USA).

Human Neonatal Keratinocytes

Human neonatal keratinocytes were purchased from Thermo Fisher Scientific, Gibco.

3.4.2 Tissue Culture Media, Buffer and Supplements

Tissue Culture Media

Dulbecco's Minimum Essential Medium (DMEM), DMED (phenol red free), RPMI, Defined Keratinocyte Serum Free Medium (DKSFM), HEPES (1M), L-glutamine (200Mm), Sodium Pyruvate (100mM) and Human Serum were purchased from Gibco, Life Technologies (Carlsbad, CA). Foetal Bovine Serum (FBS) was supplied by Serana Europe GmBH. (Pessin, Germany). Complete media comprised the various base media (DMEM, RPMI, DMEM (phenol red free)) supplemented with 10 mM HEPES, 1 mM sodium pyruvate, 2 mM glutamine and 10% FBS.

0.05M Ethylenediaminetetraacetic acid (EDTA) Stock Solution

EDTA (Spectrum Chemical) was dissolved in 40 mL of doubled distilled water (ddH_2O) at the final concentration of 0.05M. Then, 1M NaOH was added to dissolve EDTA and the pH level was adjusted to 7.4. The volume was made up to 50 mL using ddH_2O.

3.4.3 Cell Counting

Cells 3T3 and C2C12, were counted using the Z™ Series COULTER COUNTER® (Beckmann Coulter, Indianapolis, IN). Harvested cells (100 µL or 200 µL) were diluted in 10 mL isotonic saline and 500 µL of this sample was counted by the instrument in which gates were set to exclude both dead cells and cellular debris from the analysis, meaning that the cell concentration was determined only for live cells. The actual cell concentration was calculated by taking into consideration the dilution factor.

Keratinocytes and HDFs cells were counted by using a hemocytometer. 10 µL of resuspended cells were transferred into a microcentrifuge tube, mixed with 10 µL of 0.4% trypan blue (Sigma) and then 10 µL of cell suspension was applied into the hemocytometer. Live, unstained cells were counted from all four corners and the middle of the hemocytometer grid (Figure 3.7; number 1-5). The number of viable cells/mL was calculated as follows:

$$\text{Cells/mL} = \text{Total Cell Count} \div 5 \times 10^4 \times 2 \text{ fold dilution} \quad (6)$$

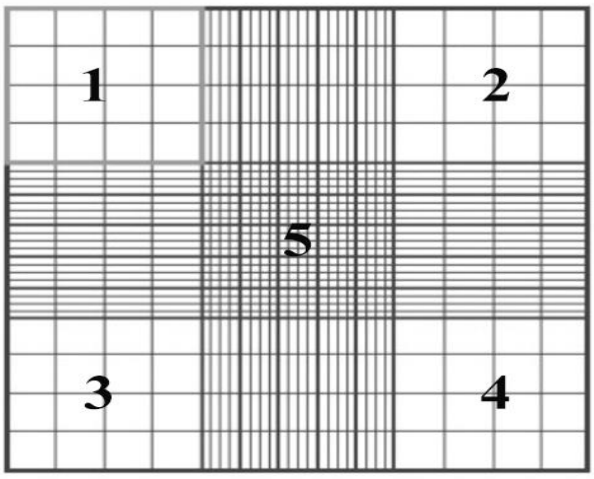

Figure 3.7 A representative diagram of a haemacytometer indicating one corner of the square that should be used for counting (Adapted from Abcam website).

3.4.4 Freezing and Thawing Cell Lines

Freezing Fibroblasts and Myoblasts

Cells (HDFs, 3T3 and C2C12) were harvested and resuspended in complete media (DMEM complete media for HDFs and C2C12 cells and RPMI complete media for

3T3 cells), which was followed by centrifugation at 1100 rpm for 5 min. Without disturbing the cells pellet, media was removed and the cell pellet was resuspended in freezing medium (50% of complete tissue culture media, 40% FBS and 10% DMSO). The cell concentration of 50×10^4 cells/mL was transferred into cryogenic vials and placed in a "Mr Frosty" freezing chamber (Nalgene Labware, Nalge Nunc International, Rochester, NY, USA). The cryogenic vials were placed in a -80 °C freezer, and then transferred to liquid nitrogen storage.

Freezing Keratinocytes

Conditioned DKSFM was recovered from keratinocyte cultures and filtered using a 0.22 µm syringe filter unit. Then freezing media A (*i.e.,* 50% conditioned DKSFM/ 50% fresh DKSFM) and freezing media B (*i.e.,* 40% spent DKSFM/ 40% fresh DKSFM/ 20% DMSO) were prepared. The keratinocytes were harvested and resuspended in PBS/4% human serum/1mg/mL soybean trypsin inhibitor (Gibco, Thermo Fisher Scientific), counted and centrifugation at 1,100 RPM for 5 minutes. Without disturbing the pellet, the media was gently discarded. The cell pellet was resuspended in freezing media A, then 5×10^4 cells were mixed with freezing media B and transferred into cryovials. The cryovials were placed first in a "Mr Frosty" freezing chamber (Nalgene Labware, Nalge Nunc International, Rochester, NY) and then in a -80 °C freezer overnight followed by transferring to liquid nitrogen storage.

Thawing Fibroblasts and Myoblasts

Pre-warmed complete media (DMEM complete medium for HDFs and C2C12 cells and RPMI complete medium for 3T3 cells) were added into a 25 cm^2 tissue culture (T25) flask. Frozen cells were defrosted by placing in a 37 °C water bath and then the warmed media was added dropwise to the thawed cells and mixed. When the cells had been diluted by a ratio of 1:3 (cell solution: media), this mixture was placed into a 25 cm^2 tissue culture flask and total volume in the flask slowly increased to 5 mL by the addition of the pre-warmed media. The media was changed after the cells adhered (~ 60 min).

Thawing Keratinocytes

The 25 cm^2 tissue culture flask was coated with 3 µg/cm^2 of type I collagen (diluted in PBS), for 2 h at 37 °C. Cells were quickly thawed in a 37 °C water bath and diluted to a ratio of 1:3 (cell solution: media) by adding warmed DKSFM media drop wise to

the cells. The diluted cell solution was then transferred into the T25 tissue culture flask, and further warm DKSFM was slowly added to make up 5 mL final volume. After the cells attached (~3-4 hours), the media was replaced.

3.4.5 Cell Culture and Maintenance

3T3 Murine Fibroblasts

3T3 fibroblast cells were maintained in complete RPMI medium in a humidified 37 °C incubator at 5% CO_2. When the cells reached 70-80% confluency, they were subcultured. Briefly the media was removed and the cells were rinsed with 5 mL PBS. Then 500 µL trypsin-EDTA (0.05%, Life Technologies) was added to the flask and incubated at 37 °C for 5 min to detach cells. Cells were suspended in 3 mL of RPMI complete media and then counted. Cells were seeded at 15 x 10^4 density per T25 flask for maintenance. Experiments were conducted with cells passaged less than 25 times.

HDFs Fibroblasts

HDFs fibroblast cells were cultured in a complete DMEM and incubated in a humidified 37 °C incubator at 5% CO_2. Cells were subcultured when they reached 80-90% confluency by discarding medium from the flask and rinsing with 5 mL PBS. Then 500 µL of 0.05% trypsin-EDTA (Life Technologies) was added and incubated for 5 min at 37 °C. Cells were resuspended in 2.5 mL complete DMEM and then were counted. Cells were seeded at 25 × 10^4 cells per T25 flask for maintenance, and were used at less than 16 passages for all experiments.

C2C12 Murine Myoblasts

C2C12 myoblasts were maintained in a complete DMEM in an incubator at 37 °C with 5% CO_2. Cells were subcultured at 60-70% confluence and used for experiments with the passage less than 20. To subculture the cells, the medium was discarded and the growth surface washed with 5 mL PBS. Cells were dissociated from the flask by incubating with 0.05% trypsin-EDTA at 37 °C for 5 min, and then suspended in 3 mL complete DMEM and counted. Cells were seeded at a density of 4 × 10^4 cells per T25 flask for maintenance.

Keratinocytes

Keratinocytes were maintained in DKSFM and housed in a humidified 37 °C incubator equilibrated at 5 % CO_2. Keratinocytes were passaged when they reached 80%

confluence and cells below passage 4 or 5 were used for all experiments. Briefly, the medium was removed from the T25 flask and cells were washed gently with 5 mL PBS before 5 mL of 0.5mM EDTA/PBS was added to the flask and incubated at RT for 5 min. The EDTA/PBS solution was then discarded and replaced with 500 µL of 0.05% trypsin-EDTA and incubated for 5 min at 37 °C. Cells were resuspended in 5 mL of PBS/4% human serum/1mg/mL soybean trypsin inhibitor and were then transferred to a centrifuge tube to be pelleted by the centrifugation at 1100 rpm for 5 min. Keratinocytes were resuspended in DKSFM and counted using a haemocytometer followed by being seeded at density of 20×10^4 cells per T25 flask for maintenance.

3.4.6 Cell Morphology

3T3 fibroblast cell morphology on SF/HNT scaffolds was observed using SEM and fluorescent imaging. The procedure for sample preparation in relation to each technique is summarised in the following subsections.

3.4.6.1 Solutions, Buffers & Cell seeding

HEPES Buffered Saline (HBS)

This buffer comprised 150 mM NaCl (Sigma Aldrich), 10 mM HEPES, 1 mM $MgCl_2$ (Sigma Aldrich) and 1 mM $CaCl_2$ (Sigma Aldrich) and was stored at 4 °C.

4% (w/v) Paraformaldehyde

2.4 g of paraformaldehyde (Sigma Aldrich) was added to 50 mL HBS and heated at 55 °C until the solution was clear. The PH was adjusted to 7.4 with 1M NaOH and the volume made up to 60 mL by the addition of HBS. The solution was filtered and stored at 4 °C and used within a month.

Blocking Solution

Blocking solution consisted of HBS containing BSA (1% (v/v), Hyclone) and 5% (v/v) of FBS.

Scaffold Preparation

Scaffolds (1×1 cm^2) were sterilised by ultra violet radiation (UV) for 40 min on each side, and then incubated at 37 °C in complete DMEM (phenol red free) media.

Cell Seeding

3T3 cells were harvested, pelleted and then resuspended in DMEM (phenol red free) medium, at a concentration of 16×10^4 cells/mL. Scaffolds prepared as indicated above, were wiped with autoclaved cotton buds and transferred to a 6-well tissue culture plate (NUNC). Two replicate scaffolds were used from each group of nanocomposites. 500 µL of the cell suspension (8×10^4 cells) was added to the scaffolds and incubated at 37 °C for 30 min. Then 3 mL DMEM (phenol red free) medium was added to each well. The culture medium was changed every 48 h. Scaffolds without cells were incubated in medium as negative controls.

3.4.6.2 Scanning Electron Microscopy

To observe the 3T3 cell morphology on day 1 and day 3 culture, Field emission scanning electron microscope (FE-SEM, Zeiss NEON 40 EsB Cross Beam) at the accelerating voltage of 5 kV was used. Scaffolds were rinsed twice with HBS and fixed with 4% paraformaldehyde in HBS for 15 min at RT. They were washed twice with HBS before being blocked for 1 h at RT with blocking solution. Scaffolds were transferred to a 12-well plate and chemically dehydrated via serial dilutions in ethanol (100%, 90%, 70%, 30% and 10%, Sigma) for 10 min each. Then they were dried in a freeze dryer and coated with platinum for imaging.

3.4.6.3 Immunofluorescence Staining

On day 1 and day 3 of cell culture, scaffolds were rinsed twice with HBS, fixed with 4% paraformaldehyde for 15 min and washed HBS followed by permeabilisation with cold 0.1% Triton X-100 (Sigma)/HBS for 3 min. Then, cells were rinsed twice with HBS before being blocked in blocking solution (1 h). Blocking solution was removed, and scaffolds were stained for Filamentous actin (F-actin) by incubating in phalloidin-Alexa Fluor® 488 (1:200 in blocking solution, Thermo Fisher Scientific) for 1 h at RT. Afterwards, scaffolds were rinsed 3 times with HBS (5 min each) before being incubated with 500 µL DAPI (1:2000 in HBS) for 10 min at RT. The µscaffold were rinsed 3 times with 1 mL HBS as before and mounted on glass slides using 30 µL Vectashield antifade mounting medium (Vector Laboratories). Coverslips were put on the scaffolds and sealed with nail varnish. Images were captured using a Nikon A1+

Confocal Microscope (Nikon, Tokyo, Japan) in 3 different locations on each scaffold. To generate a three-dimensional (3D) image, Z-stack images were obtained and merged to generate a single image using NIS-Elements AR analysis software.

3.4.7 Proliferation Assay

Cell proliferation on SF/HNT scaffolds was examined using 3T3 fibroblasts and C2C12 myoblasts. On SF/gelatin and SF/Col I scaffolds 3T3 cell proliferation was studied. Sample preparation and protocols are described below.

Scaffold Preparation

Scaffolds of uniform size were obtained by using a 6 mm punch. These discs were sterilised and prepared as described above (Section 3.4.6.1).

3D Collagen Type I (Col I) Hydrogel

Rat tail type I collagen (Col I) (4 mg/ml) was purchased from Advanced Biomatrix (Carlsbad, CA). Circular moulds were prepared (diameter: 9 mm, height: 7 mm) and placed in 24-well tissue culture plates (NUNC) and sterilised with UV for 1h. Hydrogels of Col I were prepared according to the manufacturer's protocol. Briefly, the desired volume of collagen was calculated and one part of chilled neutralisation solution at 4 °C were mixed with 9 parts of Rat Tail Collagen. Then 120 µl of Col I mixture was added to each mould and incubated at 37 °C for 1h for the gel formation.

SF/Col I Scaffolds

SF methanol treated scaffolds were punched into 12 mm discs, placed in 24 well tissue culture plates and sterilised with UV for 40 min on each side. Then 25 µl of the Col I mixture (prepared as above) was added to the scaffolds and incubated at 37 °C for 1h for the gel formation.

Cell Seeding

3T3 and C2C12 cells were harvested using 0.05% trypsin-EDTA (500 µL) at 37 °C for 5 min and suspended in 5 mL complete DMEM (phenol red free) medium. Cells were washed, resuspended in 0.5 mL of complete DMEM (phenol red free) medium and counted. The 3T3 and C2C12 cells were made up to concentrations of 40×10^4 and 22×10^4 cells/mL, respectively. The prepared scaffolds were wiped with autoclaved cotton buds to remove excess medium, and transferred to 12-well plates. The cells were seeded to each scaffold by adding 5 µL cell per scaffold (6 replicates)

and incubated at 37 °C for 30 min before adding 2 mL DMEM (phenol red free). Scaffolds (4 replicates) without cells (background controls) were incubated in medium. Culture medium was changed every 48 h.

3.4.7.1 Assay Protocol

Cell growth was measured in 96-well tissue culture black plates (NUNC) using CellTiter-Blue® (Promega). As the different cell types grew at different rates, cell growth was analysed at different times: day 1 and day 3 for 3T3 cells, and day 1and day 2 for C2C12 cells. At the specified times, scaffolds were transferred to a 96-well black plate and 100 µL DMEM (phenol red free) medium was added to each scaffold, followed by the addition of 20 µL CellTiter-Blue reagent. To generate a standard curve for calculating cell numbers, cells of a known number (titrated from 20×10^4- 3×10^3 cells/well) were added to the black plate and labelled with 20 µL CellTiter-Blue. The plates were incubated in a humidified 37 °C incubator equilibrated at 5 % CO_2 for 4 h before measuring the fluorescence intensity using EnSpire Multimode plate reader (Perkin Elmer, Waltham, MA).

3.4.8 Differentiation Assay

The differentiation of C2C12 cells on SF/HNT scaffolds was investigated as described below.

Differentiation Medium

Differentiation medium consisted of DMEM (phenol red free) medium containing 10 mM HEPES, 1 mM sodium pyruvate, 2 mM glutamine and 2% Horse serum (HS).

Blocking Solution

Blocking solution was HBS supplemented with BSA (1% (v/v), and 10% (v/v) goat serum.

Scaffold Preparation

Scaffolds (1×1 cm^2) were sterilised and prepared as described above (Section 3.4.6.1).

Cell Seeding

C2C12 myoblasts were harvested, pelleted and resuspended in DMEM (phenol red free) complete medium, at a concentration of 8×10^4 cells/mL. Two replicate scaffolds

were placed in a 6-well plate and 50 µL of cells (4×10^3) per scaffold were added and incubated for 30 min at 37 °C before the addition of 3 mL complete DMEM (phenol red free) medium. After 4 days, the medium was replaced with differentiation medium, which was changed every second day. After 4 days, differentiation of C2C12 was assessed by immunofluorescence staining.

Scaffolds were rinsed with HBS, fixed in 4% paraformaldehyde for 15 min, washed and the cells permeabilised using cold 0.1 % Triton X-100/PBS for 3 min at RT and washed with HBS. Scaffolds were blocked with blocking solution for 1 h at RT and then incubated for 1 h at RT with anti-slow muscle myosin antibody (Millipore) diluted 1:200 in blocking solution. Scaffolds were washed by soaking in HBS with two changes of buffer, and then incubated in 200 µL of secondary antibody (anti-mouse Alexa Flour 488, diluted 1:400 in blocking solution) for 1 h at RT. Samples were then washed by immersion in HBS before being incubated for 10 min in 500 µL DAPI (diluted 1:2000 in HBS) and washed as previously. Scaffolds were mounted on glass slides using 30 µL Vectashield antifade mounting medium and coverslips were sealed using nail varnish. Images were captured using a Nikon A1+ confocal microscope.

3.4.9 Fibroblast Derived Extracellular Matrix (ECM) Deposition

3.4.9.1 Media, Buffers and Solutions

Normal ECM Deposition Media (NDM)

This medium was DMEM (phenol red free) medium supplemented with 10% FBS, 10 m HEPES, 2 mM L glutamine, 1 mM sodium pyruvate and 30 µg/mL ascorbic acid (Wako Chemicals).

Macromolecular Crowding ECM Deposition Medium (MCDM)

To prepare this medium, 37.5 mg/mL Ficoll 70 (Sigma) and 25 mg/mL Ficoll 400 (Amersham) were dissolved in DMEM (phenol red free) medium and the solution was filtered before the addition of the supplementary reagents: 10 mM HEPES, 2 mM L glutamine, 1 mM sodium pyruvate, 30 µg/mL ascorbic acid and 10% FBS.

Phosphate Buffered Saline (PBS) & Blocking solution

1 PBS tablet (Ameresco, Ohio, USA) was dissolved in 100 mL of ddH_2O. Blocking solution was PBS containing BSA (1% (v/v) and 10% (v/v) goat serum.

1M Tris Buffer (pH 7/8) Stock Solution

12.11 g of Tris-base (Sigma) was dissolved in 90 mL of ddH_2O and to adjust the PH (7 or 8), 1M HCL was used. The final volume was adjusted to 100 mL with adding ddH_2O.

5% Sodium Deoxycholate Stock Solution

To prepare 5% (w/v) sodium deoxycholate, 1 g of sodium deoxycholate (Sigma) was dissolved in 20 mL ddH_2O and filterd with a 0.22 µm syringe filter and stored at RT.

DNase I Buffer and Working Solution

The 10x DNase I Reaction was 100 mM Tris Buffer (pH 7) containing 25 mM $MgCl_2$ (Sigma) and 5 mM $CaCl_2$ (Sigma). This was filtered with a 0.22 µm syringe filter and stored at -20 °C. DNase I working solution consisted of 0.02 mg/mL DNase I (Amresco), 1X DNase I reaction buffer, and 0.16x EDTA-Free protease inhibitor (Roche). Fresh solution was made up before use.

5x Phospholipase A_2 (PLA_2) Reaction Buffer and Working Solution

The buffer was 250 mM Tris Buffer (pH 7), 5mM $MgCl_2$ (Sigma) and 5mM $CaCl_2$ (Sigma). It was filtered with a 0.22 µm syringe filter and stored at -20 °C. The PLA_2 working solution contained 20 U/mL of PLA_2 (Sigma Aldrich), 1x PLA_2 reaction buffer, 0.5% sodium deoxycholate (Sigma) and 1x EDTA-Free protease inhibitor (Roche). Fresh solution was made up for each use.

3.4.9.2 Deposition of Fibroblast Derived Extracellular Matrix on Scaffolds

Scaffold Preparation

Scaffolds (four replicates) were punched into 6 mm discs, sterilised with UV, as described and incubated in either MCDM or NDM media for 1h.

Fibroblast Cell Seeding

3T3 and HDFs cells were harvested, pelleted, and resuspended in either MCDM or NDM media at densities of 50×10^4 cells/mL and 200×10^4 cells/mL, respectively. Scaffolds were placed in 24-well plates and 5 µL of either 3T3 or HDFs cell suspensions applied to them and incubated at 37 °C for 30 min to allow cell adhesion. Then 1 mL of either MCDM or NDM media was gently added to each well. Scaffolds

were incubated for 7 days at 37 °C in an incubator equilibrated at 5% CO_2 and the medium was changed every two days.

Decellularisation of Fibroblast-Derived Matrix

At day 7 of cell culture, medium was removed and scaffolds were rinsed twice with PBS before being incubated in PLA_2 working solution at 37 °C for 30 min. Samples were then washed twice with PBS, and then incubated in DNase I working solution at 37 °C for 30 min. Thereafter, samples were washed three times with PBS.

3.4.9.3 Immunofluorescent Staining for Extracellular Matrix Deposition

Auto-fluorescence Check: Prior to immunofluorescent staining, the auto-fluorescent of SF/gelatin scaffolds were checked. Scaffolds (1 × 1 cm^2) were sterilised with UV for 40 min on each side followed by incubation at 37 °C in complete DMEM (phenol red free) medium for 24 h. Afterwards, samples were rinsed twice with PBS buffer, and then fixed with 4% paraformaldehyde for 15 min. After rinsing 3 times with PBS, they were incubated in a blocking solution of PBS/10% goat serum/1% BSA for 1 h at RT. Scaffolds were mounted onto a glass slide using 30 µl Vectashield antifade mounting medium (Vector Laboratories), coverslips were put on each scaffold and sealed with nail varnish. Images were captured with a Nikon A1+ Confocal Microscope.

Immunofluorescence Staining: Decellularised scaffolds were fixed with 4% paraformaldehyde in PBS for 15 min at RT. After washing with PBS, the ECM on the scaffolds were incubated in blocking solution for 1 h at RT. Blocking solution was removed and one replicate from each sample was incubated for 1 h at RT with primary antibody (recognising ECM proteins) *i.e.,* fibronectin, type I collagen, type IV Collagen (Abcam) or rabbit IgG control (Invitrogen). These antibodies were prepared in blocking solution. Samples were then washed three times with PBS and incubated for 1 h at RT with secondary antibody (Goat anti-rabbit Alexa Fluor® 647, Invitrogen) diluted in blocking solution (1:400). After washing three times with PBS (5 min/wash), scaffolds were mounted on glass slides as described and images were captured with a Nikon A1+ confocal microscope.

3.4.10 Immunofluorescence Staining of Keratinocytes Grown on Different Substrates

Immunofluorescent staining of keratinocytes was conducted on either pristine scaffolds (SF or SF/HNT 1 wt% treated with methanol) or scaffolds coated with either 3T3 or HDFs derived acellular matrix.

Scaffold Preparation

Scaffolds were punched into 6 mm discs and sterilised under UV for 40 min followed by incubation in DKSFM media for 1h. In case of scaffolds coated with fibroblast derived ECM, they were incubated in DKSFM media for 1 h. Moulds were prepared (diameter: 9 mm and height: 7 mm), and sterilised with UV for 40 min. Scaffolds were transferred to a 24-well plate and placed in the moulds.

Cell Seeding

Keratinocytes were harvested, pelleted and resuspended in DKSFM, at a concentration of 2.7×10^4 cells/mL. 150 µL of this cell suspension (0.4×10^4 cells) was added into the moulds containing scaffolds and incubated at a 37 °C or 3h. Then 1 mL DKSFM was added to each well and the culture medium changed every 48 h.

Immunofluorescence Staining

At day 4 or day 8 of cell culture, keratinocytes were fixed with 4% paraformaldehyde (in HBS) for 15 min and washed twice with HBS before being permeabilised with cold 0.1% Triton X-100 /HBS buffer for 3 min. Keratinocytes were washed twice with HBS and blocked for 1 h in blocking solution at RT. After discarding the blocking solution, one replicate from each sample was incubated in antibodies recognising keratin 10 (K10) and keratin 14 (K14) (these antibodies were provided by Prof. Birgit Lane, A*STAR Institute of Medical Biology, Singapore). In addition, an antibody recognising involucrin (Sigma) was also used. All antibodies were diluted in blocking solution and incubated on the cells for 1h at RT. Cells were washed 3 × 5 min with HBS and then incubated for 1 h at RT with the secondary antibody, Alexa488 anti-mouse IgG (Molecular Probes, ThermoFisher Scientific; OR, USA) prepared in blocking solution (1:400). Cells and scaffolds were washed three times with HBS (5 min each) and mounted on glass slides as described. Images were captured with a Nikon A1+ confocal microscope.

3.5 Statistical Analysis

Data were presented as means ± standard deviation (SD). Data analysis were performed by using GraphPad Prism 6 software (GraphPad, San Diego, CA, USA). Data were tested for normality of distribution. If the data were normally distributed, a parametric test was conducted; if not, a non-parametric test was conducted. P-value ($p < 0.05$) was considered statistically significant.

For normally distributed data, statistical comparisons were performed using one-way analysis of variance (ANOVA) followed by Tukey's posthoc test.

Non-normally distributed data were analysed using the Kruskal-Wallis one way analysis of variance followed by Dunn's multiple comparison test.

Chapter IV: Development and Characterisation of Silk/Halloysite (SF/HNT) Nanocomposites

4.1 Introduction

The ultimate goal of tissue engineering is to assist the repair of damaged or lost tissue by surgically inserting a fabricated scaffold *in vivo* at the site of tissue damage. Ideally these scaffolds should have functional properties resembling the native extracellular matrix (ECM) of that tissue. Hence, the ideal tissue scaffold should support cell adhesion, cell proliferation and the correct pattern of cell differentiation and so facilitate the formation of new, functional tissue [55, 529-531]. In this context electrospinning has been considered as having the potential to produce nanoscale fibrous structures that resemble the ECM [7, 177]. In order to satisfy the prerequisite specifications in regeneration of tissues via electrospinning, extensive research has been conducted on scaffolds fabricated by electrospinning with the result that methods have been developed to vary fibre morphology, to incorporate bioactive molecules into the fibres and to blend together different polymers into the fibres. These approaches have made promising advances towards achieving the desired mechanical and bioactive properties for scaffolds designed for different tissues [188, 532]. Apart from the fabrication method the other key element for creating desirable scaffolds, is choosing the appropriate starting material, or materials.

Bombyx. Mori silk fibroin (SF) is a natural protein polymer that is attractive for biomedical applications because of its excellent biocompatibility, adaptable biodegradability and good oxygen/water vapour permeability [11, 533, 534]. Recent advances in SF processing technology has enabled the preparation of SF in either aqueous or organic solutions such that it can be easily formed into various structures [228, 535]. It has been well documented that SF has potential to serve as a platform for supporting stem cell based tissue engineering in the generation of bone, cartilage, vascular or ligament-like tissues [228, 264, 536]. However conventional electrospun SF scaffolds usually demonstrate weak mechanical properties relative to natural tissues which limits their biomedical applications [221]. Two main strategies were employed to counter such limitations: either a post treatment method which usually involves water vapour annealing, or the inclusion of a reinforcing agent to prepare composite fibres [228, 537]. For instance embedding a low amount of MWCNTs into SF was found to be beneficial for improving tensile properties [222]. Blending SF with other polymers such as poly(L-lactic acid-co-ϵ-caprolactone) (P(LLA-CL)) [538], poly(e-caprolactone) (PCL) [539], poly ethylene oxide (PEO) [228], sericin [294], Polyhydroxybutyrate-co-

hydroxyvalerate [540] and collagen [541] has also enhanced mechanical properties of SF scaffolds.

Halloysite with a layered-tubular structure (HNT) is a double-layered aluminosilicate that naturally occurs as hollow tubular structures with sizes in the submicron range. It has gained considerable attention as a novel biomaterial because of its good biocompatibility and dispersion properties, low toxicity and the presence of active groups on the nanotube surfaces. HNT can be used as a drug delivery vehicle availing the controlled released of a drug. In addition, incorporation of HNT to polymers has the potential to substantially improve strength [296, 542, 543] and bioactivity [261] of nanocomposites [31, 544]. Interestingly, only a small amount of HNT (*i.e.* 5 wt%) is needed to provide the requisite increase in scaffold performance for the properties indicated, and such low concentrations HNT are not expected to be toxic in a biological setting [31, 545]. HNT has been embedded in various electrospun polymeric nanofibres (*e.g.* polylactic acid (PLA) [29], PLLA [30, 546], polyvinyl alcohol (PVA) [24], PCL [547], poly (glycolic acid) [548], poly (lactic-co-glycolic acid) (PLGA) [32]and alginate [27]) for use in biomedical applications. The biocompatibility of HNT was demonstrated by the study where it was incorporated into PLGA fibres and this scaffold was shown to support fibroblast proliferation [36]. The addition of HNT to the PLLA polymer enhanced its tensile strength and Young's modulus, and improved the adhesion and proliferation of mouse embryo osteoblast precursor cells (MC3T3-E1) [34]. Moreover, inclusion of HNT can promote the adsorption of proteins, which was shown to facilitate cell attachment and accelerate wound healing processes [31]. In light of these findings, it may be expected that incorporation of HNT into SF matrices could improve both the scaffold's the mechanical properties as well as its ability to support cell behaviour resembling that seen *in vivo*.

In this chapter, different amounts of HNT were used to modify the electrospun SF fibres. The effects of HNT content on morphology, porosity, hydrophilicity, thermal and mechanical properties of the electrospun fibres were investigated. The *in vitro* biocompatibility of SF/HNT nanocomposites for wound healing applications was examined by investigating the proliferation, differentiation and morphology of cells plated on SF/HNT scaffolds. Fibroblasts and myoblasts were chosen for these experiments. The former is the most abundant cell type in connective tissue and the

latter have the potential to differentiate into myotubes (the first step towards producing a muscle fibre).

4.2 Method Development

4.2.1 Electrospinning Optimisation of SF/HNT Scaffolds

The morphology and final structure of electrospun nanofibres are dependent upon the concentration of the polymer solution and the electrospinning parameters [188]. In order to fabricate smooth and bead free fibres, SF spinning solutions of various SF concentrations (8, 10, 12, 13 and 14 w/v%) were electrospun at a high voltage of 16 kV applied to the blunt needle with inner diameter of 0.6 mm, needle-to-collector distance of 13 cm and flow rate of 0.3 mL/h. The morphology of the resulting fibres was observed by scanning electron microscopy (SEM) and the micrographs are shown in Figure 4.1 (a-e).

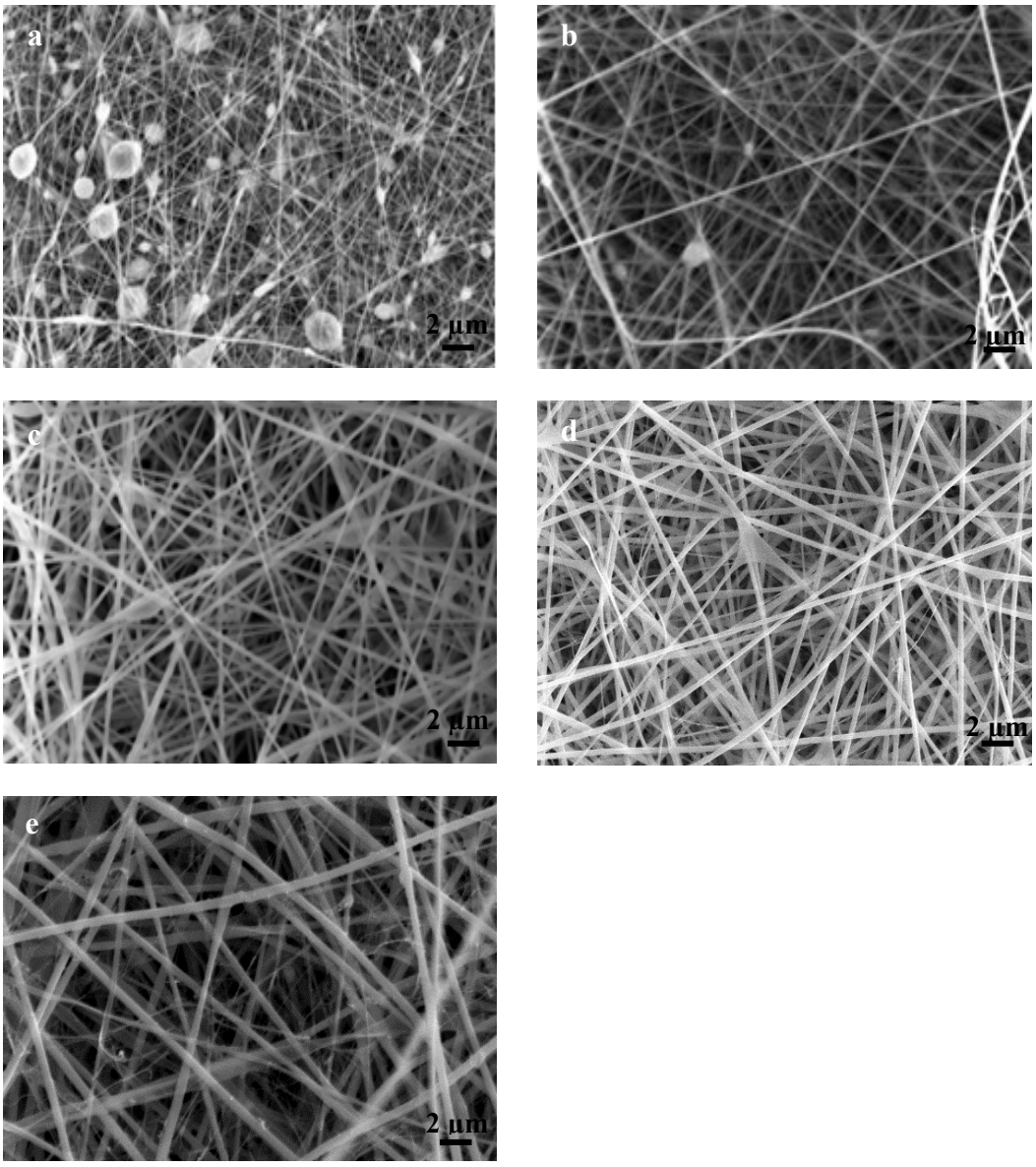

Figure 4.1 SEM micrographs of electrospun SF fibres at applied voltage of 16 kV, needle-to-collector of 13 cm, flow rate 0.3 mL/h with SF concentrations of a) 8 w/v%, b) 10 w/v%, c) 12 w/v%, d) 13 w/v% e) 14 w/v%; scale bar = 2 μm.

These data (Figure 4.1 a-e) indicated the role of SF concentration in fibre formation, as uneven and beaded fibres were obtained at SF concentrations below 13 w/v%. With increasing SF concentration, the number of beads decreased, and uniform, bead-free fibrous structures were fabricated. At a SF concentration of 14 w/v% uniform fibres were formed, but the spinning procedure was not continuous and was interrupted due to the high SF concentration. Therefore, all further electrospinning was conducted with a SF concentration of 13 w/v%, an applied voltage of setting 16 kV, a needle-to-collector distance of 13 cm and a flow rate of 0.3 mL/h.

4.2.2 Proliferation Assay Optimisation

To assess whether scaffolds support cell growth, a proliferation assay was performed. A number of different methods were trialled to determine the most appropriate set of assay conditions to use with the scaffolds. These methods are detailed in the following subsections.

4.2.2.1 AQueous One Assay

The AQueous One assay (CellTiter 96 AQueous One solution, Promega, Madison, WI, USA) is a colorimetric assay for determining the number of viable cells in a sample. The assay is based on a tetrazolium compound (3-(4,5-dimethylthiazol-2-yl)-5-(3-carboxymethoxyphenyl)-2-(4-sulfophenyl)-2H-tetrazolium; commonly called MTS) that is reduced by cells to form a soluble coloured formazan product. This formazan product is measured by absorbance at 490nm and the value obtained is directly proportional to the number of living cells in a tissue culture plate. However, on occasion chemical interference may cause non-enzymatic reduction of MTS and the generation of the formazan product in the absence of cells giving rise to significant background absorbance values. To determine the extent to which the SF scaffolds generate background readings the assay was performed on medium and methanol treated SF scaffolds without cells (three replicates). Two different media were tested: Dulbecco's modified Eagle's medium (DMEM) and DMEM (phenol red free) complete media. These assays were performed in 96-welled plates, 100 μl of media being added to the scaffolds in the wells followed by 20 μl of the Aqueous One reagent

and the plates were incubated at 37^{0}C for either 1.5 h or 3 h before absorbance at 490 nm was assessed. These data are presented in Figure 4.2 (a, b). It is clear from this Figure that regardless of media type, scaffolds had significant signal. Hence, the AQueous One assay cannot be used to measure cell numbers on the SF scaffolds because the background signal is too high.

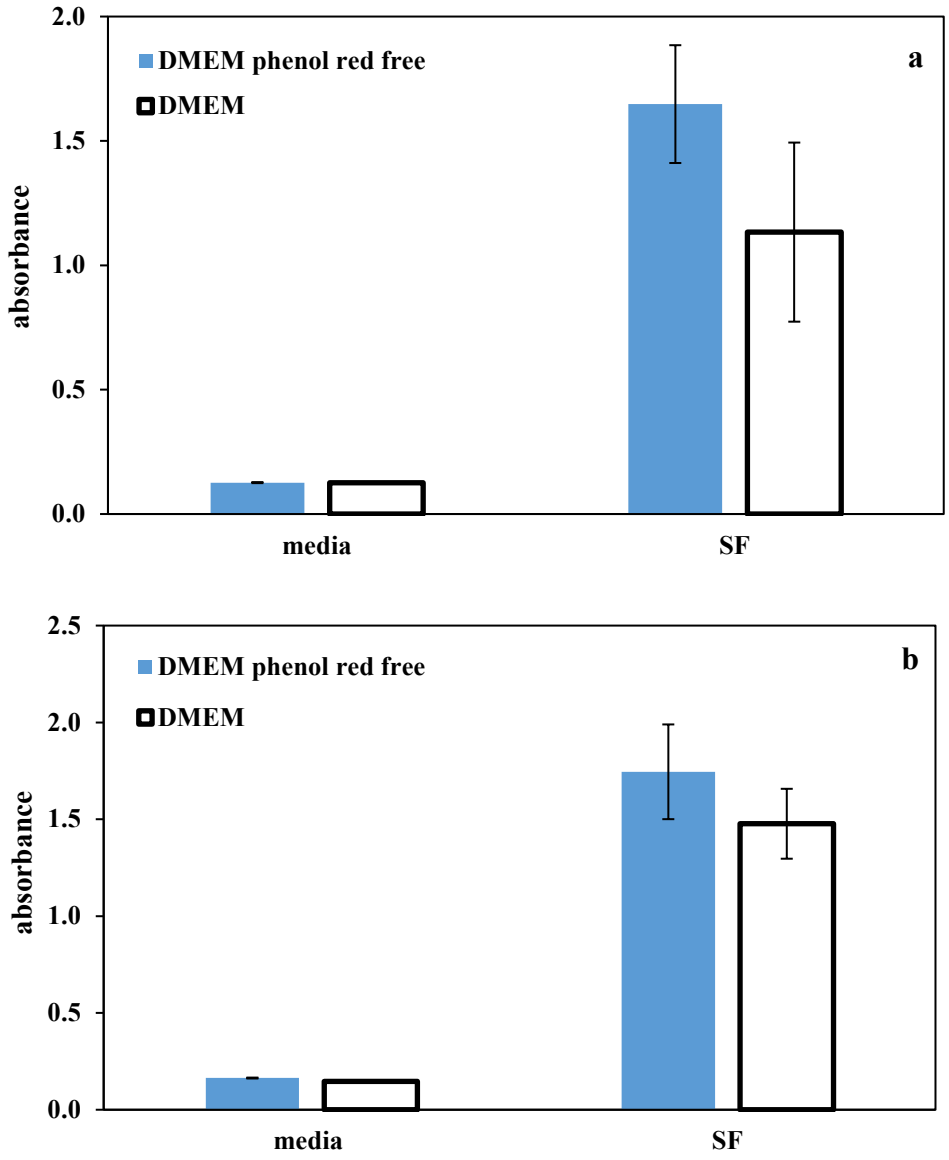

Figure 4.2 Background signal generated by SF scaffolds with Aqueous One reagent. Media with or without SF scaffolds were labelled with AQueous One and incubated for (a) 1.5 h and (b) 3 h. Absorbance at 490 nm is shown and means of 3 replicates are plotted.

4.2.2.2 CellTiter Blue Assay

The CellTiter Blue ® (Promega) assay was tested as an alternative. This assay is based on the active component, resazurin, a weak fluorescent compound which is converted to the highly fluorescent resorufin by living cells and the fluorescent signal is proportional to the number of viable cells. To investigate the suitability of this assay, methanol treated SF scaffolds, DMEM (phenol red free) medium and 3T3 cells titrated from a concentration of 10×10^4 to 1.56×10^3 in 100 µl medium were labelled with 20 µl CellTiter Blue and incubated for 4 h and plates the fluorescent signal was measured using an EnSpire Multimode plate reader. As shown in Figure 4.3 both medium and methanol treated SF scaffolds in medium had a low background signal for all 5 replicates relative to 3T3 standard curve and the difference was quite high confirming the potential of cell quantification on scaffold based on this assay.

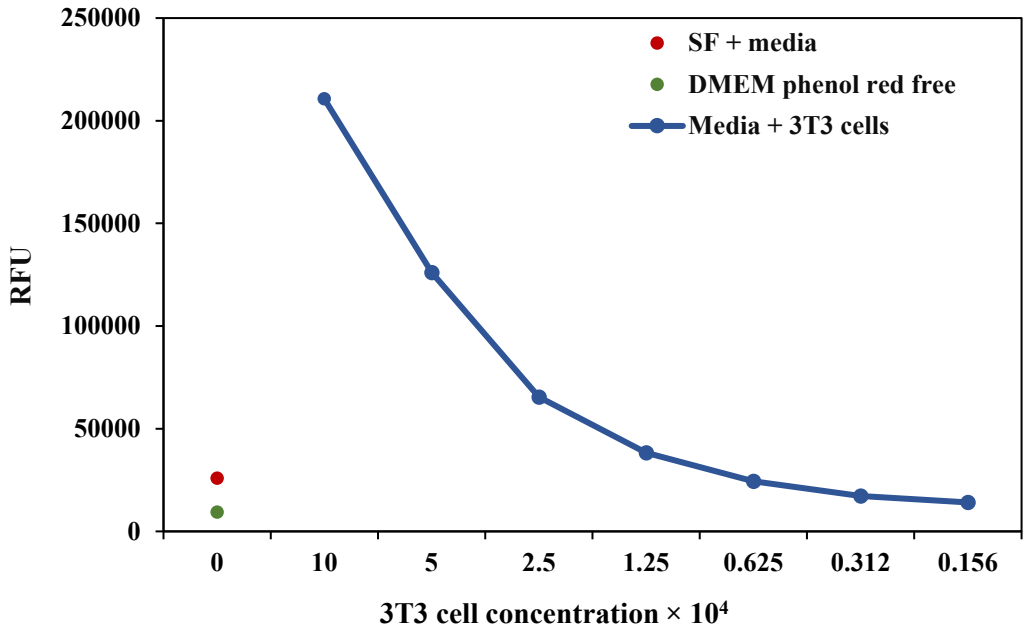

Figure 4.3 Standard curve for CellTiter Blue assay. Relative fluorescent Units (RFU) are shown for medium, scaffolds with and without 3T3 cells labelled with CellTiter Blue for 4 h.
Plotted data were based on the mean values of 5 replicates for SF and DMEM (phenol red free) medium and 3 replicates for 3T3 standard curve. Note that the error bars are much smaller than data point symbols.

4.2.3 Cell Morphology Optimisation

4.2.3.1 Confocal Microscopy

To observe whether the 3T3 cells adhered and spread on the scaffolds, or remained un-spread nuclei and filamentous actin (F-actin) were stained with DAPI and Rhodamine phalloidin (10 Units/mL, Molecular Probes) respectively diluted in PBS. Briefly, 3T3 cells were harvested, pelleted and resuspended in DMEM (phenol red free) medium, at a concentration of 8×10^4 cells/ mL. 250 µL and 50 µL of the cell suspension were seeded on collagen coated coverslips (4.8 cm^2) and SF scaffolds (1 cm^2) respectively. After culturing for three days, cell morphology was observed using a Olympus IX-81 high content screening inverted fluorescent microscope (Olympus, Tokyo, Japan). Figure 4.4 (a, b) are images of cells on collagen coated coverslips (control) and SF scaffolds after 3 days of culture. The scaffolds produced a high background signal which interfered with observing the cell morphology.

To reduce the scaffold signal and improve the images Nikon A1+ confocal microscope (Nikon, Tokyo, Japan) was used. Scaffolds were loaded with two different 3T3 cell concentrations (either 0.4×10^4 or 0.8×10^4 cells), cultured for 3 days and stained with DAPI and rhodamine phalloidin. As before cells on collagen coated coverslips served as controls and to maintain an equivalent cell density on the larger surface 3T3 cells were seeded at concentrations of 2×10^4 and 4×10^4. Representative images are shown in Figure 4.5 (a - d). The background was considerably decreased using confocal microscopy and the cell morphology was clearer (compare Figure 4.4 and 4.5), so confocal microscopy was used for observing cell morphology. Moreover cell density of 0.8×10^4 was appeared to be more reasonable for further experiments.

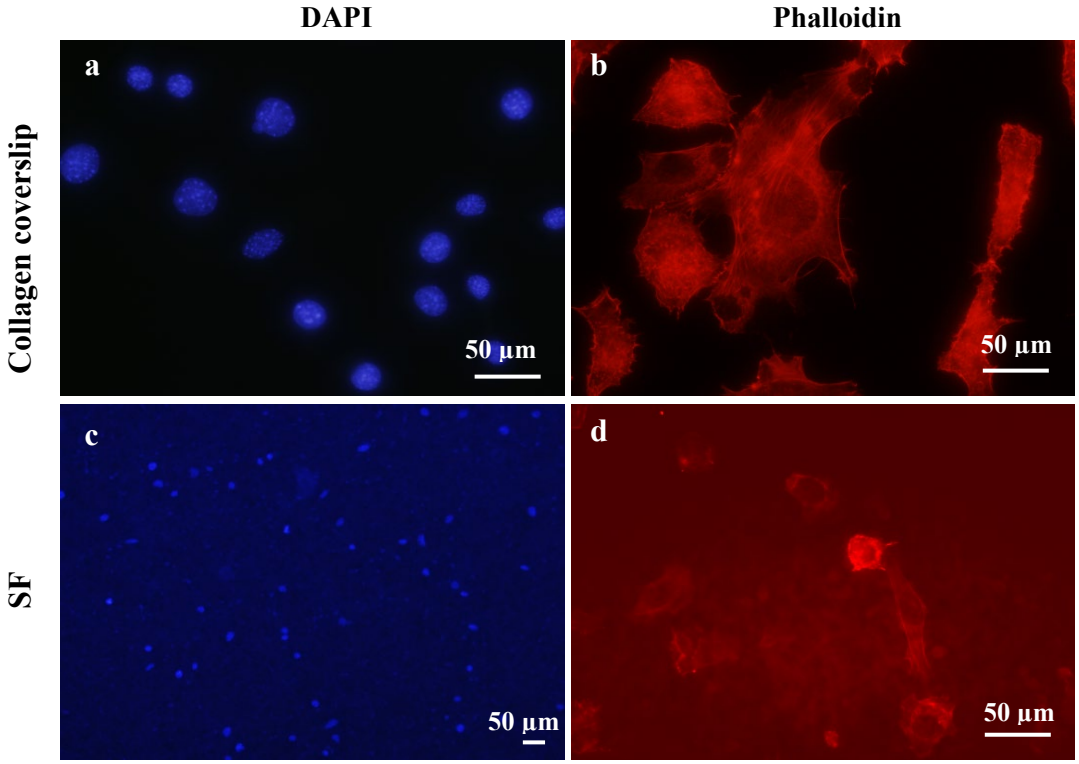

Figure 4.4 Representative images of 3T3 cells seeded on collagen coated coverslips at a density 2×10^4 cells per well (a, b) and on SF scaffolds at cell density of 0.4×10^4 (c, d) and cultured for 3 days. Images of DAPI and rhodamine phalloidin stained cells were obtained using an Olympus IX-81 microscope. Scale bar = 50 µm

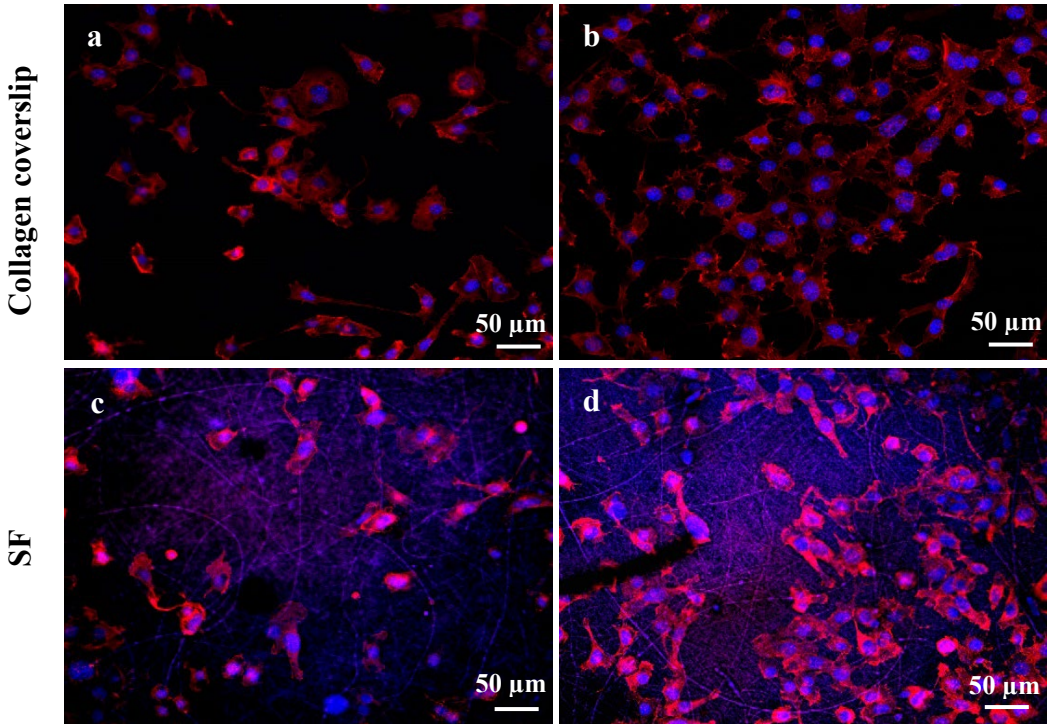

Figure 4.5 Representative images of 3T3 cells seeded for 3 days on collagen coverslip at cell concentration of (a) 2×10^4 and b) 4×10^4 and on SF scaffolds at cell density of (c) 0.4×10^4 and d) 0.8×10^4. F-actin were stained with rhodamine phalloidin (red) and nuclei were stained with DAPI (Blue). Images were obtained using Nikon A1+ confocal microscope. Scale bar = 50 µm.

4.2.3.2 SEM Microscopy

To investigate the influence of HNT on cytocompatibility of SF scaffolds scanning electron microscopy (SEM) was employed. Initially, samples were prepared for SEM as follows: 3T3 cells (0.8×10^4 /scaffold) were seeded on SF scaffolds (1 cm^2) and cultured for 3 days. Scaffolds were then dehydrated by immersion in serial dilutions of increasing ethanol concentrations, air-dried, platinum coated and observed under a Zeiss EVO 40XVP SEM at an accelerating voltage of 10 kV. Representative images for methanol treated SF and SF/HNT 1 wt% are shown in Figure 4.6 (a - d). In these images the cells are opaque and their morphology is unclear. This is especially the case when viewed at high magnification. This may have been due to the delicate nature of the cells causing them to be damaged during the dehydration and drying procedure, or by the high SEM accelerating voltage. To improve image quality samples were freeze dried and observed at a lower accelerating voltage of 5 kV, as described in detail in Section 3.4.6.2, Chapter III. The images obtained are presented and discussed in 4.3.10.2.

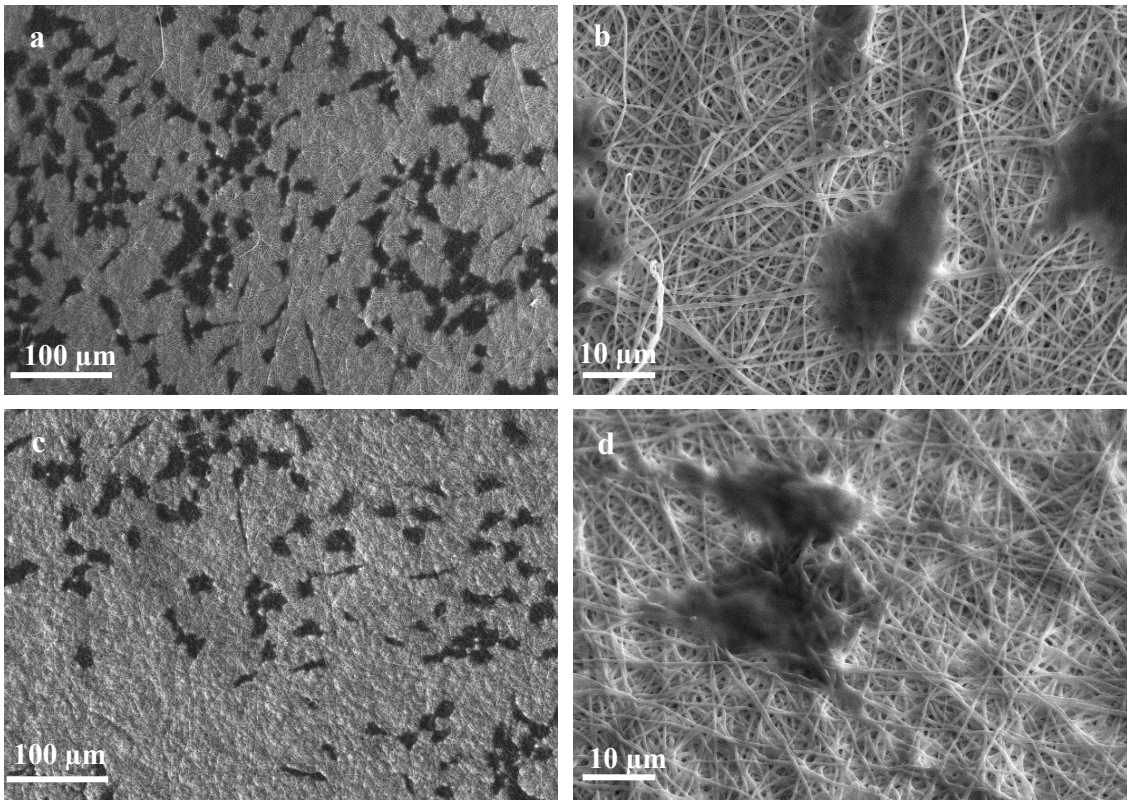

Figure 4.6 SEM micrographs of scaffolds seeded with 3T3 cells and cultured for 3 days. SF (a, b) and SF/HNT 1wt% (c, d).

4.2.4 Differentiation Assay Optimisation

To address whether SF/HNT scaffolds support differentiation of C2C12 myoblasts, cells (0.4×10^4) were seeded on 1 cm^2 scaffolds and maintained in DMEM (phenol red free) complete medium for 4 days, before being switched into differentiation medium (DMEM/ 2% Horse Serum) for 4 further days (see details in Section 3.4.8, Chapter III). To evaluate myotube formation, scaffolds were immuno-stained with than an antibody recognising alpha-smooth muscle actin (α-SMA) and counter-stained with DAPI. Alpha-smooth muscle actin is a differentiation marker of muscle cells. The images obtained by fluorescent microscopy are presented in Figure 4.7 (a - e). Although the α-SMA antibody staining indicated that myotubes had formed and DAPI staining suggested these were multi-nucleate, this staining protocol was not optimal with respect to the myotube structure that was revealed. In an effort to improve the images of myotube morphology, immunostaining with an anti-myosin antibody was performed. It was found that the anti-myosin antibody staining better revealed myoblast differentiation into myotubes and myotube morphology. Relevant images are shown in Section 4.3.11.

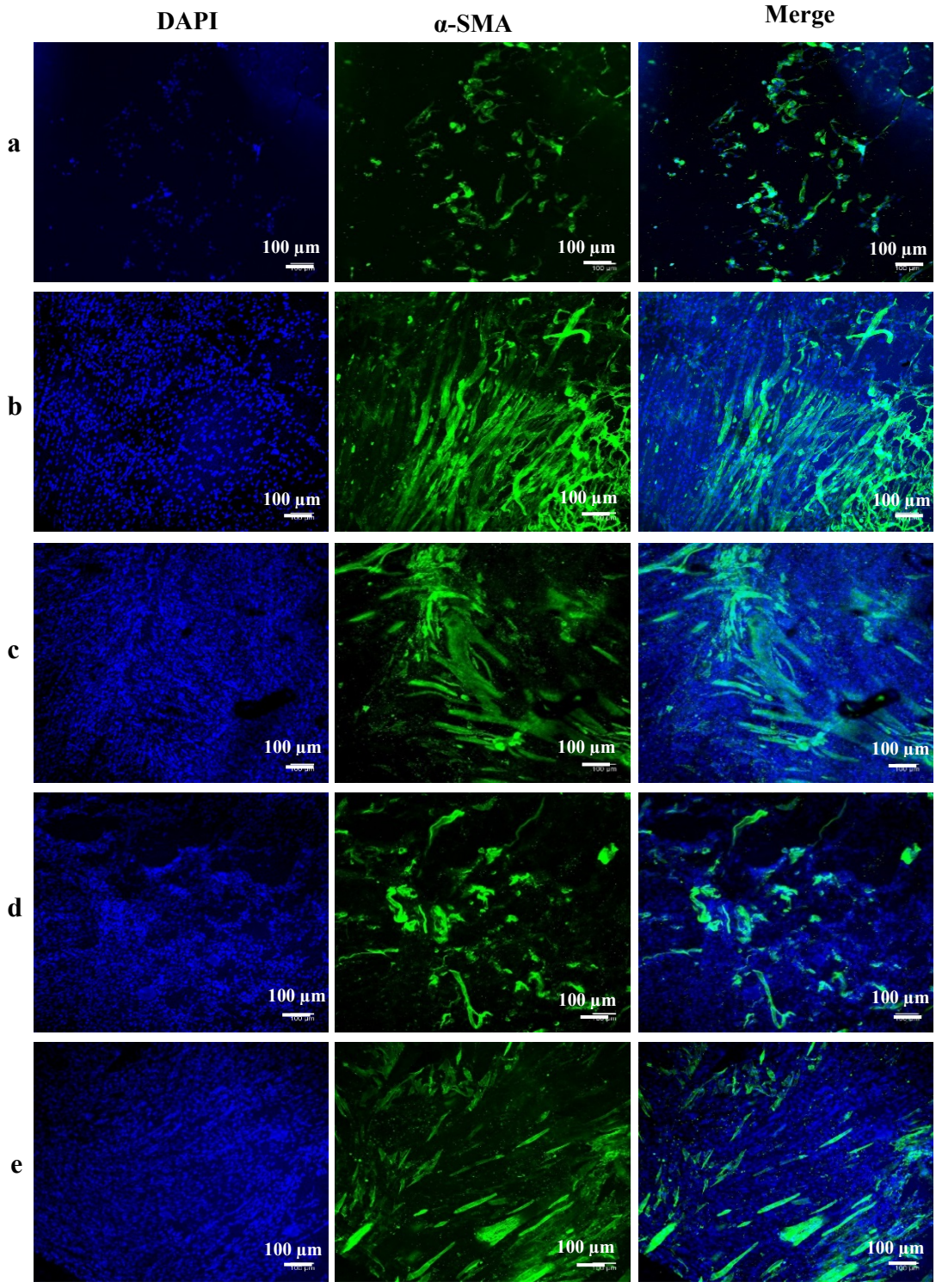

Figure 4.7 C2C12 cell differentiation on SF/HNT scaffolds.

The scaffolds seeded with C2C12 cells were stained with DAPI (blue) and an α-SMA antibody (green). Images were obtained using fluorescent microscopy. (a) SF, (b) SF/ HNT 1 wt%, (c) SF/ HNT 3 wt%, (d) SF/ HNT 5 wt%, (e) SF/ HNT 7 wt%; Scale bar = 100 µm.

4.3 Results and Discussion

4.3.1 Fibre Morphology

Electrospun SF/HNT scaffolds were fabricated under the optimised conditions outlined above (Section 4.2.1) and their surface morphologies were observed by SEM. Figure 4.8 (a-e) shows representative SEM images of plain SF and SF/HNT with different HNT content. Pristine SF fibres have smooth and bead-free surfaces and the simultaneous addition of HNT to the SF scarcely had any effect on the fibre surface. The high magnification images (Figure 4.8 (a-e) insets) revealed infrequent irregularities in the SF/HNT nanocomposite fibres with HNT content of 1 wt% and 3 wt%, which could be attributed to HNT that were well embedded into the SF fibres. At higher HNT content of 5 and 7 wt%, more frequent irregularities were visible and had the appearance of nanotubes protruding from the side or end of the SF nanofibres. The morphology of the nanofibres were not markedly changed by methanol treatment; the fibrous structure was retained, but methanol treatment did cause a little swelling (Figure 4.8 (f-j)).

Nanofibre diameters in the scaffolds were determined and these data are represented as frequency distribution histograms (Figure 4.9 (a-e)). Pristine silk produced fibres with an average diameter of 358.3 (±65.8) nm and with the inclusion of HNT the average diameter increased in accordance with the concentration of HNT. The average diameter of SF/HNT nanofibres with the addition of 1, 3, 5, and 7 wt% HNT was found to be 388.1 (±64.18), 394.4 (±63.01), 410.3 (±51.3) and 437.2 (±50.7) nm respectively (Table 4.1). The inclusion of HNT moderately increased the fibre diameter of SF nanofibres. This finding was consistent with other studies. These studies have shown that inclusion of HNT into PLA [29], PCL [31], PLGA [36] and polydioxanone [385] resulted in formation of fibres with larger diameters. This phenomenon can be attributed to the enhanced solution viscosity due to the addition of HNT; increasing solution viscosity is known to induce increasing resistance against the jet leading to increased fibre diameters [31].

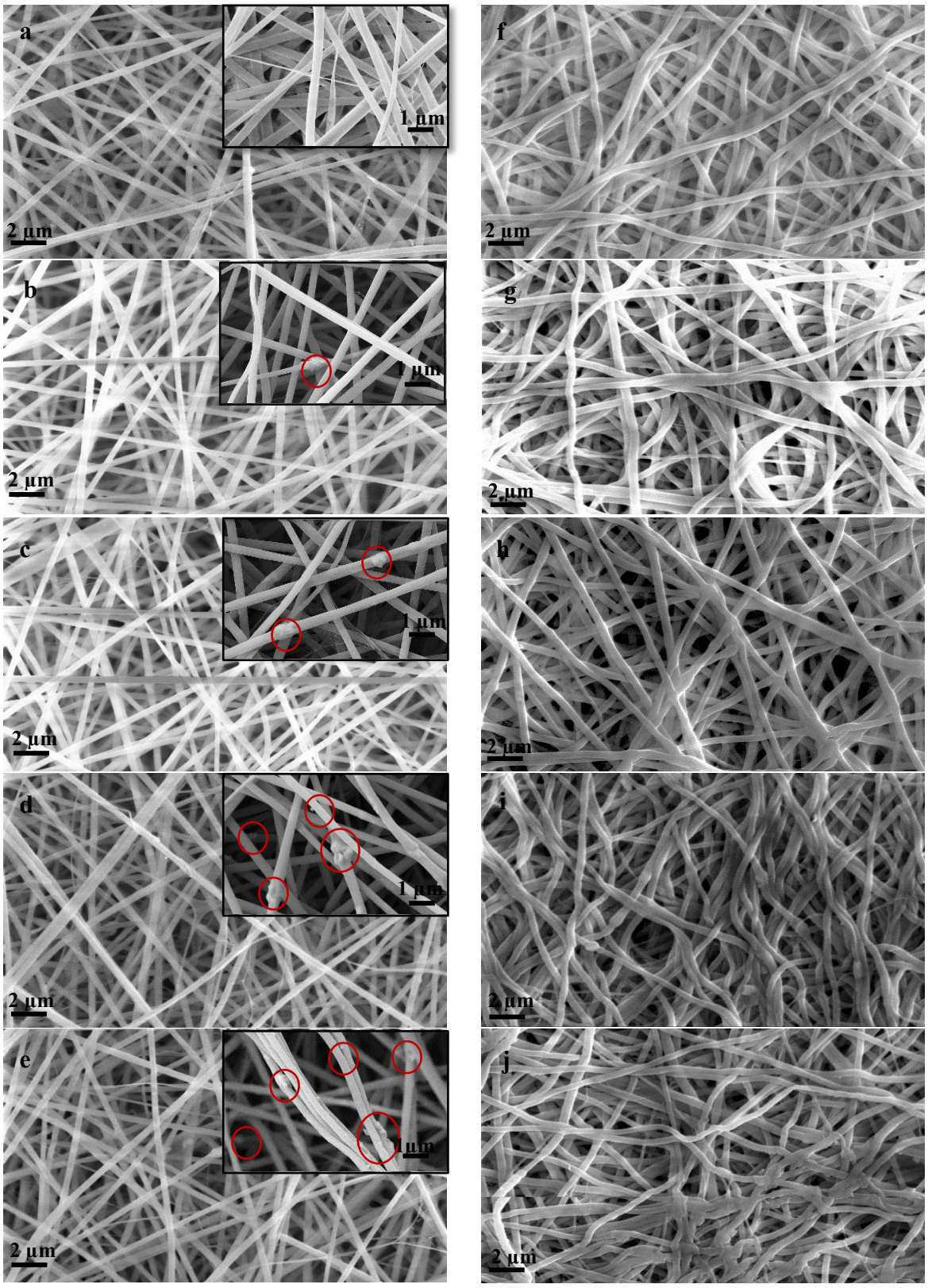

Figure 4.8 SEM images of as spun SF/HNT scaffolds: (a) SF, (b) SF/ HNT 1 wt%, (c) SF/ HNT 3 wt%, (d) SF/ HNT 5 wt%, (e) SF/ HNT 7 wt%; and (f-j) are the corresponding methanol treated scaffold; scale bar = 2 µm. SF concentration was 13 w/v% throughout. Insets show high magnification images of each scaffold scale bar = 1 µm. Circles within built-in EDS images indicate embedded HNT.

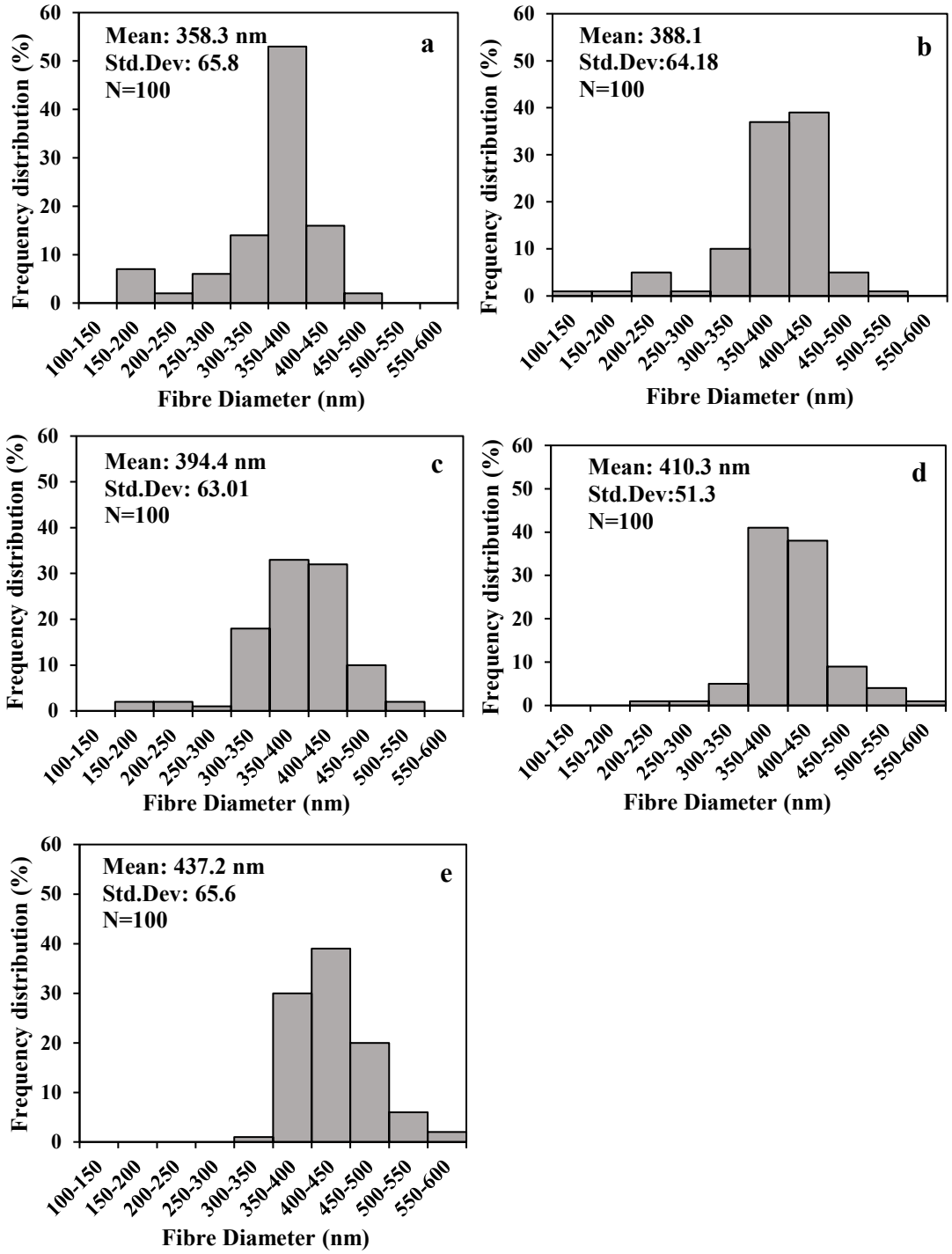

Figure 4.9 Fibre diameter distribution of methanol treated: (a) SF, (b) SF/ HNT 1 wt%, (c) SF/ HNT 3 wt%, (d) SF/ HNT 5 wt%, and (e) SF/ HNT 7 wt% nanofibres.

Table 4.1 Fibre diameter results of SF/HNT nanocomposites.

Sample	Diameter (nm)
SF	358.3 ± 65.8[a]
SF/HNT 1 wt%	388.1 ± 64.18[b]
SF/HNT 3 wt%	394.4 ± 63.01[b]
SF/HNT 5 wt%	410.3 ± 51.3[b]
SF/HNT 7 wt%	437.2 ± 50.72[c]

Statistical analyses using ANOVA followed by Tukey's test were conducted. [a-c] Different superscripts indicate significant differences between scaffolds ($p < 0.05$).

4.3.2 X-ray energy dispersive spectroscopy (EDS)

X-ray energy dispersive spectroscopy (EDS) was used to identify the elemental composition of the nanofibres. As shown in Figure 4.10 (a)-(e), the EDS analysis indicates the chemical composition of silk fibroin comprises carbon, oxygen and nitrogen elements. Whereas, the presence of aluminium and silicon elemental peaks correlates with the addition of HNT to the SF solution prior to electrospinning, and evidence of nanotubes in the fibres as revealed by SEM (Figure 4.10). Given that the typical chemical formula for HNT is ($Al_2Si_2O_5(OH)_4 . nH_2O$) [29], these data indicate that HNT have become incorporated into the SF fibres.

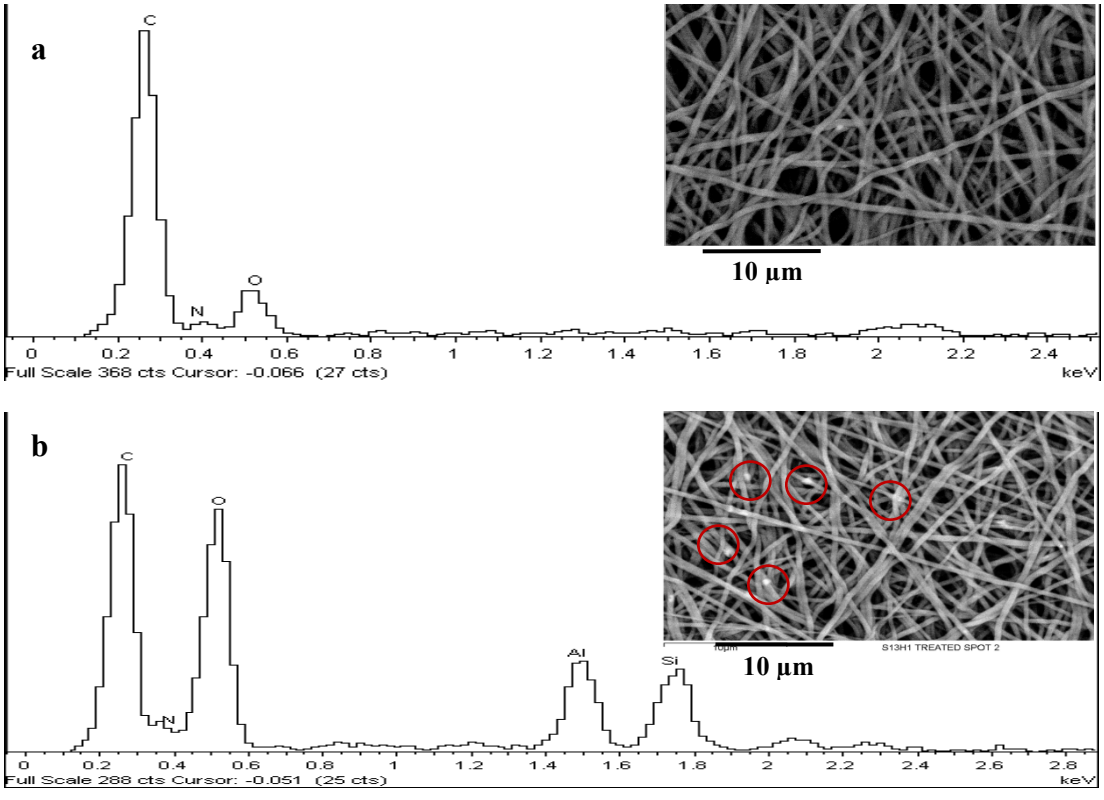

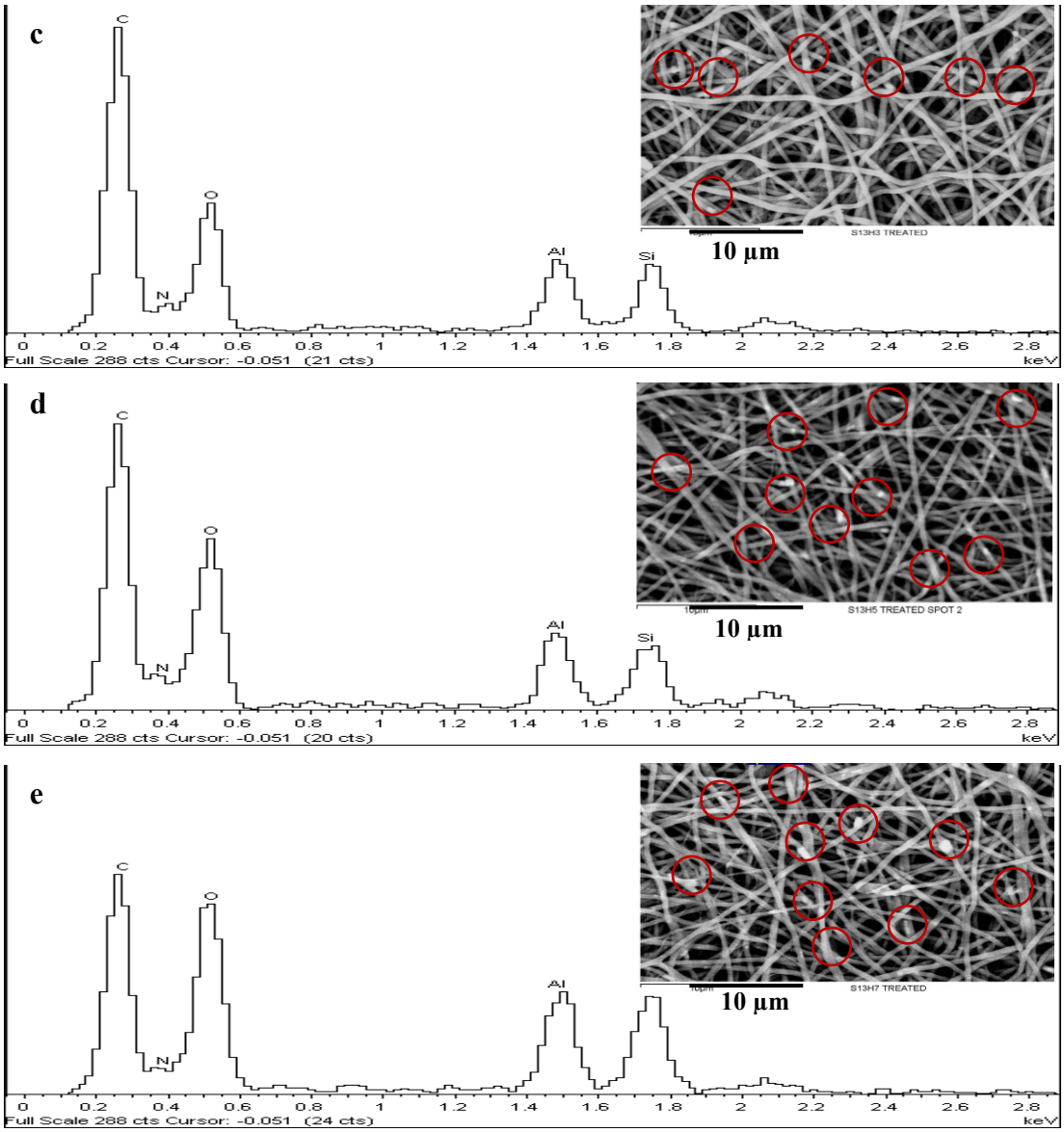

Figure 4.10 EDS spectra of methanol treated Silk/HNT scaffolds (a) SF, (b) SF/ HNT 1 wt%, (c) SF/ HNT 3 wt%, (d) SF/ HNT 5 wt%, (e) SF/ HNT 7 wt%. Scanning electron micrographs of the samples analysed are shown in the inserts. Red circles: HNT incorporated in the SF fibres.

4.3.3 BET Surface Area and Porous Structures

The pore size is an important parameter of scaffolds for tissue engineering. Inadequate pore size can limit the diffusion of nutrients or reduce cell attachment [549]. It has been well documented that the proliferation of cells is dependent on scaffold pore size [550-553]. Thus the BET surface areas, pore size and pore volume of SF and SF/HNT scaffolds were measured and the results are summarised in Table 4.2. The data appear to suggest that the addition of HNT into SF enhances the BET specific surface area of

the resulting nanocomposites. The BET specific surface area of electrospun SF nanofibres membrane was 4.47 m^2/g and it increased with increasing HNT up to 9.06 m^2/g when 7 wt% HNTs were added. This can be attributed to the increased surface roughness of SF/HNT nanofibres due to presence of HNTs on their surfaces. Although the incorporation of HNT resulted in an increase in the diameters of electrospun fibres, such increased diameters did not lead to a reduction in surface area. These results are consistent with those of Makarmei *et al*. [554], who also indicated that incorporation of HNTs led to an increasing BET surface area of electrospun polyacrylonitrile nanofibres.

In contrast, pore volume and pore width of nanocomposites did not change uniformly with increasing HNT content. The pore volume and pore width of SF fibres were 0.0081 cm^3/g and 7.61 nm as well as 0.0146 cm^3/g and 9.51 nm respectively, for scaffolds with the inclusion of 1 wt% HNTs, but decreased to 0.0084 cm^3/g and 4.13 nm respectively, when 7 wt% HNTs were added. HNTs have a lumen structure with inner pores, the incorporation of HNTs within polymer matrices can enhance pore volume of the construct when HNTs are well dispersed [28]. At low HNT content of 1 wt% the pore volume increased due to the presence of lumen inside the HNTs whilst as the HNTs content increased the agglomeration block the inner pores of HNT lumens and caused the reduction in pore volume.

Table 4.2 BET results of SF and SF/HNT nanocomposites.

Sample	Pore width (nm)	Pore volume (cm^3/g)	BET surface area (m^2/g)
SF	7.61	0.0081	4.47
SF/HNT 1 wt%	9.51	0.0146	6.14
SF/HNT 3 wt%	8.66	0.0122	8.06
SF/HNT 5 wt%	4.66	0.0103	8.43
SF/HNT 7 wt%	4.13	0.0084	9.06

4.3.4 Contact Angle and Water Uptake Capacity

The suitable hydrophilicity of the scaffolds is required for cell adhesion, proliferation and tissue integration [555-558]. To gain an insight into the wettability of the scaffolds, the water contact angle test was conducted. Water droplets placed on the scaffold surfaces were photographed (Figure 4.11 (a-e)) and the data are presented in Table 4.3. It was

found that on all scaffolds the contact angle of the water droplet was less than 90°, which is the criterion for categorising a surface as hydrophilic [559]. For scaffolds with the inclusion of 1 wt% HNT, the contact angle was 57.52° as opposed to 64.23° for SF, and this decrease can be ascribed to the hydrophilic nature of HNT [34, 560]. Surprisingly, further increasing the HNT content had an adverse effect and increased the contact angle up to 70.76° for SF/HNT 7 wt%. This discrepancy can be attributed to the changes in specific surface area which can be an indicator of surface roughness [561, 562]. To alter the wettability of a material two strategies can be employed: changing the chemical nature of the surface [563] or modulation of the surface roughness [561, 564]. Hydrophobic surfaces can be formed by hydrophilic substances if the surface roughness enhanced [562, 565, 566]. As surface roughness increases, the material's surface energy reduces (*i.e.,* interfacial tension between polymer and water reduces) and becomes hydrophobic (*i.e.* a similar phenomenon as superhydrophobic materials) [567]. As evidenced by SEM images of SF/HNT nanocomposites (Figure 4.8 insets (c-e)) and the BET surface area results, as the HNT content increased, more irregularities were formed thereby yielding rougher surface. Thus, the peculiar effect of HNT on hydrophilicity of the SF/HNT nanocomposites may be due to increases in surface roughness. Similar results and conclusions have been reported for other HNT containing materials, for example HNT nanocomposite materials based on polypropylene, PLA and PLLA [34, 561, 564, 567].

Table 4.3 Static contact angles of SF/HNT fibrous scaffolds. Statistical analyses using ANOVA followed by Tukey's test were conducted. * $P \leq 0.05$.

Sample	Water contact angle (degree)
SF	64.23°± 4.01°
SF/HNT 1 wt%	57.52° ± 6.73°*
SF/HNT 3 wt%	65.73° ± 7.29°
SF/HNT 5 wt%	66.33° ± 5.46°
SF/HNT 7 wt%	70.76° ± 4.82°*

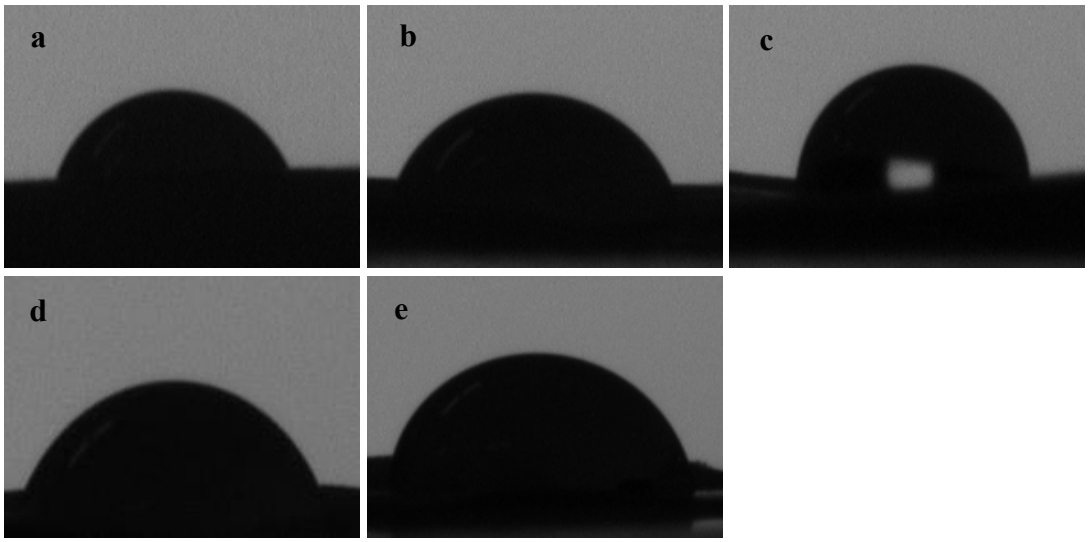

Figure 4.11 Contact angle images: (a) SF, (b) SF/ HNT 1 wt%, (c) SF/ HNT 3 wt%, (d) SF/ HNT 5 wt%, (e) SF/ HNT 7 wt%.

Another important factor for scaffolds is their ability for water diffusion, which allows the transportation of nutrients, and helps the growth of new cells. [568-570]. Figure 4.12 depicts the water uptake capacity for SF and SF/HNT nanocomposites after 24 h. The water uptake capacity (WUC) determined for SF/HNT 1 wt% was significantly higher than that measured for SF and for the other nanocomposites that contained more HNT. The value for SF/HNT 1 wt% was 462% in comparison to 326% for SF, and values between 290-314% for nanocomposites with the inclusion of 3-7 wt% HNT. As hydrophilicity, high surface area and pore volume all contribute to increasing the WUC [571], hence given SF/HNT 1 wt% scaffolds had the highest WUC it is not surprising that these scaffolds also had the lowest contact angle and highest pore volume (0.0146 cm^3/g) relative to other nanocomposites. These data are in accordance with other published report indicating the role of pore volume on WUC of scaffolds [572].

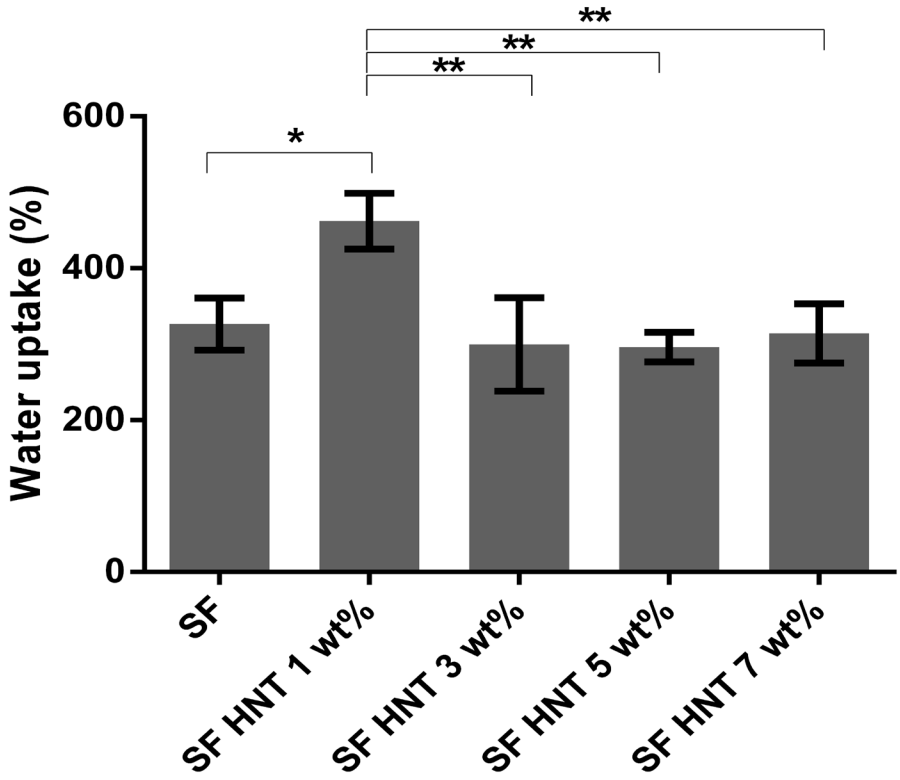

Figure 4.12 Water uptake capacity of SF and SF/HNT nanocomposites. In all cases the tests were performed on 5 replicates. Means +/- SDs are shown. Statistical analyses using ANOVA followed by Tukey's test were conducted. * $P \leq 0.05$, **$P \leq 0.01$.

4.3.5 FTIR Analysis

To determine if incorporation of HNT into the SF scaffolds caused a change in the molecular structure of the SF, FTIR was performed and these data are shown in Figure 4.13. The main peaks at 1651 cm^{-1} (amide I) and 1536 cm^{-1} (amide II) were detected in "as-spun" SF fibres which is attributed to the random coil conformation [280, 573]. After methanol treatment, the characteristic peaks of SF scaffolds were found at 1627 and 1520 cm^{-1}, which can be assigned to amide I and amide II in the β-sheet conformations, respectively [316, 574]. This is an indicator of a change in the chemical conformation of SF from random coil to β-sheet state. SF has two types of molecular conformation of the secondary structure, called silk I and silk II. Silk I is a metastable form of SF that is soluble in water and non-crystalline; random coil conformations are usually called silk I. On the other hand, silk II is a highly stable and organised structure that is insoluble in water; the β-sheet conformation is called silk II. Generally, both silk I and silk II are present in SF products, but it is their relative proportions that can define the

final properties [575, 576]. Previous studies documented that the conformational transition of SF from random coil to β-sheet state could be induced by methanol treatment through the effects of dehydration [274, 275, 577].

Two peaks were evident in HNT powders, at 3621 and 3694 cm^{-1}, arising from the OH stretching vibration of the inner Al-OH groups of the HNTs [372, 578]. The other relevant peaks at 1005 and 910 cm^{-1} can be assigned to the stretching of Si-O and Al-OH groups, respectively [29]. SF/HNT nanocomposite scaffolds have not demonstrated the peaks characteristic of HNTs, which is probably because of the small loading of HNT relative to the quantity of SF. Moreover, SF/HNT nanocomposite scaffolds with different HNT contents produced the same absorption peaks as that of pure SF, implying that the addition of HNTs does not influence the overall structure of SF.

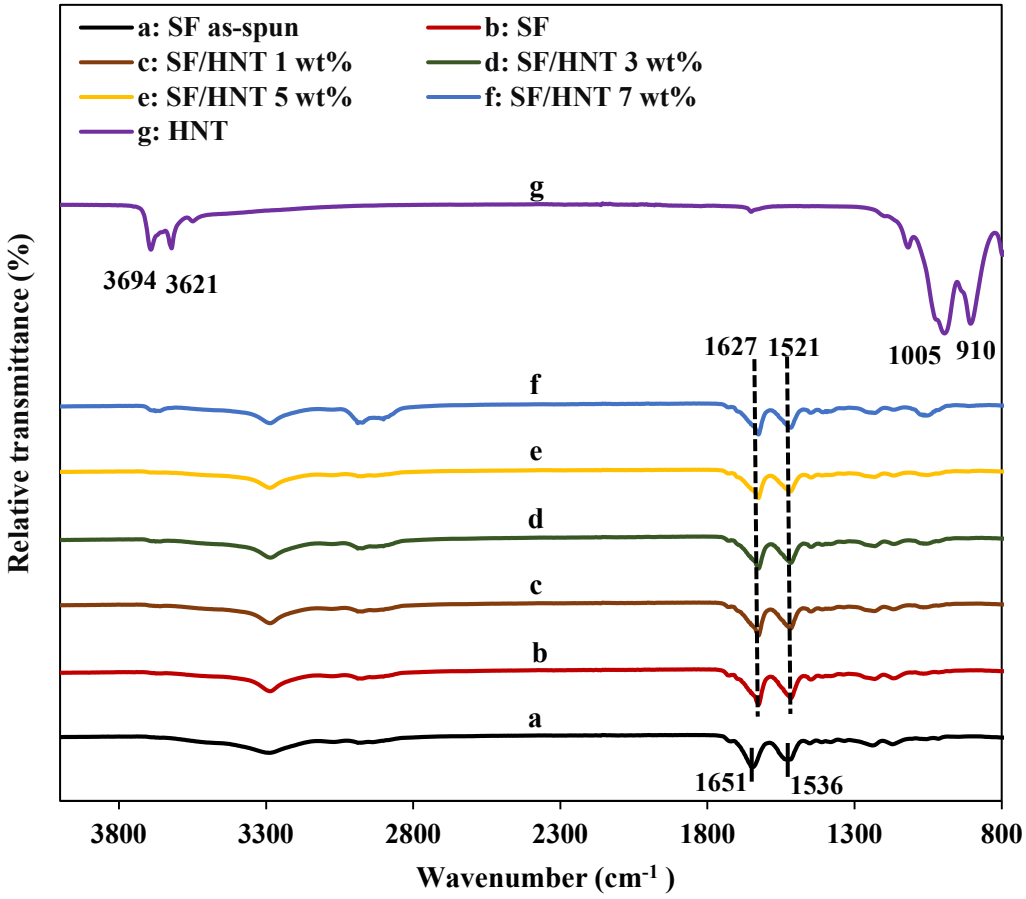

Figure 4.13 FTIR spectra of as-spun, methanol treated SF and SF/HNT nanocomposites scaffolds.

4.3.6 XRD Diffraction Analysis

In order to identify the structure of SF, X-ray diffraction was used. Figure 4.14 illustrates the XRD pattern of as-received HNTs, as-spun SF nanofibres and methanol treated SF/HNT nanocomposites. Three major diffraction peaks at 2θ angle of 12.49°, 20.44° and 25.04° were found for HNT powder which were assigned to (001), (020)/(110) and (020) crystal planes, respectively [34]. Based on Bragg's law, these peaks are associated with *d*-spacing values of approximately 0.73, 0.44 and 0.35 nm, respectively. The amorphous structure of as-spun SF was evident with the absence of its XRD peak, whereas after methanol treatment, SF had a peak at $2\theta = 20.3°$ corresponding to the β-sheet structure (Silk II) [294, 535]. This peak was observed for all scaffolds regardless of the HNT content, confirming their β-sheet structure, however it overlaps with the diffraction pattern of HNT at 20.44°. Moreover, in all the nanocomposites the HNT peak pattern was also evident and as the HNT content increased, the diffraction patterns at $2\theta = 12.5°$ and 25.1° intensified. Notably, the d-spacing values for these corresponding peaks remained almost unchanged at 0.7 and 0.35 nm indicating that HNT intercalation by SF molecular chains does not noticeably take place.

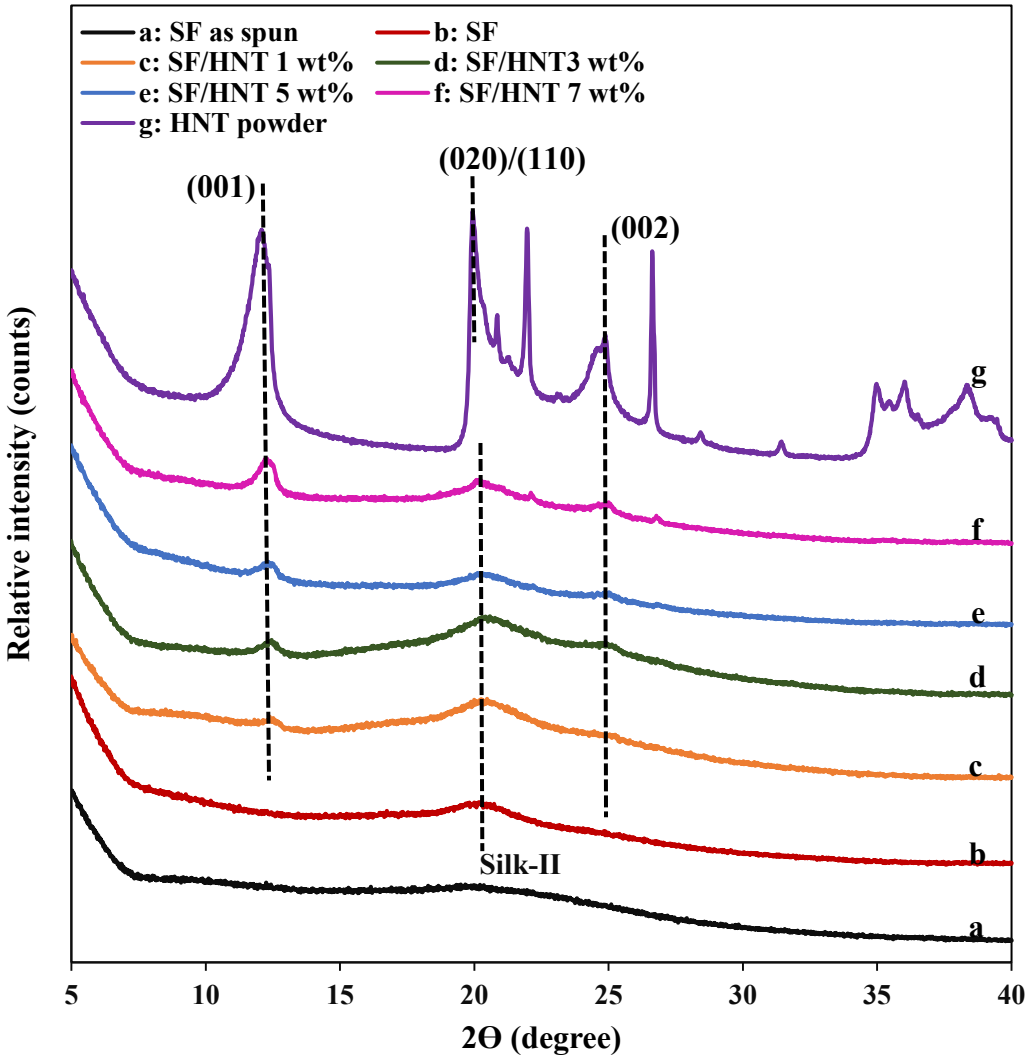

Figure 4.14 XRD pattern of SF/HNT scaffolds and as received HNTs.

4.3.7 Mechanical Properties

For tissue engineering applications where scaffolds are implanted in the body, it is desirable that mechanical properties of the scaffold match that of the corresponding tissue [36, 579]. Hence the effects of HNT content on mechanical properties of the resulting scaffolds were investigated and the results are shown in Figure 4.15 (a-d). Scaffolds comprising only SF possessed a Young's modulus of 158.08 ± 51.82 MPa and a tensile strength of 7.94 ± 2.54 MPa. For scaffolds modified with 1 and 3 wt% HNTs, Young's moduli were 159 ± 43.23 and 233.67 ± 18.40 MPa, respectively, and the corresponding tensile strengths were 8.07 ± 2.92 and 11.35 ± 1.79 MPa. These increases are due to the inherent toughness of HNT [29, 34, 580] and good dispersion of

HNTs, thus, the applied external load can be effectively transferred to HNT giving rise to the improvement in mechanical properties of scaffolds [547].

However, increasing the HNT content from 5 to 7 wt% had a detrimental effect on the tensile properties of nanocomposites at which Young's modulus and tensile strength were reduced to 90.20 ± 40.07 and 4.64 ± 1.34 MPa, respectively with the inclusion of 7 wt% HNT. This could be explained by the agglomeration of HNT at higher filler contents, a suggestion supported by the SEM images (Figure 4.8 (d-e)) showing HNT agglomeration when 5 and 7 wt% HNT were incorporated. These agglomerates can potentially hinder the good filler–matrix interfacial adhesion and reduce the effective load transfer from the polymer matrix to the fillers. As a result, these agglomerates act as the source of flaws, causing deterioration in mechanical performance [537, 547]. Pan *et al.* [537] also reported 2.8- and 4.4-fold increase in breaking strength and Young's modulus respectively when incorporating 1 wt % of functionalised MWCNTs into SF as opposed to SF mats, but further HNT content weakened the mechanical properties of SF/MWCNTs nanocomposites. The elongation at break was not affected by HNT loading and was 20.39% for SF, whereas it reached 15.21% at the HNT content of 7 wt% which can be considered negligible. Similar results were reported by others [381, 545, 547] where the elongation at break of nanocomposites decreased with the addition of HNT due to the formation of typical aggregates.

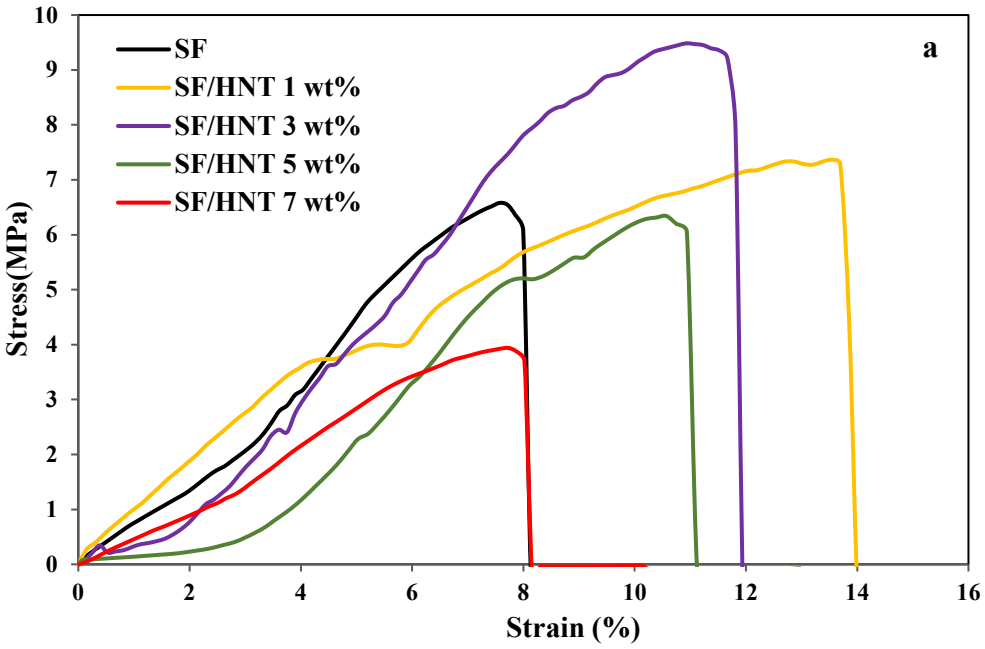
a
SF
SF/HNT 1 wt%
SF/HNT 3 wt%
SF/HNT 5 wt%
SF/HNT 7 wt%
Stress(MPa)
Strain (%)
0
1
2
3
4
5
6
7
8
9
10
0
2
4
6
8
10
12
14
16

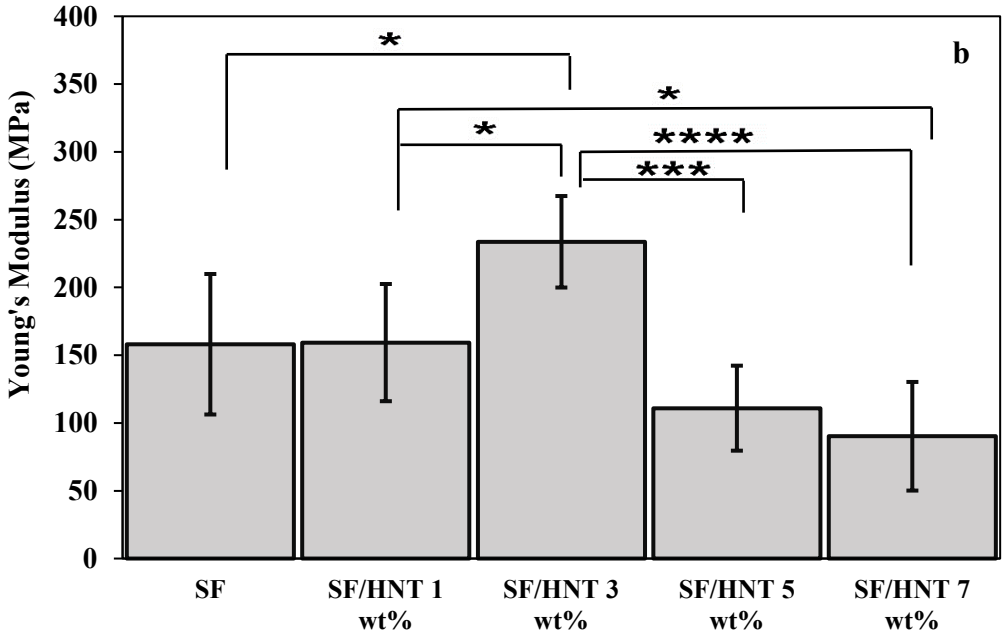
b
Young's Modulus (MPa)
0
50
100
150
200
250
300
350
400
*
*
*
****
***
SF
SF/HNT 1 wt%
SF/HNT 3 wt%
SF/HNT 5 wt%
SF/HNT 7 wt%

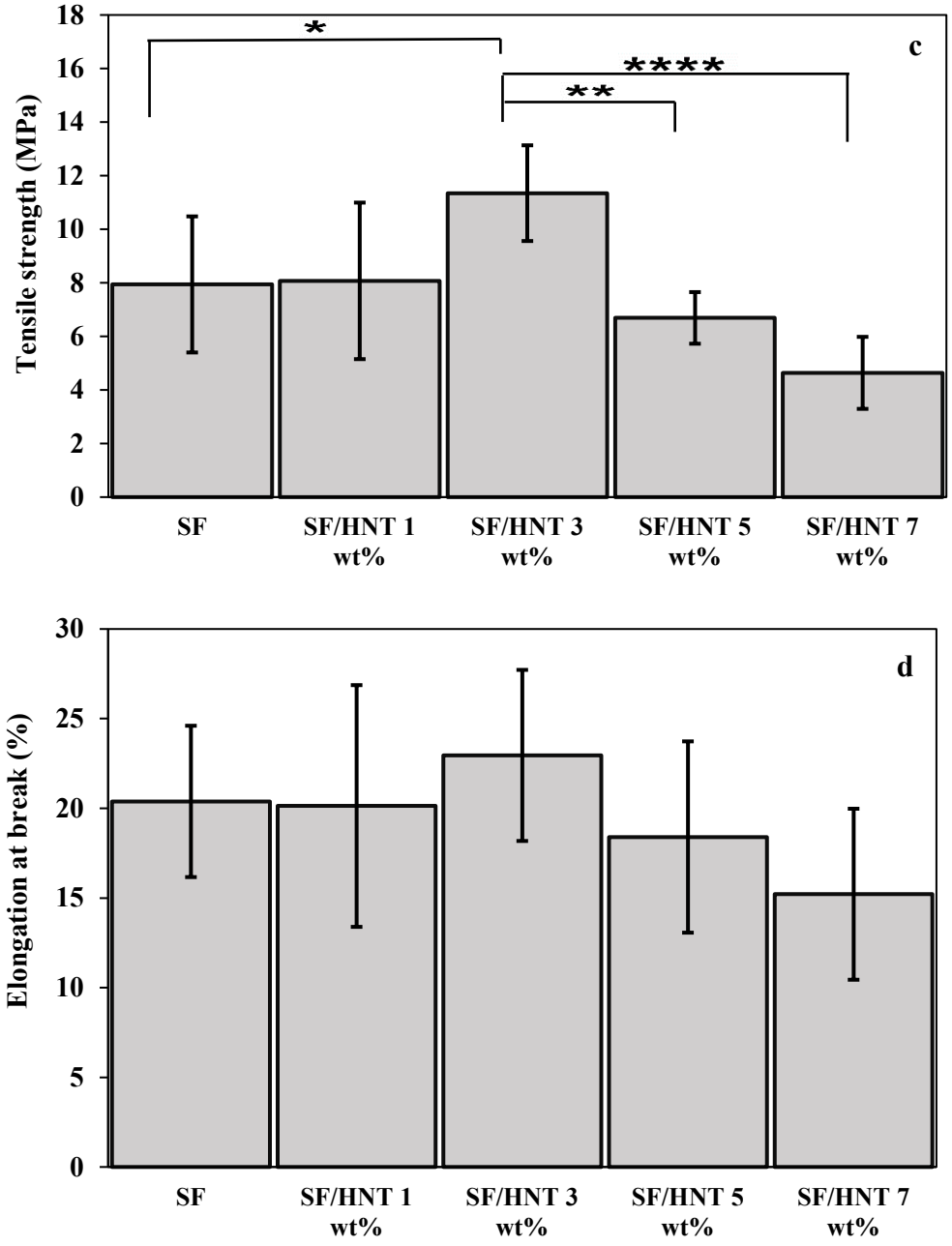

Figure 4.15 (a) A representative stress-strain curves of SF/HNT nanofiber mats. Mechanical properties of SF/HNT scaffolds at different HNT contents: scaffold (b) Young's modulus (c) tensile strength (d) elongation at break of SF with different HNT loadings. In all cases, the analyses were performed on 10 replicates for each scaffold batch. Means +/- SDs are shown. Statistical analyses using ANOVA followed by Tukey's test were conducted. * $P \leq 0.05$, ** $P \leq 0.01$, *** $P \leq 0.001$, **** $P \leq 0.0001$. Elongation at break data demonstrated no statistically significant differences ($P > 0.05$).

4.3.8 Thermal Properties

4.3.8.1 Thermal Stability

In order to study the effect of HNT on thermal decomposition/stability of SF/HNT nanocomposites, TGA was performed and results are given in Figure 4.16 (a-b) and summarised in Table 4.4. The decomposition temperatures at weight losses of 10 and 50% were labelled as $T_{10\%}$ and $T_{50\%}$ respectively and these values were determined from the TGA curves. Based on thermogravimetric curves in Figure 4.16 (a), all scaffolds demonstrated two distinct phases. The first phase of weight loss was recorded at less than 100 °C, which can be attributed to the evaporation of water. The second phase which occurred at around 270-350 °C is probably due to fibroin degradation associated with the breakdown of peptide bonds [335]. The incorporation of HNT can increase the thermal stability of SF fibres, demonstrating increased decomposition temperatures and reduced weight loss, as shown in Figure 4.16 (a). The onset temperatures of $T_{10\%}$ for SF/HNT scaffold become higher in range from 230-240 °C relative to 201.65 °C for SF scaffold. Similarly, $T_{50\%}$ increased with increasing HNT content in the range of 407-412 °C as opposed to 395.3 °C for plain SF. However at higher HNT contents (5 and 7 wt%) both $T_{10\%}$ and $T_{50\%}$ decreased slightly, as a result of HNT agglomeration. The results suggest that inclusion of HNT into the SF nanofibres improved the thermal stability of the scaffolds. This improvement can be attributed to the high thermal stability of HNT as well as barrier effect toward both mass and heat transport. In addition, it is possible polymer chains and degradation products can enter the lumens of HNT, thus delaying mass transport and further improving the thermal stability [28].

To study the thermal and decomposition behaviour of the SF/HNT nanocomposites in detail, DTG scans of the scaffolds were obtained, as illustrated in Figure 4.16 (b). Three distinguishable peak temperatures of weight loss for pure SF and SF/HNT scaffolds were detected, which were symbolised using T_{d1}, T_{d2}, and T_{d3}. The peak T_{d1}, at around 66.77 °C is probably due to moisture loss, whereas T_{d3} at about 291.32 °C is more likely due to decomposition of the SF protein. Both peaks revealed increasing tendencies with increments in HNT content, in particular T_{d3} reached its maximum value at 312.4 °C when 3 wt% HNT was added. Like the TGA values, all three decomposition temperature peaks decreased at HNT contents of 5 and 7 wt%,

but this was still higher than plain SF. This phenomenon may be attributed to good HNT dispersion and HNT agglomeration at both low and high HNT loadings, respectively. A similar trend was reported by Abdullah *et al.* [581] in that the thermal stability of PVA/starch/HNT nanocomposites at high HNT loadings decreased due to the typical effect of HNT agglomeration.

Table 4.4 TGA, DTG and DSC data of SF and SF/HNT scaffolds. Temperature unit is degrees Celsius.

Sample	TGA		DTG			DSC		
	$T_{10\%}$	$T_{50\%}$	T_{d1}	T_{d2}	T_{d3}	T_g	T_C	T_m
SF	201.65	395.3	68.22	222.41	290.65	139.82	284.95	296.87
HNT particles	—	—	—	—	499.56	—	—	—
SF/HNT 1 wt%	230.84	407.6	70.97	231.37	311.54	138.93	281.19	297.40
SF/HNT 3 wt%	240.63	412.68	70.85	234.35	312.42	138.55	283.51	304.33
SF/HNT 5 wt%	239..88	409.3	69.9	228.26	309.26	137.62	282.14	303.98
SF/HNT 7 wt%	234.52	408.4	68	226.49	308.57	137.44	282.16	298.06

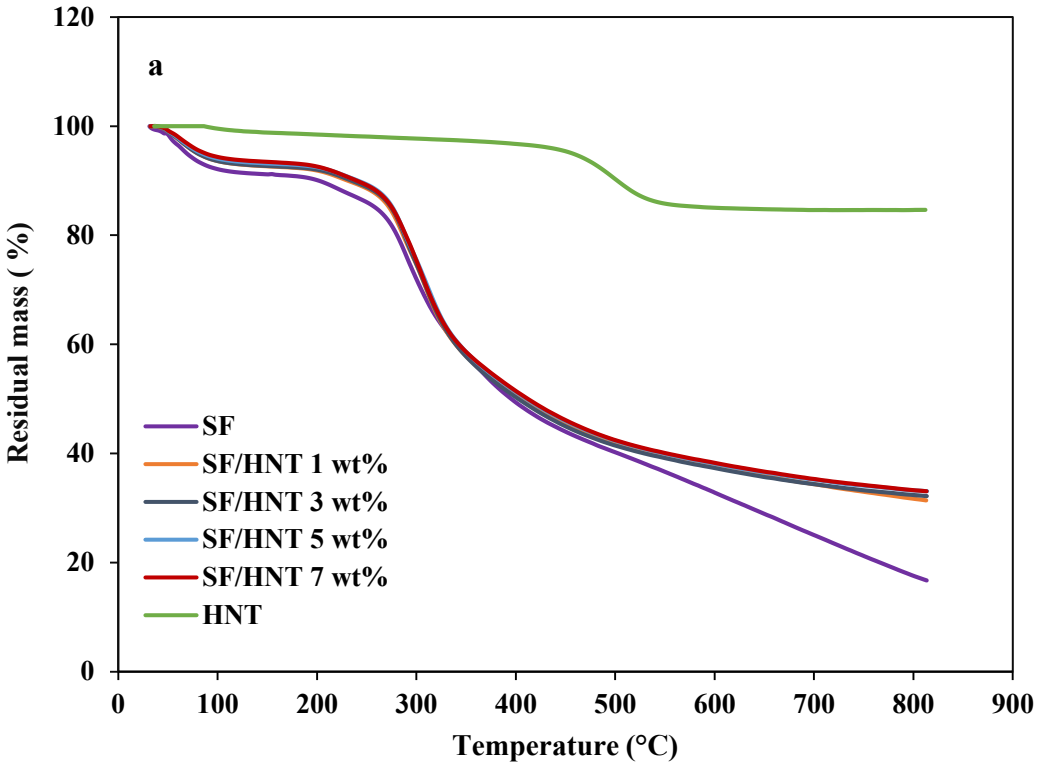

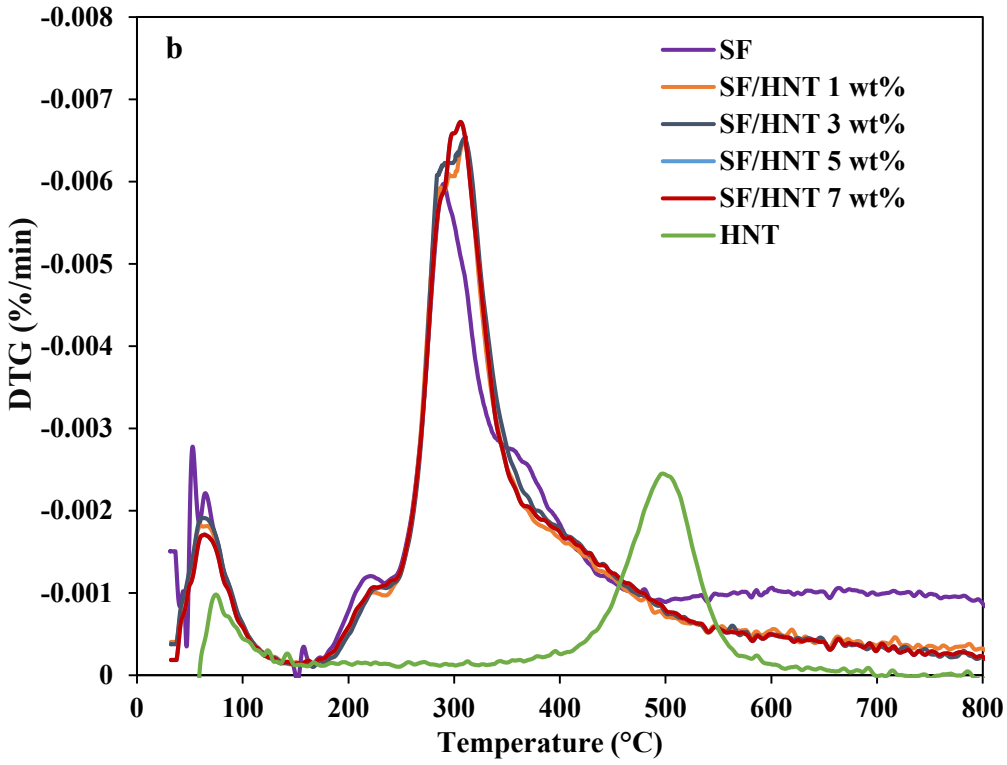

Figure 4.16 Thermal stability of SF, SF/HNT scaffolds and as-received HNTs: (a) TGA curves (b) and DTG curves.

4.3.8.2 DSC Analysis

Figure 4.17 shows the DSC curves of SF and SF/HNT nanocomposites. Endothermic peak at around 60 °C – 70 °C were observed for all samples, which is assigned to the evaporation of water or remaining solvent in the samples [582]. The curve of SF scaffolds exhibits an endothermic peak at 126.71 °C that corresponds to the glass transition temperature (T_g) of SF, an exothermic peak at 284.95 °C related to the crystallisation via the conformational transition to a β-sheet structure of amorphous SF chains (T_C), and an endothermic peak at 294.87°C assigned to the melting/decomposition of SF chains (T_m). It can be found that T_g slightly decreased from 139.82 °C for SF nanofibres to 137-138 °C for the SF/HNT nanocomposites. This may be due to a reduction in chain entanglement of SF caused by the presence of the HNTs, which may have enhanced the motion of the polymeric chains [29, 583].

The addition of HNT shifted the T_C peaks to lower temperature levels, in range of 281–283 °C as opposed to 284.95 °C for SF nanofibres. This trend may be due to the nucleating effect of HNT when embedded within polymer matrices in nanocomposite systems [28, 581, 584], however in my system this effect (if it exists at all) is very trivial.

On the other hand, T_m values of nanocomposite fibres increased with the addition of 3 and 5 wt% HNT, but this was not so evident with the addition of 1 wt% HNT and curiously with the inclusion of 7 wt% HNT, the T_m value was very similar to that of SF alone despite being still higher. The reported inherent high thermal stability of HNT as well as their barrier effect on mass and heat transfer [581] could be contributing to the effects observed.

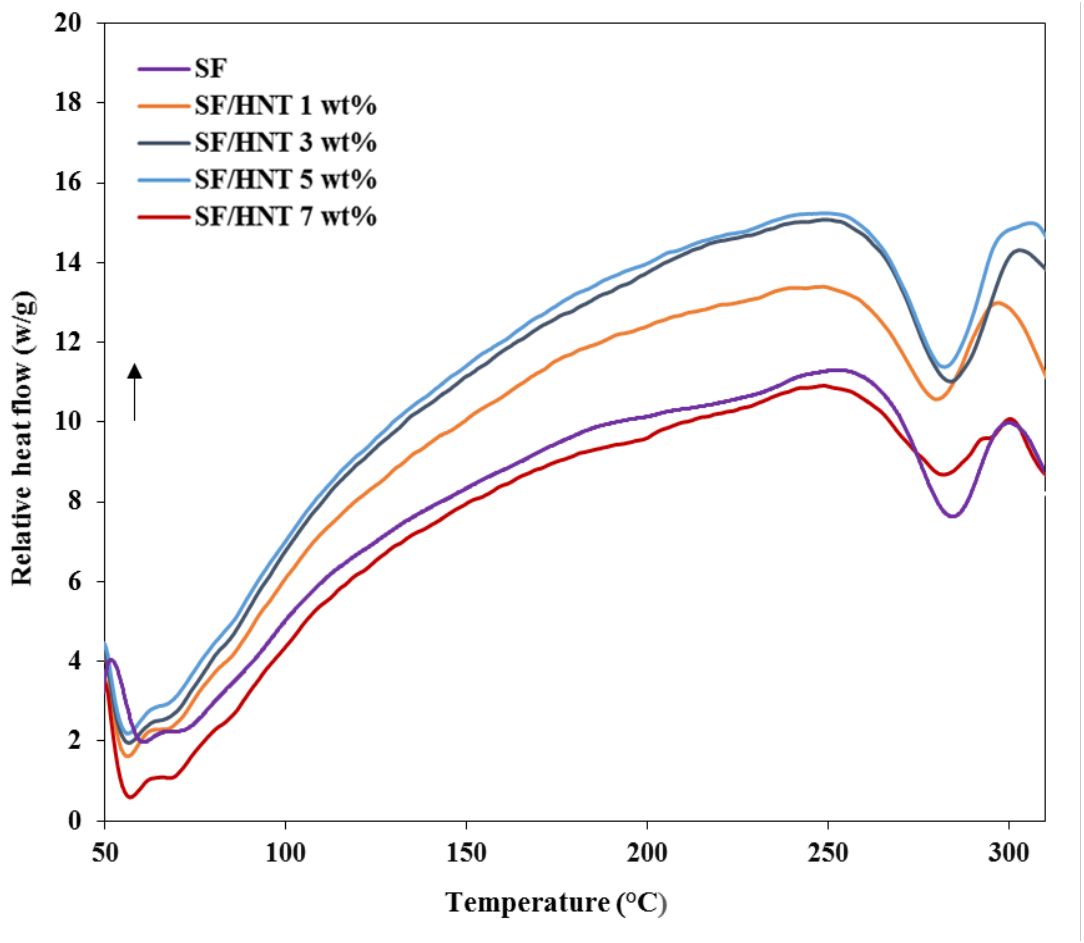

Figure 4.17 DSC curves of SF/HNT scaffolds at different HNT contents.

4.3.9 Proliferation Assay

To assess whether HNT in SF scaffolds could alter cell behaviour the growth of 3T3 cells on the various scaffolds was measured using the CellTiter Blue assay. Cell numbers were determined at days 1 and 3 after cells were seeded onto the scaffolds. As shown in Figure 4.18, cell numbers increased with increasing culture duration for

all scaffolds, and the difference between scaffolds was not significant although the relative number of cells on the SF/HNT 1 wt% was higher than that on plain SF ($p \leq 0.05$). The reason for this is not clear but the increased hydrophilicity of this scaffold (discussed above, Section 4.3.4) may have been a contributing factor. This effect was lost when more HNT were incorporated.

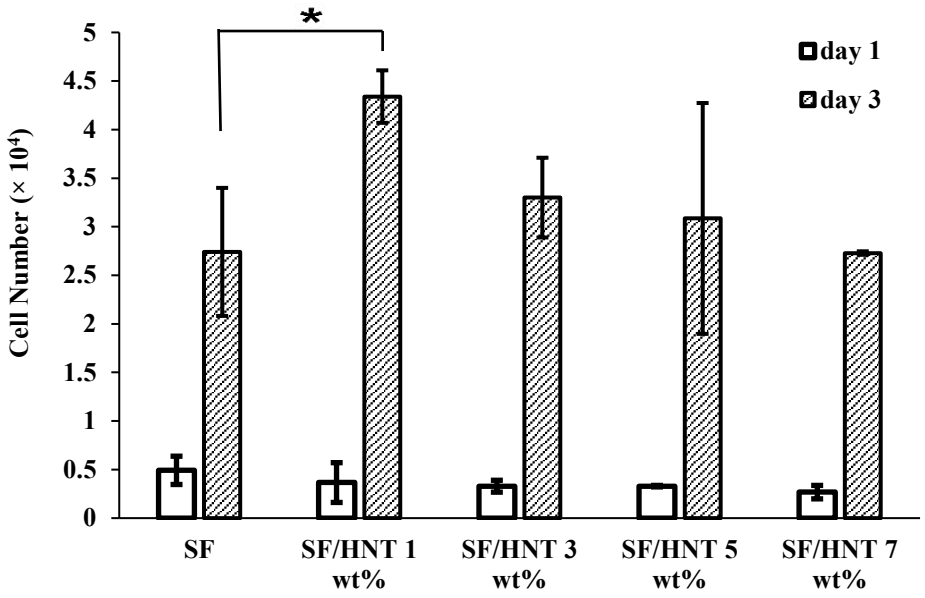

Figure 4.18 Proliferation of 3T3 fibroblasts seeded on SF and SF/HNT nanocomposite after 1 and 3 days of culture.

These data are means +/- SD of 6 replicates. The data are representative of three independent experiments. Statistical analyses was conducted using ANOVA with Fisher's least significant difference (LSD) test. * $P \leq 0.05$.

4.3.10 Cell Morphology

4.3.10.1 Confocal Microscopy

Viability and growth of the 3T3 cells was further assessed by observation of the cell morphology using fluorescence microscopy. Cell nuclei were stained with DAPI (blue) and filamentous actin was stained with phalloidin (green). As shown by the images captured after 1 and 3 days of culture (Figure 4.19, 4.20) cell adhesion and cell spreading on all the scaffolds were visible. The area covered by the cells increased with the culture time as is expected if the cells are proliferating. From day 1 images it

is clear that the cells on the substrates with less HNT (either SF or SF/1 wt% HNT) (Figure 4.19 (a - b)) were more elongated compared with those on substrates with a higher HNT content where the cell shape was more spherical (Figure 4.19 (c - e)). Importantly the cells are uniformly distributed on the materials, however lower densities of cell nuclei were observed for scaffolds with HNT contents of 5 and 7 wt% (Figures 4.19 and 4.20). These data suggest the materials are homogenous. These confocal microscopy data were consistent with the proliferation assay data (Figure 4.18).

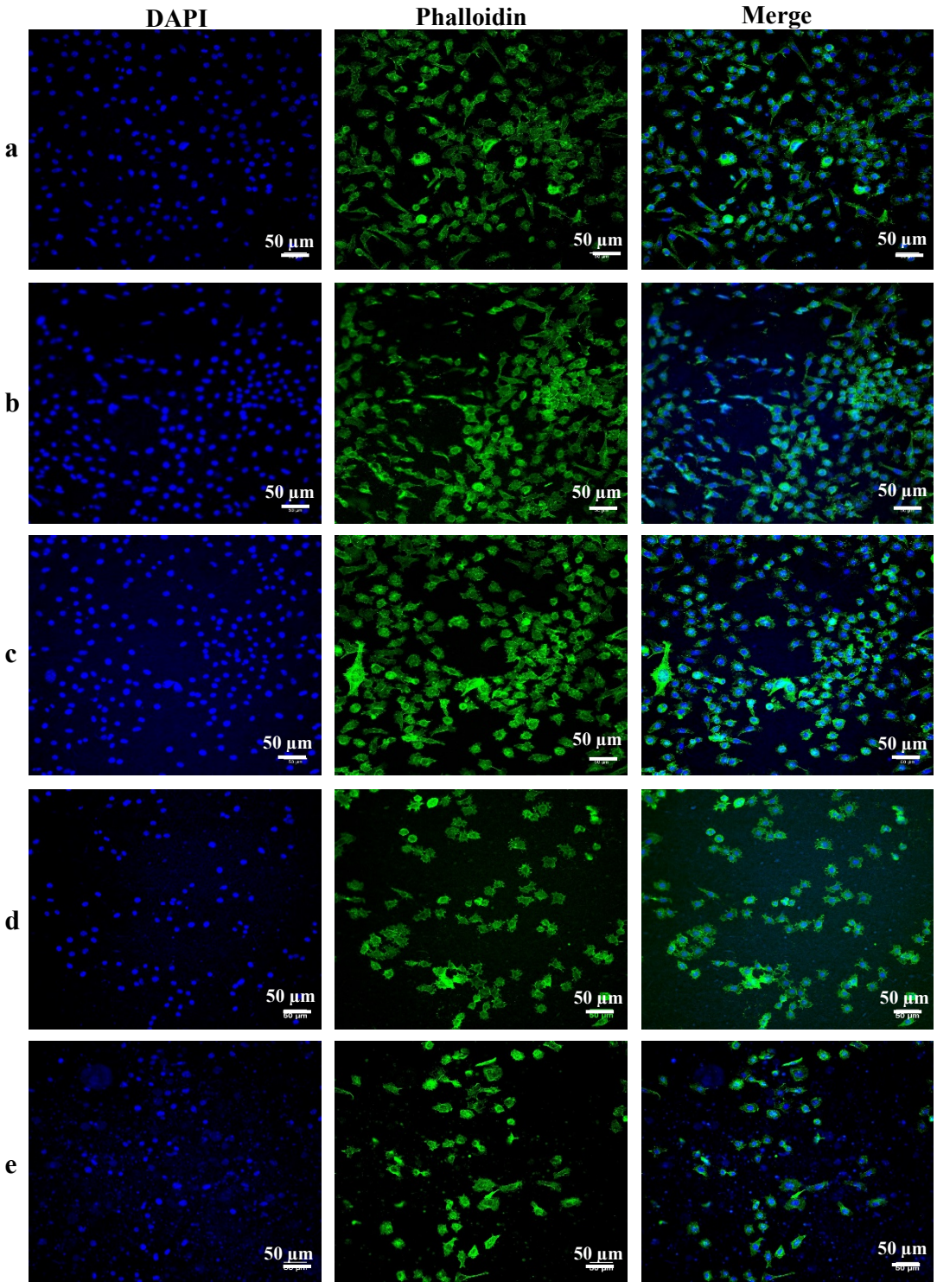

Figure 4.19 Representative images of 3T3 cells cultured for 1 day on a) SF, (b) SF/ HNT 1 wt%, (c) SF/ HNT 3 wt%, (d) SF/ HNT 5 wt%, (e) SF/ HNT 7 wt%.

3T3 cells were fixed with 4% paraformaldehyde before being stained with phalloidin-Alexa Fluor® 488 (Green). Nuclei were stained with DAPI (Blue). Scale bar = 50 µm.

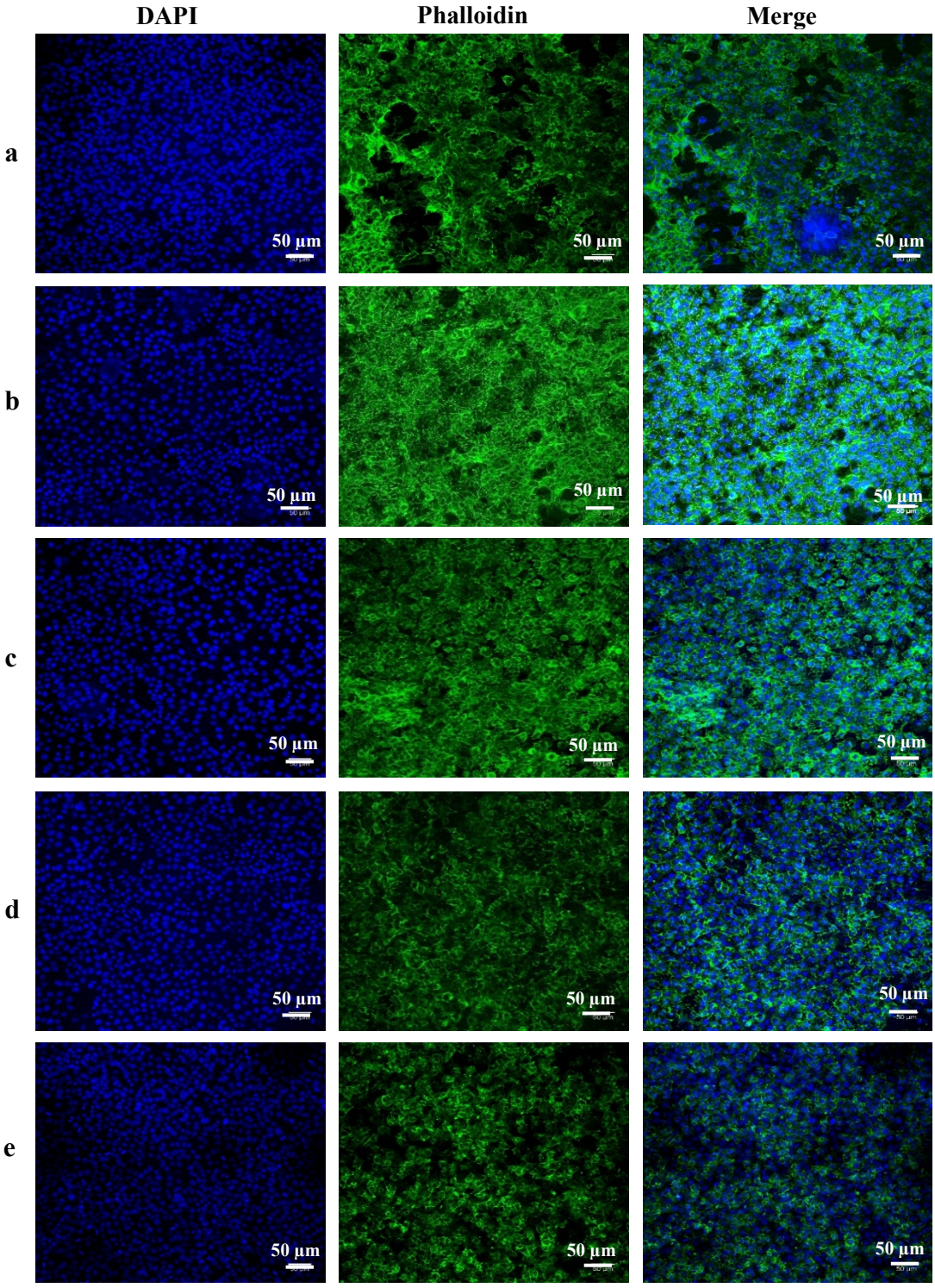

Figure 4.20 Representative images of 3T3 cells cultured for 3 days on a) SF, (b) SF/ HNT 1 wt%, (c) SF/ HNT 3 wt%, (d) SF/ HNT 5 wt%, (e) SF/ HNT 7 wt%.

3T3 cells were fixed with 4% paraformaldehyde before being stained with phalloidin-Alexa Fluor® 488 (Green). Nuclei were stained with DAPI (Blue). Scale bar = 50 µm.

4.3.10.2 SEM Microscopy

Figure 4.21 (a-e) are representative SEM images of SF and SF/HNT scaffolds with or without 3T3 cells after 1 and 3 days of culture. The SEM micrographs indicated that all scaffolds provided a three-dimensional environment with interconnected pores that supported cell attachment confirming the cytocompatibility of HNT containing scaffolds, in accordance with the literature[36] and our immunofluorescent images (Figures 4.19 and 4.20). The cells were less spread on scaffolds with 7 wt% HNT relative to other scaffolds. Cells on the other scaffolds (SF and SF/HNT 1, 3, 5 wt%) were quite elongated indicating adhesion and spreading had occurred. On day 3 of culture the cells were almost a confluent layer on all scaffolds. However, images of the cell layer on SF/HNT 1 wt% scaffolds indicated smaller regions of unoccupied scaffold compared to the other substrates (Figure 4.21). These data are consistent with the cell proliferation data (Figure 4.18) and the confocal microscopy images (Figure 4.20). Thus, introducing low amount of HNT (1 wt%) into SF scaffolds did not change the morphology of cells on this material compared to that of cell on SF scaffolds and the NHT content seemed to have favoured cell growth.

Cell morphology data obtained from both confocal and SEM microscopy are consistent with the cytocompatibility of other HNT based composites that were previously reported[27, 34]. For example, Lue *et al.* [34] investigated the cytocompatibility of HNT and surface modified HNT on poly(l-lactide) (PLLA) composites. They observed superior proliferation rates and cell spreading of mouse embryo osteoblast precursor cells on HNT containing nanocomposites as opposed to pure PLLA. Liu at al. [27] similarly found enhanced attachment and proliferation of mouse fibroblasts on alginate/HNT composites relative to pristine alginate. Furthermore, the addition of HNT into PVA [545], PLGA [36] and chitosan [362] had a negligible effects on cell proliferation and cell morphology. From my data incorporation of 5-7 wt% HNT into SF scaffolds decreased cell spreading, but at lower contents, HNTs did not alter cell morphology.

It is known that some factors of a substrate material for cell growth such as chemical composition, hydrophilicity, roughness and porosity can greatly influence cell adhesion and growth. For example, it was shown by Christopherson *et al.* [585] that smaller fibre diameters were beneficial for neural cell attachment and proliferation when these cells were cultured on non-woven electrospun fibre meshes. In addition, a

decrease in the porosity of a nanofibre matrix was shown to affect cell attachment, resulting in less cell viability [335]. Murphy el al. [553] noted that scaffold surface area plays an important role in initial cell adhesion and also indicated the advantage of larger pores in reducing cell aggregation that develops along the edges of the scaffolds. Another feature which should be considered is hydrophilicity of a scaffold, as this has been shown to favour the attachment and proliferation of cells [586, 587]. Svachova *et al.* [547] noted that NIH-3T3 fibroblasts cells proliferated more on uniform distribution of HNT in polycaprolactane/gelatin nanocomposites rather than in presence of HNT agglomerates. Qi *et al.* [32] reported that the incorporation of HNT did not have a significant impact on cell proliferation when compared to pure poly(lactic-co-glycolic acid) (PLGA) fibres suggesting good biocompatibility of HNT, which is consistent with other literatures [36, 386, 544]. Moreover, it was demonstrated that HNT possess high biocompatibility for human Caucasian lung carcinoma cells at a low concentration [588]

Taken altogether it can be deduced that higher hydrophilicity, WUC, pore volume and better dispersion of HNT at 1 wt% loading cooperate to make the scaffold a more favourable microenvironment for fibroblasts to attach, grow in, and proliferate in respect with other substrates.

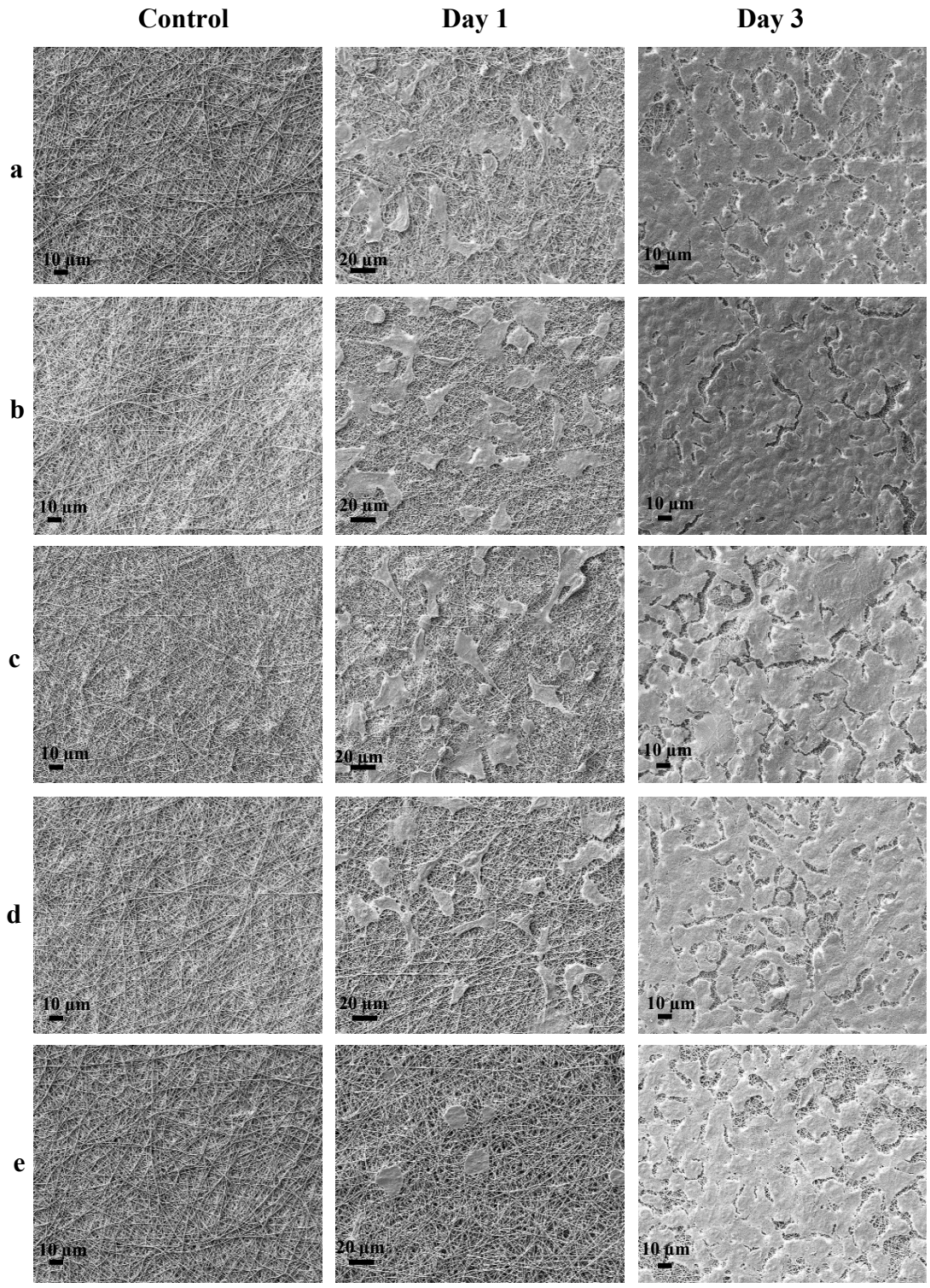

Figure 4.21 SEM Images of cell morphology when cells were grown for 1-3 days on various scaffolds: (a) SF, (b) SF/ HNT 1 wt%, (c) SF/ HNT 3 wt%, (d) SF/ HNT 5 wt%, (e) SF/ HNT 7 wt%; Control: scaffolds incubated in media without cells, scale bar = 10 µm; middle column: day 1 3T3 culture, scale bar = 20 µm; right column day 3 3T3 culture scale bar = 10 µm.

4.3.11 Differentiation Assay

The murine myoblast cell line C2C12 was used to investigate the effect of various scaffolds on cell differentiation. The first step was to determine the compatibility of the scaffolds for C2C12 cell proliferation. Therefore, C2C12 cells were cultured in DMEM (phenol red free) complete media on SF/HNT scaffolds and cell numbers at day 1 and day 2 after seeding were determined using the CellTiter Blue assay. The data in Figure 4.22 are representative of 3 independent experiments. The number of viable C2C12 cells on SF and all the SF/HNT scaffolds after two days in culture were comparable.

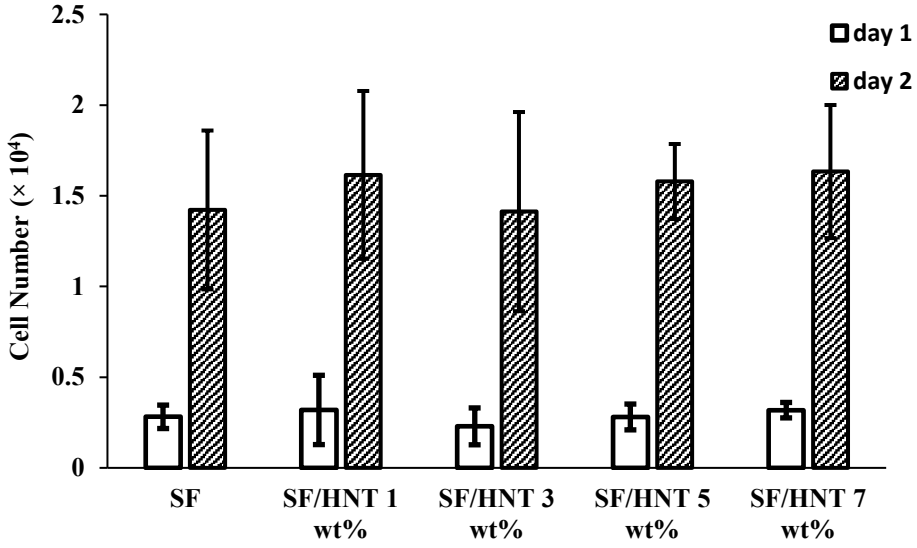

Figure 4.22 C2C12 proliferation on SF and SF/HNT scaffolds after 1 and 2 days of culture.
These data are means +/- SD of 6 replicates. The data are representative of three independent experiments. Statistical analyses using ANOVA followed by Tukey's test were conducted. No significance difference between scaffolds were detected ($P > 0.05$).

The development of skeletal muscle is a multistep process, involving myoblast proliferation initially, then withdrawal from the cell cycle and differentiation into multinucleated myotubes [589]. To determine the effect of SF/HNT scaffolds on C2C12 cell differentiation, C2C12 cells were first allowed to proliferate close to confluence and then were switched into differentiation medium. As shown in Figure 4.23 (a-e) myotube formation, as revealed by staining with an anti-myosin antibody, occurred on all scaffolds. However, the nature of the myotubes formed consistently varied according to the scaffolds on which the cells were growing. Myotubes were longer and

better aligned on SF/HNT 1 wt% scaffolds than on any other substrate. The myotubes that formed on scaffolds containing 3 wt%, 5 wt% and 7 wt% HNT were short, thick and disorganised, and this effect was particularly apparent for the scaffolds containing the high concentrations of HNT. Myotubes on SF scaffolds were aligned but were shorter than those on SF/HNT 1 wt% scaffolds.

It has been reported by others that structural and mechanical properties of scaffolds can play an important role in regulating myoblast differentiation and differentiation generally [590-593]. For instance, Yang *et al*. [594] reported a higher rate of neural stem cell differentiation on PLLA mats with fibre diameters in the nanometre range rather than in the micrometre rage. Some studies showed that hydrophilic surfaces also facilitated interactions with cells and enhanced cell behaviour like the initial attachment, proliferation and differentiation [595, 596]. For example grafting silk fibroin to polyurethane (PU) scaffolds improved the hydrophilicity of the composite and this led to higher proliferation and better differentiation of myoblasts compared to when myoblasts were on pristine PU [597]. Scaffold stiffness, as measured by the Young's modulus is another factor that should be considered, as nonflexible scaffolds are not suitable for myoblast differentiation [592]. An elastic, yet comparatively stiff scaffold would allow myoblasts to differentiate into myotubes without the myotubes from the surface [598]. For optimal myotube length, alignment, and maturation a scaffold elasticity resembled to that of normal muscle is required [599]. Levy-Mishali *et al.* [600] investigated a range of PLGA scaffolds with different stiffness and found that those with a Young's modulus of greater than 200 kPa, enabled myotube formation, but scaffolds with a lower Young's modulus collapsed under the forces generated by the myotubes. Evrova *et al.* [601] demonstrated that the cell response can be manipulated by regulating the microenvironment. It was found that blending poly(ethylene oxide) (PEO) to PLGA resulted in increased myotube formation and self-alignment, when compared to PLGA-only scaffolds, and these functionality differences were attributed difference in scaffold flexibility [602]. Gilmore *et al.* [603] investigated the effect of surface roughness of polypyrrole films on differentiation of C2C12 cells and observed enhanced myofibre formation correlated with films that had less roughness.

In our study, the Young's modulus of all scaffolds were much higher than 320 kPa (in the range of MPa, Figure 4.15 (a)). Thus, it can be presumed that the change in Young's modulus of the scaffolds did not play a critical role in myoblast responses,

moreover, all scaffolds had a modulus that allowed myoblast differentiation. However, other factors including specific surface area, pore volume, hydrophilicity and WUC were different between the scaffolds. From our data one can infer that higher hydrophilicity, and porosity, plus the smoother surface of SF/HNT 1wt% scaffold may have contributed to guiding the alignment and elongation of the myotubes that formed. In contrast, incremental increases in HNT (3, 5, and 7 wt%) in the SF scaffolds resulted in more hydrophobic, rougher surfaces and the number of thin, striated myotubes that formed was markedly reduced, and this was particularly evident at the higher HNT concentrations. Thus, the results obtained here suggest that scaffold stiffness is only one component, and other factors such as WUC and surface roughness should also be taken into account when designing a material to support myoblast differentiation.

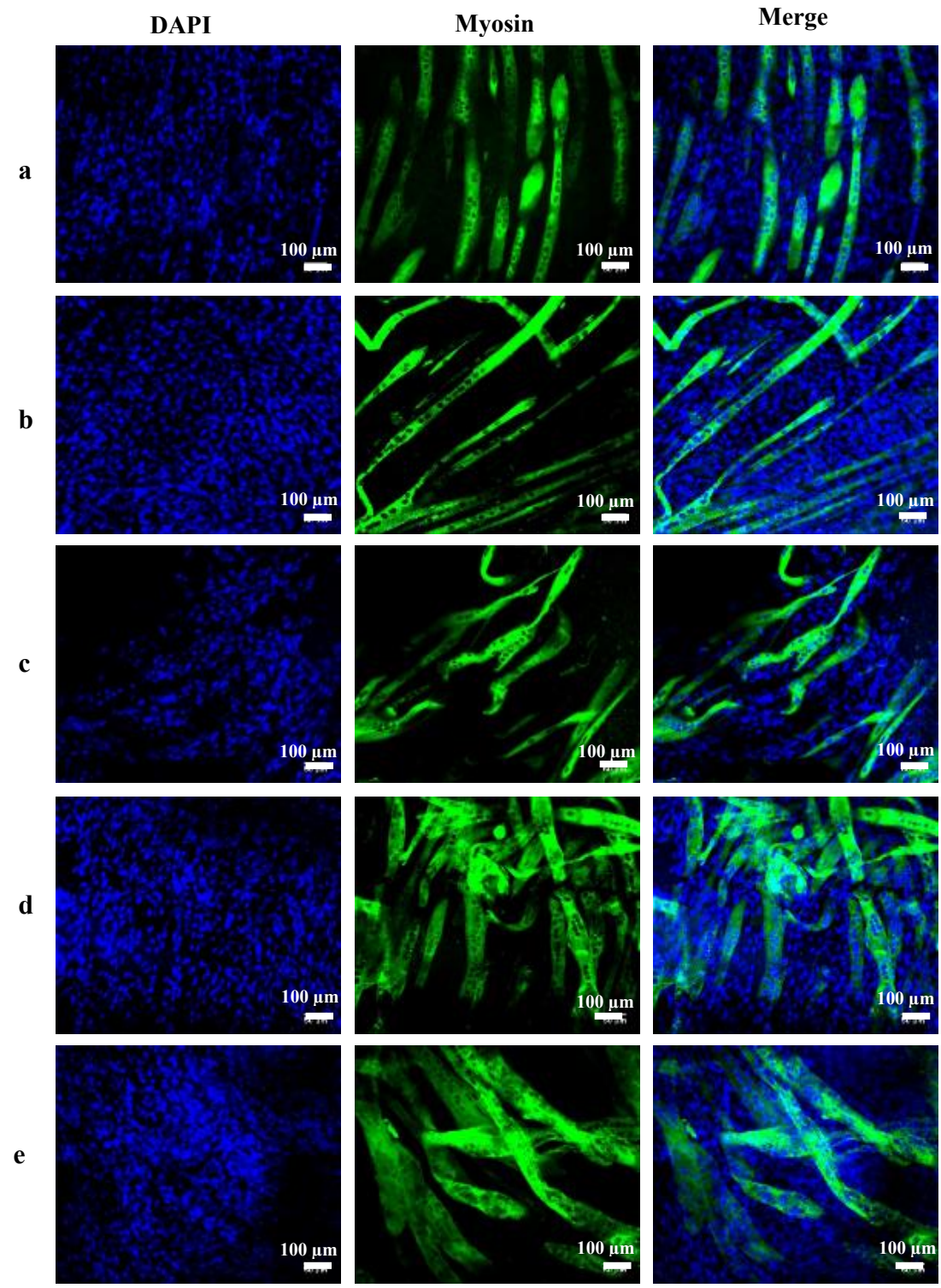

Figure 4.23 C2C12 cell differentiation on SF/HNT scaffolds.

Cells were stained with DAPI (blue) and an anti-myosin antibody (green) to reveal myotube formation: (a) SF, (b) SF/ HNT 1 wt%, (c) SF/ HNT 3 wt%, (d) SF/ HNT 5 wt%, (e) SF/ HNT 7 wt%; Scale bar = 100 µm.

4.3.12 Summary

In this chapter a series of silk/HNT nanocomposites with different HNT contents (1, 3, 5, and 7 wt %) were fabricated by electrospinning. The average fibre diameter of SF was 358.3 (± 65.8) nm and the inclusion of HNT led to increased fibre diameters of up to 437.2 (± 50.72) nm for scaffolds with the inclusion of 7 wt% HNT. Incorporating 1 and 3 wt% HNT improved the stiffness and tensile strength by 47 and 42% respectively, however higher HNT loadings caused a deterioration in the mechanical properties of the scaffold, probably as a result of HNT agglomeration. An increase in thermal stability and a reduction in weight loss for all SF/HNT nanocomposites were also observed; a result consistent with the barrier effect of HNT against mass and heat transfer. In comparison with pristine SF, the addition of 1 wt% HNT, decreased the contact angle and improved WUC of the fibrous mats by 1.5 times. Furthermore, *in vitro* cytocompatibility of all SF/HNT scaffolds were confirmed by the good viability and the spread morphology of 3T3 fibroblasts when they were cultured for up to 3 days on these scaffolds. Additionally SF/HNT scaffolds supported the formation of myotubes by C2C12 myoblasts. However, a combination of low specific surface area and high WUC of the substrate appeared to be the most favourable elements for differentiation of C2C12 cells. Collectively these results suggest that introducing a very low amount of HNT (1 wt%) provides advantageous physical properties, and the cytocompatibility assessment suggests that SF/HNT fibrous scaffolds are promising scaffolding biomaterials for tissue engineering.

Chapter V: Development and Characterisation of Silk/gelatin (SF/gelatin) Blended Nanofibres

5.1 Introduction

The development of decellularisation techniques, to separate the extracellular matrix (ECM) of a tissue from the cells that reside in that tissue, has made attractive the notion of using tissue ECMs as biological scaffolds for clinical applications. Decellularisation removes cells and cell antigens that could trigger an immune response in a recipient, but preserves the ultrastructure and composition of the tissue ECM. Natural ECMs contain many bioactive molecules that drive tissue homeostasis and regeneration. In addition, in the absence of cells, natural ECMs possess excellent biocompatibility and do not elicit adverse effects such as inflammatory responses and graft rejection [604-606]. Reports of the clinical use of decellularised tissues document various levels of success [607, 608]. This may be because cells usually are attached or deeply enclosed within the ECM, and the elimination of all cellular antigens during the decellularisation process without compromising the ECM integrity is a challenge. Moreover, native ECMs are fragile, and can be perturbed upon subsequent cell adhesion and cell generated tension [607, 609].

Polymeric biomaterials are more robust materials and can be produced with tuneable and reproducible mechanical and material properties [1, 610, 611]. However, these materials lack the molecular complexities of the native ECM and as a result they also lack bioactivity. Hence, attempts have been made to incorporate specific ECM components into polymeric biomaterials to enhance their bioactivity [612-614]. Nevertheless, these scaffolds failed to recapitulate the natural sophisticated tissue microenvironment because of the limited set of synthetic or purified ECM components that are available [40, 604, 606].

Consequently, an alternative approach was developed in recent years where the native ECM is integrated into polymeric biomaterials. This method exploits the advantages of both classes of materials and produces scaffolds where material properties can be controlled by the choice of synthetic components, and the bioactivity can be controlled by the cells used to deposit the ECM [609, 615]. The potential of polymer/ECM composites for tissue scaffolding applications has been explored by a few research groups. Gu *et al*. [41] used chitosan/SF scaffolds coated with schwann cell derived (SC)-ECM proteins to repair a 10 mm gap in the sciatic nerve of rats. They found superior regenerative outcomes for SC-ECM modified scaffolds compared to that seen with scaffolds

lacking the SC-ECM proteins. Harvestine *et al*. [39] reported that coating bioactive glass /PLG scaffolds with MSC-secreted ECM proteins potentiated the efficacy of these substrates by promoting cell persistence/viability and function *in vitro* and *in vivo*. Sadr *et al*. [40], manufactured hybrid ECM-polymer materials based on the combination of 3D polyesterurethane (PEU) scaffolds and human MSC (hMSC) secreted ECM. Relative to plain PEU, ECM/PEU composites better supported the osteoblastic differentiation of newly seeded hMSC by up-regulating the expression of typical osteoblastic genes, and increasing calcium deposition (6-fold higher). Goyal *et al*. [609] fabricated poly (desamino tyrosyl-tyrosine carbonate) electrospun nanofibres and coated these with NIH 3T3 cell generated ECM. This hybrid ECM-scaffold displayed enhanced functionality compared to its counterpart without ECM, as it promoted not only cell adhesion, but also new ECM assembly. Levorson *et al*. [38] produced constructs composed of electrospun PCL nanofibres coated with cartilage-like ECM, by coculturing chondrocytes and MSCs on the electrospun nanofibres. However in this case their goal was not to produce an acellular scaffold, but rather to assess the best ratio of chondrocytes:MSCs required to produce a cartilage-like ECM using the least possible number of chondrocytes.

Gelatin is an inexpensive natural polymer derived from the partial hydrolysis of collagen. It is non-immunogenic, biodegradable, easy to process and biocompatible for clinic use [389, 392]. This protein also contains the cell binding motif, arginine-glycine-aspartic acid (RGD), within its sequence making it favourable for cell adhesion. However, gelatin is rarely used alone owing to its high brittleness, and thus to be an effective biomaterial it needs to be modified by crosslinking, or grafting to, and or, blending with other polymers [616-618].

Considering the strengths and weaknesses of SF (discussed in Chapter IV) and gelatin we hypothesised that blending SF with gelatin would overcome the shortcomings of the individual proteins as materials for tissue engineering scaffolds. Moreover, as others have successfully blended SF with gelatin and prepared films and electrospun mats [289, 433, 616, 619] it was assumed that combining the approach of using cell-secreted ECMs on SF/gelatin blended electrospun mats would boost the efficiency of these scaffolds for tissue engineering. In this chapter, we investigated this hypothesis by developing SF/gelatin electrospun nanofibres with different gelatin weight ratios and assessing their material properties using various analyses including scanning electron

microscope (SEM), Fourier transform infrared spectroscopy (FTIR), mechanical testing, water uptake capacity (WUC) tests, water contact angle measurement and X-ray diffraction (XRD) analysis. Subsequently, 3T3 fibroblasts were seeded onto SF/gelatin scaffolds and their proliferation as well as the ECM these cells secreted were evaluated.

5.2 Method Development

5.2.1 Optimisation of SF/gelatin Electrospinning

To optimise the concentration of the SF/gelatin solution for electrospinning two concentrations of 11 and 13 w/v% with SF/gelatin blending ratios of 100/0, 90/10 and 70/30 were used. Electrospinning was set up at an applied voltage of 16 kV, flow rate of 0.3 mL/h and a needle-to-collector distance of 13 cm. Figure 5.1 shows SEM images of electrospun SF/gelatin fibres using a final SF/gelatin concentation of 11 wt% with the different blending ratios. It is clear that regardless of the ratio of SF/gelatin, beads formed on all the nanofibres generated. However, the number of beads decreased with increasing the gelatin content, suggesting that blending gelatin improved both the viscosity and spinability of the 11 w/v% solution [432, 620]. On the other hand, a 13 w/v% SF/gelatin solution resulted in smooth, bead free fibrous structures. The SEM micrographs of these scaffolds are given and discussed in Section 5.3.2.

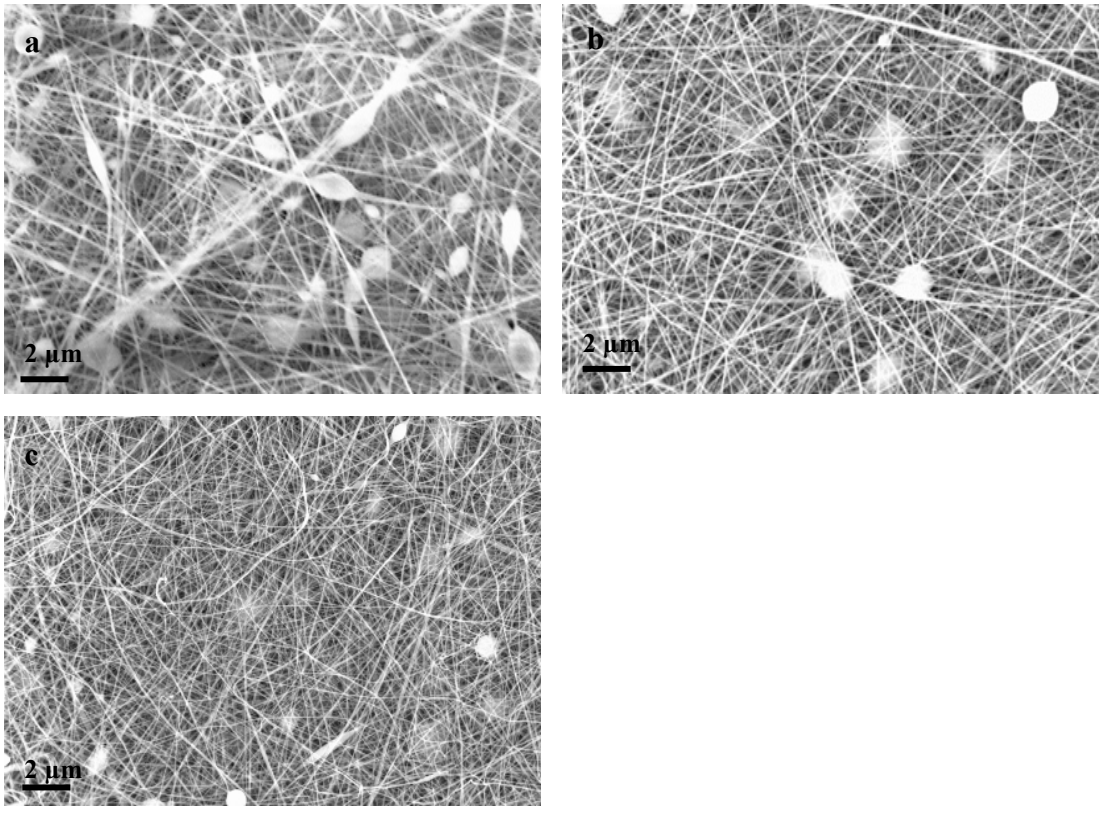

Figure 5.1 SEM micrographs of as-spun SF/gelatin nanofibres at the final concentration of 11 w/v%, with different blending ratios: a) 100/0, b) 90/10 and c) 70/30.

5.2.2 SF/gelatin Post-treatment Optimisation

As the SF/gelatin nanofibres were fabricated for tissue engineering applications their stability in aqueous conditions was essential. Stability of as–spun SF/gelatin scaffolds was examined initially. Scaffolds with different blending ratios were cut into 1×1 cm^2 pieces and incubated in DMEM complete media for 24 h at 37°C in an incubator equilibrated at 5% CO_2. After incubation, all scaffolds regardless of blending ratio were partially dissolved and difficult to transfer. Therefore three post-spinning treatments were investigated namely, immersion in 100% methanol for 15 min and air-dried, GC and GTA (see details in Section 3.2.2.1). Figure 5.2 shows the representative images of SF/gelatin 90/10 scaffolds following the different post-spinning treatments. It can be seen that both methanol and GC resulted in brittle mats that were not usable for further material characterisation. On the contrary, GTA successfully crosslinked the SF/gelatin scaffolds without being brittle. However, the colour of the nanofibres changed from white to light yellow. Consequently, GTA treatment was used subsequently to stabilise SF/gelatin scaffolds.

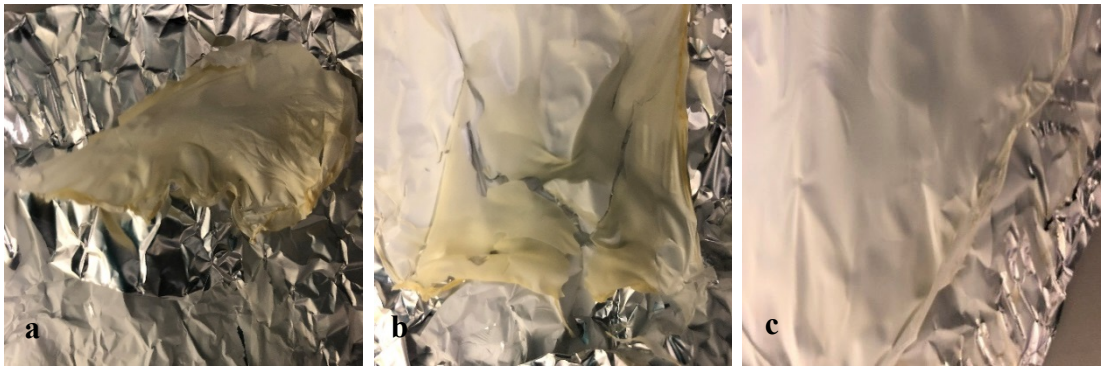

Figure 5.2 Representative images of SF/gelatin 90/10 electrospun nanofibres treated with a) methanol, b) GC and c) GTA.

5.2.3 Extracellular Matrix Deposition Development

To examine whether ECM proteins secreted from fibroblasts remained attached to the scaffolds following decellularisation, immunostaining was performed. 3T3 fibroblast-secreted ECM were prepared, as described in detail in Section 3.4.9.2, Chapter III and stained with primary antibodies that recognise various ECM proteins, for example anti-fibronectin, anti-collagen type I and anti-collagen type IV. Initially, anti-rabbit Alexa Flour 488 was used as a secondary antibody and the results are shown in Figure 5.3

(A). Immunostaining of SF scaffolds treated with methanol revealed that a deposited ECM was preserved during the decellularisation process and all of these ECM proteins were retained on the scaffold. However by this method, the ECM proteins could not be detected for GTA crosslinked SF and SF/gelatin scaffolds with different gelatin blend ratios. A comparison of the isotype control and auto-fluorescent images of each scaffold in Figure 5.3, revealed the GTA crosslinked scaffolds displayed high auto-fluorescence in the absence of antibody and these images were brighter than their corresponding isotype controls. The high auto-fluorescence of scaffolds masked any signals from antibody binding and therefore the presence of the ECM proteins could not be detected. Moreover, the auto-fluorescence of methanol treated SF scaffolds was considerably lower than either GTA cross-linked SF or SF/gelatin scaffolds, indicating GTA cross-linking is responsible for the high background signal observed. Zhu *et al*. [621] also found that GTA crosslinking induced auto-fluorescence of collagen/silk fibres, and this was corroborated by the increased fluorescence intensity of the band between 520–560 nm in fluorescence spectra of collagen fibres upon GTA crosslinking. The formation of a Schiff base (C=N) between the collagen and GTA as well as the increased fibre stiffness that restricted the intramolecular rotation were found to be responsible for this effect.

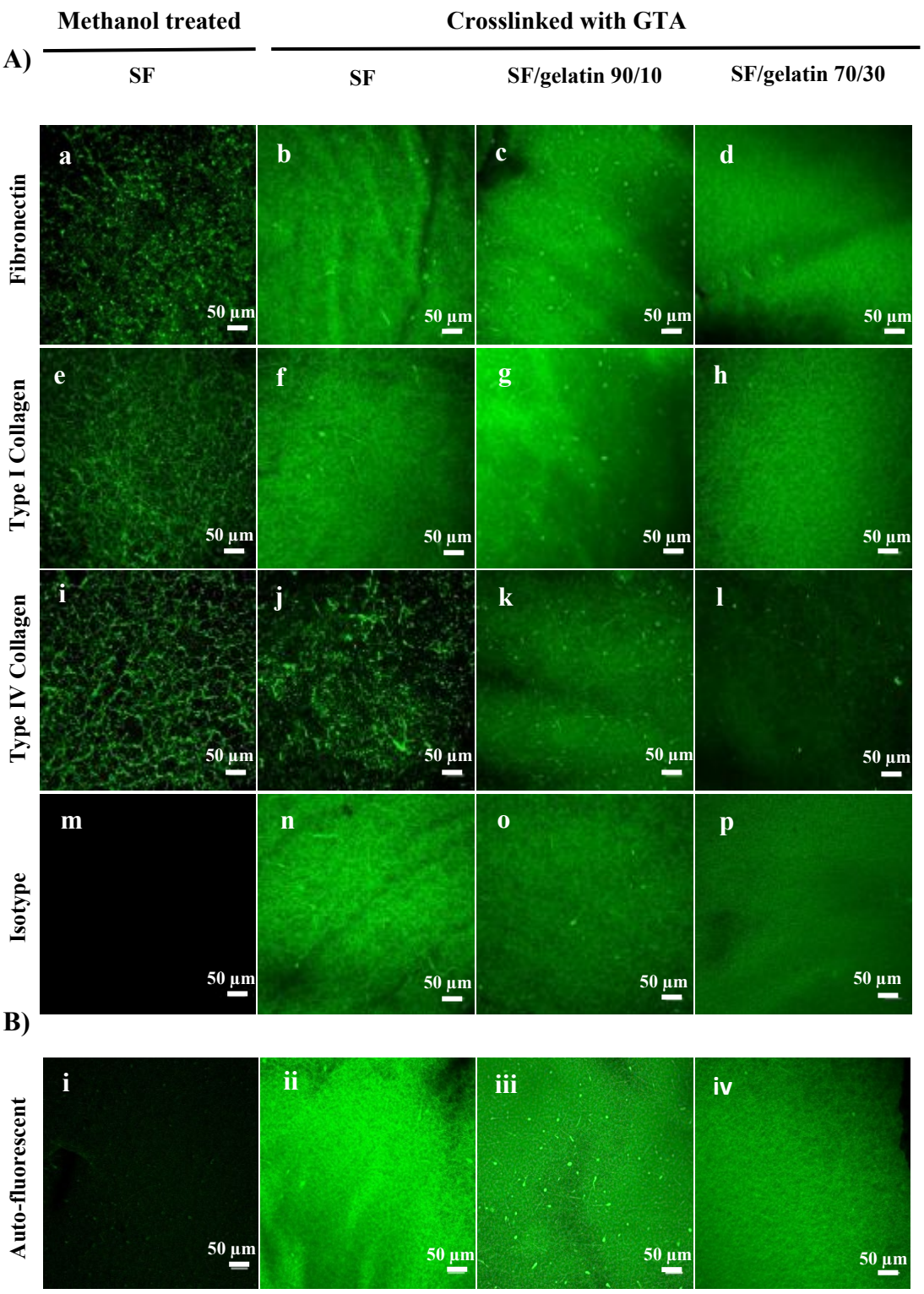

Figure 5.3 A) Immunofluorescence labelling of 3T3-secreted ECM on scaffolds methanol treated SF and GTA treated SF/ gelatin scaffolds with different gelatin ratios.

3T3 cells were cultured for seven days, cells were removed and the ECM was fixed with 4% paraformaldehyde and stained with antibodies recognising fibronectin (a-d), type I collagen (e-h), type

IV collagen (i-l) and isotype control (m-p). The secondary antibody was an anti-rabbit Alexa Fluor® 488. Images were taken using Nikon A1+ confocal microscope. Scale bar = 50 µm.

B) Auto-fluorescent images of scaffolds under 488 nm wavelength. Scaffolds were incubated in media fixed with 4% paraformaldehyde and imaged by confocal microscopy at 480 nm (i) methanol treated SF, (ii) GTA treated SF, (iii) SF/gelatin 90/10, (iv) SF/gelatin 70/30. Scale bars = 50 µm.

To find a wavelength that produced lower background fluorescence, GTA crosslinked SF scaffolds were examined at different wavelengths (*i.e.,* 488, 560 and 674 nm) using the fluorescence microscope, and these images were compared with those for SF methanol treated scaffolds. From Figure 5.4, it is clear that methanol treated scaffolds produced very low background signals at all wavelengths. In contrast, the GTA crosslinked scaffolds produced a very high signal at a wavelength of 488 nm, but the auto-fluorescence was significantly reduced at higher wavelengths and the lowest background was at 647 nm. Hence, an Alexa Fluor 647-conjugated second antibody was used subsequently to detect primary antibody binding to proteins on GTA cross-linked scaffolds. The detailed method is given in Section 3.4.9.3, Chapter III, and the corresponding images and discussion are presented in Section 5.3.10.

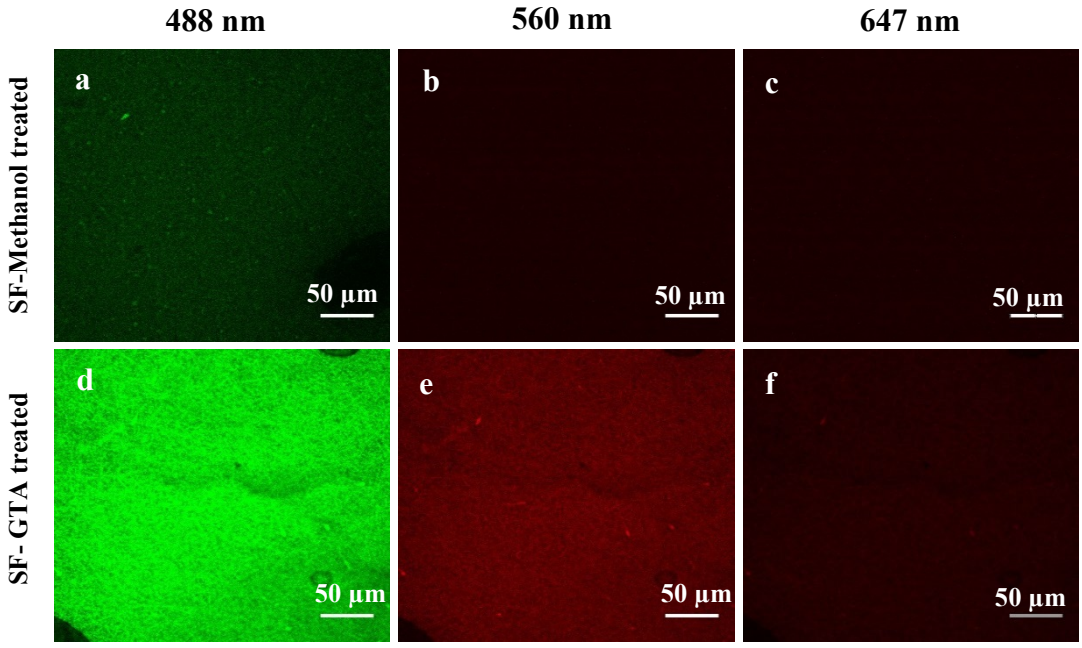

Figure 5.4 Auto-fluorescent check of methanol treated SF under different wavelength.
Scaffolds were incubated in MMC media for 24 h at 37 °C followed by fixation with 4% paraformaldehyde and imaged by Nikon A1+ confocal microscope at (a,d) 480 nm, (b,e) 560 nm and (c, f) 647 nm.

5.3 Results and Discussion

5.3.1 Viscosity

A key factor in determining the fibre morphology is solution viscosity, and this is directly proportional to the solution concentration and polymer molecular weight [622]. Since the concentration of SF/gelatin solution is constant at 13 w/v%, the ratio of SF/gelatin is the only parameter to impact the solution viscosity. Figure 5.5(a) shows the viscosity of SF/gelatin solutions with different blending ratios. Regardless of gelatin content, all SF/gelatin solutions exhibited typical Newtonian fluid behaviour [623]. Because the viscosity of solutions is relatively unaffected by the shear rate, the shear viscosity at a fixed shear rate (*i.e.,* 100 s^{-1}) was measured and these data are presented in Figure 5.5 (b). It was found that solution viscosity gradually increased with the increased weight ratio of gelatin in the SF/gelatin mixture. A similar trend was reported by Bao *et al.* [619] where they showed that blending gelatin with SF improved the solution viscosity and spinnability of these solutions for electrospinning.

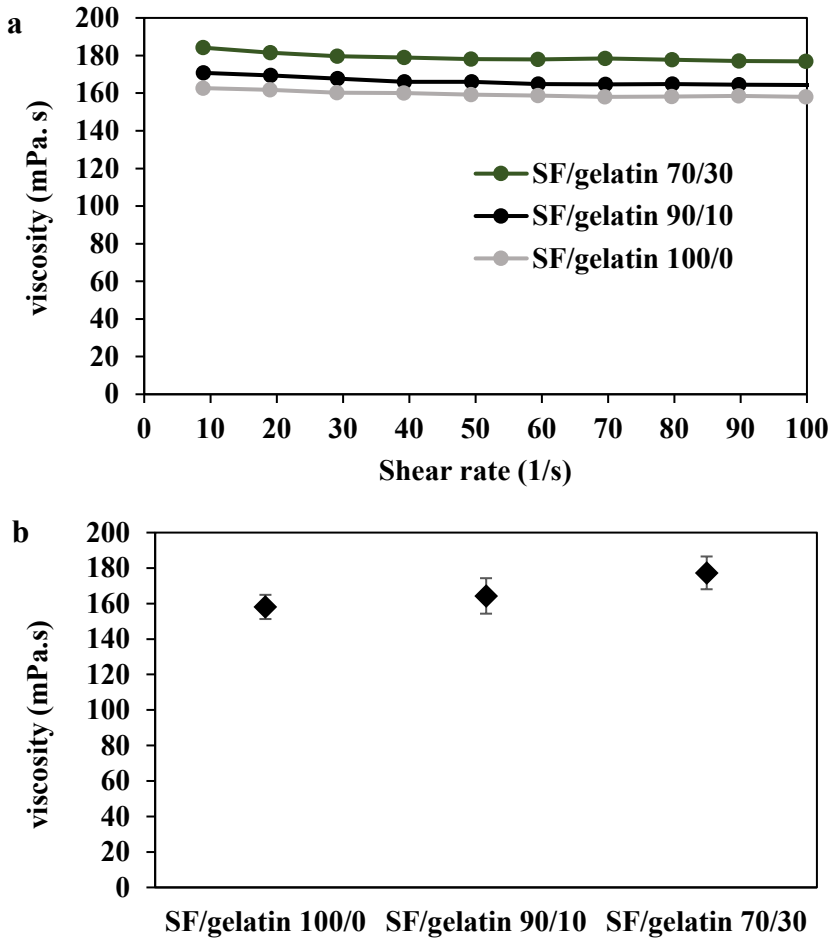

Figure 5.5 (a) Viscosity as a function of shear rate for SF/gelatin solutions in formic acid at constant concentration of 13 w/v %, (b) viscosity of SF/gelatin solution at a constant shear rate of 100 s^{-1}. These data are mean and SDs of 3 replicates.

5.3.2 Fibre Morphology

Figures 5.6 (a-c) show SEM images of as-spun SF and SF/gelatin fibres at various blending ratios. All scaffolds were comprised of homogeneous, bead-free nanofibrous structures. After cross-linking the fibrous structure of all scaffolds was preserved (Figures 5.6 (d–f)); however, the fibres were expanded and the space between the fibres was reduced. Fibre swelling and fibre fusion (particularly evident in Figure 5.6e) may have been caused by partial dissolution of the fibres following exposure to the moisture-rich glutaraldehyde vapour.

From Figures 5.7 (a-c), average fibre diameters for SF, SF/gelatin (90/10), SF/gelatin (70/30) were 403.5, 422.7, and 426.4 nm, respectively. The addition of gelatin into SF formed fibres with marginally larger diameters and less variability. However, this

effect was not statistically significant. These data are in agreement with those obtained by Chomachayi *et al.* [433] for similar fibre materials. This behaviour can be explained by slight increase in solution viscosity with the addition of gelatin (discussed above). Although this increased viscosity would have induced higher resistance against the electrospinning jet, it could be minor because the fibres were not significantly thicker. Additionally, the more uniform fibre distribution implied an improvement of electrospinnability of SF/gelatin solution when the gelatin content was increased [434].

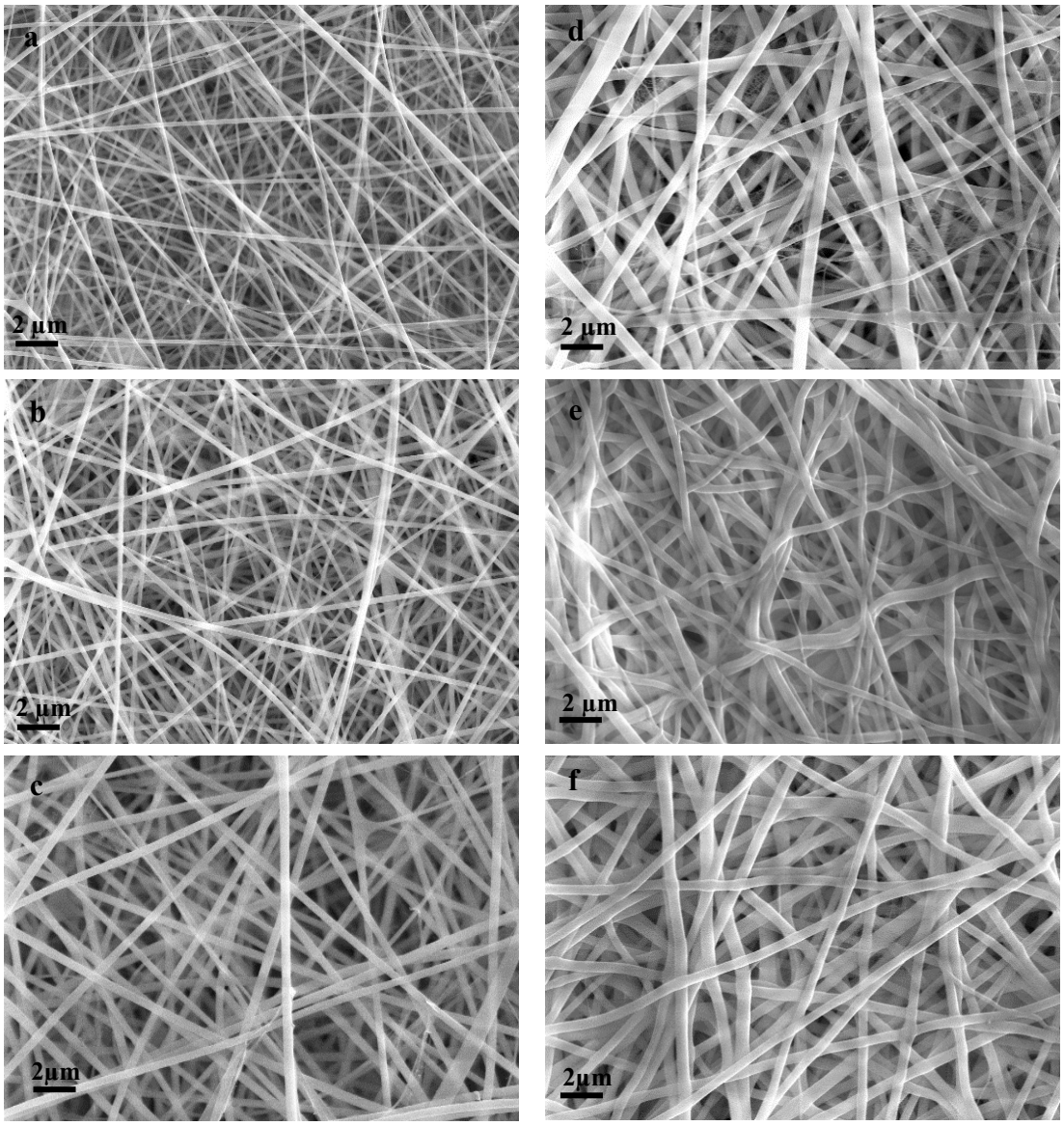

Figure 5.6 SEM micrograph of as-spun a) SF, b) SF/gelatin 90/10, c) SF/gelatin 70/30 and GTA crosslinked d) SF, e) SF/gelatin 90/10 and f) SF/gelatin 70/30.

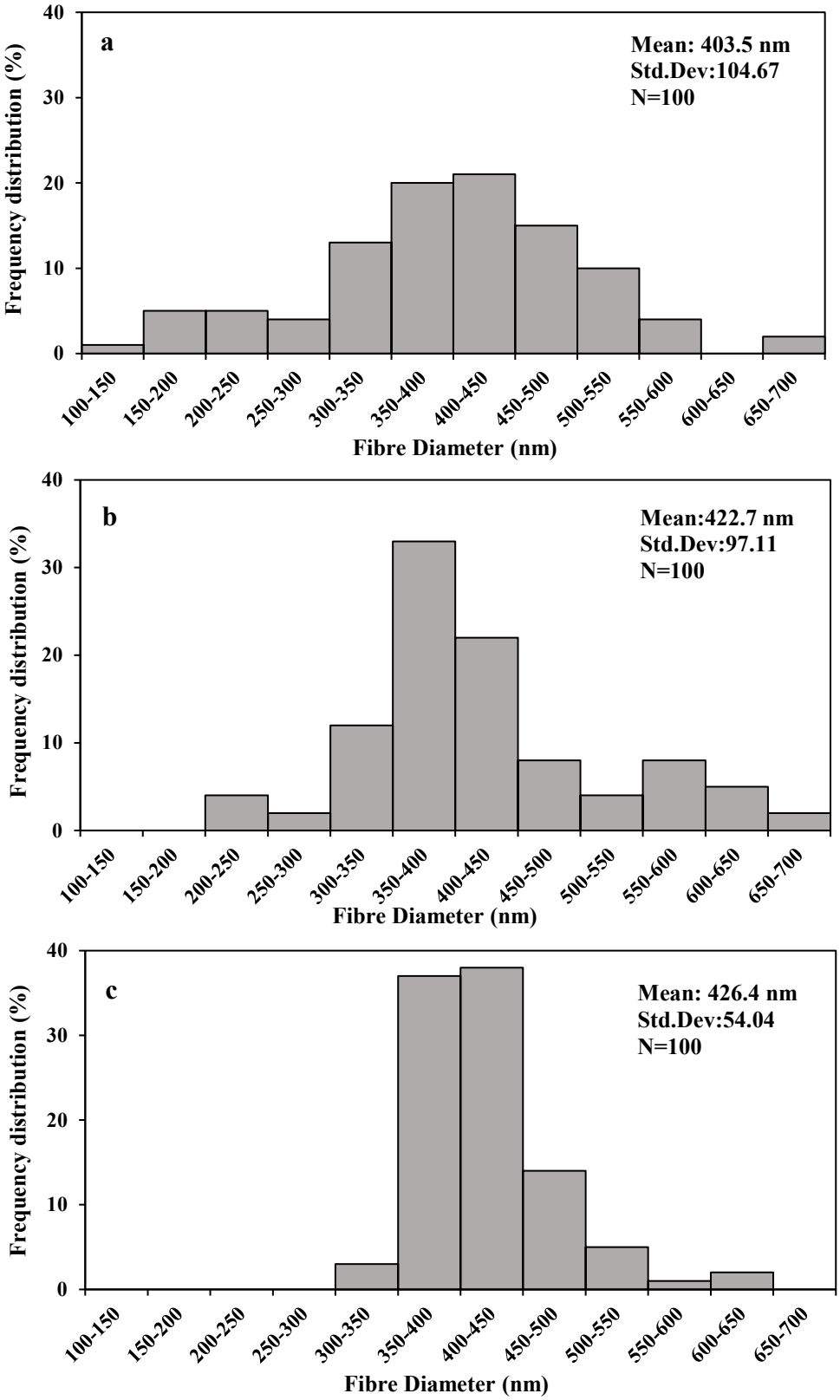

Figure 5.7 Fibre diameter distribution diagrams of GTA crosslinked a) SF, b) SF/gelatin 90/10, c) SF/gelatin 70/30 nanofibres. Statistical analyses using ANOVA followed by Tukey's test were conducted. Fibre diameter demonstrated no statistically significant differences at different gelatin blend ratios ($P > 0.05$).

5.3.3 FTIR Analysis

The FTIR spectra of GTA modified fibre mats are shown in Figure 5.8. The spectrum of gelatin sample showed characteristic peaks at around 3304 cm^{-1} for amide A (N–H stretching vibration), 1640 cm^{-1} for amide I (C═O stretch), 1539 cm^{-1} for amide II (C–N stretching and N–H bending) and 1240 cm^{-1} for amide III (N–H in phase bending and C–N stretching vibration) [405, 406, 624, 625].

In the GTA cross-linked SF fibre mats, FTIR peaks centred at 1627 and 1522 cm^{-1} (Figure 5.8 (a)) and could be assigned to amide I and amide II, respectively, which was indicative of β-sheet structures. FTIR spectra of SF/gelatin fibre mats at the blend ratios of 90/10 and 70/30 revealed characteristic peaks similar to SF implying that the presence of gelatin did not hinder the GTA induced transformation of SF from random-coil to β-sheet conformation [288, 626, 627].

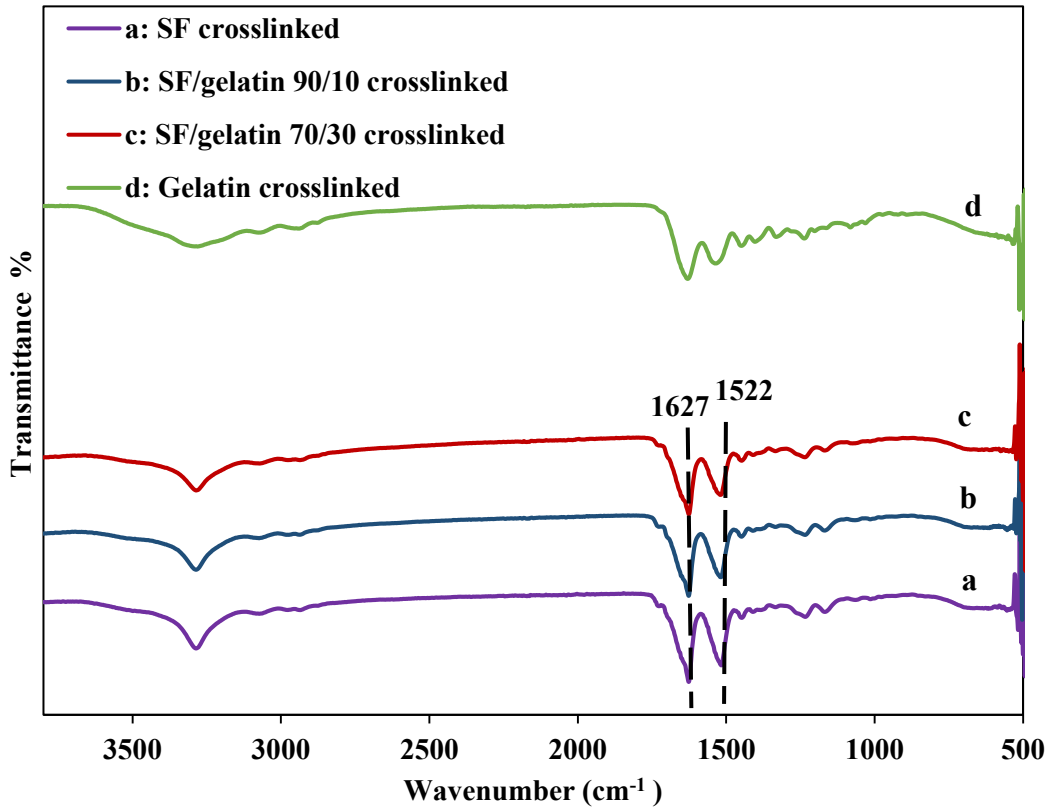

Figure 5.8 FTIR spectra of GTA crosslinked (a) SF, (b) SF/gelatin 90/10, (c) SF/gelatin 70/30 and (d) gelatin.

5.3.4 XRD Diffraction Analysis

Figure 5.9 showed the X-ray diffraction patterns of crosslinked SF, gelatin and SF/gelatin fibre mats. Gelatin possessed a reflection at 2θ = 18.2° corresponding to α-helical structures [420]. The XRD curve of SF demonstrated diffraction peaks at 14.51° and 17.29°, as well as a less intense peak at 20.74° to confirm the existence of β-sheet structures [628-630]. In SF/gelatin fibre mats, the diffraction patterns were almost the same as that for the SF mats, which implied that the β-sheet conformation of the SF was retained in SF within SF/gelatin fibre mats, which is consistent with the FTIR data obtained in this study.

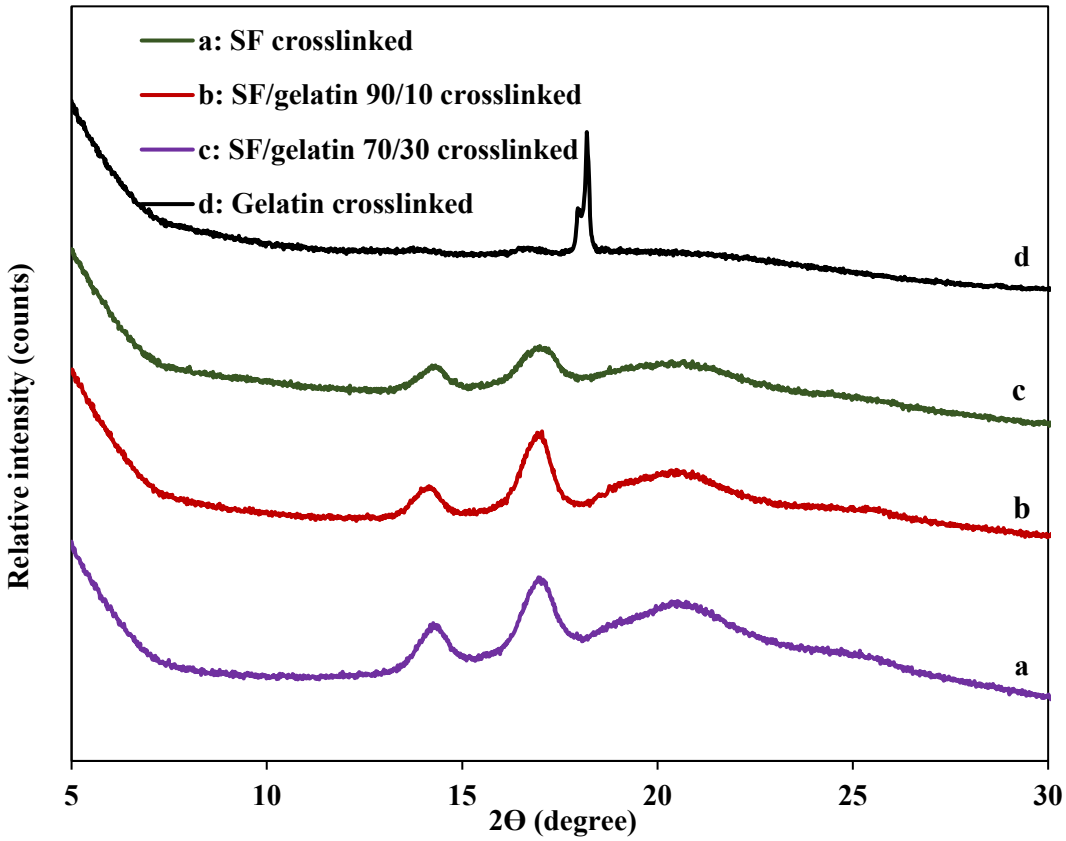

Figure 5.9 XRD patterns of GTA crosslinked (a) SF, (b) SF/gelatin at the blend ratio of 90/10 (c) SF/gelatin at the blend ratio of 70/30 and (d) gelatin.

5.3.5 Degree of Crosslinking

GTA crosslinks proteins through its aldehyde groups. The aldehyde groups react with the free amino groups of lysine and hydroxylysine in the gelatin and SF, forming bonds similar to those of Schiff bases [631, 632]. SF/gelatin mats prepared at the blend ratio of 70/30 had the highest degree of crosslinking of 43%, as opposed to the lowest value

of 34% for SF alone (Figure 5.10). It is probable that incorporation of gelatin with high number of free $–NH_2$ groups enhances the extent of crosslinking for SF/gelatin scaffolds [621, 633].

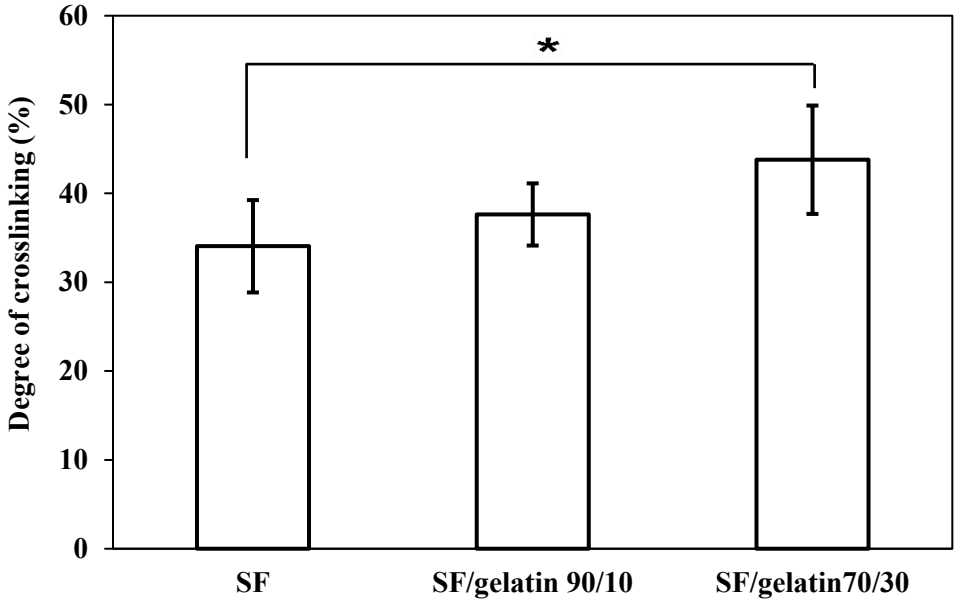

Figure 5.10 Degree of crosslinking for GTA modified SF/gelatin mats using TNBS assay. These data are mean and SDs of 3 replicates. Statistical analyses was performed with Kruskal–Wallis test followed by Dunn's multiple comparison test. * $P \leq 0.05$.

5.3.6 Porosity Measurements

Tissue scaffolds to be used for tissue engineering require a certain level of porosity, as has been discussed previously. Moreover, the porosity requirement varies depending on the tissue that is being repaired and the degradation rate of the scaffold. Increasing the gelatin content appeared to decrease the porosity of the GTA treated SF/gelatin fibre mats (Figure 5.11). The porosity of SF/gelatin fibre mats at the blend ratios of 90/10 and 70/30 were 59% and 47%, respectively as opposed to 62% for pure SF mats. The crosslinking data indicated the addition of gelatin to SF gave rise to a higher degree of crosslinking, which in turn yielded more fibre twining (see Figure 5.6) with more evident reduction of mat porosity at the SF/gelatin ratio of 70/30. It has been reported that an increase in fibre diameter at higher gelatin levels can contribute to the decreased porosity of their fibre mats [634, 635]. However the fibre diameters were not significantly different in this study.

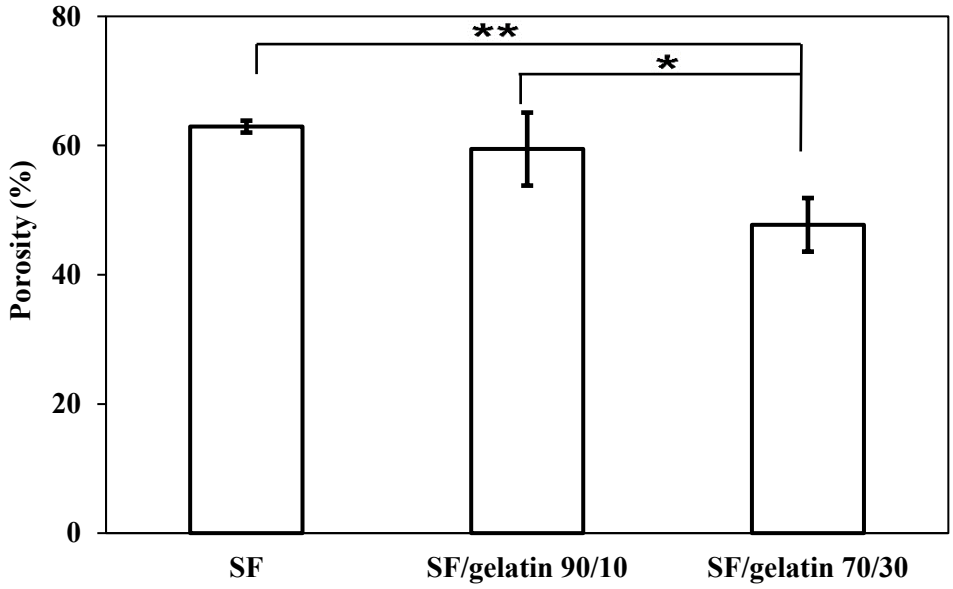

Figure 5.11 Porosity of GTA treated nanofibres SF/gelatin mats. These data are mean and SDs of 5 replicates. Statistical analyses using ANOVA followed by Tukey's test were conducted. * $P \leq 0.05$, ** $P \leq 0.01$.

5.3.7 Contact Angle and Water Uptake Capacity

To investigate the effect of gelatin on the hydrophilic properties of SF/gelatin fibre mats, the water contact angle and water uptake capacity of crosslinked mats were measured and the results are presented in Figure 5.12. The water contact angles measured on all of the fibre mats were less than 90°, which is indicative of hydrophilic features. The addition of gelatin did not significantly alter the contact angle of fibre mats, the contact angles varied from 75.31 ± 7.5° for SF to 69.94 ± 7.68° for SF/gelatin at the blend ratio of 70/30. These data can be explained by the hydrophilic nature of gelatin [425]. On the other hand, as shown in Figure 5.12, the WUC of SF was much higher with value of 405% for pure SF as opposed to 350% and 232% for SF/gelatin fibres at the blend ratios of 90/10 and 70/30, respectively. Such a finding was probably due to the incorporation of gelatin into the SF matrix and the increased GTA crosslinking resulting in more dense fibre mats, so that it was difficult for water molecules to enter the scaffolds [636]. As shown earlier higher gelatin content led to lower fibre porosity, thereby limiting water diffusion into the fibre mats. Xiao *et al.* [633] reported a similar behaviour for SF/gelatin hydrogels crosslinked with genipin, and

this study also suggested that the wettability of fibre mats could be modulated by adjusting the SF/gelatin blend ratios.

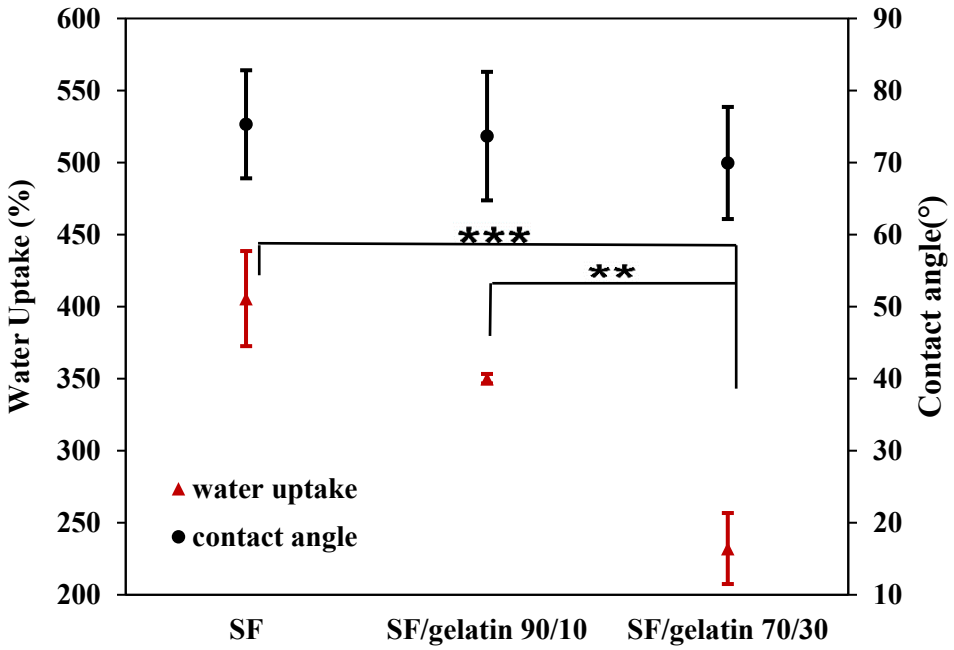

Figure 5.12 water uptake capacity and contact angle for GTA modified SF/gelatin mats. These data are mean and SDs of 5 replicates. Statistical analyses using ANOVA followed by Tukey's test were conducted. ** $P \leq 0.01$, *** $P \leq 0.001$. Contact angle data demonstrated no statistically significant differences ($P > 0.05$).

5.3.8 Mechanical Properties

Mechanical properties of crosslinked fibre mats with different gelatin content were shown in Figure 5.13. The mechanical properties of SF scaffolds were not affected by the addition of gelatin ($P > 0.05$). Tensile strength and Young's modulus of SF were 11.21 MPa and 268.67 MPa, respectively. This increased up to 14.23 MPa and 342.31 MPa accordingly when 30 wt% of gelatin was added, but the difference was not significant. Based on crosslinking data (Figure 5.10) where the crosslinking density became higher with increasing the gelatin content, and as the proteins were restrained by the crosslinking sites, it was expected that the mats would be stiffer in the presence of more gelatin. Others have reported that in their systems the formation of intermolecular interactions between SF and gelatin enhanced the mechanical properties of SF/gelatin mats [335, 408, 637]. Moreover, higher gelatin content gave rise to higher crosslinking densities resulting in fibre fusion, and thereby decreasing the

porosity and increasing fibre entanglement which was reported to result in mechanical strength enhancement [638, 639]. However our data did not fit this pattern.

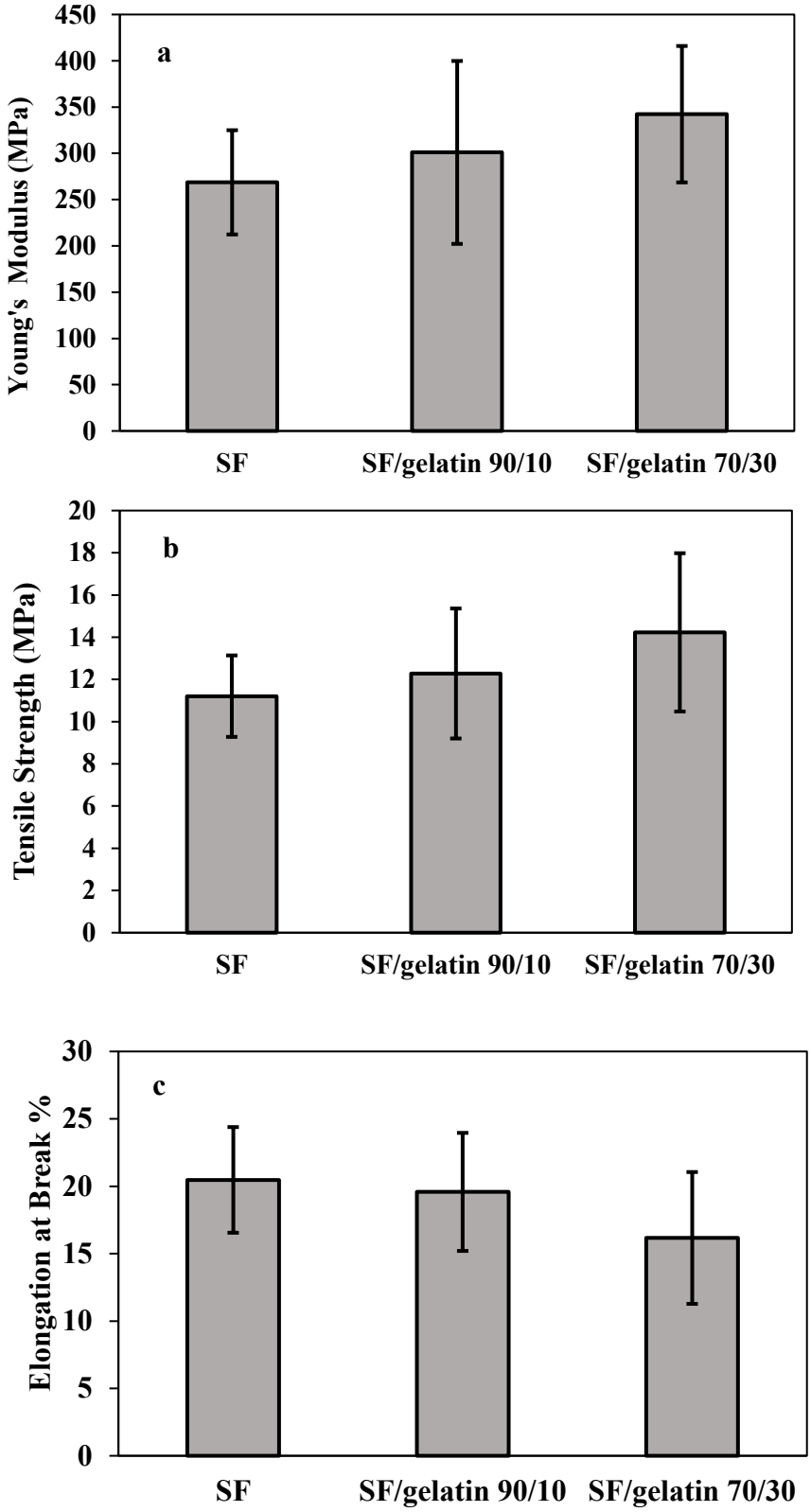

Figure 5.13 Mechanical properties of GTA modified SF/gelatin fibre mats: a) Young's modulus, b) tensile strength and c) elongation at break. These data are mean and SDs of 10 replicates. Statistical

analyses using ANOVA followed by Tukey's test were conducted. No significance difference between scaffolds were detected ($P > 0.05$).

5.3.9 Proliferation Assay

Cell viability and cell proliferation as a function of the time on a scaffold is indicative of the cell compatibility and appropriateness for tissue engineering of particular scaffolds. To acquire an insight into cytocompatibility of SF/gelatin fibre mats, 3T3 cells were seeded onto GTA treated SF/gelatin scaffolds. Cell proliferation was determined and the results are displayed in Figure 5.14. After 1 day, there was no significant difference in cell proliferation on SF or the SF/gelatin fibre mats regardless of the SF/gelatin ratio. However, after 3 days cell proliferation markedly increased in all samples and the analysis suggested that the rate of proliferation was higher on SF mats compared to the proliferation rate on the SF/gelatin fibre mats with the highest gelatin ratio. It was expected that cell proliferation would increase with increasing gelatin content, a finding seen by others and interpreted as due to the greater numbers of integrin binding sites [640-642]. Surprisingly, we found the opposite trend; with more gelatin in the SF scaffolds cell proliferation was lower. One plausible reason for this result was that crosslinking consumed the glutamate and aspartate residues in Arg-Gly-Asp (RGD) in gelatin, and thereby reduced the number of integrin binding sites [643]. Moreover, alterations in the morphology, porosity and WUC of scaffolds with the addition of gelatin, could also have contributed to the reduced cell proliferation. Previous research by Yeo *et al.* [58] showed a reduction in keratinocyte spreading and proliferation on GTA crosslinked SF/collagen mats, as compared to mats of either neat collagen or neat SF. They ascribed this finding to the different conformation of blended SF/collagen matrices due the interaction between collagen and SF. Interestingly, they did not observe the same effect for fibroblasts seeded onto these mats. Yao *et al.* [644] reported that a higher gelatin content in PCL/gelatin composites did not necessarily result in better cell responses and they indicated the important role of the physical microenvironment, characteristics such as mechanical properties, in directing cell responses. In addition, Grover *et al*. [643] found that crosslinking gelatin films with a carbodiimide had detrimental effect on cell responses and they suggested this was a consequence of changes in physical properties such as roughness and stiffness of the gelatin films as a result of the crosslinking, as well as a reduction in the number of available cell binding sites. It is well documented that highly porous structures with

interconnected pores assist with the provision of nutrients and gas exchange, which then helps cell proliferation and cell migration [551, 634]. Higher WUC and more storage of water can help to store growth factors in the scaffold as well as facilitating biofluid transport and cell migration [645]. Therefore, possibly the superior porosity and WUC of pristine SF scaffolds compared to SF/gelatin scaffolds, facilitated better nutrient transport and diffusion of signalling molecules, as well as providing more space for cell proliferation and migration, thereby giving rise to the higher proliferation rate.

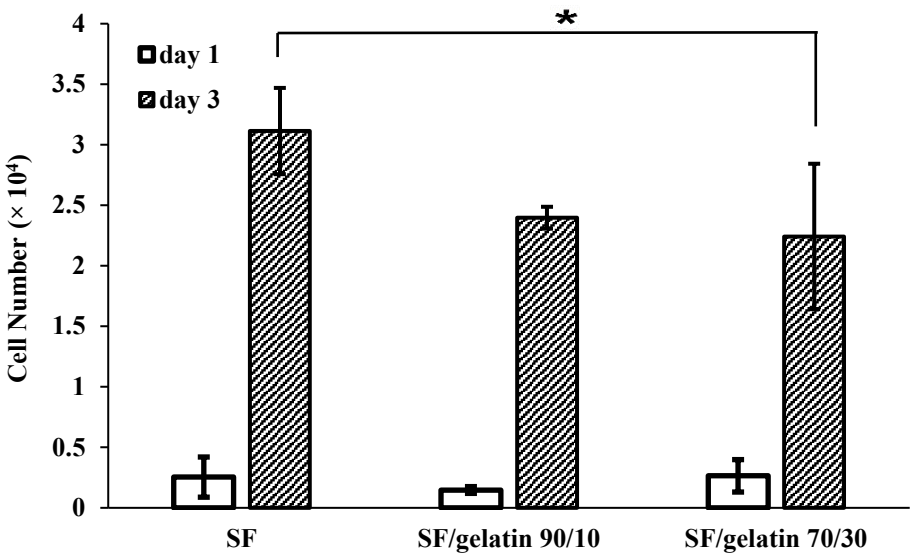

Figure 5.14 Proliferation of 3T3 fibroblasts seeded on GTA treated SF/gelatin fibre mats after the first and third days of culture. These data are means +/- SD of 6 replicates. The data are representative of 3 experiments. Statistical analyses was performed with Kruskal–Wallis test followed by Dunn's multiple comparison test. *P < 0.05.

5.3.10 Extracellular Matrix Deposition

To determine if 3T3 cells deposited an ECM onto the scaffolds that remained following decellularisation, immunostaining was performed using antibodies recognising type I collagen and fibronectin (Figure 5.15 (a-f)). These experiments confirmed that cells deposited their ECM onto the fibrous scaffolds, and the deposited ECM was preserved during the decellularisation process as staining of both type I collagen and fibronectin was detected. However, not all scaffolds triggered the same level of ECM protein deposition. Both fibronectin and collagen type I staining

intensity appeared to be the strongest on plain SF followed by SF/gelatin 90/10, and the SF/gelatin 70/30 scaffolds showed considerably lower levels of staining with the antibodies used. These findings were consistent with the proliferation assay data, as the highest gelatin content resulted in less cell growth. It is therefore expected that there would be less ECM deposited on those scaffolds that were less favoured for cell growth. As discussed in Section 5.3.9, differences in the morphology, porosity and WUC of the SF and SF/gelatin scaffolds were reflected in 3T3 cell growth patterns and accordingly the amounts of ECM that were secreted.

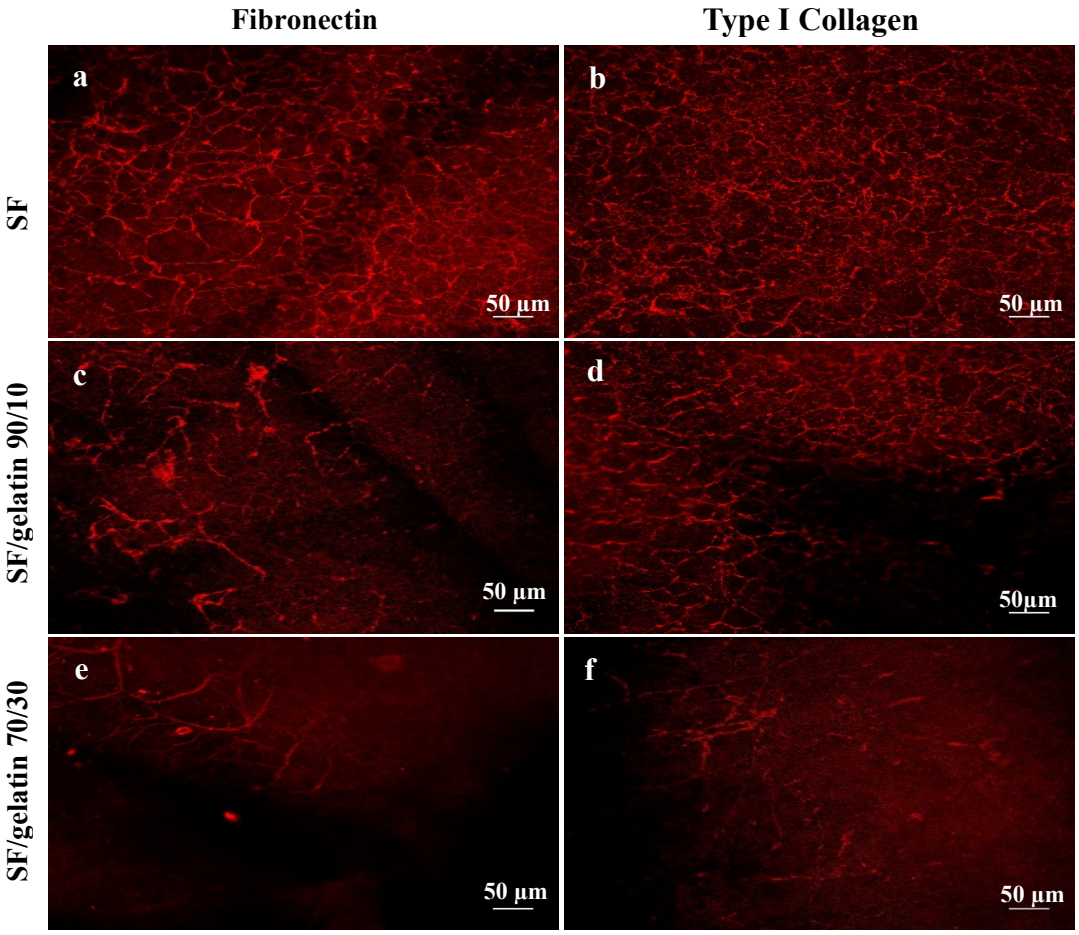

Figure 5.15 Deposition ECM proteins by 3T3 fibroblasts on GTA treated SF/ gelatin scaffolds.
3T3 fibroblast cells (0.25×10^4 cells per scaffold) were cultured for seven days, then cells were removed and the ECM was fixed and stained with antibodies recognising fibronectin (a, c, e) and type I collagen (b, d, f). The secondary antibody was an anti-rabbit Alexa Fluor® 647. Images were taken using a Nikon A1+ confocal microscope. Scale bar = 50 µm.

5.4 Summary

SF/gelatin fibre mats with different gelatin content were successfully prepared by electrospinning and then stabilised with GTA. These scaffolds possessed different properties according to the gelatin content, although incorporating 30 wt% gelatin did not significantly enhance either the tensile strength or the Young's modulus. Increasing the gelatin content decreased the porosity and WUC of SF/gelatin fibre mats relative to those of neat SF. SF/gelatin fibre mats at the blend ratio of 70/30 had the lowest 3T3 cell proliferation rates and the least ECM deposited. Such findings may be associated with the fact that GTA crosslinking induced changes in the physical characteristics of the scaffolds when the gelatin content was highest. It is probable, WUC and porosity played a role in regulating cell functions. As a result, it could be concluded that plain SF scaffolds provided a superior microenvironment for cell growth and ECM deposition compared to the SF/gelatin fibre mats.

Chapter VI: Extracellular Matrix (ECM) Deposition on Silk based Scaffolds and Their Characterisation

6.1 Introduction

The skin safeguards the body from the outside environment. The ability of the skin to self-renew enables wound repair and the replacement of dead cells. Most cutaneous wounds heal in a few days, however if the damage is extensive and extends into the dermis, medical intervention may be required [646, 647]. Split-thickness autologous skin grafting is considered as the traditional therapeutic strategy for treating severe wounds. However, this approach is not viable in cases of extensive injury where considerable amounts of skin are needed and available healthy donor sites are lacking. Thus, the development of engineered skin graft substitutes has emerged as a clinical need [648, 649].

Grafting of *in vitro*-expanded keratinocytes, is an alternative approach to augment the repair of damaged skin. For this purpose, keratinocytes are usually isolated from a small skin biopsy and are expanded in culture before being applied to the patient's wound sites [650]. However, a layer of keratinocytes is very fragile and simply covering the wound with a keratinocyte layer may not be the best engraftment procedure. The addition of a bioscaffold to support the cell layer can improve mechanical properties of the graft and facilitate cell survival and growth [462, 651].

SF has been extensively used to engineer scaffolds for repairing many tissues including skin, because of its high mechanical strength, cytocompatibility and malleability [652, 653]. SF is known to support the adhesion of human keratinocytes and fibroblasts [231, 519, 654, 655] and a recent study conducted by Zhang *et al.* [656] provided systematic preclinical and clinical evidence that SF films can be used for the healing of full-thickness skin defects using both small and large animal models. SF based scaffolds prepared by electrospinning have been shown to outperform SF films or a woven matrix of SF microfibres when these materials have been used as wound dressings. The electrospun SF scaffolds were better able to support keratinocyte adhesion and spreading and well as collagen retention [654]. Electrospun SF patches, used as wound dressings, were found to accelerate wound repair in a diabetic mouse model shown to have significantly delayed wound healing [657]. Despite various studies indicating the benefits of SF scaffolds, single-component SF scaffolds may not be sufficient for optimal dermal regeneration due to shortage of cell specific-binding sites and limited growth factor-adsorbing capacity [658]. Therefore blending SF with other polymers [658-661] or incorporating growth factors with the SF [327, 332] has been suggested as ways to enhance

the functional shortcomings while taking advantage of the structural benefits of using SF as a dermal alternative.

Type I collagen (Col I) is the major structural and functional protein of the dermal ECM. It contains abundant integrin-binding sites and has been shown to enhance cell proliferation and hence tissue regeneration [662]. Despite its role in wound re-epithelisation and healing, the use of pure Col I as a tissue scaffold is problematical because of its poor mechanical properties, fast degradation and issues associated with *in vivo* contraction [663]. Numerous studies have shown that incorporating Col I with other polymers promotes the biocompatibility of those polymers whilst retaining their mechanical properties [53, 54]. In particular, combining Col I with SF through various approaches such as coating [664-666] and blending [667, 668] could overcome the potential limitations of collagen matrices and improve SF biocompatibility.

There is a growing body of work reporting the use of biological scaffolds composed of ECM derived from the decellularisation of tissues or organs [669, 670]. Some commercial products derived from human dermis shown to be successful clinically include: FlexHD (Ethicon, Somerville, NJ), Dermamatrix (Synthes, West Chester, PA), Allo-patch HD (Conmed, Largo, FL), Memoderm (Memometal, Inc., Mahwah, NJ) and Graftjacket Regenerative Tissue Matrix (Wright Medical Technology, Inc., licensed by KCI, an Acelity company, San Antonio, TX) [671, 672]. Other studies have demonstrated the efficacy of ECM/polymer scaffolds for the regeneration of various tissues including bone [39, 40], cartilage [38] and nerves [41]. However, to my knowledge, no studies have been reported on using a polymer functionalized with ECM to successfully facilitate keratinocyte expansion. The ultimate goal of this work is to develop this biomaterial containing keratinocytes as a skin graft.

In this chapter we first evaluated the effect of a type I collagen coating on SF scaffolds using cell proliferation assays and immunofluorescent staining of the ECM secreted by 3T3 fibroblasts. The scaffolds with the best cytocompatability criteria as determined from Chapter IV were chosen to study the efficacy of two different fibroblast types: murine 3T3 fibroblasts and primary human dermal fibroblasts (HDFs), for firstly ECM deposition and secondly the ability of these ECMs to support keratinocyte growth and monolayer formation.

6.2 Method Development

6.2.1 Immunofluorescence Staining of ECM Deposited on SF/ Col I and 3D Col I scaffolds

To examine whether ECM proteins remained on the scaffolds following decellularisation, 3T3 cells were grown on scaffolds for 7 days under MMC then the scaffolds were decellularised and immunostained using antibodies against fibronectin, collagens type I and type IV (Figure 6.1 A). Decellularisation of 3T3-derived matrix and their immunofluorescent staining was performed as explained in Sections 3.4.9.2 and 3.4.9.3, Chapter III.

The deposition of fibronectin as well as collagen type I and type IV were detected for on SF scaffolds. A patchy distribution of fibronectin was detected on SF/Col I scaffolds. However, the deposition of the ECM proteins could not be detected on 3D Col I Hydrogels. The images of scaffolds incubated with the isotype control antibodies and the autofluorescence of the scaffolds without incubation with antibodies (Figure 6.1 A (xi-xiii) and B), indicated incorporating Col I gel onto the SF scaffolds created an autofluorescent effect when viewed at a wavelength of 480 nm, making visualization of ECM proteins difficult. This autofluorescence was much improved when scaffolds were viewed at 647 nm (Figure 6.1 (B)). Accordingly, ECM protein deposition immunofluorescence was performed using an Alexa Fluor 647 nm secondary antibody.

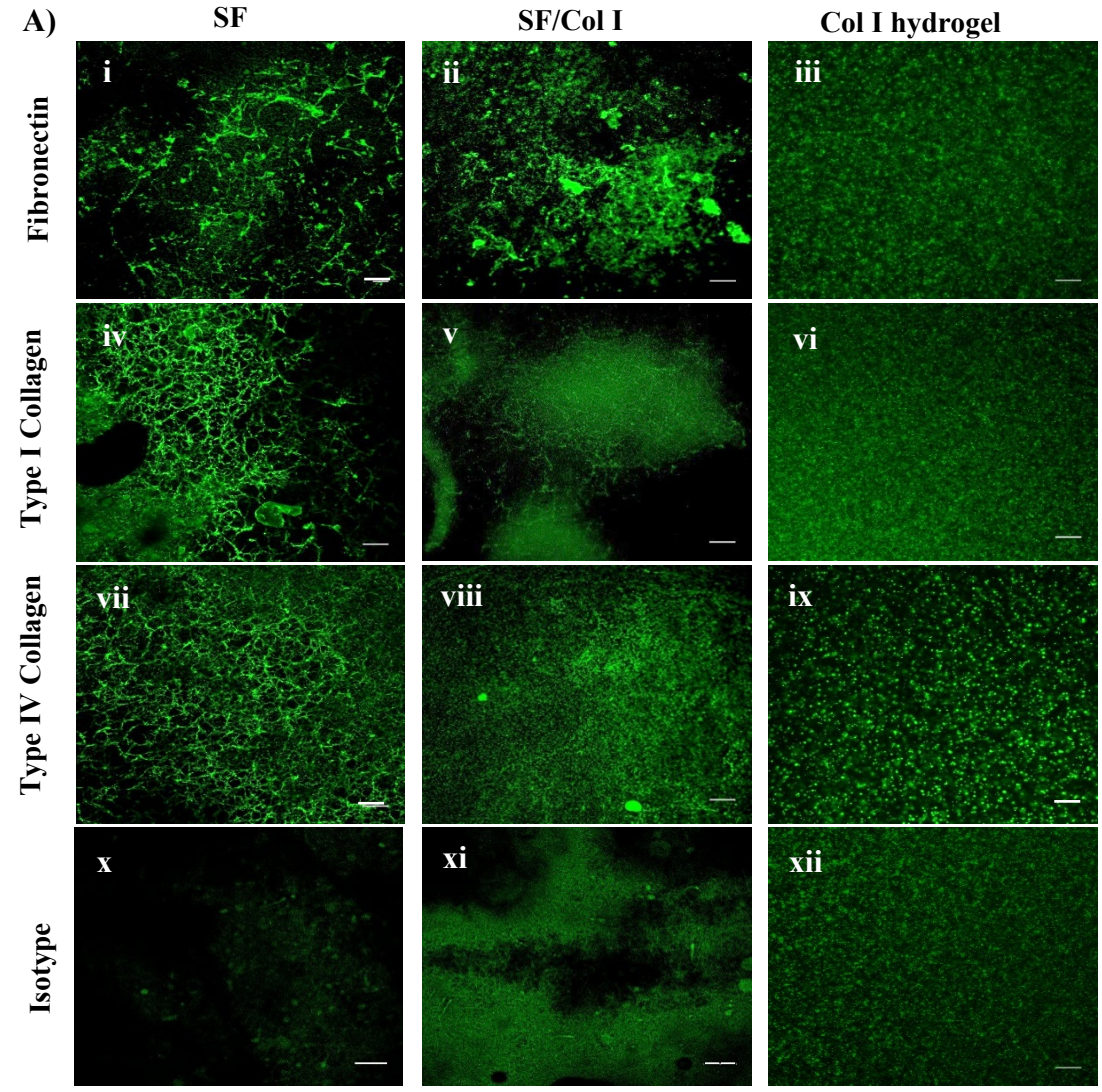
A)
SF
SF/Col I
Col I hydrogel
Fibronectin
Type I Collagen
Type IV Collagen
Isotype
i
ii
iii
iv
v
vi
vii
viii
ix
x
xi
xii

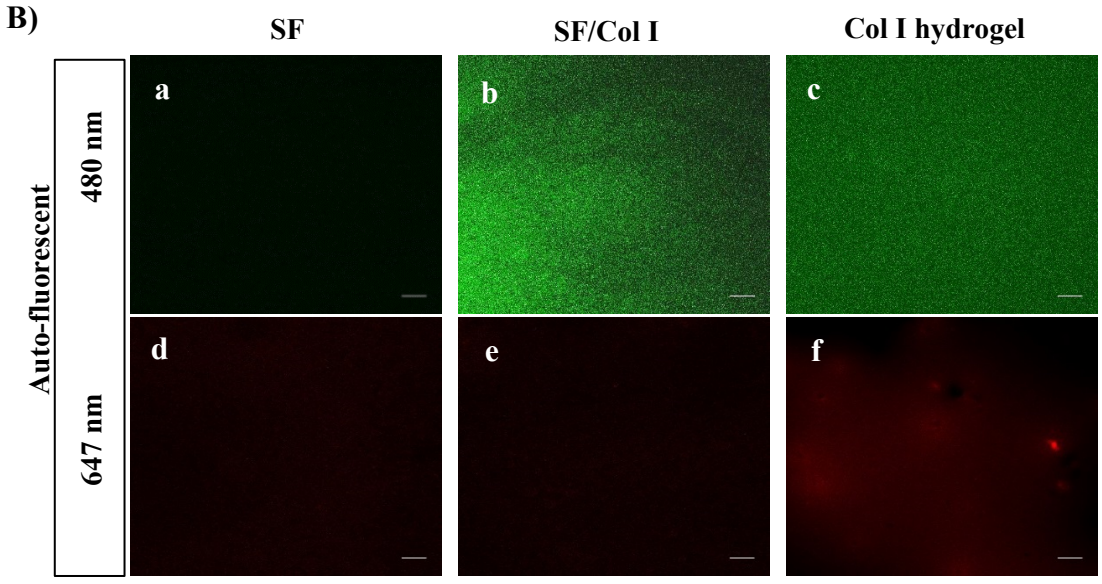
B)
SF
SF/Col I
Col I hydrogel
Auto-fluorescent
480 nm
647 nm
a
b
c
d
e
f

Figure 6.1 Immunofluorescence labelling of 3T3-secreted ECM protein on scaffolds and scaffolds autofluorescence check.

A) 3T3 cells were cultured for 7 days with MMC. Then cells were removed and the ECM was fixed with 4% paraformaldehyde and stained with antibodies recognising fibronectin (i-iii), type I collagen (iv-vi), type IV collagen (vii-ix) and isotype control (x-xii). The secondary antibody was an anti-rabbit Alexa Fluor® 488. Images were taken using Nikon A1+ confocal microscope. Scale bar = 50 μm.

B) Scaffolds were incubated in MMC media for 24 h at 37 °C followed by fixation with 4% paraformaldehyde and imaged by Nikon A1+ confocal microscope under different fluorescent channel (a-c): 480 nm and (d-f):647 nm.

6.2.2 Optimisation of Keratinocyte Growth on SF based Scaffolds Coated with ECM

Numerous reports have demonstated that MMC enhances the deposition and supramolecular assembly of ECM [147, 151, 152]. Accordingly, MMC was used for 3T3 cell ECM deposition. The deposition of three major ECM components: fibronectin, type I collagen and type IV collagen were detected on both SF and SF/HNT 1 wt% scaffolds by immunofluorescence staining (Figure 6.2 A). To investigate whether these substrates can support keratinocyte expansion, keratinocytes were initially seeded at density of 0.4×10^4 cells/scaffold onto SF and SF/HNT 1% scaffolds coated with 3T3 fibroblast-derived ECM deposited with MMC media. Keratinocytes were grown in Defined Keratinocyte Serum Free Media (DKSFM) for 4 days before being fixed with 4% paraformaldehyde and stained with antibodies recognising cytokeratin 14 (K14), a marker of basal keratinocytes. Nuclei were stained with DAPI. This experiment revealed that the keratinocytes did not grow as compact colonies and neither did they stratify on these substrates (Figure 6.2 B). Instead they remained as small single cells with a round morphology, and the very low number of nuclei that stained with DAPI indicted poor keratinocyte growth on either of the scaffolds.

To determine if the keratinocytes were reacting poorly to MMC conditions, keratinocytes were grown on 3T3-derived matrix deposited with or without MMC. Col I was used as a positive control, as it is generally used with KSFM to propagate keratinocytes [673]. All substrates were prepared in a 24 well plate. Briefly, keratinocytes were harvested, pelleted and then resuspended in DKSFM, at a concentration of 8×10^4 cells/mL. 250μL of this cell suspension (2×10^4 cells) was added to the wells. At

day 4, cell morphology was observed by phase contrast using a Zeiss Axiovert bright field inverted microscope (Zeiss, Oberkochen, Germany). Keratinocytes grew as colonies on both Col I and 3T3 ECM matrix without MMC substrates, however more cells were observed on Col I substrates (Figure 6.3 a, b). In contrast, distinct changes in cell morphology were observed when keratinocytes were cultured on 3T3 ECM matrix with MMC. These keratinocytes were disorganised, there were very few colonies and many cells had an aberrant elongated morphology (Figure 6.3 c). From these data it appeared that MMC played an adverse role in keratinocyte growth and caused the changes in cell morphology observed. All further fibroblast ECM deposition was done in DMEM without MMC.

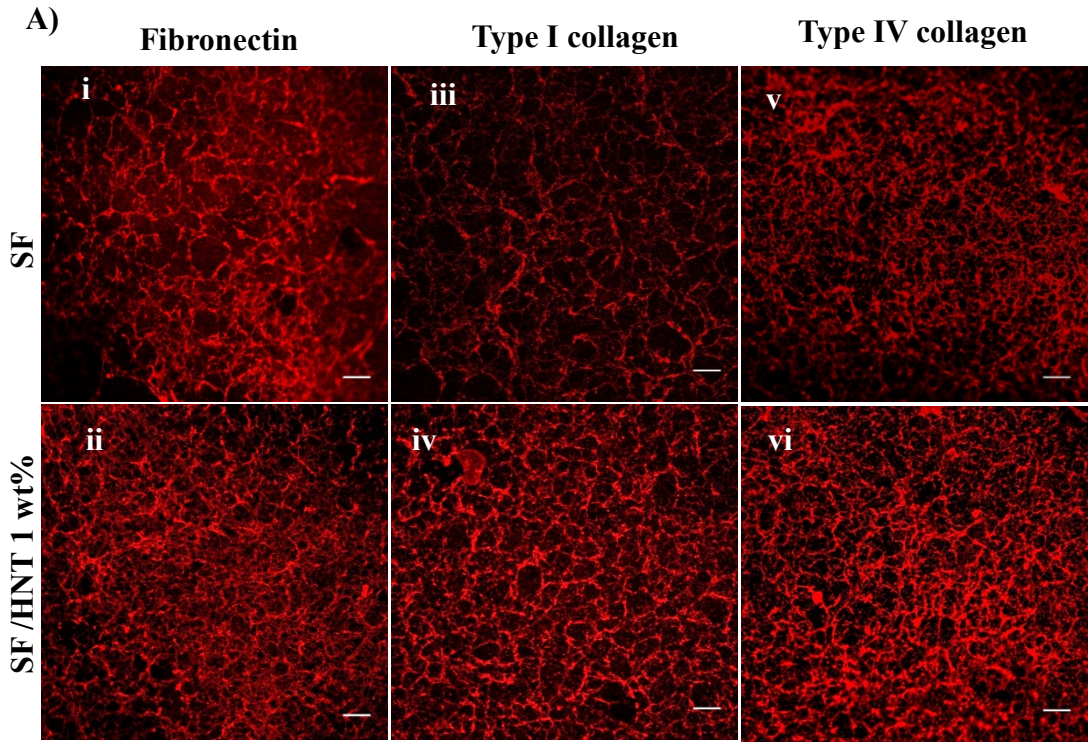

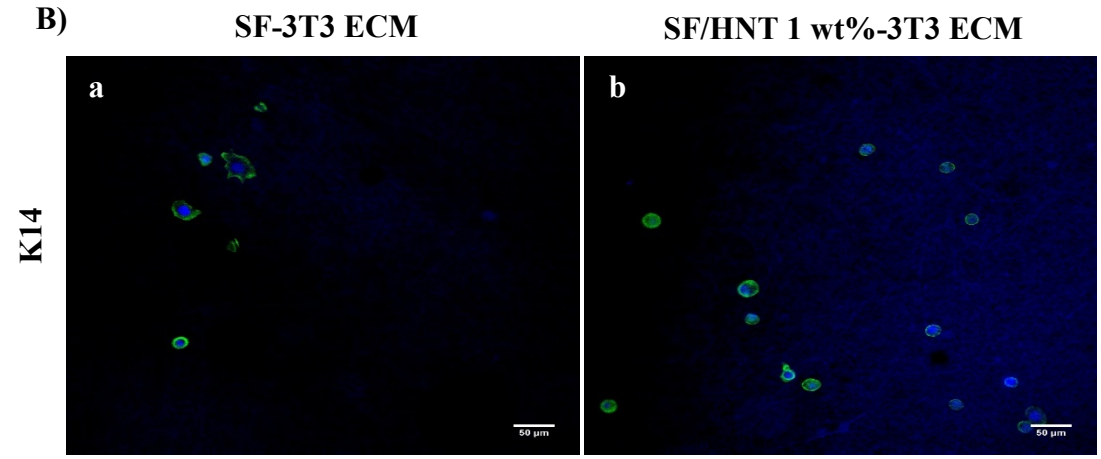

Figure 6.2 A) Deposition of fibronectin, type I collagen and type IV collagen by 3T3 fibroblasts on SF and SF/HNT 1 wt% scaffolds. 3T3 fibroblasts (0.25×10^4 cells) were cultured for 7 days with MMC. The cells were then removed and the ECM was fixed with 4% paraformaldehyde and stained with antibodies recognising fibronectin (i,ii), type I collagen (iii,iv) and type IV collagen (v.vi). Scale bars are 50 µm.

B) K14 expression by keratinocytes grown on fibroblast-derived ECM deposited on SF (SF-3T3 ECM) and SH/HNT1 wt% (SF/HNT1 wt%-3T3 ECM). Keratinocytes (0.4×10^4) were cultured on the scaffolds for 4 days in DKSFM, fixed with 4% paraformaldehyde and stained with antibodies recognising cytokeratin 14 (K14; a,b) and with DAPI. Scale bars are 50 µm.

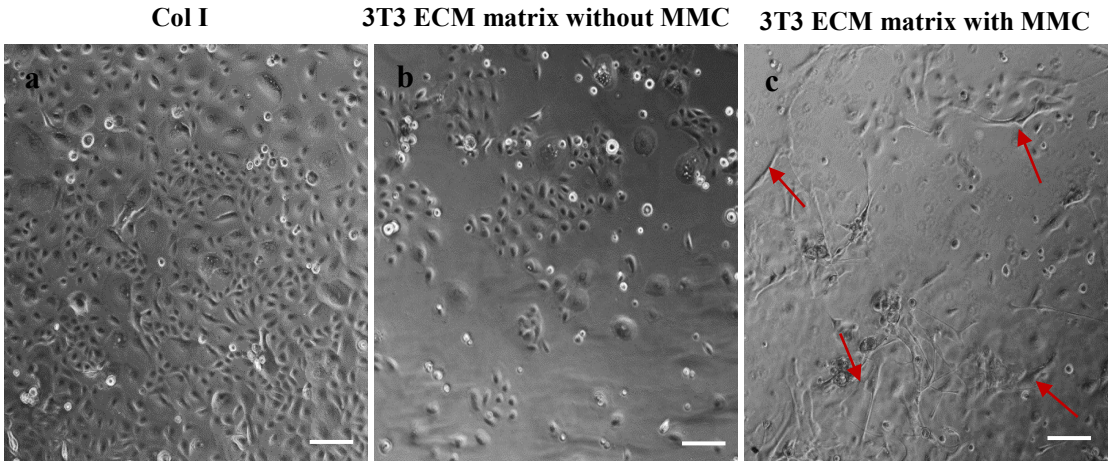

Figure 6.3 Representative phase contrast images of keratinocytes grown on (a) Col I (b) 3T3 ECM matrix without MMC and (c) 3T3 ECM matrix with MMC**.**
Keratinocytes (2×10^4) were seeded into wells of a 24-well plate that contained either 3T3 ECM matrix with MMC, 3T3 ECM matrix without MMC or Col I ($3ug/cm^2$) and cultured for 4 days in DKSFM. Arrows indicate keratinocytes with elongated morphology. Scale bars are 100 µm.

6.2.3 Determining HDF Concentration for ECM deposition on SF based Scaffolds

It was necessary to determine a HDF density that produced a confluent cell layer on the scaffolds thereby ensuring the scaffolds were well covered with the ECM secreted by these cells before the decellularisation step. Thus, HDFs were cultured at different seeding densities, either 0.3×10^4, 1×10^4 or 2×10^4 for 4 days in complete DMEM (phenol red free). The cells were fixed then stained with DAPI and phalloidin-Alexa Fluor® 488 to detect cell nuclei and polymerised actin respectively. Immunofluorescence images were captured using Nikon A1+ confocal microscope (Nikon, Tokyo, Japan). As shown in Figure 6.4, the HDFs had a uniform spindle shaped morphology that is typical of fibroblasts. The cells did not proliferate sufficiently when used at 0.3×10^4 cells/scaffold, whereas a confluent monolayer was achieved at the higher cell densities. If the monolayer became over-confluent after 7 days of culture, cells may have detached, accordingly 1×10^4 HDFs/scaffold was chosen for further work.

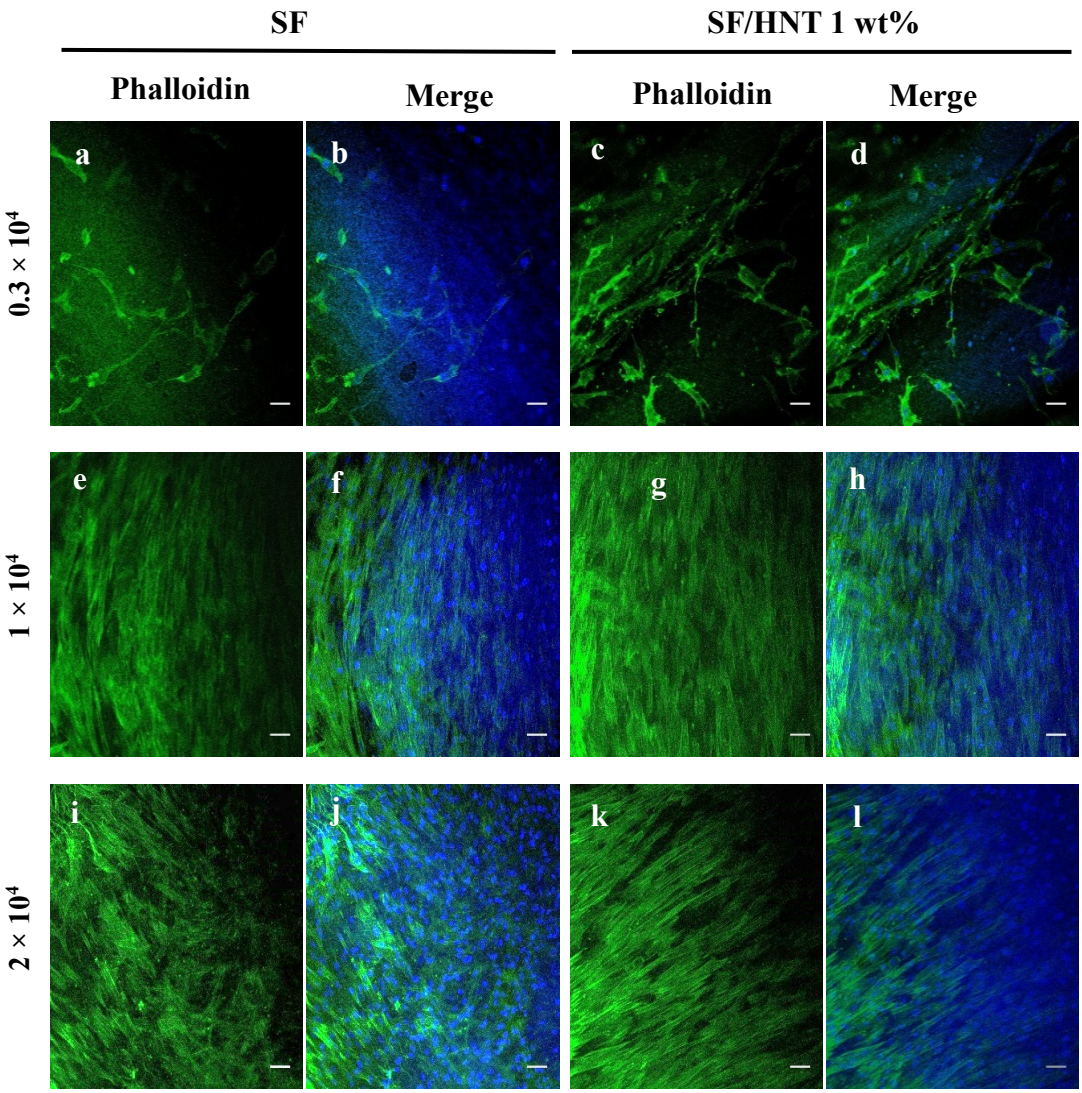

Figure 6.4 Representative images HDFs on SF or SF/HNT 1% scaffolds at day 4 post seeding. The cells were seeded at (a-d) 0.3×10^4, (e-h) 1×10^4 and (i-l) 2×10^4 on SF and SF/HNT1 wt% scaffolds. After 4 days of culture, cells were fixed with 4% paraformaldehyde and stained with phalloidin-Alexa Fluor® 488 (Green) and DAPI (Blue). Scale bars are 50 μm.

6.3 Results and Discussion

6.3.1 Scanning Electron Microscopy (SEM)

The morphology of electrospun nanofibres of SF, SF/Col I scaffolds and 3D Col I Hydrogel are shown in Figure 6.5. Plain SF scaffolds (Figure 6.5 a) exhibited smooth and homogeneous nanofibrous structures with an average diameter of 378.9 nm ± 65.6. Col I hydrogels were composed of a dense network of fibrils and many fibrils self-assembled to form massive fibrils. The fibrous structures remained for SF/Col I scaffolds however the void space was filled with collagen gel and the fibres appeared larger.

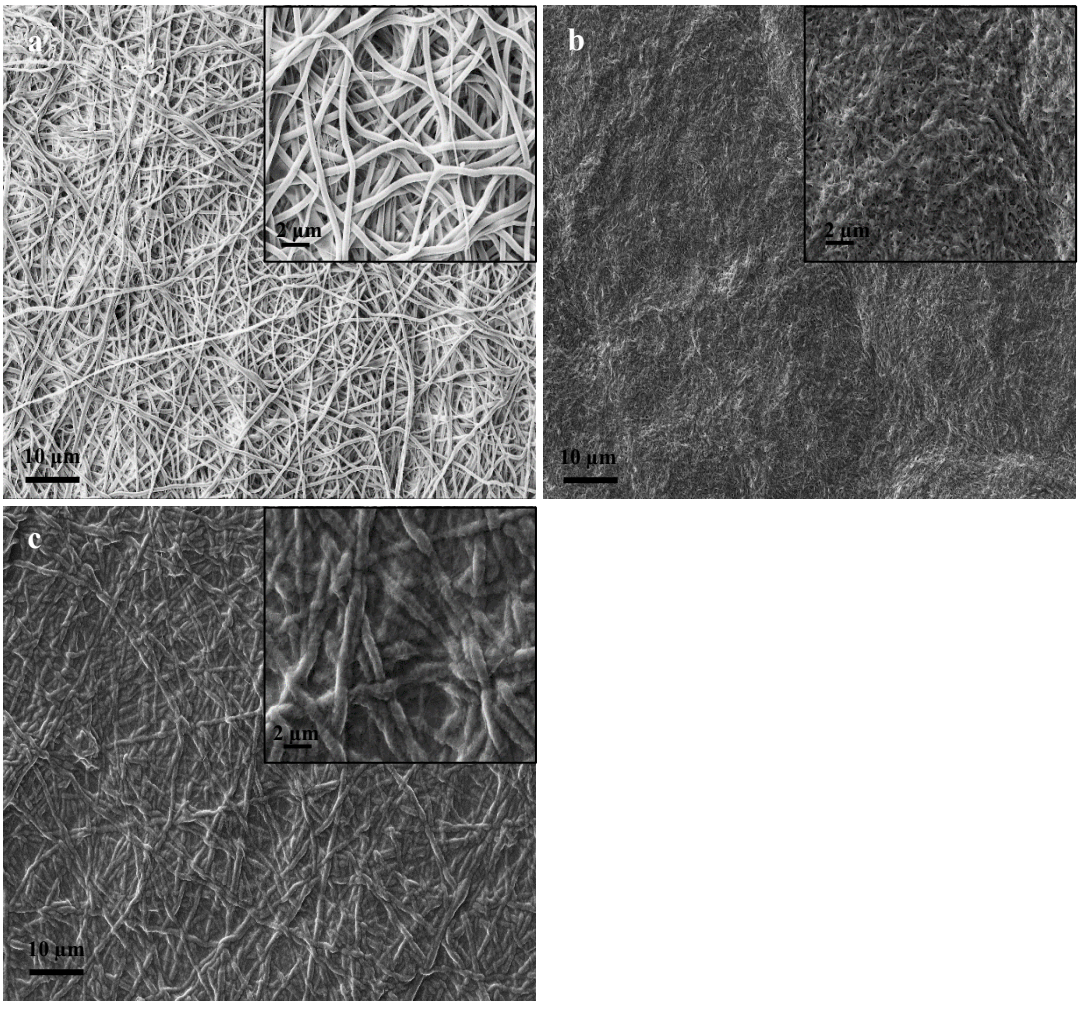

Figure 6.5 SEM micrographs of (a) SF methanol treated nanofibres scaffold, (b) 3D Col I hydrogel and (c) SF/Col I scaffold (scale bar = 10 µm). Insets show images of the corresponding scaffolds at higher magnification (scale bar = 2 µm).

6.3.2 FTIR Analysis

The FTIR spectra of SF, SF/Col I scaffold and 3D Col I hydrogel are depicted in Figure 6.6. Since SF and Col I are both proteins composed of a high number of glycines and alanines, their FTIR spectra are quite similar. The spectra of Col I scaffolds showed the amide I band at 1635 cm^{-1} resulting from C=O stretching and amide II at 1556 cm^{-1} derived from N-H bending coupled to C–N stretching vibrations. In addition, a broad peak at about 3300–3400 cm^{-1} was assigned to amide A due to N-H stretching [674, 675]. In SF nanofibres amide I and amide II peaks were centred at 1627 and 1522 cm^{-1}, respectively indicating the β-sheet structure of SF as a result of methanol treatment [665, 676]. The FTIR spectrum of the SF/Col I scaffolds demonstrates the characteristic bands of the parent molecules. However, the transmittance band intensities of amide I and amide II increased relative to both pure collagen and SF.

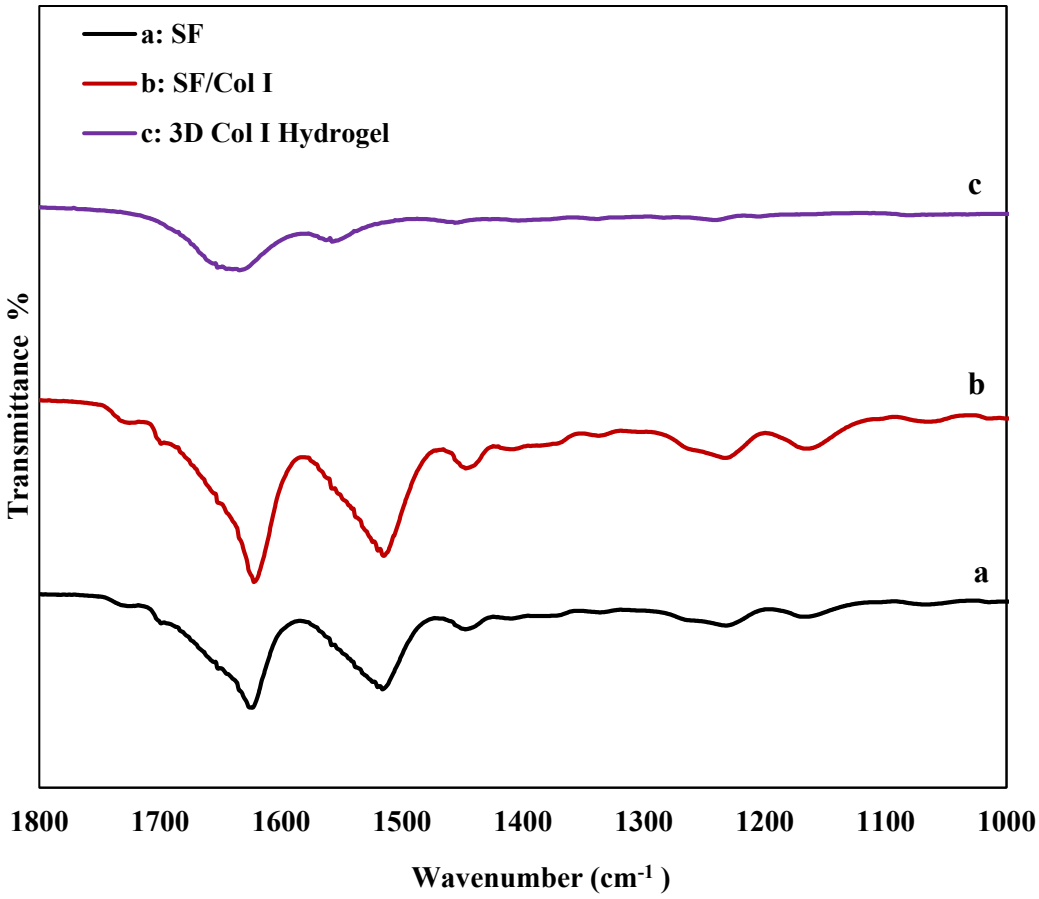

Figure 6.6 FTIR spectra of (a) SF, (b) SF/Col I scaffold (c) 3D Col I Hydrogel.

6.3.3 Water Contact Angle Measurements

Water contact angles of SF, SF/Col I scaffolds and 3D Col I hydrogels were measured and the results are presented in Table 6.1. The higher the contact angle the lower the hydrophilicity of the material. The 3D Col I hydrogel possessed the lowest contact angle of 17.54° indicating highly hydrophilic nature due to its amino acid and water content [677]. The average contact angle of the SF scaffolds was 70.1° and this reduced to 60.83° for SF/Col I scaffolds. These results suggested that the collagen coating improved the surface hydrophilicity of SF.

Table 6.1 Water contact angles of SF, SF/Col I scaffold and Col I hydrogel.

Sample	Water contact angle (degree)
SF	70.50 ± 5.05
SF/Col I	60.83 ± 4.06
Col I hydrogel	17.54 ± 1.11

6.3.4 Proliferation Assay

The proliferation of 3T3 fibroblasts on SF, SF/Col I scaffolds and 3D Col I hydrogels were evaluated after 1 and 3 days of cell culture. As illustrated in Figure 6.7 , it is apparent that cell number increased with time for all three scaffolds, indicating that the scaffolds were cytocompatible. The proliferation rates for the different substrates were not statistically different ($p > 0.05$) and comparable results were observed for SF and Col I hydrogels. This may have been due to the high collagen concentration used in this study (3.6 mg/mL). Collagen density can alter the cell response, as reported by Abreu *et al.* [678]. It was shown increasing the collagen density from 2 to 4 mg/mL results in stiffer scaffolds, which suppresses fibroblast proliferation and exerts more resistance to retraction of the hydrogels. The collagen concentration also affects the characteristics of the hydrogel. For example, high collagen concentrations decrease both the diffusion rate and the length of the collagen fibres, which affects the

organization of the gel that forms [679-681], and as demonstrated by Xie *et al.* [682] the fibrous structure of the collagen gel can induce different cellular responses. For example, high fibre stiffness, along with shorter fibre lengths, restrained the transfer of cell traction forces to nearby fibres thereby impeding human mesenchymal stem cell spreading, proliferation, and migration. Thus, it is possible that hydrogels formed with lower Col I concentrations may enhance fibroblast proliferation above that seen with plain SF, which is not the case in here, as Col I concentrations were not optimised for cell proliferation in the present experiments.

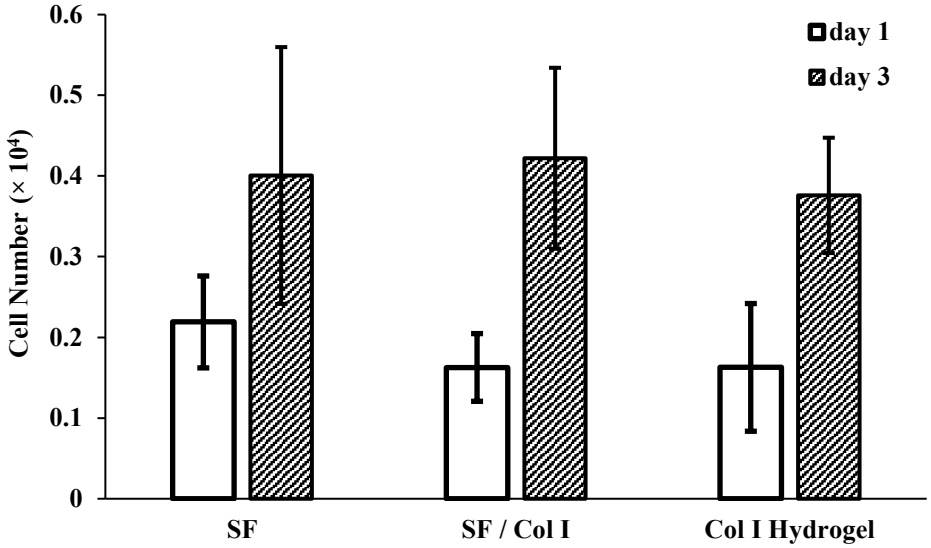

Figure 6.7 Proliferation of 3T3 fibroblasts seeded on SF, SF/Col I scaffolds and 3D Col I hydrogel after the first and third days of culture.

The data are representative of three separate experiments. Values are means +/- SD of 6 replicates. Statistical analyses using ANOVA followed by Tukey's test were conducted. No significance difference between scaffolds were detected ($P > 0.05$).

6.3.5 Immunofluorescent Staining of ECM Proteins Deposited on different scaffolds

To determine whether 3T3 fibroblasts deposit ECM on SF, SF/Col I scaffolds and 3D Col I hydrogel, 3T3 cells were grown for 7 days on these substrates and immunostaining was performed using antibodies recognising fibronectin, collagens type I and type IV following decellularisation (Figure 6.8). Scaffolds without any ECM deposition were also immunestained with these antibodies to confirm that the

observed staining in Figure 6.8 were indicative of ECM deposited proteins (Figure A.6, Appendix A). The staining intensities of the collagen type IV and the collagen type I antibodies was very similar on all three scaffolds, albeit the staining pattern is different on plain SF compared to the other scaffolds. Fibronectin staining intensity was the strongest on pristine SF, followed by SF/Col I scaffold and fibronectin was not detected on 3D Col I hydrogel. It seemed that incorporation of Col I into the scaffolds reduced the amount of fibronectin expressed by the 3T3 cells. A similar finding was observed by Davenport and Nettesheim [683]; they found lower fibronectin expression by epithelial cells on collagen type I gel coated membrane compared to the amounts of fibronectin deposited on uncoated membranes.

Fibronectin plays a crucial role in a number of cellular mechanisms including cell adhesion, growth, migration, differentiation, wound healing, and matrix assembly [684, 685]. The interaction between α5β1 integrin and fibronectin has shown to inhibit the terminal differentiation of keratinocytes [686], and there is a decrease in the affinity of α5β1 integrin for fibronectin when the keratinocytes are committed to terminal differentiation [687]. The main purpose of coating the SF scaffold with collagen was to enhance its biofuctional properties thereby creating better microenvironment for keratinocyte proliferation. However, the immunofluorescence images (Figure 6.8) revealed that incorporation of Col I into the SF scaffold down regulated the fibroblast derived ECM protein deposition, in particular fibronectin protein, which plays an important role in maintaining keratinocytes in an undifferentiated state. As the addition of Col I did not have the desired function, in following sections the scaffolds used were methanol treated SF (which from Chapter V and the results here outperformed both SF/gelatin and SF/Col I scaffolds) and SF/HNT 1 wt% (developed in Chapter IV).

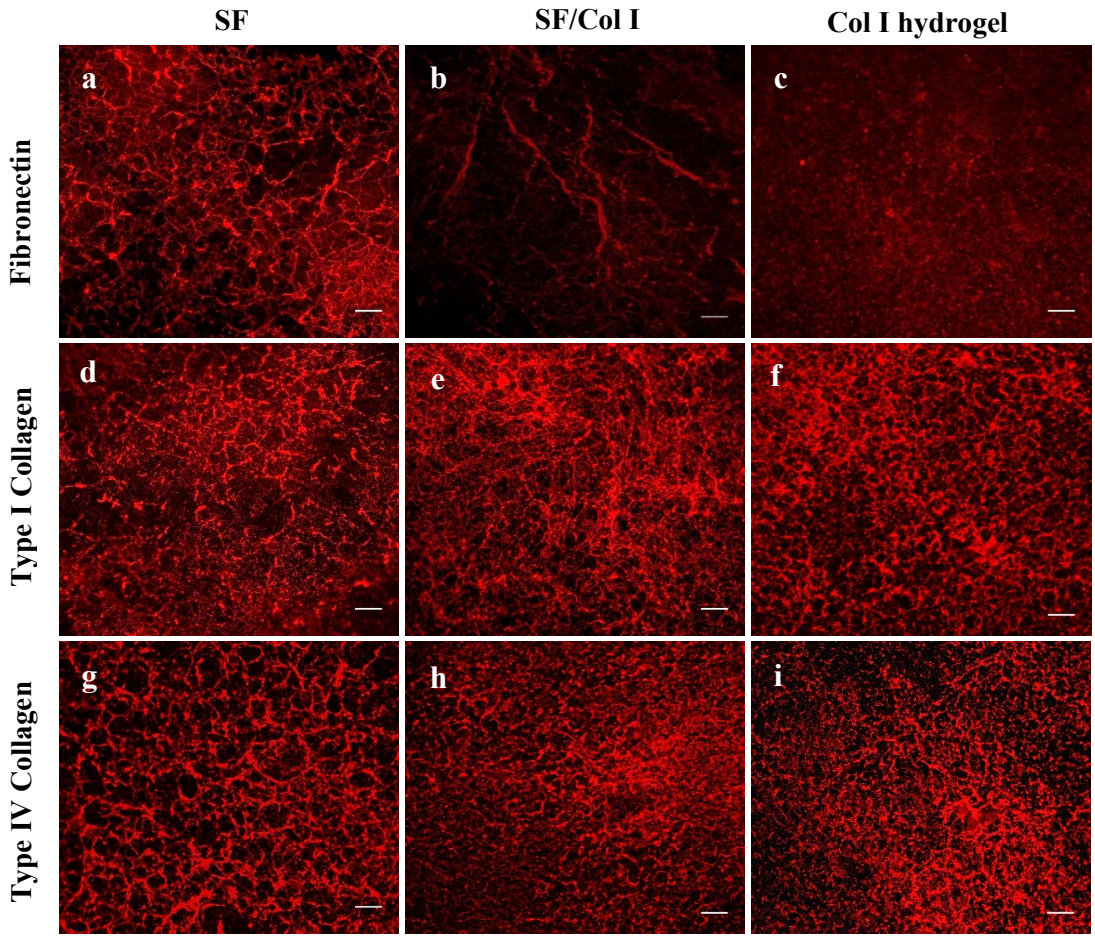

Figure 6.8 Deposition of fibronectin, type I collagen and type IV collagen by 3T3 fibroblasts on SF, SF/Col I scaffold and 3D Col I Hydrogel.

3T3 fibroblast cells (0.25×10^4) were cultured for 7 days with MMC media. Then cells were removed and the ECM was fixed with 4% paraformaldehyde and stained with antibodies recognising fibronectin (a-c), type I collagen (d-f) and type IV collagen (g-i). The secondary antibody was an anti-rabbit Alexa Fluor® 647. Images were taken using Nikon A1+ confocal microscope. Scale bar = 50 μm.

6.3.6 Immunofluorescent Staining of 3T3 cell ECM Proteins Deposited on SF and SF/HNT 1 wt% scaffolds

Numerous studies have shown that acellular ECM can assist in maintaining a stem cell phenotype and improve stem cell self-renewal during *in vitro* expansion [688-690]. For instance, ECM derived from mesenchymal stem cells (MSCs) promotes the proliferation of MSCs and maintains their high responsiveness to the osteogenic inductive effect of bone morphogenetic protein 2 (BMP-2) during culture expansion

[691]. Interestingly, ECMs are tissue-specific, *i.e.,* the ECM from one tissue best maintains cells from the same tissue [692, 693]. Here the goal is to develop scaffolds that could be used in skin grafts, and so the ECM from mouse 3T3 fibroblasts, cells that have previously been shown to support human primary keratinocyte proliferation *in vitro* (data from Prof. Deirdre Coombe's lab, not shown), were used to coat SF and SF/HNT 1 wt% scaffolds.

To verify whether 3T3 cell ECM was deposited on SF and SF/HNT1% scaffolds, immunofluorescence staining was conducted. These experiments revealed that three of the major ECM molecules (fibronectin, type I collagen and type IV collagen) were deposited by the 3T3 cells on both substrates (Figure 6.9). However, a slightly more dense deposition of type I collagen and type IV collagen was observed on the SF/HNT 1 wt% scaffolds compared to the plain SF scaffolds. This visual interpretation from the immunofluorescence images is consistent with the 3T3 fibroblast proliferation and morphology data (Sections: 4.3.9 and 4.3.10, Chapter IV), as they showed a superior proliferation rate and were more spread on SF/HNT 1wt% relative to the pure SF scaffolds.

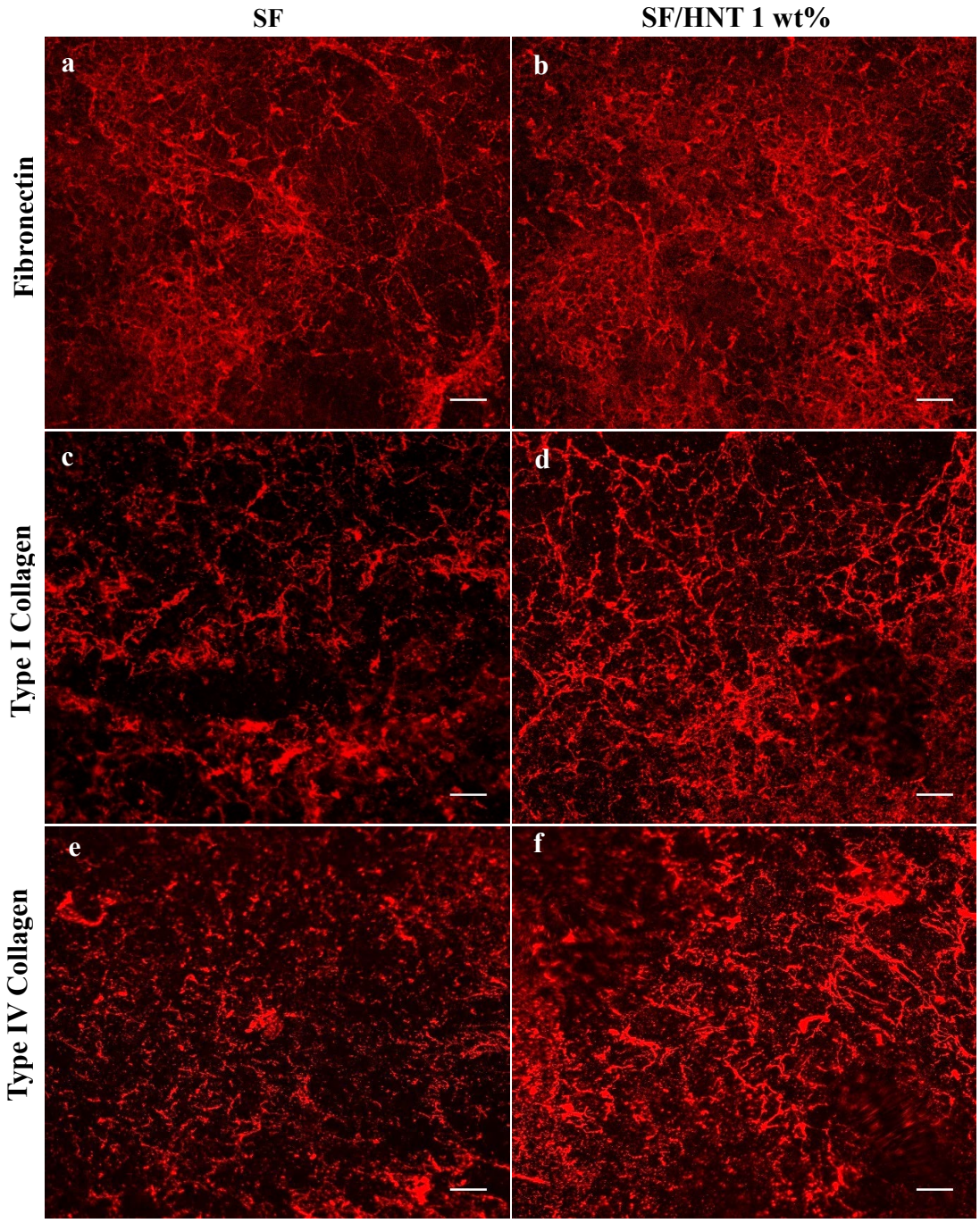

Figure 6.9 Deposition of fibronectin, type I collagen and type IV collagen by 3T3 fibroblasts on SF and SF/HNT 1 wt% scaffolds**.**

3T3 fibroblasts (0.25×10^4) were cultured for 7 days in DMEM (phenol red free), subjected to decellularisation and the ECM fixed with 4% paraformaldehyde and stained with antibodies recognising fibronectin (a,b), type I collagen (c,d) and type IV collagen (e,f). The secondary antibody was an anti-rabbit Alexa Fluor® 647. Images were taken using Nikon A1+ confocal microscope. Scale bar = 50 μm.

6.3.7 Keratinocyte Growth on SF based Scaffolds Coated with 3T3 Fibroblast Derived ECM

One goal of this work was to determine if SF based scaffolds could support keratinocyte proliferation and whether 3T3 fibroblast-derived ECM was beneficial for keratinocyte growth. To this end, keratinocytes were cultured on SF and SF/HNT 1wt% scaffolds with and without the 3T3 fibroblast ECM coating (*i.e.,* the ECM coated scaffolds were: SF-3T3 ECM and SF/HNT1wt%-3T3 ECM). After 4 or 8 days of culture immunofluorescent staining was performed using antibodies that recognised: cytokeratin 14 (K14), cytokeratin 10 (K10) and involucrin to investigate the keratinocyte differentiation status on each substrate. K14 is a marker of basal keratinocytes, while K10 and involucrin are early markers of terminal differentiation. Immunofluorescence images from day 4 revealed that K14 expression was observed in keratinocytes on all four substrates, indicating the presence of basal keratinocytes (Figure 6.10 i-iv). Interestingly, keratinocytes behaved differently on each substrate. On plain SF and SF/HNT 1wt% keratinocytes grew as single cells, whereas on both 3T3 ECM coated scaffolds keratinocytes grew as colonies with distinct boundaries. While the expression of K10 was not observed in keratinocytes on any substrate, involucrin expression was noted in cells on all scaffolds (Figure 6.10 v-xii).

From the data given in Figure. 6.11, it is clear that after 8 days of culture, K14 staining was evident in keratinocytes on all four scaffolds. However on SF scaffolds clear, intense staining was restricted to a subpopulation of cells. In contrast, staining was more pronounced on the other scaffolds and on SF/HNT1wt%-3T3 ECM scaffolds where the staining was quite uniform with virtually all keratinocytes expressing this basal cell marker; the uneven nature of the scaffold surface means that a portion of the keratinocyte layer is not within the field of focus and hence the staining is less visible in this region. Importantly, on all scaffolds there are areas where the keratinocytes appear to have formed cell-cell junctions and they have assumed the cobblestoned morphology that is characteristic of proliferating keratinocytes. The DAPI staining suggested that the keratinocytes had reached a near confluent monolayers on both 3T3 ECM functionalised scaffolds. However, not all cells were of the same size and it is likely the larger cells were differentiating. This conclusion is consistent with the staining pattern observed with the involucrin antibody, as predominantly the large cells

were positive for this differentiation marker. In contrast, no keratinocytes stained with the K10 antibody regardless as to the scaffold upon which they were growing.

Previous studies have demonstrated the potential of electrospun nanofibres for human keratinocyte adhesion and proliferation [694, 695] . In particular, Min *et al*. [654, 696] reported that electrospun SF nanofibres enhanced keratinocyte adhesion and spreading, because they provide a large surface area for cell attachment as well as good biocompatibility. Likewise our data show that both SF and SF/HNT1wt% scaffolds supported keratinocyte growth. Others have also shown that cell-secreted ECM deposited on polymeric scaffolds enhance their biological performance. Harvestine *et al*. [39] reported that the addition of MSC-secreted ECM onto bioactive glass /poly(lactide-co-glycolide) scaffolds potentiated the efficacy of this substrate by promoting cell survival and function *in vitro* and *in vivo*. Similarly Goyal *et al.* [609] showed that coating poly(desamino tyrosyl-tyrosine carbonate) with NIH 3T3 cell generated ECM promoted not only cell adhesion but also the assembly of new ECM. Our results also indicated that coating the scaffolds with 3T3 cell ECM enhanced keratinocyte adhesion, an expected result given that we demonstrated the presence of type I collagen, type IV collagen and fibronectin on both SF and SF/HNT1% scaffold following decellularisation of the 3T3 cell layer (Figure 6.9) and what is known about these ECM proteins and keratinocyte behaviour. Both type I collagen and fibronectin are important ECM components of skin. Fibronectin has a major role in promoting cell adhesion, migration and differentiation [685]. Type IV collagen is also crucial for the maintenance of the stem cell-like characteristics of basal keratinocytes [697, 698]. Type IV collagen and type I collagen enhance human keratinocyte migration *in vitro* [699, 700].

Although all 4 substrates support keratinocytes adhesion, but it seemed that SF/HNT 1wt% scaffolds were more favourable, as there were more keratinocytes growing as colonies-forming of small cells on SF/HNT1% with or without ECM compared to their SF counterparts. It is known that physiochemical properties of scaffolds such as hydrophilicity/hydrophobicity, surface morphology, functionality and roughness effect their cellular response [701, 702]. Hence, this result may be attributed to the superior water uptake capacity and pore volume of SF/HNT 1 wt% scaffolds (Sections 4.3.3 and 4.3.4, Chapter IV). In addition, the ECMs secreted by the 3T3 cells SF/HNT 1 wt% scaffolds were slightly more dense than those on SF scaffolds (Figure 6.9), possibly providing more protein binding sites favourable for keratinocytes adhesion.

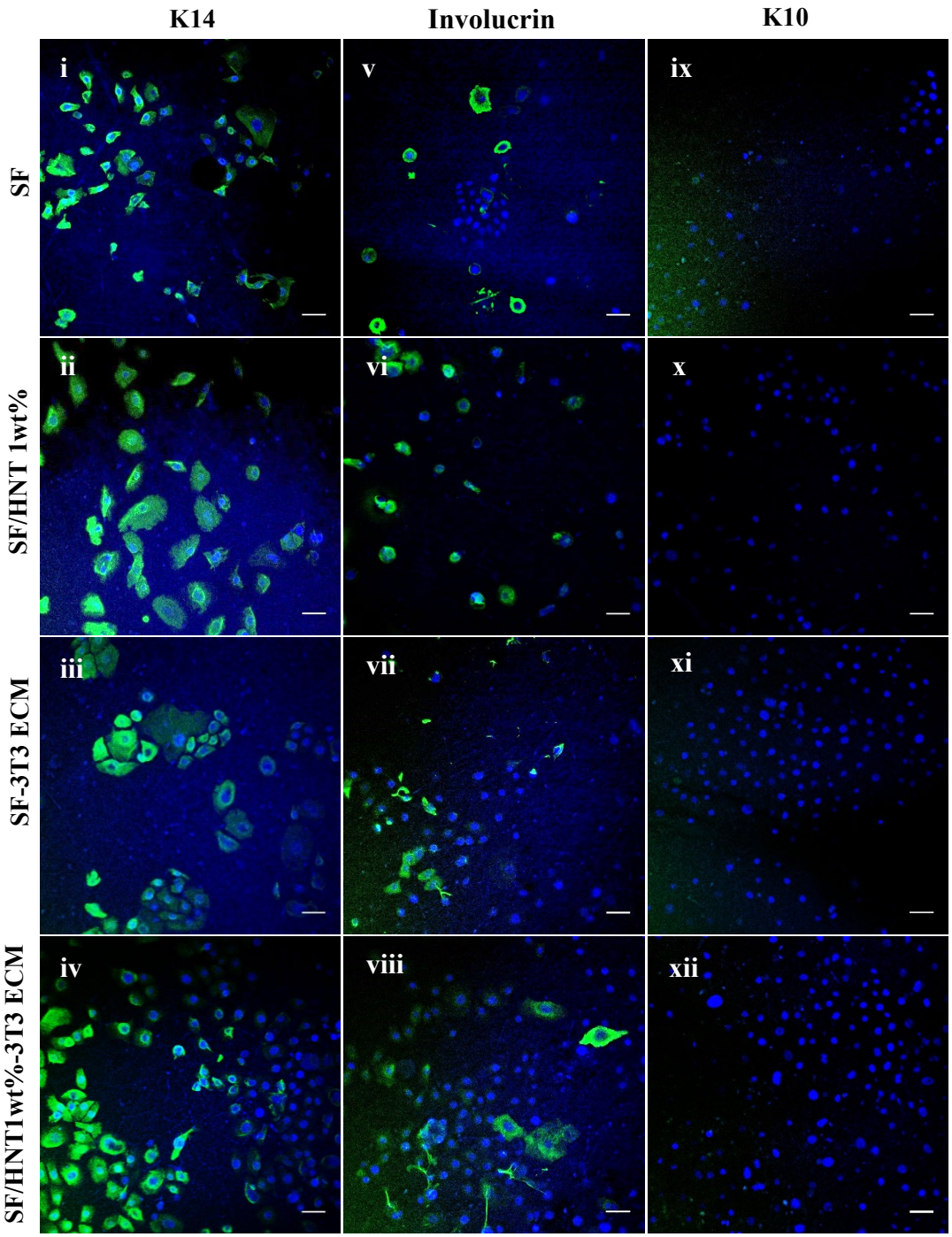

Figure 6.10 Expression of K10, K14 and involucrin by keratinocytes grown for 4 days on the SF based scaffolds with or without 3T3 ECM coating.

Keratinocytes (0.4 x 10^4) were cultured in DKSFM on different substrates. Keratinocytes were fixed with 4% paraformaldehyde and stained with antibodies recognising cytokeratin 14 (K14; i-iv), involucrin (v-viii) and cytokeratin 10 (K10; ix-xii). Nuclei were stained using DAPI (Blue). Scale bars are 50 μm.

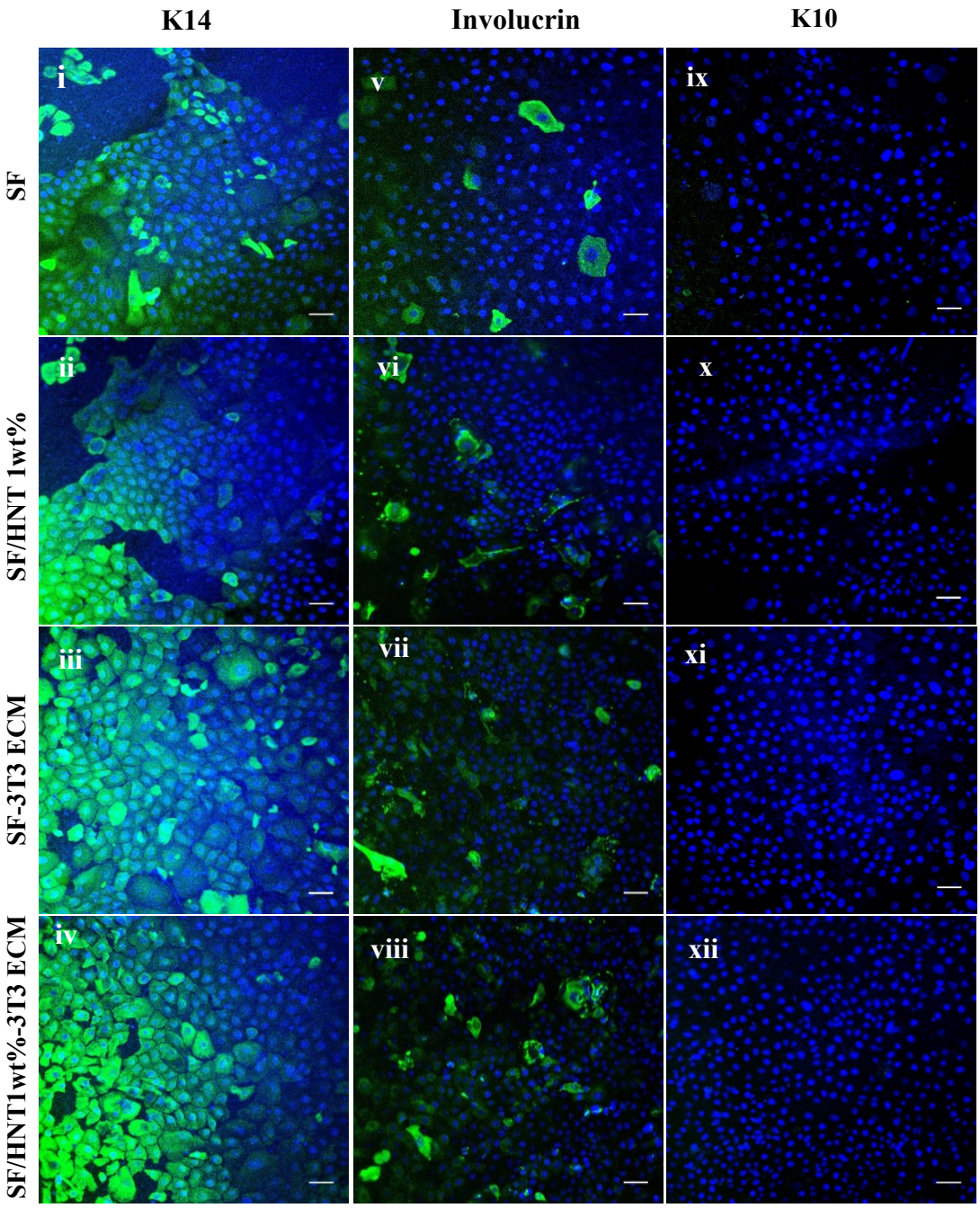

Figure 6.11 Expression of K10, K14 and involucrin by keratinocytes grown for 8 days on the SF based scaffolds with or without 3T3 ECM coating.

Keratinocyte culture and immunostaining conditions were as described in Figure 6.10. Antibodies recognising: cytokeratin 14 (K14; i-iv), involucrin (v-viii) and cytokeratin 10 (K10; ix-xii). Nuclei were stained with DAPI (Blue). Scale bars are 50 μm.

6.3.8 Immunofluorescent Staining of HDF Derived ECM on SF and SF/HNT 1wt% Scaffolds

Given that SF and SF/HNT1wt% scaffolds support keratinocyte growth and ECM proteins from the murine 3T3 fibroblasts further promoted their expansion the question was asked as to whether ECM from human dermal fibroblasts (HDFs) similarly assisted keratinocyte growth. If SF and SF/HNT 1 wt% scaffolds coated with HDF derived ECM was effective it is likely such scaffolds would be more favourably viewed by Regulatory Agencies for use in the clinic.

Hence, the appearance of the matrix produced by HDFs grown on both SF and SF/HNT1 wt% scaffolds was examined by immunostaining. As can be seen in Figure 6.12, fibronectin, type I collagen and type IV collagen were expressed by HDFs grown on both scaffolds. Fibronectin staining was patchy and it seemed that it was almost equally expressed by HDFs on both SF and SF/HNT 1wt% scaffolds as the staining intensities were similar. Immunofluorescent staining revealed Type I collagen and type IV collagen were deposited in a more organised, and a slightly more dense fashion on SF/HNT 1wt% scaffolds compared to that seen for pristine SF scaffolds.

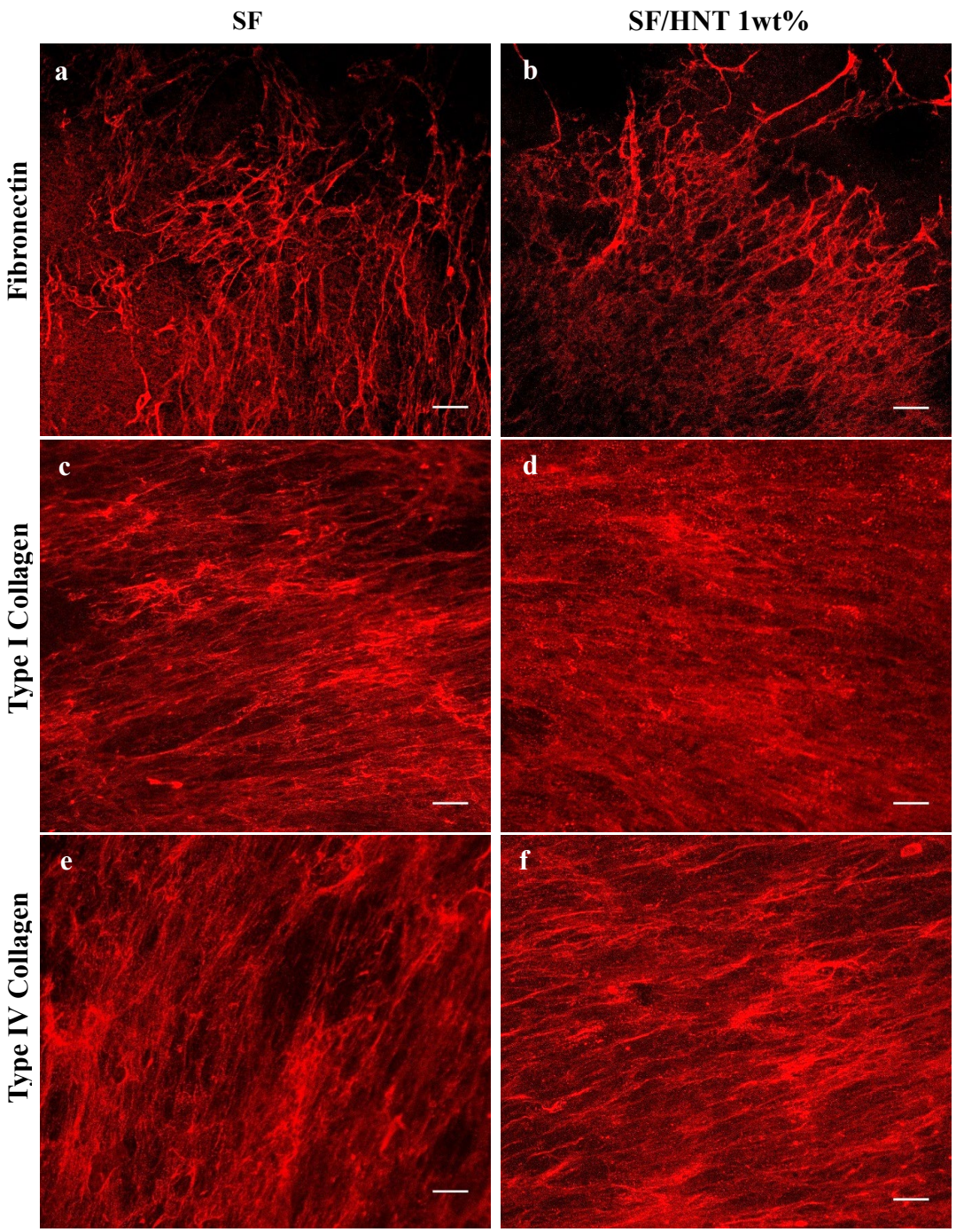

Figure 6.12 Deposition of fibronectin, type I collagen and type IV collagen by HDFs on SF and SF/HNT1wt% scaffolds.

HDFs (1×10^4) were grown in DMEM (phenol red free) until day 7 and then decellularised. The ECM was fixed with 4% paraformaldehyde and immunostained with antibodies recognising fibronectin (a,b), Type I Collagen (c,d) and Type IV Collagen (e,f). The secondary antibody was Goat anti-rabbit Alexa Fluor® 647. Scale bars are 50 μm.

6.3.9 Keratinocyte growth on SF based scaffolds Coated with HDF Derived ECM

In an effort to recapitulate the dermal niche that the keratinocytes inhabit *in vivo*, HDF-derived ECMs were used to coat the SF and SF/HNT1wt% scaffolds (*i.e.,* SF-HDF ECM and SF/HNT1wt%-HDF ECM). Keratinocytes were grown on SF and SF/HNT1wt% scaffolds with or without the ECM coating. After 4 and 8 days of culture, immunofluorescent staining was performed using antibodies recognising K14, K10 and involucrin. As can be seen in Figure 6.13, after 4 days keratinocytes grown on all surfaces were positive for K14 staining. No marked differences were observed between the cells on these surfaces except that more colonies were formed on scaffolds coated with HDF-derived ECM. K10 expression was not observed in keratinocytes on any of the scaffolds, in contrast, the different scaffolds appeared to trigger different levels of involucrin expression. It was interesting that keratinocytes on HDF-derived ECM coated substrates expressed less involucrin compared to keratinocytes on uncoated scaffolds.

Figure 6.14 presents immunofluorescence images of keratinocytes cultured for 8 days on the various scaffolds. Keratinocytes clearly increased in number from day 4 to day 8 on all four scaffolds and the majority of these cells expressed K14. Thus, all scaffolds support keratinocyte growth, but a more confluent keratinocyte monolayer was obtained on HDF-derived ECM coated scaffolds compared to that obtained on scaffolds without the ECM coating. Most of the keratinocytes on HDF ECM coated substrates were of a uniform small cell size and gave rise to monolayers with a cobblestone-like morphology, which was not so much the case for cells on the uncoated scaffolds and particularly not for cells on the plain SF scaffolds. Like the day 4 results (Figure 6.13), staining with the anti-involucrin antibody indicated that a higher proportion of keratinocytes expressed involucrin when grown on uncoated substrates, as compared to keratinocytes grown on scaffolds functionalised with HDF ECM (Figure 6.14 v-viii). K10 expression was not detected in keratinocytes on any of the scaffolds. Moreover, SF/HNT 1wt% scaffolds with or without HDF ECM coating better facilitated keratinocyte adhesion and proliferation than the plain SF scaffolds. This is similar to what was observed earlier when keratinocytes were grown on SF and SF/HNT 1wt% substrates with or without 3T3 ECM functionalisation (Figures 6.10-6.11, 6.13-6.14).

Collectively the data described here indicated that keratinocytes cultured on substrates coated with HDF-derived ECM are less differentiated than those grown on either scaffolds coated with 3T3 ECM or on uncoated scaffolds. The functional significance of ECM for controlling epidermal stem cell fate has been highlighted in many studies [703-705]. Recent evidence indicates that stem cell-ECM interactions contribute to maintaining the self-renewal ability of stem cells by preventing differentiation [706]. Watt *et al*. [686] reported that the combination of type IV collagen and fibronectin hampered the differentiation of keratinocytes during *in vitro* culture. As shown earlier (Figure 6.12), the ECM generated by HDFs contained numerous ECM proteins, including fibronectin, type I collagen and type IV collagen, the combination of signals from which may have helped to suppress keratinocyte differentiation.

It has been reported that ECMs are tissue-specific, and ECM from one tissue best maintains cells from the same tissue. For example, Marinkovic *et al.* [692] showed that the proliferation of bone marrow mesenchymal stem cells and adipose mesenchymal stem cells was better sustained when these cells were cultured on their corresponding tissue-derived ECM. Similarly, Sellaro *et al.* [693] reported that ECM derived from liver is more able to sustain the phenotype of hepatic sinusoidal endothelial cells during *in vitro* culture compared to ECM derived from urinary bladder, or from the small intestinal submucosa. While many ECM components are similar in different tissues, within specific regions of the skin and at different developmental stages, there is considerable anatomical and molecular variation in the ECM proteins expressed [704, 707]. In our study, ECM from two different fibroblast types (murine 3T3 fibroblasts and HDFs) were shown to similarly deposit fibronectin, type I collagen and type IV collagen, but many of the minor ECM components are likely to be qualitatively or quantitatively different. As the HDF cells are from human skin, it is probable that HDF-derived ECM coated scaffolds provided a more physiologically compliant microenvironment that assisted in suppressing, or down regulating keratinocyte differentiation pathways rather more than 3T3 fibroblast derived ECM coated scaffolds. Others have similarly found that human dermal fibroblast feeder layers can both maintain keratinocyte proliferation and delay terminal differentiation [708]. They suggested that human fibroblasts prevented the early terminal differentiation of keratinocytes through a molecular pathway that involves the transcription factor Sp1.

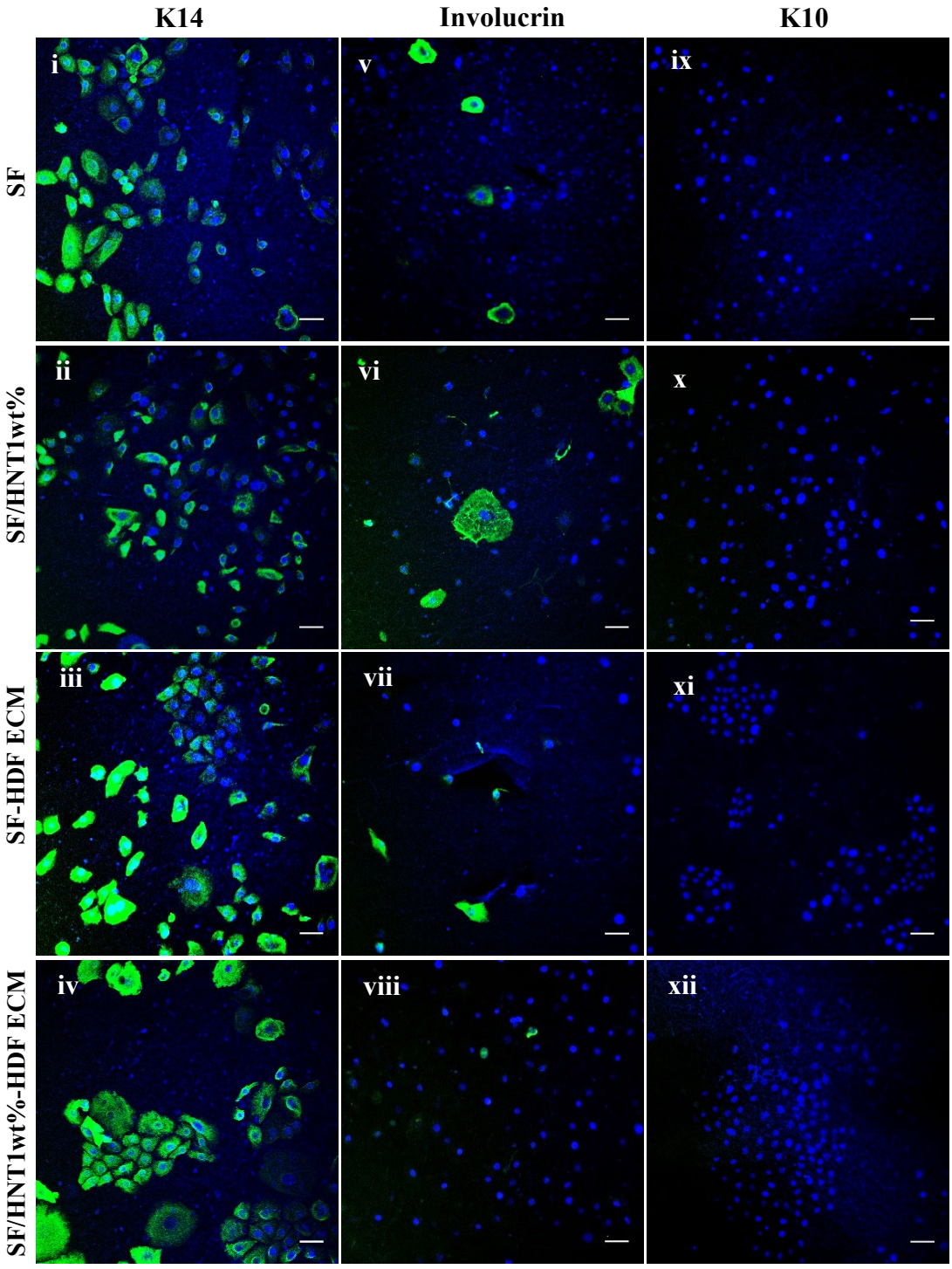

Figure 6.13 K10, K14 and involucrin expression by keratinocytes grown for 4 days on the SF based scaffolds with or without HDFs ECM coating.

Keratinocytes (0.4 x 10^4) were cultured in DKSFM on different substrates, they were fixed with 4% paraformaldehyde and stained with antibodies recognising cytokeratin 14 (K14; i-iv), involucrin (v-viii) and cytokeratin 10 (K10; ix-xii). Nuclei were stained with DAPI (Blue). Scale bars are 50 µm.

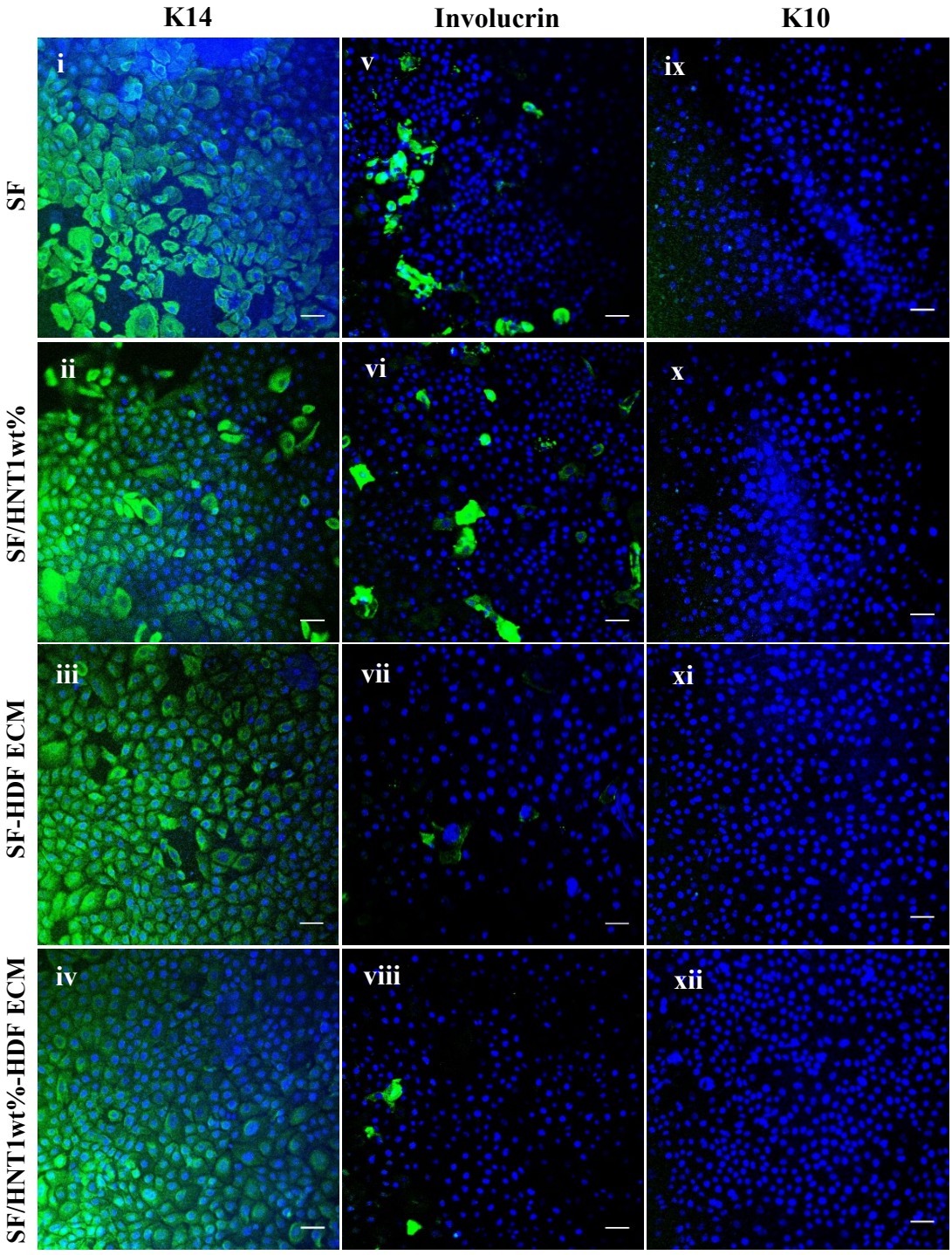

Figure 6.14 K10, K14 and involucrin expression by keratinocytes grown for 8 days on the SF based scaffolds with or without HDFs ECM coating.

Keratinocyte culture and immunostaining conditions were as described in Figure 6.13. Antibodies recognised: cytokeratin 14 (K14; i-iv), involucrin (v-viii) and cytokeratin 10 (K10; ix-xii). Nuclei were stained with DAPI (Blue). Scale bars are 50 μm.

6.4 Conclusion

The main objective of this chapter was to investigate the potential of SF based scaffolds for keratinocytes adhesion and whether a fibroblast ECM coating further improved keratinocyte proliferation. Immunofluorescence images revealed that the incorporation of type I collagen hydrogel into the SF scaffold decreased the ECM deposited by the fibroblasts, and in particular the levels of fibronectin were higher in the absence of the collagen hydrogel. Hence, SF scaffolds and SF/HNT 1wt% scaffolds (developed in Chapter IV) were used as substrates. The both 3T3 fibroblasts and or HDFs deposited fibronectin, type I collagen and type IV collagen onto SF and SF/HNT 1wt% substrates. However, the deposition of the ECM proteins appeared to be denser and more organised on SF/HNT 1wt% scaffolds relative to that seen on SF scaffolds.

The data obtained from experiments with primary human keratinocytes, seeded on the SF and SF/HNT 1wt% scaffolds in defined serum free medium, indicated these scaffolds supported keratinocytes growth. However, the addition of decellularised ECM from either 3T3 fibroblasts or HDFs markedly enhanced keratinocyte expansion. Interestingly, HDF coated substrates appeared to better suppress, or down-regulate keratinocyte differentiation pathways than the 3T3 fibroblast derived ECM coated scaffolds. This may have been because the HDF ECM provided a more physiologically compliant microenvironment for proliferative basal keratinocytes. In general, SF/HNT1wt%-HDF ECM was shown to be a superior substrate for the growth of primary human keratinocytes compared to 3T3 ECM on either of the SF-based scaffolds. The keratinocytes on SF/HNT1wt%-HDF ECM proliferated more and were undifferentiated, as indicated by firstly, a very small number of cells that were involucrin positive and secondly, the cobblestone-like morphology of the small keratinocytes that comprised the monolayer. Collectively these data suggest that the SF/HNT1wt% scaffold coated with HDF ECM has potential as a biomaterial to assist in the healing of large, deep wounds.

Chapter VII: Conclusions and Future Work

7.1 Conclusions

The primary objective of this thesis was to develop new electrospun silk fibroin (SF) based nanocomposites for tissue engineering applications. To this end, three different SF based electrospun scaffolds were fabricated by (1) incorporating halloysite nanotubes (HNTs) into the SF scaffolds, (2) by blending SF with gelatin, and (3) by coating SF scaffolds with collagen type I (Col I). For each scaffold type, physical properties of the material and their biological compatibility *in vitro* were examined. From this work, the scaffold that had the most favourable characteristics was coated with extracellular matrices (ECM) secreted by two different types of fibroblasts and investigated for its ability to support keratinocyte expansion. The latter work involved comparing keratinocyte expansion on both selected SF-based scaffold and plain SF scaffold with and without the ECM coating. The following are the main conclusions drawn from this work.

It has been published by others [25, 33, 34] that the incorporation of HNTs into various polymer matrices accelerated wound healing, cell adhesion and cell proliferation, whilst also enhancing the mechanical performance of the nanocomposites. In this study (**Chapter IV**), electrospun SF/HNT nanocomposites were manufactured. Our data indicated that the addition of HNTs into the SF solution barely affected the scaffold morphology, such as fibre collapse or breakage. However, the average fibre diameters were found to be increased by the addition of HNTs and at higher HNTs contents of 5 and 7 wt%, HNT aggregation and surface irregularity of the SF fibres were detected. The addition of a low amount of HNTs (*i.e.,* 1 wt%) enhanced the hydrophilicity and increased the water uptake capacity (WUC) of the composite nanofibre scaffolds above those fabricated from plain SF. This was probably because of the hydrophilic nature of HNTs,

When the HNT content was increased to 3 wt%, noticeable increases in Young's modulus and tensile strength of the nanocomposites were achieved. These findings were ascribed to the inherent toughness of HNTs and the good HNTs dispersion throughout the SF scaffolds; meaning that applied external loads can be effectively transferred to HNTs. However, further increasing the HNT content up to 7 wt% caused poor HNT dispersion and agglomeration, as confirmed from the results of morphological structures for SF/HNT nanocomposites, leading to decreasing

mechanical properties in terms of their Young's modulus, tensile strength and elongation at break. The incorporation of HNTs also enhanced the thermal stability of SF/HNT scaffolds, and as the HNT content increased so did the thermal stability. The increase thermal stability of the scaffolds is believed to be associated with high thermal stability of HNTs as well as the HNTs exerting a barrier effect towards both mass and heat transport.

Our data confirmed the cytocompatibility of all SF/HNTs scaffolds. However, scaffolds containing SF/HNT 1 wt% better supported firstly, the viability and spreading of 3T3 fibroblasts, and secondly, the differentiation of C2C12 myoblasts into aligned myotubes. The incorporation of HNTs into the scaffolds induced physiochemical changes in the scaffolds, which in turn altered the cells' microenvironment and accordingly cell responses. In this study, the incorporation of a very low amount of HNTs (1 wt%) rendered a microenvironment with a combination of low surface roughness and high WUC, thereby favoring cell proliferation and differentiation.

Gelatin has an inherent potential to promote cell proliferation, migration and adhesion as it is derived from collagen, a major ECM protein, and gelatin has many sites, like the RGD motif, that facilitate cell activities [42, 43]. In **Chapter V,** SF/gelatin blended fibres crosslinked with glutaraldehyde (GTA) were examined to determine whether the addition of gelatin boosted the effectiveness of the scaffolds for tissue engineering. Our results showed that the addition of gelatin to SF gave rise to a higher degree of crosslinking, which in turn yielded more fibre twining and adhesive features with a reduction of scaffold porosity. As a consequence, scaffolds with high gelatin ratios possessed lower WUC. In addition, the incorporation of gelatin did not enhance the tensile strength and Young's modulus.

Results from proliferation assays and ECM deposition experiments revealed that SF/gelatin fibre mats with the highest gelatin weight ratio (*i.e.,* 70/30) supported the lowest 3T3 fibroblast proliferation rates and the lowest levels of ECM deposition. These findings may be due to the fact that GTA crosslinking induced changes in the physical characteristics of the scaffold microenvironment presented to the cells at the higher gelatin levels. In particular, WUC and porosity of the scaffolds were likely to have influenced cell behaviour. As a result, plain SF scaffolds gave rise to a superior

microenvironment for cell growth and ECM deposition compared to the SF/gelatin fibre mats.

Col I, is a natural protein and key component of connective tissue ECM. Like gelatin it contains abundant binding sites for cell surface adhesion molecules, of the integrin family, and as a result it has been reported to enhance cell proliferation and hence tissue regeneration [50]. However, our results from **Chapter VI**, indicated that coating SF with Col I did not enhanced 3T3 fibroblast proliferation. Probably the high collagen concentration that was used in this study, and which led to a high density gel, suppressed fibroblast proliferation. Additionally, ECM deposition images showed that the incorporation of Col I reduced the amount of fibronectin deposited by 3T3 fibroblasts, compared to that seen when cells were growing on plain SF.

Consequently, from the three different SF based scaffolds that were developed in this thesis, methanol treated SF and SF/HNT 1wt% scaffolds were found to be the materials with the preferred characteristics for tissue engineering applications.

Numerous studies have shown that acellular ECM assists in maintaining the stem cell phenotype, including the ability of stem cells to self-renew ability during *in vitro* expansion [688, 689, 709] . In **Chapter VI** the two best SF based scaffolds, (*i.e.*, SF, and SF/HNT 1wt%) were examined for their ability to support keratinocyte expansion. This study was in two parts: firstly, because keratinocyte expansion *in vitro* is frequently performed with a feeder layer of 3T3 cells, the possibility that 3T3 cell ECM may enhance the ability of these scaffolds to support keratinocyte expansion was examined, and secondly, whether a tissue relevant ECM (*i.e.,* from HDFs) deposited on these scaffold may enhance keratinocyte expansion was also examined. Our data indicated that both 3T3 cells and HDFs deposited an ECM on the SF-based scaffolds, as immunofluorescence experiments indicated the presence of three key ECM proteins on SF and SF/HNT 1wt% surfaces following decellularisation. However, the ECM proteins secreted appeared denser and more organised on SF/HNT 1wt% scaffolds.

Our results indicated that although SF and SF/HNT 1wt % scaffolds supported keratinocyte growth, coating these scaffolds with either 3T3 cell or HDF ECMs enhanced keratinocyte expansion. Interestingly, HDF ECM coated substrates appeared to provide a more physiologically compliant microenvironment because keratinocyte differentiation pathways, (indicated by involucrin expression) were down-regulated

more on scaffolds coated with HDF ECM, than that seen with 3T3 fibroblast derived ECM coated scaffolds. Moreover, keratinocytes on SF/HNT1wt%-HDF ECM also proliferated more. Thus, the SF/HNT 1wt% scaffolds coated with dermal ECM best supported the retention of undifferentiated/basal keratinocytes during *in vitro* culture.

In conclusion, this study has highlighted the potential of SF based scaffolds for tissue engineering applications. Furthermore the novel HDF coated SF/HNT 1wt% scaffolds developed in this study may serve as an appropriate substrate for expanding undifferentiated keratinocytes *in vitro* for clinical applications. In addition, this scaffold may also be very useful as a dressing for wound healing, and particularly so if the ECM and the keratinocytes are autologous.

7.2 Future Work

- Our results indicate that SF/HNT nanocomposites may be useful scaffolds for tissue engineering. For medical use, the materials must be safe for cells and for insertion into human body. Although both SF and HNTs have been reported to be safe and biocompatible materials, the solvent that we used for SF/HNT fabrication was formic acid, any residual of which is harmful to humans and the environment [28, 710]. To prevent such risks, developing these scaffolds using an aqueous system could be beneficial [260, 261].
- The degradation of biomaterial scaffolds is a key factor for successful tissue regeneration. The best scaffolds degrade and reshape at a rate that matches the formation of new tissue [711, 712]. Material composition and structures of scaffold are the most important factors that can influence their degradation rates [713-715]. As the inclusion of HNTs into the SF altered the physiochemical properties of resulting scaffolds, it may accordingly alter the degradation rates of these SF-based nanocomposites. Hence, it will be most important to determine how HNTs affect the biodegradation of SF based scaffolds *in vitro* and *in vivo*.
- The potential application of HNTs as drug delivery vehicles is widely reported in the literatures. It is reported that polymer/HNT nanocomposites are promising drug containers as HNTs facilitate drug loading processes as well as slowing down the release of drugs from nanocomposites [372, 716-719]. Loading SF/HNT scaffolds with antimicrobial and antibiotic drugs, growth factors or

vitamins may further enhance their applications for tissue engineering and as wound dressings.

- Our results showed that the addition of gelatin failed to enhance the efficiency of SF scaffolds possibly due to the high degree of crosslinking induced by the GTA fixation step. It would be useful to optimise the crosslinking step so that SF/gelatin constructs are stabilised without sacrificing the physiochemical features of the scaffolds and thereby the favourable bioactive properties of gelatin can be better exploited. This could be achieved by using different GTA concentrations at various time intervals, or by using alternative crosslinking agents with less toxicity such as genipin, γ-glycidoxy propyl trimethoxy silane, oxidized polysaccharide and disaccharide and proanthocyanidin [392, 413, 417].
- It has been reported that collagen concentration influences its mechanical properties, thereby regulating cellular behaviour [679, 682]. Abreu *et al.* [678] revealed that increasing the collagen density of collagen-platelet hydrogels from 2 to 4 mg/mL resulted in stiffer scaffolds, which suppressed fibroblast proliferation. These scaffolds were also more resistant to retraction when seeded with fibroblasts. As such, further optimisation of collagen concentration is required to develop a SF/Col I biomaterial with desirable properties for tissue engineering applications.
- This study clearly demonstrated the beneficial effect of an ECM coating for supporting the proliferation of undifferentiated keratinocytes. It is likely that differences in ECM composition between the matrices from primary human dermal fibroblasts and 3T3 murine fibroblasts could have contributed to the different effects observed on the terminal differentiation of the keratinocytes. It will be interesting to quantitatively assess the differences in the ECM composition from these two cell types. Such information is necessary to understand the critical ECM components that regulate keratinocyte differentiation. Other studies [704, 720] have suggested that matrix stiffness rather than ECM concentration or composition is essential for keratinocyte differentiation, suggesting that biophysical factors may be important in determining keratinocyte stem cell fate. Alternatively, Huang *et al.* [721] showed that substrate stiffness and ECM protein composition cooperatively regulate wound healing in axolotls *in vivo*. Gupta *et al.* [722] reported that variation in the stiffness of the substrate results in modulation of the morphology, proliferation

and signal cascades of keratinocytes. Therefore, it will be of interest to explore the stiffness of the both 3T3 cell and HDF ECM coated SF scaffolds to see whether this will be a factor influencing keratinocyte behaviour.

Bibliography

1. O'Brien FJ. Biomaterials & scaffolds for tissue engineering. *Mater. Today*. 2011; 14:88-95.
2. Zhou Y, Chyu J, Zumwalt M. Recent Progress of Fabrication of Cell Scaffold by Electrospinning Technique for Articular Cartilage Tissue Engineering. *Int. J. Biomater*. 2018; 2018:10.
3. Carletti E, Motta A, Migliaresi C. Scaffolds for tissue engineering and 3D cell culture. *Methods mol. biol.(Clifton, N.J.)*. 2011; 695:17-39.
4. Hasan A, Memic A, Annabi N, et al. Electrospun scaffolds for tissue engineering of vascular grafts. *Acta Biomater.* 2014; 10:11-25.
5. Sundaramurthi D, Krishnan UM, Sethuraman S. Electrospun Nanofibers as Scaffolds for Skin Tissue Engineering. *Polym. Rev*. 2014; 54:348-376.
6. Barnes CP, Sell SA, Boland ED, Simpson DG, Bowlin GL. Nanofiber technology: Designing the next generation of tissue engineering scaffolds. *Adv. Drug Del. Rev.* 2007; 59:1413-1433.
7. Liu H, Ding X, Zhou G, et al. Electrospinning of nanofibers for tissue engineering applications. *Journal of Nanomaterials*. 2013; 2013
8. Jun I, Han H-S, Edwards JR, Jeon H. Electrospun Fibrous Scaffolds for Tissue Engineering: Viewpoints on Architecture and Fabrication. *Int. J. Mol. Sci.* 2018; 19:745.
9. Wang X, Ding B, Li B. Biomimetic electrospun nanofibrous structures for tissue engineering. *Mater. Today*. 2013; 16:229-241.
10. Kwon KJ, Seok H. Silk protein-based membrane for guided bone regeneration. *Applied Sciences (Switzerland)*. 2018; 8
11. Kundu B, Rajkhowa R, Kundu SC, Wang X. Silk fibroin biomaterials for tissue regenerations. *Adv. Drug Del. Rev.* 2013; 65:457-470.
12. Ma D, Wang Y, Dai W. Silk fibroin-based biomaterials for musculoskeletal tissue engineering. *Mater. Sci. Eng., C*. 2018; 89:456-469.
13. Xiong S, Zhang X, Lu P, et al. A Gelatin-sulfonated Silk Composite Scaffold based on 3D Printing Technology Enhances Skin Regeneration by Stimulating Epidermal Growth and Dermal Neovascularization. *Sci. Rep.* 2017; 7:4288.
14. Wang Y, Rudym DD, Walsh A, et al. In vivo degradation of three-dimensional silk fibroin scaffolds. *Biomaterials*. 2008; 29:3415-3428.
15. Numata K, Cebe P, Kaplan DL. Mechanism of enzymatic degradation of beta-sheet crystals. *Biomaterials*. 2010; 31:2926-2933.
16. Behera S, Naskar D, Sapru S, et al. Hydroxyapatite reinforced inherent RGD containing silk fibroin composite scaffolds: Promising platform for bone tissue engineering. *Nanomed. Nanotechnol. Biol. Med.* 2017; 13:1745-1759.
17. Morgan AW, Roskov KE, Lin-Gibson S, et al. Characterization and optimization of RGD-containing silk blends to support osteoblastic differentiation. *Biomaterials*. 2008; 29:2556-2563.
18. Su D, Jiang L, Chen X, Dong J, Shao Z. Enhancing the Gelation and Bioactivity of Injectable Silk Fibroin Hydrogel with Laponite Nanoplatelets. *ACS Appl. Mater. Interfaces*. 2016; 8:9619-9628.
19. Wang Y, Kim H-J, Vunjak-Novakovic G, Kaplan DL. Stem cell-based tissue engineering with silk biomaterials. *Biomaterials*. 2006; 27:6064-6082.
20. Thurber AE, Omenetto FG, Kaplan DL. In vivo bioresponses to silk proteins. *Biomaterials*. 2015; 71:145-157.
21. Naumenko EA, Guryanov ID, Yendluri R, Lvov YM, Fakhrullin RF. Clay nanotube-biopolymer composite scaffolds for tissue engineering. *Nanoscale*. 2016; 8:7257-7271.
22. Poland CA, Duffin R, Kinloch I, et al. Carbon nanotubes introduced into the abdominal cavity of mice show asbestos-like pathogenicity in a pilot study. *Nat. Nanotechnol.* 2008; 3:423.

23. Abdullayev E, Lvov Y. Halloysite clay nanotubes as a ceramic “skeleton” for functional biopolymer composites with sustained drug release. *J. Mater. Chem. B*. 2013; 1:2894-2903.
24. Lee IW, Li J, Chen X, Park HJ. Electrospun poly(vinyl alcohol) composite nanofibers with halloysite nanotubes for the sustained release of sodium d -pantothenate. *J. Appl. Polym. Sci.* 2016; 133
25. Liu M, Shen Y, Ao P, et al. The improvement of hemostatic and wound healing property of chitosan by halloysite nanotubes. *RSC Advances*. 2014; 4:23540-23553.
26. Ji L, Qiao W, Zhang Y, et al. A gelatin composite scaffold strengthened by drug-loaded halloysite nanotubes. *Materials Science and Engineering: C*. 2017; 78:362-369.
27. Liu M, Dai L, Shi H, Xiong S, Zhou C. In vitro evaluation of alginate/halloysite nanotube composite scaffolds for tissue engineering. *Mater. Sci. Eng., C*. 2015; 49:700-712.
28. Liu M, Jia Z, Jia D, Zhou C. Recent advance in research on halloysite nanotubes-polymer nanocomposite. *Prog. Polym. Sci.* 2014; 39:1498-1525.
29. Dong Y, Marshall J, Haroosh HJ, et al. Polylactic acid (PLA)/halloysite nanotube (HNT) composite mats: Influence of HNT content and modification. *Composites Part A: Applied Science and Manufacturing*. 2015; 76:28-36.
30. Zhang X, Guo R, Xu J, et al. Poly(l-lactide)/halloysite nanotube electrospun mats as dual-drug delivery systems and their therapeutic efficacy in infected full-thickness burns. *J. Biomater. Appl.* 2015; 30:512-525.
31. Nitya G, Nair GT, Mony U, Chennazhi KP, Nair SV. In vitro evaluation of electrospun PCL/nanoclay composite scaffold for bone tissue engineering. *J. Mater. Sci. Mater. Med.* 2012; 23:1749-1761.
32. Qi R, Cao X, Shen M, et al. Biocompatibility of electrospun halloysite nanotube-doped poly(Lactic-co-Glycolic Acid) composite nanofibers. *J. Biomater. Sci. Polym. Ed.* 2012; 23:299-313.
33. Du M, Guo B, Jia D. Newly emerging applications of halloysite nanotubes: A review. *Polym. Int.* 2010; 59:574-582.
34. Luo C, Zou Z, Luo B, et al. Enhanced mechanical properties and cytocompatibility of electrospun poly(l-lactide) composite fiber membranes assisted by polydopamine-coated halloysite nanotubes. *Appl. Surf. Sci.* 2016; 369:82-91.
35. Chen L, Hu J, Ran J, Shen X, Tong H. Preparation and evaluation of collagen-silk fibroin/hydroxyapatite nanocomposites for bone tissue engineering. *Int. J. Biol. Macromol.* 2014; 65:1-7.
36. Qi R, Guo R, Shen M, et al. Electrospun poly(lactic-co-glycolic acid)/halloysite nanotube composite nanofibers for drug encapsulation and sustained release. *J. Mater. Chem.* 2010; 20:10622-10629.
37. Gilpin A, Yang Y. Decellularization Strategies for Regenerative Medicine: From Processing Techniques to Applications. *BioMed Research International*. 2017; 2017
38. Levorson EJ, Mountziaris PM, Hu O, Kasper FK, Mikos AG. Cell-derived polymer/extracellular matrix composite scaffolds for cartilage regeneration, Part 1: investigation of cocultures and seeding densities for improved extracellular matrix deposition. *Tissue Eng Part C Methods*. 2014; 20:340-57.
39. Harvestine JN, Vollmer NL, Ho SS, et al. Extracellular Matrix-Coated Composite Scaffolds Promote Mesenchymal Stem Cell Persistence and Osteogenesis. *Biomacromolecules*. 2016; 17:3524-3531.
40. Sadr N, Pippenger BE, Scherberich A, et al. Enhancing the biological performance of synthetic polymeric materials by decoration with engineered, decellularized extracellular matrix. *Biomaterials*. 2012; 33:5085-5093.
41. Gu Y, Zhu J, Xue C, et al. Chitosan/silk fibroin-based, Schwann cell-derived extracellular matrix-modified scaffolds for bridging rat sciatic nerve gaps. *Biomaterials*. 2014; 35:2253-2263.
42. Djagny KB, Wang Z, Xu S. Gelatin: A valuable protein for food and pharmaceutical industries: Review. *Crit. Rev. Food Sci. Nutr.* 2001; 41:481-492.

43. Echave MC, Burgo LS, Pedraz JL, Orive G. Gelatin as biomaterial for tissue engineering. *Curr. Pharm. Des.* 2017; 23:3567-3584.
44. Shalumon KT, Deepthi S, Anupama MS, et al. Fabrication of poly (l-lactic acid)/gelatin composite tubular scaffolds for vascular tissue engineering. *Int. J. Biol. Macromol.* 2015; 72:1048-1055.
45. Rong D, Chen P, Yang Y, et al. Fabrication of gelatin/PCL electrospun fiber mat with bone powder and the study of its biocompatibility. *J. Funct. Biomater.* 2016; 7
46. Meng ZX, Wang YS, Ma C, et al. Electrospinning of PLGA/gelatin randomly-oriented and aligned nanofibers as potential scaffold in tissue engineering. *Mater. Sci. Eng., C*. 2010; 30:1204-1210.
47. Detta N, Errico C, Dinucci D, et al. Novel electrospun polyurethane/gelatin composite meshes for vascular grafts. *J. Mater. Sci. Mater. Med.* 2010; 21:1761-1769.
48. Yang Z, Xu LS, Yin F, et al. In vitro and in vivo characterization of silk fibroin/gelatin composite scaffolds for liver tissue engineering. *J. Dig. Dis.* 2011; 13:168-178.
49. Zeltz C, Gullberg D. The integrin-collagen connection--a glue for tissue repair? *J. Cell Sci.* 2016; 129:653-64.
50. Parenteau-Bareil R, Gauvin R, Berthod F. Collagen-based biomaterials for tissue engineering applications. *Materials*. 2010; 3:1863-1887.
51. Liu S-J, Kau Y-C, Chou C-Y, et al. Electrospun PLGA/collagen nanofibrous membrane as early-stage wound dressing. *J. Membr. Sci.* 2010; 355:53-59.
52. Fu X, Xu M, Liu J, et al. Regulation of migratory activity of human keratinocytes by topography of multiscale collagen-containing nanofibrous matrices. *Biomaterials*. 2014; 35:1496-1506.
53. Sell SA, McClure MJ, Garg K, Wolfe PS, Bowlin GL. Electrospinning of collagen/biopolymers for regenerative medicine and cardiovascular tissue engineering. *Adv. Drug Del. Rev.* 2009; 61:1007-1019.
54. Sionkowska A. Current research on the blends of natural and synthetic polymers as new biomaterials: Review. *Progress in Polymer Science (Oxford)*. 2011; 36:1254-1276.
55. Langer R, Vacanti JP. Tissue engineering. *Science*. 1993; 260:920-926.
56. Dzobo K, Thomford NE, Senthebane DA, et al. Advances in regenerative medicine and tissue engineering: Innovation and transformation of medicine. *Stem cells international*. 2018; 2018
57. O'Brien FJ. Biomaterials & scaffolds for tissue engineering. *Mater. Today*. 2011; 14:88-95.
58. Yeo IS, Oh JE, Jeong L, et al. Collagen-based biomimetic nanofibrous scaffolds: Preparation and characterization of collagen/silk fibroin bicomponent nanofibrous structures. *Biomacromolecules*. 2008; 9:1106-1116.
59. Law JX, Liau LL, Saim A, Yang Y, Idrus R. Electrospun Collagen Nanofibers and Their Applications in Skin Tissue Engineering. *Tissue Engineering and Regenerative Medicine*. 2017; 14:699-718.
60. Griffith LG, Swartz MA. Capturing complex 3D tissue physiology in vitro. *Nature Reviews Molecular Cell Biology*. 2006; 7:211.
61. Williams DF. On the mechanisms of biocompatibility. *Biomaterials*. 2008; 29:2941-2953.
62. Chan BP, Leong KW. Scaffolding in tissue engineering: General approaches and tissue-specific considerations. *Eur. Spine J.* 2008; 17:S467-S479.
63. Babensee JE, Anderson JM, McIntire LV, Mikos AG. Host response to tissue engineered devices. *Adv. Drug Del. Rev.* 1998; 33:111-139.
64. Bitar KN, Zakhem E. Design Strategies of Biodegradable Scaffolds for Tissue Regeneration. *Biomedical Engineering and Computational Biology*. 2014; 6:13-20.
65. Le X, Poinern GEJ, Ali N, Berry CM, Fawcett D. Engineering a biocompatible scaffold with either micrometre or nanometre scale surface topography for promoting protein adsorption and cellular response. *International Journal of Biomaterials*. 2013; 2013
66. Kloxin AM, Benton JA, Anseth KS. In situ elasticity modulation with dynamic substrates to direct cell phenotype. *Biomaterials*. 2010; 31:1-8.

67. Discher DE, Janmey P, Wang YL. Tissue cells feel and respond to the stiffness of their substrate. *Science*. 2005; 310:1139-43.
68. Rowlands AS, George PA, Cooper-White JJ. Directing osteogenic and myogenic differentiation of MSCs: Interplay of stiffness and adhesive ligand presentation. *American Journal of Physiology - Cell Physiology*. 2008; 295:C1037-C1044.
69. Uludag H, De Vos P, Tresco PA. Technology of mammalian cell encapsulation. *Adv. Drug Del. Rev.* 2000; 42:29-64.
70. Nicodemus GD, Bryant SJ. Cell encapsulation in biodegradable hydrogels for tissue engineering applications. *Tissue Engineering - Part B: Reviews*. 2008; 14:149-165.
71. Yang J, Yamato M, Shimizu T, et al. Reconstruction of functional tissues with cell sheet engineering. *Biomaterials*. 2007; 28:5033-5043.
72. Sekiya S, Shimizu T, Yamato M, Kikuchi A, Okano T. Bioengineered cardiac cell sheet grafts have intrinsic angiogenic potential. *Biochem. Biophys. Res. Commun.* 2006; 341:573-582.
73. Shimizu T, Sekine H, Yang J, et al. Polysurgery of cell sheet grafts overcomes diffusion limits to produce thick, vascularized myocardial tissues. *FASEB J.* 2006; 20:708-710.
74. Kim TG, Shin H, Lim DW. Biomimetic scaffolds for tissue engineering. *Adv. Funct. Mater.* 2012; 22:2446-2468.
75. Dhandayuthapani B, Yoshida Y, Maekawa T, Kumar DS. Polymeric scaffolds in tissue engineering application: A review. *International Journal of Polymer Science*. 2011; 2011
76. Dutta RC, Dey M, Dutta AK, Basu B. Competent processing techniques for scaffolds in tissue engineering. *Biotechnol. Adv.* 2017; 35:240-250.
77. Sin D, Miao X, Liu G, et al. Polyurethane (PU) scaffolds prepared by solvent casting/particulate leaching (SCPL) combined with centrifugation. *Mater. Sci. Eng., C*. 2010; 30:78-85.
78. Akbarzadeh R, Yousefi AM. Effects of processing parameters in thermally induced phase separation technique on porous architecture of scaffolds for bone tissue engineering. *Journal of Biomedical Materials Research - Part B Applied Biomaterials*. 2014; 102:1304-1315.
79. Dehghani F, Annabi N. Engineering porous scaffolds using gas-based techniques. *Curr. Opin. Biotechnol.* 2011; 22:661-666.
80. Khan F, Tanaka M, Ahmad SR. Fabrication of polymeric biomaterials: a strategy for tissue engineering and medical devices. *Journal of Materials Chemistry B*. 2015; 3:8224-8249.
81. Seol YJ, Kang TY, Cho DW. Solid freeform fabrication technology applied to tissue engineering with various biomaterials. *Soft Matter*. 2012; 8:1730-1735.
82. Landers R, Hübner U, Schmelzeisen R, Mülhaupt R. Rapid prototyping of scaffolds derived from thermoreversible hydrogels and tailored for applications in tissue engineering. *Biomaterials*. 2002; 23:4437-4447.
83. Parks KL, Beckman EJ. Generation of microcellular polyurethane foams via polymerization in carbon dioxide. II: Foam formation and characterization. *Polym. Eng. Sci.* 1996; 36:2417-2431.
84. Barbetta A, Rizzitelli G, Bedini R, Pecci R, Dentini M. Porous gelatin hydrogels by gas-in-liquid foam templating. *Soft Matter*. 2010; 6:1785-1792.
85. Costantini M, Barbetta A. Gas foaming technologies for 3D scaffold engineering. In: Functional 3D Tissue Engineering Scaffolds: Woodhead Publishing; 2018. p. 127-149.
86. Lu T, Li Y, Chen T. Techniques for fabrication and construction of three-dimensional scaffolds for tissue engineering. *International Journal of Nanomedicine*. 2013; 8:337-350.
87. Smith IO, Liu XH, Smith LA, Ma PX. Nanostructured polymer scaffolds for tissue engineering and regenerative medicine. *Wiley Interdisciplinary Reviews: Nanomedicine and Nanobiotechnology*. 2009; 1:226-236.
88. Sultana N, Hassan MI, Lim MM. Scaffold Fabrication Protocols. In: Sultana N, Hassan MI, Lim MM, editors. Composite Synthetic Scaffolds for Tissue Engineering and Regenerative Medicine. Cham: Springer International Publishing; 2015. p. 13-24.

89. Thomson RC, Wake MC, Yaszemski MJ, Mikos AG. Biodegradable polymer scaffolds to regenerate organs. *Adv. Polym. Sci.* 1995; 122:218-274.
90. Mikos AG, Bao Y, Cima LG, et al. Preparation of poly(glycolic acid) bonded fiber structures for cell attachment and transplantation. *J. Biomed. Mater. Res.* 1993; 27:183-189.
91. Subia B, Kundu J, Kundu S. Biomaterial scaffold fabrication techniques for potential tissue engineering applications. In: Tissue Eng.: InTech; 2010.
92. Hartgerink JD, Beniash E, Stupp SI. Self-assembly and mineralization of peptide-amphiphile nanofibers. *Science*. 2001; 294:1684-1688.
93. Barnes CP, Sell SA, Boland ED, Simpson DG, Bowlin GL. Nanofiber technology: Designing the next generation of tissue engineering scaffolds. *Adv. Drug Del. Rev.* 2007; 59:1413-1433.
94. Ibrahim DM, Kakarougkas A, Allam NK. Recent advances on electrospun scaffolds as matrices for tissue-engineered heart valves. *Materials Today Chemistry*. 2017; 5:11-23.
95. Cheng H, Yang X, Che X, Yang M, Zhai G. Biomedical application and controlled drug release of electrospun fibrous materials. *Materials Science and Engineering: C*. 2018; 90:750-763.
96. Lee JW, Kim JY, Cho DW. Solid free-form fabrication technology and its application to bone tissue engineering. *International Journal of Stem Cells*. 2010; 3:85-95.
97. Hesaraki S, Zamanian A, Moztarzadeh F. The influence of the acidic component of the gas-foaming porogen used in preparing an injectable porous calcium phosphate cement on its properties: Acetic acid versus citric acid. *Journal of Biomedical Materials Research - Part B Applied Biomaterials*. 2008; 86:208-216.
98. Maniglio D, Bonani W, Migliaresi C, Motta A. Silk fibroin porous scaffolds by N2O foaming. *J. Biomater. Sci. Polym. Ed.* 2018; 29:491-506.
99. Chen VJ, Smith LA, Ma PX. Bone regeneration on computer-designed nano-fibrous scaffolds. *Biomaterials*. 2006; 27:3973-3979.
100. Wei G, Ma PX. Macroporous and nanofibrous polymer scaffolds and polymer/bone-like apatite composite scaffolds generated by sugar spheres. *Journal of Biomedical Materials Research - Part A*. 2006; 78:306-315.
101. Ibrahim DM, Kakarougkas A, Allam NK. Recent advances on electrospun scaffolds as matrices for tissue-engineered heart valves. *Materials Today Chemistry*. 2017; 5:11-23.
102. Zhu N, Chen X. Biofabrication of tissue scaffolds. In: Advances in biomaterials science and biomedical applications: InTech; 2013.
103. Ratheesh G, Venugopal JR, Chinappan A, et al. 3D Fabrication of Polymeric Scaffolds for Regenerative Therapy. *ACS Biomaterials Science and Engineering*. 2017; 3:1175-1194.
104. Hench LL. Bioceramics. *Journal of the American Ceramic Society*. 1998; 81:1705-1727.
105. Sai Nievethitha S, Subhapradha N, Saravanan D, et al. Nanoceramics on osteoblast proliferation and differentiation in bone tissue engineering. *Int. J. Biol. Macromol.* 2017; 98:67-74.
106. Gunatillake P, Mayadunne R, Adhikari R. Recent developments in biodegradable synthetic polymers [Review]. 2006.
107. Fitzgerald JF, Kumar AS. Biologic versus synthetic mesh reinforcement: What are the pros and cons? *Clin. Colon Rectal Surg.* 2014; 27:140-148.
108. Kurella A, Dahotre NB. Review paper: Surface modification for bioimplants: The role of laser surface engineering. *J. Biomater. Appl.* 2005; 20:5-50.
109. Brodie JC, Goldie E, Connel G, Merry J, Grant MH. Osteoblast interactions with calcium phosphate ceramics modified by coating with type I collagen. *Journal of Biomedical Materials Research - Part A*. 2005; 73:409-421.
110. ALEXANDER H, BRUNSKI JB, COOPER SL, et al. Classes of materials used in medicine. In: Biomaterials Science: Elsevier; 1996. p. 37-130.
111. Sano A, Maeda M, Nagahara S, et al. Atelocollagen for protein and gene delivery. *Adv. Drug Del. Rev.* 2003; 55:1651-1677.
112. Ma PX. Biomimetic materials for tissue engineering. *Adv. Drug Del. Rev.* 2008; 60:184-198.

113. Lee E, Milan A, Urbani L, De Coppi P, Lowdell MW. Decellularized material as scaffolds for tissue engineering studies in long gap esophageal atresia. *Expert Opin. Biol. Ther.* 2017; 17:573-584.
114. Gilbert TW, Sellaro TL, Badylak SF. Decellularization of tissues and organs. *Biomaterials*. 2006; 27:3675-3683.
115. Kim BS, Kim H, Gao G, Jang J, Cho DW. Decellularized extracellular matrix: A step towards the next generation source for bioink manufacturing. *Biofabrication*. 2017; 9
116. Wang L, Johnson JA, Chang DW, Zhang Q. Decellularized musculofascial extracellular matrix for tissue engineering. *Biomaterials*. 2013; 34:2641-2654.
117. Wong ML, Griffiths LG. Immunogenicity in xenogeneic scaffold generation: Antigen removal vs. decellularization. *Acta Biomater.* 2014; 10:1806-1816.
118. Fitzpatrick LE, McDevitt TC. Cell-derived matrices for tissue engineering and regenerative medicine applications. *Biomaterials Science*. 2015; 3:12-24.
119. Rana D, Zreiqat H, Benkirane-Jessel N, Ramakrishna S, Ramalingam M. Development of decellularized scaffolds for stem cell-driven tissue engineering. *J. Tissue Eng. Regen. Med.* 2017; 11:942-965.
120. Elliott RA, Jr., Hoehn JG. Use of commercial porcine skin for wound dressings. *Plast. Reconstr. Surg.* 1973; 52:401-405.
121. Saldin LT, Cramer MC, Velankar SS, White LJ, Badylak SF. Extracellular matrix hydrogels from decellularized tissues: Structure and function. *Acta Biomater.* 2017; 49:1-15.
122. Badylak SF, Lantz GC, Coffey A, Geddes LA. Small intestinal submucosa as a large diameter vascular graft in the dog. *J. Surg. Res.* 1989; 47:74-80.
123. Lu H, Hoshiba T, Kawazoe N, et al. Cultured cell-derived extracellular matrix scaffolds for tissue engineering. *Biomaterials*. 2011; 32:9658-9666.
124. Uygun BE, Soto-Gutierrez A, Yagi H, et al. Organ reengineering through development of a transplantable recellularized liver graft using decellularized liver matrix. *Nat. Med.* 2010; 16:814-820.
125. Cheng CW, Solorio LD, Alsberg E. Decellularized tissue and cell-derived extracellular matrices as scaffolds for orthopaedic tissue engineering. *Biotechnol. Adv.* 2014; 32:462-484.
126. Frantz C, Stewart KM, Weaver VM. The extracellular matrix at a glance. *J. Cell Sci.* 2010; 123:4195-4200.
127. Theocharis AD, Skandalis SS, Gialeli C, Karamanos NK. Extracellular matrix structure. *Adv. Drug Del. Rev.* 2016; 97:4-27.
128. Bosman FT, Stamenkovic I. Functional structure and composition of the extracellular matrix. *J. Pathol.* 2003; 200:423-428.
129. Turoverova LV, Khotin MG, Yudintseva NM, et al. Analysis of extracellular matrix proteins produced by cultured cells. *Cell and Tissue Biology*. 2009; 3:497-502.
130. Manabe RI, Tsutsui K, Yamada T, et al. Transcriptome-based systematic identification of extracellular matrix proteins. *Proc. Natl. Acad. Sci. U. S. A.* 2008; 105:12849-12854.
131. Batzios SP, Zafeiriou DI, Papakonstantinou E. Extracellular matrix components: An intricate network of possible biomarkers for lysosomal storage disorders? *FEBS Lett.* 2013; 587:1258-1267.
132. Lu P, Weaver VM, Werb Z. The extracellular matrix: A dynamic niche in cancer progression. *J. Cell Biol.* 2012; 196:395-406.
133. Jaspreet KK, Shouvik B, Ram IS. The extracellular matrix: Structure, composition, age-related differences, tools for analysis and applications for tissue engineering. *Journal of Tissue Engineering*. 2014; 5:2041731414557112.
134. Hoshiba T, Chen G, Endo C, et al. Decellularized extracellular matrix as an in vitro model to study the comprehensive roles of the ECM in stem cell differentiation. *Stem Cells International*. 2016; 2016
135. Fernandes H, Moroni L, Van Blitterswijk C, De Boer J. Extracellular matrix and tissue engineering applications. *J. Mater. Chem.* 2009; 19:5474-5484.

136. Yi S, Ding F, Gong L, Gu X. Extracellular matrix scaffolds for tissue engineering and regenerative medicine. *Current Stem Cell Research and Therapy*. 2017; 12:233-246.
137. Kim Y, Ko H, Kwon IK, Shin K. Extracellular Matrix Revisited: Roles in Tissue Engineering. *Int. Neurourol. J.* 2016; 20:S23-29.
138. Zhang W, Zhu Y, Li J, et al. Cell-derived extracellular matrix: Basic characteristics and current applications in orthopedic tissue engineering. *Tissue Engineering - Part B: Reviews*. 2016; 22:193-207.
139. Hoshiba T. Cultured cell-derived decellularized matrices: A review towards the next decade. *Journal of Materials Chemistry B*. 2017; 5:4322-4331.
140. Liao J, Guo X, Grande-Allen KJ, Kasper FK, Mikos AG. Bioactive polymer/extracellular matrix scaffolds fabricated with a flow perfusion bioreactor for cartilage tissue engineering. *Biomaterials*. 2010; 31:8911-8920.
141. Lau TT, Lee LQP, Vo BN, Su K, Wang D-A. Inducing ossification in an engineered 3D scaffold-free living cartilage template. *Biomaterials*. 2012; 33:8406-8417.
142. Lu H, Hoshiba T, Kawazoe N, Chen G. Comparison of decellularization techniques for preparation of extracellular matrix scaffolds derived from three-dimensional cell culture. *Journal of Biomedical Materials Research - Part A*. 2012; 100 A:2507-2516.
143. Lu H, Hoshiba T, Kawazoe N, et al. Cultured cell-derived extracellular matrix scaffolds for tissue engineering. *Biomaterials*. 2011; 32:9658-9666.
144. Hoshiba T, Lu H, Yamada T, et al. Effects of extracellular matrices derived from different cell sources on chondrocyte functions. *Biotechnol. Prog.* 2011; 27:788-795.
145. Prewitz MC, Stißel A, Friedrichs J, et al. Extracellular matrix deposition of bone marrow stroma enhanced by macromolecular crowding. *Biomaterials*. 2015; 73:60-69.
146. Chen C, Loe F, Blocki A, Peng Y, Raghunath M. Applying macromolecular crowding to enhance extracellular matrix deposition and its remodeling in vitro for tissue engineering and cell-based therapies. *Adv. Drug Del. Rev.* 2011; 63:277-290.
147. Zeiger AS, Loe FC, Li R, Raghunath M, Van Vliet KJ. Macromolecular Crowding Directs Extracellular Matrix Organization and Mesenchymal Stem Cell Behavior. *PLoS One*. 2012; 7:e37904.
148. Mittal S, Chowhan RK, Singh LR. Macromolecular crowding: Macromolecules friend or foe. *Biochimica et Biophysica Acta (BBA) - General Subjects*. 2015; 1850:1822-1831.
149. Benny P, Raghunath M. Making microenvironments: A look into incorporating macromolecular crowding into in vitro experiments, to generate biomimetic microenvironments which are capable of directing cell function for tissue engineering applications. *Journal of Tissue Engineering*. 2017; 8:2041731417730467.
150. Ang XM, Lee MHC, Blocki A, et al. Macromolecular Crowding Amplifies Adipogenesis of Human Bone Marrow-Derived Mesenchymal Stem Cells by Enhancing the Pro-Adipogenic Microenvironment. *Tissue Engineering. Part A*. 2014; 20:966-981.
151. Kumar P, Satyam A, Fan X, et al. Macromolecularly crowded in vitro microenvironments accelerate the production of extracellular matrix-rich supramolecular assemblies. *Sci. Rep.* 2015; 5
152. Satyam A, Kumar P, Cigognini D, Pandit A, Zeugolis DI. Low, but not too low, oxygen tension and macromolecular crowding accelerate extracellular matrix deposition in human dermal fibroblast culture. *Acta Biomater.* 2016; 44:221-231.
153. Benny P, Badowski C, Lane EB, Raghunath M. Making More Matrix: Enhancing the Deposition of Dermal–Epidermal Junction Components In Vitro and Accelerating Organotypic Skin Culture Development, Using Macromolecular Crowding. *Tissue Engineering. Part A*. 2015; 21:183-192.
154. Crapo PM, Gilbert TW, Badylak SF. An overview of tissue and whole organ decellularization processes. *Biomaterials*. 2011; 32:3233-3243.
155. Jackson DW, Grood ES, Arnoczky SP, Butler DL, Simon TM. Cruciate reconstruction using freeze dried anterior cruciate ligament allograft and a ligament augmentation device LAD:An experimental study in a goat model. *The American Journal of Sports Medicine*. 1987; 15:528-538.

156. Hashimoto Y, Funamoto S, Kimura T, et al. The effect of decellularized bone/bone marrow produced by high-hydrostatic pressurization on the osteogenic differentiation of mesenchymal stem cells. *Biomaterials*. 2011; 32:7060-7067.
157. Phillips M, Maor E, Rubinsky B. Nonthermal irreversible electroporation for tissue decellularization. *J. Biomech. Eng.* 2010; 132
158. Hung SH, Su CH, Lee FP, Tseng H. Larynx Decellularization: Combining Freeze-Drying and Sonication as an Effective Method. *J. Voice*. 2013; 27:289-294.
159. Schenke-Layland K, Vasilevski O, Opitz F, et al. Impact of decellularization of xenogeneic tissue on extracellular matrix integrity for tissue engineering of heart valves. *J. Struct. Biol.* 2003; 143:201-208.
160. Rieder E, Kasimir MT, Silberhumer G, et al. Decellularization protocols of porcine heart valves differ importantly in efficiency of cell removal and susceptibility of the matrix to recellularization with human vascular cells. *J. Thorac. Cardiovasc. Surg.* 2004; 127:399-405.
161. Bader A, Schilling T, Teebken OE, et al. Tissue engineering of heart valves - Human endothelial cell seeding of detergent acellularized porcine valves. *Eur. J. Cardiothorac. Surg.* 1998; 14:279-284.
162. Wu Z, Zhou Y, Li N, et al. The use of phospholipase A2 to prepare acellular porcine corneal stroma as a tissue engineering scaffold. *Biomaterials*. 2009; 30:3513-3522.
163. Schenke-Layland K, Vasilevski O, Opitz F, et al. Impact of decellularization of xenogeneic tissue on extracellular matrix integrity for tissue engineering of heart valves. *J. Struct. Biol.* 2003; 143:201-208.
164. Kim JS, Reneker DH. Mechanical properties of composites using ultrafine electrospun fibers. *Polym. Compos.* 1999; 20:124-131.
165. Mohammadzadehmoghadam S, Dong Y, Jeffery Davies I. Recent progress in electrospun nanofibers: Reinforcement effect and mechanical performance. *J. Polym. Sci., Part B: Polym. Phys.* 2015; 53:1171-1212.
166. Mohammadzadehmoghadam S, Dong Y, Barbhuiya S, et al. Electrospinning: Current Status and Future Trends. In: Nano-size Polymers: Springer; 2016. p. 89-154.
167. Cooley J. Apparatus for electrically dispersing fluids US Patent Specification 692631. 1902;
168. Formhals A. US patent 1975504. *US Pat*. 1934; 1975504
169. Taylor GI. Electrically driven jets. *Proc. R. Soc. Lond. A*. 1969; 313:453-475.
170. Larrondo L, St. John Manley R. Electrostatic fiber spinning from polymer melts. I. Experimental observations on fiber formation and properties. *Journal of Polymer Science: Polymer Physics Edition*. 1981; 19:909-920.
171. S AK, Sanpui P, Chatterjee K. Fabrication of Poly(Caprolactone) Nanofibers by Electrospinning. *Journal of Polymer and Biopolymer Physics Chemistry*. 2014; 2:62-66.
172. Xue J, Xie J, Liu W, Xia Y. Electrospun Nanofibers: New Concepts, Materials, and Applications. *Acc. Chem. Res.* 2017; 50:1976-1987.
173. Teo W-E, Inai R, Ramakrishna S. Technological advances in electrospinning of nanofibers. *Science and Technology of Advanced Materials*. 2011; 12:013002.
174. Persano L, Camposeo A, Tekmen C, Pisignano D. Industrial Upscaling of Electrospinning and Applications of Polymer Nanofibers: A Review. *Macromolecular Materials and Engineering*. 2013; 298:504-520.
175. Bhardwaj N, Kundu SC. Electrospinning: A fascinating fiber fabrication technique. *Biotechnol. Adv.* 2010; 28:325-347.
176. Haider A, Haider S, Kang I-K. A comprehensive review summarizing the effect of electrospinning parameters and potential applications of nanofibers in biomedical and biotechnology. *Arabian Journal of Chemistry*. 2015;
177. Sill TJ, von Recum HA. Electrospinning: Applications in drug delivery and tissue engineering. *Biomaterials*. 2008; 29:1989-2006.
178. Liu Y, He JH, Yu JY, Zeng HM. Controlling numbers and sizes of beads in electrospun nanofibers. *Polym. Int.* 2008; 57:632-636.

179. Liao Y, Loh CH, Tian M, Wang R, Fane AG. Progress in electrospun polymeric nanofibrous membranes for water treatment: Fabrication, modification and applications. *Prog. Polym. Sci.* 2018; 77:69-94.
180. Hu J, Wang X, Ding B, et al. One-step electro-spinning/netting technique for controllably preparing polyurethane nano-fiber/net. *Macromol. Rapid Commun.* 2011; 32:1729-1734.
181. Lin T, Wang H, Wang H, Wang X. The charge effect of cationic surfactants on the elimination of fibre beads in the electrospinning of polystyrene. *Nanotechnology*. 2004; 15:1375-1381.
182. Agarwal S, Greiner A, Wendorff JH. Functional materials by electrospinning of polymers. *Prog. Polym. Sci.* 2013; 38:963-991.
183. Ingavle GC, Leach JK. Advancements in electrospinning of polymeric nanofibrous scaffolds for tissue engineering. *Tissue Engineering - Part B: Reviews*. 2014; 20:277-293.
184. Li C, Vepari C, Jin HJ, Kim HJ, Kaplan DL. Electrospun silk-BMP-2 scaffolds for bone tissue engineering. *Biomaterials*. 2006; 27:3115-3124.
185. Wang X, Ding B, Yu J, Yang J. Large-scale fabrication of two-dimensional spider-web-like gelatin nano-nets via electro-netting. *Colloids Surf. B. Biointerfaces*. 2011; 86:345-352.
186. De Vrieze S, Van Camp T, Nelvig A, et al. The effect of temperature and humidity on electrospinning. *Journal of Materials Science*. 2009; 44:1357-1362.
187. Kim Js, Reneker DH. Mechanical properties of composites using ultrafine electrospun fibers. *Polym. Compos.* 1999; 20:124-131.
188. Agarwal S, Wendorff JH, Greiner A. Use of electrospinning technique for biomedical applications. *Polymer*. 2008; 49:5603-5621.
189. Dvir T, Timko BP, Kohane DS, Langer R. Nanotechnological strategies for engineering complex tissues. *Nature Nanotechnology*. 2011; 6:13-22.
190. Ngadiman NHA, Noordin MY, Idris A, Kurniawan D. A review of evolution of electrospun tissue engineering scaffold: From two dimensions to three dimensions. *Proceedings of the Institution of Mechanical Engineers, Part H: Journal of Engineering in Medicine*. 2017; 231:597-616.
191. Hu X, Liu S, Zhou G, et al. Electrospinning of polymeric nanofibers for drug delivery applications. *J. Controlled Release*. 2014; 185:12-21.
192. Liu C, Hsu PC, Lee HW, et al. Transparent air filter for high-efficiency PM 2.5 capture. *Nature Communications*. 2015; 6
193. Molaeipour Y, Gharehaghaji AA, Bahrami H. Filtration performance of cigarette filter tip containing electrospun nanofibrous filter. *J. Ind. Text.* 2015; 45:187-198.
194. Ahmed FE, Lalia BS, Hashaikeh R. A review on electrospinning for membrane fabrication: Challenges and applications. *Desalination*. 2015; 356:15-30.
195. Liao Y, Loh C-H, Tian M, Wang R, Fane AG. Progress in electrospun polymeric nanofibrous membranes for water treatment: Fabrication, modification and applications. *Prog. Polym. Sci.* 2018; 77:69-94.
196. Ding B, Wang M, Yu J, Sun G. Gas sensors based on electrospun nanofibers. *Sensors*. 2009; 9:1609-1624.
197. Ding B, Wang M, Wang X, Yu J, Sun G. Electrospun nanomaterials for ultrasensitive sensors. *Mater. Today*. 2010; 13:16-27.
198. Thenmozhi S, Dharmaraj N, Kadirvelu K, Kim HY. Electrospun nanofibers: New generation materials for advanced applications. *Materials Science and Engineering: B*. 2017; 217:36-48.
199. Huang KK, Chu XF, Feng WC, et al. Catalytic behavior of electrospinning synthesized La0.75Sr0.25MnO3 nanofibers in the oxidation of CO and CH4. *Chem. Eng. J.* 2014; 244:27-32.
200. Guo R, Jiao T, Xing R, et al. Hierarchical AuNPs-loaded Fe3O4/Polymers nanocomposites constructed by electrospinning with enhanced and magnetically recyclable catalytic capacities. *Nanomaterials*. 2017; 7

201. Chen S, Du H, Wei Y, et al. Fine-tuning the cross-sectional architecture of antimonydoped tin oxide nanofibers as Pt catalyst support for enhanced oxygen reduction activity. *International Journal of Electrochemical Science*. 2017; 12:6221-6231.
202. Gorji M, Bagherzadeh R, Fashandi H. Electrospun nanofibers in protective clothing. In: Electrospun Nanofibers; 2016. p. 571-598.
203. Gorji M, Karimi M, Nasheroahkam S. Electrospun PU/P(AMPS-GO) nanofibrous membrane with dual-mode hydrophobic–hydrophilic properties for protective clothing applications. *J. Ind. Text.* 2018; 47:1166-1184.
204. Vitchuli N, Shi Q, Nowak J, et al. Electrospun ultrathin nylon fibers for protective applications. *J. Appl. Polym. Sci.* 2010; 116:2181-2187.
205. Lee S, Obendorf SK. Use of Electrospun Nanofiber Web for Protective Textile Materials as Barriers to Liquid Penetration. *Textile Research Journal*. 2007; 77:696-702.
206. Moy RL, Lee A, Zalka A. Commonly used suture materials in skin surgery. *Am. Fam. Physician*. 1991; 44:2123-8.
207. Noorunnisa Khanam P, Al-Maadeed MA, Naseema Khanam P. Silk as a reinforcement in polymer matrix composites. In: Basu A, editor. Advances in Silk Science and Technology: Woodhead Publishing; 2015. p. 143-170.
208. Maghdouri-White Y, Bowlin GL, Lemmon CA, Dréau D. Bioengineered silk scaffolds in 3D tissue modeling with focus on mammary tissues. *Materials Science and Engineering: C*. 2016; 59:1168-1180.
209. Alessandrino A, Marelli B, Arosio C, et al. Electrospun silk fibroin mats for tissue engineering. *Eng. Life Sci.* 2008; 8:219-225.
210. Yukseloglu SM, Sokmen N, Canoglu S. Biomaterial applications of silk fibroin electrospun nanofibres. *Microelectron. Eng.* 2015; 146:43-47.
211. Melke J, Midha S, Ghosh S, Ito K, Hofmann S. Silk fibroin as biomaterial for bone tissue engineering. *Acta Biomater.* 2016; 31:1-16.
212. Mhuka V, Dube S, Nindi MM. Chemical, structural and thermal properties of Gonometa postica silk fibroin, a potential biomaterial. *Int. J. Biol. Macromol.* 2013; 52:305-311.
213. Rockwood DN, Preda RC, Yücel T, et al. Materials fabrication from Bombyx mori silk fibroin. *Nat. Protoc.* 2011; 6:1612-1631.
214. Aramwit P, Kanokpanont S, De-Eknamkul W, Srichana T. Monitoring of inflammatory mediators induced by silk sericin. *J. Biosci. Bioeng.* 2009; 107:556-561.
215. Wang Z, Zhang Y, Zhang J, et al. Exploring natural silk protein sericin for regenerative medicine: an injectable, photoluminescent, cell-adhesive 3D hydrogel. *Sci. Rep.* 2014; 4:7064.
216. Mottaghitalab F, Hosseinkhani H, Shokrgozar MA, et al. Silk as a potential candidate for bone tissue engineering. *J. Controlled Release*. 2015; 215:112-128.
217. Vepari C, Kaplan DL. Silk as a Biomaterial. *Prog. Polym. Sci.* 2007; 32:991-1007.
218. Wang M, Jin HJ, Kaplan DL, Rutledge GC. Mechanical properties of electrospun silk fibers. *Macromolecules*. 2004; 37:6856-6864.
219. Zhang X, Baughman CB, Kaplan DL. In vitro evaluation of electrospun silk fibroin scaffolds for vascular cell growth. *Biomaterials*. 2008; 29:2217-2227.
220. Ohgo K, Zhao C, Kobayashi M, Asakura T. Preparation of non-woven nanofibers of Bombyx mori silk, Samia cynthia ricini silk and recombinant hybrid silk with electrospinning method. *Polymer*. 2003; 44:841-846.
221. Ayutsede J, Gandhi M, Sukiraga S, et al. Carbon nanotube reinforced Bombyx mori silk nanofibers by the electrospinning process. *Biomacromolecules*. 2006; 7:208-214.
222. Kang M, Chen P, Jin H-J. Preparation of multiwalled carbon nanotubes incorporated silk fibroin nanofibers by electrospinning. *Current Applied Physics*. 2009; 9:S95-S97.
223. Zhang K, Wang H, Huang C, et al. Fabrication of silk fibroin blended P(LLA-CL) nanofibrous scaffolds for tissue engineering. *Journal of Biomedical Materials Research - Part A*. 2010; 93:984-993.
224. Liu Z, Zhang F, Ming J, et al. Preparation of electrospun silk fibroin nanofibers from solutions containing native silk fibrils. *J. Appl. Polym. Sci.* 2014; 132

225. Kim H, Che L, Ha Y, Ryu W. Mechanically-reinforced electrospun composite silk fibroin nanofibers containing hydroxyapatite nanoparticles. *Mater. Sci. Eng., C*. 2014; 40:324-335.
226. Kakade MV, Givens S, Gardner K, et al. Electric Field Induced Orientation of Polymer Chains in Macroscopically Aligned Electrospun Polymer Nanofibers. *J. Am. Chem. Soc.* 2007; 129:2777-2782.
227. McClure MJ, Sell SA, Ayres CE, Simpson DG, Bowlin GL. Electrospinning-aligned and random polydioxanone-polycaprolactone-silk fibroin-blended scaffolds: Geometry for a vascular matrix. *Biomedical Materials*. 2009; 4
228. Jiang N, Huang X, Li Z, et al. Silk fibroin tissue engineering scaffolds with aligned electrospun fibers in multiple layers. *RSC Advances*. 2014; 4:47570-47575.
229. Ha SW, Tonelli AE, Hudson SM. Structural studies of Bombyx mori silk fibroin during regeneration from solutions and wet fiber spinning. *Biomacromolecules*. 2005; 6:1722-1731.
230. Fan S, Zhang Y, Shao H, Hu X. Electrospun regenerated silk fibroin mats with enhanced mechanical properties. *Int. J. Biol. Macromol.* 2013; 56:83-88.
231. Min BM, Jeong L, Lee KY, Park WH. Regenerated silk fibroin nanofibers: Water vapor-induced structural changes and their effects on the behavior of normal human cells. *Macromol. Biosci.* 2006; 6:285-292.
232. Unger RE, Wolf M, Peters K, et al. Growth of human cells on a non-woven silk fibroin net: a potential for use in tissue engineering. *Biomaterials*. 2004; 25:1069-1075.
233. Yang Y, Chen X, Ding F, et al. Biocompatibility evaluation of silk fibroin with peripheral nerve tissues and cells in vitro. *Biomaterials*. 2007; 28:1643-1652.
234. Talukdar S, Mandal M, Hutmacher DW, et al. Engineered silk fibroin protein 3D matrices for in vitro tumor model. *Biomaterials*. 2011; 32:2149-2159.
235. Hakimi O, Knight DP, Vollrath F, Vadgama P. Spider and mulberry silkworm silks as compatible biomaterials. *Composites Part B: Engineering*. 2007; 38:324-337.
236. Kapoor S, Kundu SC. Silk protein-based hydrogels: Promising advanced materials for biomedical applications. *Acta Biomater.* 2016; 31:17-32.
237. Zhou J, Cao C, Ma X, et al. In vitro and in vivo degradation behavior of aqueous-derived electrospun silk fibroin scaffolds. *Polym. Degradation Stab.* 2010; 95:1679-1685.
238. Catto V, Farè S, Cattaneo I, et al. Small diameter electrospun silk fibroin vascular grafts: Mechanical properties, in vitro biodegradability, and in vivo biocompatibility. *Materials Science and Engineering: C*. 2015; 54:101-111.
239. Guo Y, Chen Z, Wen J, et al. A simple semi-quantitative approach studying the in vivo degradation of regenerated silk fibroin scaffolds with different pore sizes. *Materials Science and Engineering: C*. 2017; 79:161-167.
240. Fan H, Liu H, Toh SL, Goh JCH. Anterior cruciate ligament regeneration using mesenchymal stem cells and silk scaffold in large animal model. *Biomaterials*. 2009; 30:4967-4977.
241. Wang Y, Rudym DD, Walsh A, et al. In vivo degradation of three-dimensional silk fibroin scaffolds. *Biomaterials*. 2008; 29:3415-3428.
242. Santin M, Motta A, Freddi G, Cannas M. In vitro evaluation of the inflammatory potential of the silk fibroin. *Journal of Biomedical Materials Research: An Official Journal of The Society for Biomaterials, The Japanese Society for Biomaterials, and The Australian Society for Biomaterials and the Korean Society for Biomaterials*. 1999; 46:382-389.
243. Lundmark K, Westermark GT, Olsén A, Westermark P. Protein fibrils in nature can enhance amyloid protein A amyloidosis in mice: Cross-seeding as a disease mechanism. *Proceedings of the National Academy of Sciences*. 2005; 102:6098-6102.
244. Vert M, Li SM, Spenlehauer G, Guerin P. Bioresorbability and biocompatibility of aliphatic polyesters. *J. Mater. Sci. Mater. Med.* 1992; 3:432-446.
245. Wang Y, Rudym DD, Walsh A, et al. In vivo Degradation of Three-Dimensional Silk Fibroin Scaffolds. *Biomaterials*. 2008; 29:3415-3428.
246. Kim U-J, Park J, Joo Kim H, Wada M, Kaplan DL. Three-dimensional aqueous-derived biomaterial scaffolds from silk fibroin. *Biomaterials*. 2005; 26:2775-2785.

247. Luo Z, Zhang Q, Shi M, et al. Effect of pore size on the biodegradation rate of silk fibroin scaffolds. *Advances in Materials Science and Engineering*. 2015; 2015
248. Horan RL, Antle K, Collette AL, et al. In vitro degradation of silk fibroin. *Biomaterials*. 2005; 26:3385-3393.
249. You R, Zhang Y, Liu Y, Liu G, Li M. The degradation behavior of silk fibroin derived from different ionic liquid solvents. *Natural Science*. 2013; 05:10-19.
250. You R, Xu Y, Liu Y, Li X, Li M. Comparison of the in vitro and in vivo degradations of silk fibroin scaffolds from mulberry and nonmulberry silkworms. *Biomedical Materials (Bristol)*. 2015; 10
251. Kim JH, Park CH, Lee OJ, et al. Preparation and in vivo degradation of controlled biodegradability of electrospun silk fibroin nanofiber mats. *Journal of Biomedical Materials Research - Part A*. 2012; 100 A:3287-3295.
252. Pritchard EM, Valentin T, Boison D, Kaplan DL. Incorporation of proteinase inhibitors into silk-based delivery devices for enhanced control of degradation and drug release. *Biomaterials*. 2011; 32:909-918.
253. Zarkoob S, Reneker DH, Eby RK, et al. Structure and morphology of nano electrospun silk fibers. American Chemical Society, Polymer Preprints, Division of Polymer Chemistry; 1998. 244-245 p.
254. Jeong L, Lee KY, Park WH. Effect of solvent on the characteristics of electrospun regenerated silk fibroin nanofibers [Conference Paper]. 2007.
255. Sukigara S, Gandhi M, Ayutsede J, Micklus M, Ko F. Regeneration of Bombyx mori silk by electrospinning - Part 1: Processing parameters and geometric properties. *Polymer*. 2003; 44:5721-5727.
256. Ayutsede J, Gandhi M, Sukigara S, et al. Regeneration of Bombyx mori silk by electrospinning. Part 3: Characterization of electrospun nonwoven mat. *Polymer*. 2005; 46:1625-1634.
257. Jin HJ, Fridrikh SV, Rutledge GC, Kaplan DL. Electrospinning Bombyx mori silk with poly(ethylene oxide). *Biomacromolecules*. 2002; 3:1233-1239.
258. Wang H, Zhang Y, Shao H, Hu X. Electrospun ultra-fine silk fibroin fibers from aqueous solutions. *Journal of Materials Science*. 2005; 40:5359-5363.
259. Zhu J, Shao H, Hu X. Morphology and structure of electrospun mats from regenerated silk fibroin aqueous solutions with adjusting pH. *Int. J. Biol. Macromol.* 2007; 41:469-474.
260. Zhu J, Zhang Y, Shao H, Hu X. Electrospinning and rheology of regenerated Bombyx mori silk fibroin aqueous solutions: The effects of pH and concentration. *Polymer*. 2008; 49:2880-2885.
261. Kishimoto Y, Morikawa H, Yamanaka S, Tamada Y. Electrospinning of silk fibroin from all aqueous solution at low concentration. *Mater. Sci. Eng., C*. 2017; 73:498-506.
262. Kishimoto Y, Kobashi T, Yamanaka S, Morikawa H, Tamada Y. Comparisons between silk fibroin nonwoven electrospun fabrics using aqueous and formic acid solutions. *International Journal of Polymeric Materials and Polymeric Biomaterials*. 2017:1-6.
263. Singh BN, Panda NN, Pramanik K. A novel electrospinning approach to fabricate high strength aqueous silk fibroin nanofibers. *Int. J. Biol. Macromol.* 2016; 87:201-207.
264. Meinel AJ, Kubow KE, Klotzsch E, et al. Optimization strategies for electrospun silk fibroin tissue engineering scaffolds. *Biomaterials*. 2009; 30:3058-3067.
265. Chutipakdeevong J, Ruktanonchai UR, Supaphol P. Process optimization of electrospun silk fibroin fiber mat for accelerated wound healing. *J. Appl. Polym. Sci.* 2013; 130:3634-3644.
266. Sukigara S, Gandhi M, Ayutsede J, Micklus M, Ko F. Regeneration of Bombyx mori silk by electrospinning. Part 2. Process optimization and empirical modeling using response surface methodology. *Polymer*. 2004; 45:3701-3708.
267. Amiraliyan N, Nouri M, Kish MH. Electrospinning of silk nanofibers. I. An investigation of nanofiber morphology and process optimization using response surface methodology. *Fibers and Polymers*. 2009; 10:167-176.
268. Chomachayi MD, Solouk A, Mirzadeh H. Electrospun silk-based nanofibrous scaffolds: fiber diameter and oxygen transfer. *Progress in biomaterials*. 2016; 5:71-80.

269. Ko JS, Yoon K, Ki CS, et al. Effect of degumming condition on the solution properties and electrospinnablity of regenerated silk solution. *Int. J. Biol. Macromol.* 2013; 55:161-168.
270. Aznar-Cervantes SD, Lozano-Pérez AA, García Montalbán M, et al. Importance of refrigeration time in the electrospinning of silk fibroin aqueous solutions. *Journal of Materials Science*. 2015; 50:4879-4887.
271. Kim SH, Nam YS, Lee TS, Park WH. Silk fibroin nanofiber. Electrospinning, properties, and structure. *Polym. J.* 2003; 35:185-190.
272. Li M, Tao W, Kuga S, Nishiyama Y. Controlling molecular conformation of regenerated wild silk fibroin by aqueous ethanol treatment. *Polym. Adv. Technol.* 2003; 14:694-698.
273. Liu T, Zhang F, Zuo B. Effect of different post-treatment on the morphology, structure and property of electrospun SF nanofiber mats [Conference Paper]. 2012.
274. Fan L, Wang H, Zhang K, et al. Regenerated silk fibroin nanofibrous matrices treated with 75% ethanol vapor for tissue-engineering applications. *J. Biomater. Sci. Polym. Ed.* 2012; 23:497-508.
275. Nogueira GM, Rodas ACD, Leite CAP, et al. Preparation and characterization of ethanol-treated silk fibroin dense membranes for biomaterials application using waste silk fibers as raw material. *Bioresour. Technol.* 2010; 101:8446-8451.
276. Min BM, Jeong L, Lee KY, Park WH. Regenerated silk fibroin nanofibers: Water vapor-induced structural changes and their effects on the behavior of normal human cells. *Macromol. Biosci.* 2006; 6:285-292.
277. Jeong L, Lee KY, Liu JW, Park WH. Time-resolved structural investigation of regenerated silk fibroin nanofibers treated with solvent vapor. *Int. J. Biol. Macromol.* 2006; 38:140-144.
278. Fukuda Y, Aytemiz D, Higuchi A, et al. Relationship between structure and physical strength of silk fibroin nanofiber sheet depending on insolubilization treatment. *J. Appl. Polym. Sci.* 2017; 134
279. Silva SS, Maniglio D, Motta A, et al. Genipin-modified silk-fibroin nanometric nets. *Macromol. Biosci.* 2008; 8:766-774.
280. Calamak S, Aksoy EA, Ertas N, et al. Ag/silk fibroin nanofibers: Effect of fibroin morphology on Ag+ release and antibacterial activity. *Eur. Polym. J.* 2015; 67:99-112.
281. Li L, Li H, Qian Y, et al. Electrospun poly (ε-caprolactone)/silk fibroin core-sheath nanofibers and their potential applications in tissue engineering and drug release. *Int. J. Biol. Macromol.* 2011; 49:223-232.
282. Lee H, Kim G. Biocomposites electrospun with poly(ε-caprolactone) and silk fibroin powder for biomedical applications. *J. Biomater. Sci. Polym. Ed.* 2010; 21:1687-1699.
283. Tian L, Prabhakaran MP, Hu J, et al. Coaxial electrospun poly(lactic acid)/silk fibroin nanofibers incorporated with nerve growth factor support the differentiation of neuronal stem cells. *RSC Advances*. 2015; 5:49838-49848.
284. Bhutto MA, Wu T, Sun B, et al. Fabrication and characterization of vitamin B5 loaded poly (l-lactide-co-caprolactone)/silk fiber aligned electrospun nanofibers for schwann cell proliferation. *Colloids Surf. B. Biointerfaces*. 2016; 144:108-117.
285. Zhan J, Liu J, Wang C, et al. Electrospun silk fibroin-poly (lactic-co-glycolic acid) membrane for nerve tissue engineering. *J. Bioact. Compatible Polym.* 2016; 31:208-224.
286. Zoccola M, Aluigi A, Vineis C, et al. Study on cast membranes and electrospun nanofibers made from keratin/fibroin blends. *Biomacromolecules*. 2008; 9:2819-2825.
287. Yen KC, Chen CY, Huang JY, Kuo WT, Lin FH. Fabrication of keratin/fibroin membranes by electrospinning for vascular tissue engineering. *Journal of Materials Chemistry B*. 2015; 4:237-244.
288. Zhou J, Cao C, Ma X, Lin J. Electrospinning of silk fibroin and collagen for vascular tissue engineering. *Int. J. Biol. Macromol.* 2010; 47:514-519.
289. Shan Y-H, Peng L-H, Liu X, et al. Silk fibroin/gelatin electrospun nanofibrous dressing functionalized with astragaloside IV induces healing and anti-scar effects on burn wound. *Int. J. Pharm.* 2015; 479:291-301.

290. Yin G, Zhang Y, Bao W, et al. Study on the properties of the electrospun silk fibroin/gelatin blend nanofibers for scaffolds. *J. Appl. Polym. Sci.* 2009; 111:1471-1477.
291. Park WH, Jeong L, Yoo DI, Hudson S. Effect of chitosan on morphology and conformation of electrospun silk fibroin nanofibers. *Polymer*. 2004; 45:7151-7157.
292. Lai G-J, Shalumon KT, Chen S-H, Chen J-P. Composite chitosan/silk fibroin nanofibers for modulation of osteogenic differentiation and proliferation of human mesenchymal stem cells. *Carbohydr. Polym.* 2014; 111:288-297.
293. Hang Y, Zhang Y, Jin Y, Shao H, Hu X. Preparation of regenerated silk fibroin/silk sericin fibers by coaxial electrospinning. *Int. J. Biol. Macromol.* 2012; 51:980-986.
294. Shayannia M, Sajjadi H, Motaghitalab V, Haghi AK. Effect of multi wall carbon nanotubes on characteristics and morphology of nanofiber scaffolds composited of MWNTs/silk fibroin. *Adv. Powder Technol.* 2017; 28:775-784.
295. Zhao Y, Gong J, Niu C, et al. A new electrospun graphene-silk fibroin composite scaffolds for guiding Schwann cells. *J. Biomater. Sci. Polym. Ed.* 2017; 28:2171-2185.
296. Yang Y, Ding X, Zou T, et al. Preparation and characterization of electrospun graphene/silk fibroin conductive fibrous scaffolds. *RSC Advances*. 2017; 7:7954-7963.
297. Brito-Pereira R, Correia DM, Ribeiro C, et al. Silk fibroin-magnetic hybrid composite electrospun fibers for tissue engineering applications. *Composites Part B: Engineering*. 2018; 141:70-75.
298. Jin HJ, Chen J, Karageorgiou V, Altman GH, Kaplan DL. Human bone marrow stromal cell responses on electrospun silk fibroin mats. *Biomaterials*. 2004; 25:1039-1047.
299. Kim K-H, Jeong L, Park H-N, et al. Biological efficacy of silk fibroin nanofiber membranes for guided bone regeneration. *J. Biotechnol.* 2005; 120:327-339.
300. Singh BN, Panda NN, Mund R, Pramanik K. Carboxymethyl cellulose enables silk fibroin nanofibrous scaffold with enhanced biomimetic potential for bone tissue engineering application. *Carbohydr. Polym.* 2016; 151:335-347.
301. Yang SY, Hwang TH, Che L, et al. Membrane-reinforced three-dimensional electrospun silk fibroin scaffolds for bone tissue engineering. *Biomedical Materials (Bristol)*. 2015; 10
302. Wei K, Li Y, Kim KO, et al. Fabrication of nano-hydroxyapatite on electrospun silk fibroin nanofiber and their effects in osteoblastic behavior. *Journal of Biomedical Materials Research - Part A*. 2011; 97 A:272-280.
303. Wei K, Li Y, Kim KO, et al. Fabrication of nano-hydroxyapatite on electrospun silk fibroin nanofiber and their effects in osteoblastic behavior. *Journal of Biomedical Materials Research - Part A*. 2011; 97 A:272-280.
304. Wei K, Li Y, Kim KO, et al. Fabrication of nano-hydroxyapatite on electrospun silk fibroin nanofiber and their effects in osteoblastic behavior. *Journal of Biomedical Materials Research - Part A*. 2011; 97 A:272-280.
305. Du GY, He SW, Sun CX, Mi LD. Bone Morphogenic Protein-2 (rhBMP2)-Loaded Silk Fibroin Scaffolds to Enhance the Osteoinductivity in Bone Tissue Engineering. *Nanoscale Research Letters*. 2017; 12
306. Yuan H, Shi H, Qiu X, Chen Y. Mechanical property and biological performance of electrospun silk fibroin-polycaprolactone scaffolds with aligned fibers. *J. Biomater. Sci. Polym. Ed.* 2016; 27:263-275.
307. Chen JP, Chen SH, Lai GJ. Preparation and characterization of biomimetic silk fibroin/chitosan composite nanofibers by electrospinning for osteoblasts culture. *Nanoscale Research Letters*. 2012; 7:1-11.
308. Soffer L, Wang X, Zhang X, et al. Silk-based electrospun tubular scaffolds for tissue-engineered vascular grafts. *J. Biomater. Sci. Polym. Ed.* 2008; 19:653-664.
309. Zhou J, Cao C, Ma X. A novel three-dimensional tubular scaffold prepared from silk fibroin by electrospinning. *Int. J. Biol. Macromol.* 2009; 45:504-510.
310. Marelli B, Alessandrino A, Farè S, et al. Compliant electrospun silk fibroin tubes for small vessel bypass grafting. *Acta Biomater.* 2010; 6:4019-4026.
311. Yu L, Feng Y, Li Q, et al. PLGA/SF blend scaffolds modified with plasmid complexes for enhancing proliferation of endothelial cells. *React. Funct. Polym.* 2015; 91-92:19-27.

312. Wang S-D, Zhang Y-Z, Yin G-B, Wang H-W, Dong Z-H. Fabrication of a composite vascular scaffold using electrospinning technology. *Materials Science and Engineering: C*. 2010; 30:670-676.
313. Chantawong P, Tanaka T, Uemura A, et al. Silk fibroin-Pellethane® cardiovascular patches: Effect of silk fibroin concentration on vascular remodeling in rat model. *J. Mater. Sci. Mater. Med.* 2017; 28
314. Yu E, Mi HY, Zhang J, Thomson JA, Turng LS. Development of biomimetic thermoplastic polyurethane/fibroin small-diameter vascular grafts via a novel electrospinning approach. *Journal of Biomedical Materials Research - Part A*. 2018; 106:985-996.
315. Sato M, Nakazawa Y, Takahashi R, et al. Small-diameter vascular grafts of Bombyx mori silk fibroin prepared by a combination of electrospinning and sponge coating. *Mater. Lett.* 2010; 64:1786-1788.
316. Liu H, Li X, Zhou G, Fan H, Fan Y. Electrospun sulfated silk fibroin nanofibrous scaffolds for vascular tissue engineering. *Biomaterials*. 2011; 32:3784-3793.
317. Wang G, Hu X, Lin W, Dong C, Wu H. Electrospun PLGA-silk fibroin-collagen nanofibrous scaffolds for nerve tissue engineering. *In Vitro Cellular and Developmental Biology - Animal*. 2011; 47:234-240.
318. Li S, Wu H, Hu XD, et al. Preparation of electrospun PLGA-silk fibroin nanofibers-based nerve conduits and evaluation in vivo. *Artificial Cells, Blood Substitutes, and Biotechnology*. 2012; 40:171-178.
319. Park SY, Ki CS, Park YH, et al. Functional recovery guided by an electrospun silk fibroin conduit after sciatic nerve injury in rats. *J. Tissue Eng. Regen. Med.* 2015; 9:66-76.
320. Wang CY, Zhang KH, Fan CY, et al. Aligned natural-synthetic polyblend nanofibers for peripheral nerve regeneration. *Acta Biomater.* 2011; 7:634-643.
321. Madduri S, Papaloizos M, Gander B. Trophically and topographically functionalized silk fibroin nerve conduits for guided peripheral nerve regeneration. *Biomaterials*. 2010; 31:2323-34.
322. Liu Q, Huang J, Shao H, Song L, Zhang Y. Dual-factor loaded functional silk fibroin scaffolds for peripheral nerve regeneration with the aid of neovascularization. *RSC Advances*. 2016; 6:7683-7691.
323. Madduri S, Papaloïzos M, Gander B. Trophically and topographically functionalized silk fibroin nerve conduits for guided peripheral nerve regeneration. *Biomaterials*. 2010; 31:2323-2334.
324. Das S, Sharma M, Saharia D, et al. Electrospun silk-polyaniline conduits for functional nerve regeneration in rat sciatic nerve injury model. *Biomedical Materials (Bristol)*. 2017; 12
325. Mottaghitalab F, Farokhi M, Zaminy A, et al. A Biosynthetic Nerve Guide Conduit Based on Silk/SWNT/Fibronectin Nanocomposite for Peripheral Nerve Regeneration. *PLoS One*. 2013; 8
326. Zhang J, Qiu K, Sun B, et al. The aligned core-sheath nanofibers with electrical conductivity for neural tissue engineering. *Journal of Materials Chemistry B*. 2014; 2:7945-7954.
327. Schneider A, Wang XY, Kaplan DL, Garlick JA, Egles C. Biofunctionalized electrospun silk mats as a topical bioactive dressing for accelerated wound healing. *Acta Biomater.* 2009; 5:2570-2578.
328. Lin S, Chen M, Jiang H, et al. Green electrospun grape seed extract-loaded silk fibroin nanofibrous mats with excellent cytocompatibility and antioxidant effect. *Colloids Surf. B. Biointerfaces*. 2016; 139:156-163.
329. Farokhi M, Mottaghitalab F, Fatahi Y, Khademhosseini A, Kaplan DL. Overview of Silk Fibroin Use in Wound Dressings. *Trends Biotechnol.* 2018; 36:907-922.
330. Ju HW, Lee OJ, Lee JM, et al. Wound healing effect of electrospun silk fibroin nanomatrix in burn-model. *Int. J. Biol. Macromol.* 2016; 85:29-39.
331. Calamak S, Aksoy EA, Erdogdu C, Sagıroglu M, Ulubayram K. Silver nanoparticle containing silk fibroin bionanotextiles. *J. Nanopart. Res.* 2015; 17

332. Gil ES, Panilaitis B, Bellas E, Kaplan DL. Functionalized Silk Biomaterials for Wound Healing. *Advanced Healthcare Materials*. 2013; 2:206-217.
333. Lian Y, Zhan JC, Zhang KH, Mo XM. Fabrication and characterization of curcumin-loaded silk fibroin/P(LLA-CL) nanofibrous scaffold. *Frontiers of Materials Science*. 2014; 8:354-362.
334. Fan L, Wang H, Zhang K, et al. Vitamin C-reinforcing silk fibroin nanofibrous matrices for skin care application. *RSC Advances*. 2012; 2:4110-4119.
335. Selvaraj S, Fathima NN. Fenugreek Incorporated Silk Fibroin Nanofibers - A Potential Antioxidant Scaffold for Enhanced Wound Healing. *ACS Applied Materials and Interfaces*. 2017; 9:5916-5926.
336. Yang X, Fan L, Ma L, et al. Green electrospun Manuka honey/silk fibroin fibrous matrices as potential wound dressing. *Mater. Des.* 2017; 119:76-84.
337. Kadakia PU, Growney Kalaf EA, Dunn AJ, Shornick LP, Sell SA. Comparison of silk fibroin electrospun scaffolds with poloxamer and honey additives for burn wound applications. *J. Bioact. Compatible Polym.* 2018; 33:79-94.
338. Song DW, Kim SH, Kim HH, et al. Multi-biofunction of antimicrobial peptide-immobilized silk fibroin nanofiber membrane: Implications for wound healing. *Acta Biomater.* 2016; 39:146-155.
339. Sheikh FA, Ju HW, Lee JM, et al. 3D electrospun silk fibroin nanofibers for fabrication of artificial skin. *Nanomed. Nanotechnol. Biol. Med.* 2015; 11:681-691.
340. Akturk O, Kismet K, Yasti AC, et al. Wet electrospun silk fibroin/gold nanoparticle 3D matrices for wound healing applications. *RSC Advances*. 2016; 6:13234-13250.
341. Tom H, Xue-Feng Y, Ardeshir B. Electrospun silk fibroin fiber diameter influences in vitro dermal fibroblast behavior and promotes healing of ex vivo wound models. *Journal of Tissue Engineering*. 2014; 5:2041731414551661.
342. Lee OJ, Ju HW, Kim JH, et al. Development of artificial dermis using 3D electrospun silk fibroin nanofiber matrix. *Journal of Biomedical Nanotechnology*. 2014; 10:1294-1303.
343. Yuan P, Tan D, Annabi-Bergaya F. Properties and applications of halloysite nanotubes: recent research advances and future prospects. *Applied Clay Science*. 2015; 112-113:75-93.
344. Joussein E, Petit S, Churchman J, et al. Halloysite clay minerals - A review. *Clay Minerals*. 2005; 40:383-426.
345. Abdullayev E, Price R, Shchukin D, Lvov Y. Halloysite tubes as nanocontainers for anticorrosion coating with benzotriazole. *ACS Applied Materials and Interfaces*. 2009; 1:1437-1443.
346. Yah WO, Xu H, Soejima H, et al. Biomimetic Dopamine Derivative for Selective Polymer Modification of Halloysite Nanotube Lumen. *J. Am. Chem. Soc.* 2012; 134:12134-12137.
347. Alhuthali A, Low IM. Water absorption, mechanical, and thermal properties of halloysite nanotube reinforced vinyl-ester nanocomposites. *Journal of Materials Science*. 2013; 48:4260-4273.
348. Xie XL, Mai YW, Zhou XP. Dispersion and alignment of carbon nanotubes in polymer matrix: A review. *Materials Science and Engineering R: Reports*. 2005; 49:89-112.
349. Vergaro V, Abdullayev E, Lvov YM, et al. Cytocompatibility and uptake of halloysite clay nanotubes. *Biomacromolecules*. 2010; 11:820-826.
350. Zhang Y, Tang A, Yang H, Ouyang J. Applications and interfaces of halloysite nanocomposites. *Applied Clay Science*. 2016; 119:8-17.
351. Saif MJ, Asif HM. Escalating applications of halloysite nanotubes. *Journal of the Chilean Chemical Society*. 2015; 60:2949-2953.
352. Qiu K, Netravali AN. Halloysite nanotube reinforced biodegradable nanocomposites using noncrosslinked and malonic acid crosslinked polyvinyl alcohol. *Polym. Compos.* 2013; 34:799-809.
353. Lin Y, Ng KM, Chan CM, Sun G, Wu J. High-impact polystyrene/halloysite nanocomposites prepared by emulsion polymerization using sodium dodecyl sulfate as surfactant. *J. Colloid Interface Sci.* 2011; 358:423-429.

354. Lvov Y, Price R, Gaber B, Ichinose I. Thin film nanofabrication via layer-by-layer adsorption of tubule halloysite, spherical silica, proteins and polycations. *Colloids Surf. Physicochem. Eng. Aspects*. 2002; 198-200:375-382.
355. Deen I, Pang X, Zhitomirsky I. Electrophoretic deposition of composite chitosan-halloysite nanotube-hydroxyapatite films. *Colloids Surf. Physicochem. Eng. Aspects*. 2012; 410:38-44.
356. Cavallaro G, De Lisi R, Lazzara G, Milioto S. Polyethylene glycol/clay nanotubes composites: Thermal properties and structure. *J. Therm. Anal. Calorim.* 2013; 112:383-389.
357. Tierrablanca E, Romero-García J, Roman P, Cruz-Silva R. Biomimetic polymerization of aniline using hematin supported on halloysite nanotubes. *Applied Catalysis A: General*. 2010; 381:267-273.
358. Kelly HM, Deasy PB, Ziaka E, Claffey N. Formulation and preliminary in vivo dog studies of a novel drug delivery system for the treatment of periodontitis. *Int. J. Pharm.* 2004; 274:167-183.
359. Deen I, Zhitomirsky I. Electrophoretic deposition of composite halloysite nanotube-hydroxyapatite- hyaluronic acid films. *J. Alloys Compd.* 2014; 586:S531-S534.
360. Ye Y, Chen H, Wu J, Ye L. High impact strength epoxy nanocomposites with natural nanotubes. *Polymer*. 2007; 48:6426-6433.
361. Handge UA, Hedicke-Höchstötter K, Altstädt V. Composites of polyamide 6 and silicate nanotubes of the mineral halloysite: Influence of molecular weight on thermal, mechanical and rheological properties. *Polymer*. 2010; 51:2690-2699.
362. Liu M, Wu C, Jiao Y, Xiong S, Zhou C. Chitosan-halloysite nanotubes nanocomposite scaffolds for tissue engineering. *Journal of Materials Chemistry B*. 2013; 1:2078-2089.
363. Zhao J, Deng CL, Du SL, et al. Synergistic flame-retardant effect of halloysite nanotubes on intumescent flame retardant in LDPE. *J. Appl. Polym. Sci.* 2014; 131
364. De Silva RT, Pasbakhsh P, Goh KL, Chai SP, Ismail H. Physico-chemical characterisation of chitosan/halloysite composite membranes. *Polym. Test.* 2013; 32:265-271.
365. Du M, Guo B, Jia D. Thermal stability and flame retardant effects of halloysite nanotubes on poly(propylene). *Eur. Polym. J.* 2006; 42:1362-1369.
366. Marney D, Russell L, Wu D, et al. The suitability of halloysite nanotubes as a fire retardant for nylon 6. *Polym. Degradation Stab.* 2008; 93:1971-1978.
367. Liu M, Guo B, Du M, Jia D. Drying induced aggregation of halloysite nanotubes in polyvinyl alcohol/halloysite nanotubes solution and its effect on properties of composite film. *Applied Physics A: Materials Science and Processing*. 2007; 88:391-395.
368. Liu M, Zhang Y, Zhou C. Nanocomposites of halloysite and polylactide. *Applied Clay Science*. 2013; 75-76:52-59.
369. Lee KS, Chang YW. Thermal, mechanical, and rheological properties of poly(ε-caprolactone)/halloysite nanotube nanocomposites. *J. Appl. Polym. Sci.* 2013; 128:2807-2816.
370. Ning N-y, Yin Q-j, Luo F, et al. Crystallization behavior and mechanical properties of polypropylene/halloysite composites. *Polymer*. 2007; 48:7374-7384.
371. Ghebaur A, Garea SA, Iovu H. New polymer-halloysite hybrid materials - Potential controlled drug release system. *Int. J. Pharm.* 2012; 436:568-573.
372. Kurczewska J, Pecyna P, Ratajczak M, Gajęcka M, Schroeder G. Halloysite nanotubes as carriers of vancomycin in alginate-based wound dressing. *Saudi Pharmaceutical Journal*. 2017; 25:911-920.
373. Shi R, Niu Y, Gong M, et al. Antimicrobial gelatin-based elastomer nanocomposite membrane loaded with ciprofloxacin and polymyxin B sulfate in halloysite nanotubes for wound dressing. *Materials Science and Engineering: C*. 2018; 87:128-138.
374. Kelly HM, Deasy PB, Ziaka E, Claffey N. Formulation and preliminary in vivo dog studies of a novel drug delivery system for the treatment of periodontitis. *Int. J. Pharm.* 2004; 274:167-183.
375. Bugatti V, Viscusi G, Naddeo C, Gorrasi G. Nanocomposites based on PCL and halloysite nanotubes filled with lysozyme: Effect of draw ratio on the physical properties and release analysis. *Nanomaterials*. 2017; 7

376. Biddeci G, Cavallaro G, Di Blasi F, et al. Halloysite nanotubes loaded with peppermint essential oil as filler for functional biopolymer film. *Carbohydr. Polym.* 2016; 152:548-557.
377. Shi YF, Tian Z, Zhang Y, Shen HB, Jia NQ. Functionalized halloysite nanotube-based carrier for intracellular delivery of antisense oligonucleotides. *Nanoscale Research Letters*. 2011; 6:1-7.
378. Abdullayev E, Joshi A, Wei W, Zhao Y, Lvov Y. Enlargement of halloysite clay nanotube lumen by selective etching of aluminum oxide. *ACS nano*. 2012; 6:7216-7226.
379. Joo Y, Sim JH, Jeon Y, Lee SU, Sohn D. Opening and blocking the inner-pores of halloysite. *Chem. Commun.* 2013; 49:4519-4521.
380. Touny AH, Lawrence JG, Jones AD, Bhaduri SB. Effect of electrospinning parameters on the characterization of PLA/HNT nanocomposite fibers. *J. Mater. Res.* 2010; 25:857-865.
381. Tao D, Higaki Y, Ma W, et al. Chain orientation in poly(glycolic acid)/halloysite nanotube hybrid electrospun fibers. *Polymer (United Kingdom)*. 2015; 60:284-291.
382. Haroosh HJ, Dong Y, Chaudhary DS, Ingram GD, Yusa SI. Electrospun PLA: PCL composites embedded with unmodified and 3-aminopropyltriethoxysilane (ASP) modified halloysite nanotubes (HNT). *Applied Physics A: Materials Science and Processing*. 2013; 110:433-442.
383. Luo C, Zou Z, Luo B, et al. Enhanced mechanical properties and cytocompatibility of electrospun poly(l-lactide) composite fiber membranes assisted by polydopamine-coated halloysite nanotubes. *Appl. Surf. Sci.* 2016; 369:82-91.
384. Ghaderi-Ghahfarrokhi M, Haddadi-Asl V, Zargarian SS. Fabrication and characterization of polymer-ceramic nanocomposites containing drug loaded modified halloysite nanotubes. *Journal of Biomedical Materials Research - Part A*. 2018;
385. Bottino MC, Yassen GH, Platt JA, et al. A novel three-dimensional scaffold for regenerative endodontics: Materials and biological characterizations. *J. Tissue Eng. Regen. Med.* 2015; 9:E116-E123.
386. Qi R, Guo R, Zheng F, et al. Controlled release and antibacterial activity of antibiotic-loaded electrospun halloysite/poly(lactic-co-glycolic acid) composite nanofibers. *Colloids Surf. B. Biointerfaces*. 2013; 110:148-155.
387. Xue J, Niu Y, Gong M, et al. Electrospun microfiber membranes embedded with drug-loaded clay nanotubes for sustained antimicrobial protection. *ACS nano*. 2015; 9:1600-1612.
388. Shubhra QTH, Alam AKMM, Khan MA, et al. The preparation and characterization of silk/gelatin biocomposites. *Polym. Plast. Technol. Eng.* 2010; 49:983-990.
389. Aldana AA, Abraham GA. Current advances in electrospun gelatin-based scaffolds for tissue engineering applications. *Int. J. Pharm.* 2017; 523:441-453.
390. Rose JB, Pacelli S, El Haj AJ, et al. Gelatin-based materials in ocular tissue engineering. *Materials*. 2014; 7:3106-3135.
391. Gomez-Guillen MC, Gimenez B, Lopez-Caballero ME, Montero MP. Functional and bioactive properties of collagen and gelatin from alternative sources: A review. *Food Hydrocolloids*. 2011; 25:1813-1827.
392. Babitha S, Rachita L, Karthikeyan K, et al. Electrospun protein nanofibers in healthcare: A review. *Int. J. Pharm.* 2017; 523:52-90.
393. Farris S, Schaich KM, Liu L, Piergiovanni L, Yam KL. Development of polyion-complex hydrogels as an alternative approach for the production of bio-based polymers for food packaging applications: a review. *Trends in Food Science and Technology*. 2009; 20:316-332.
394. Sakaguchi M, Inouye S. IgE sensitization to gelatin: the probable role of gelatin-containing diphtheria–tetanus–acellular pertussis (DTaP) vaccines. *Vaccine*. 2000; 18:2055-2058.
395. Foox M, Zilberman M. Drug delivery from gelatin-based systems. *Expert opinion on drug delivery*. 2015; 12:1547-1563.
396. Huang Z-M, Zhang YZ, Ramakrishna S, Lim CT. Electrospinning and mechanical characterization of gelatin nanofibers. *Polymer*. 2004; 45:5361-5368.

397. Zhang Y, Ouyang H, Chwee TL, Ramakrishna S, Huang ZM. Electrospinning of gelatin fibers and gelatin/PCL composite fibrous scaffolds. *Journal of Biomedical Materials Research - Part B Applied Biomaterials*. 2005; 72:156-165.
398. Yan S, Xiaoqiang L, Shuiping L, Hongsheng W, Chuanglong H. Fabrication and properties of PLLA-gelatin nanofibers by electrospinning. *J. Appl. Polym. Sci.* 2010; 117:542-547.
399. Ki CS, Baek DH, Gang KD, et al. Characterization of gelatin nanofiber prepared from gelatin-formic acid solution. *Polymer*. 2005; 46:5094-5102.
400. Siimon K, Siimon H, Järvekülg M. Mechanical characterization of electrospun gelatin scaffolds cross-linked by glucose. *Journal of materials science. Materials in medicine*. 2015; 26:5375.
401. Song JH, Kim HE, Kim HW. Production of electrospun gelatin nanofiber by water-based co-solvent approach. *J. Mater. Sci. Mater. Med.* 2008; 19:95-102.
402. Erencia M, Cano F, Tornero JA, et al. Electrospinning of gelatin fibers using solutions with low acetic acid concentration: Effect of solvent composition on both diameter of electrospun fibers and cytotoxicity. *J. Appl. Polym. Sci.* 2015; 132
403. Zhang S, Huang Y, Yang X, et al. Gelatin nanofibrous membrane fabricated by electrospinning of aqueous gelatin solution for guided tissue regeneration. *Journal of biomedical materials research. Part A*. 2009; 90:671-679.
404. Choktaweesap N, Arayanarakul K, Aht-Ong D, Meechaisue C, Supaphol P. Electrospun gelatin fibers: Effect of solvent system on morphology and fiber diameters. *Polym. J.* 2007; 39:622-631.
405. Ki CS, Baek DH, Gang KD, et al. Characterization of gelatin nanofiber prepared from gelatin–formic acid solution. *Polymer*. 2005; 46:5094-5102.
406. Lee JB, Ko YG, Cho D, Park WH, Kwon OH. Modification and optimization of electrospun gelatin sheets by electronbeam irradiation for soft tissue engineering. *Biomaterials Research*. 2017; 21
407. Lin WH, Tsai WB. In situ UV-crosslinking gelatin electrospun fibers for tissue engineering applications. *Biofabrication*. 2013; 5
408. Du Y, Gao XQ, Wang ZY, et al. Construction and characterization of three-dimensional silk fibroin-gelatin scaffolds. *Journal of Hard Tissue Biology*. 2016; 25:269-276.
409. Ray RR, Jana SC, Nanda G. Immobilization of β-amylase from Bacillus megaterium B6 into gelatin film by cross-linking. *J. Appl. Bacteriol.* 1995; 79:157-162.
410. Yeh MK, Liang YM, Cheng KM, et al. A novel cell support membrane for skin tissue engineering: Gelatin film cross-linked with 2-chloro-1-methylpyridinium iodide. *Polymer*. 2011; 52:996-1003.
411. Draye JP, Delaey B, Van De Voorde A, et al. In vitro and in vivo biocompatibility of dextran dialdehyde cross-linked gelatin hydrogel films. *Biomaterials*. 1998; 19:1677-1687.
412. Sung HW, Huang DM, Chang WH, Huang RN, Hsu JC. Evaluation of gelatin hydrogel crosslinked with various crosslinking agents as bioadhesives: In vitro study. *J. Biomed. Mater. Res.* 1999; 46:520-530.
413. Bigi A, Cojazzi G, Panzavolta S, Roveri N, Rubini K. Stabilization of gelatin films by crosslinking with genipin. *Biomaterials*. 2002; 23:4827-4832.
414. Kishan AP, Nezarati RM, Radzicki CM, et al. In situ crosslinking of electrospun gelatin for improved fiber morphology retention and tunable degradation. *Journal of Materials Chemistry B*. 2015; 3:7930-7938.
415. Migneault I, Dartiguenave C, Bertrand MJ, Waldron KC. Glutaraldehyde: behavior in aqueous solution, reaction with proteins, and application to enzyme crosslinking. *BioTechniques*. 2004; 37:790-6, 798-802.
416. Jayakrishnan A, Jameela SR. Glutaraldehyde as a fixative in bioprostheses and drug delivery matrices. *Biomaterials*. 1996; 17:471-484.
417. Sisson K, Zhang C, Farach-Carson MC, Chase DB, Rabolt JF. Evaluation of cross-linking methods for electrospun gelatin on cell growth and viability. *Biomacromolecules*. 2009; 10:1675-1680.

418. Panzavolta S, Gioffrè M, Focarete ML, et al. Electrospun gelatin nanofibers: Optimization of genipin cross-linking to preserve fiber morphology after exposure to water. *Acta Biomater.* 2011; 7:1702-1709.
419. Zhang YZ, Venugopal J, Huang ZM, Lim CT, Ramakrishna S. Crosslinking of the electrospun gelatin nanofibers. *Polymer*. 2006; 47:2911-2917.
420. Zhan J, Morsi Y, Ei-Hamshary H, Al-Deyab SS, Mo X. In vitro evaluation of electrospun gelatin–glutaraldehyde nanofibers. *Frontiers of Materials Science*. 2016; 10:90-100.
421. Jiang Y-C, Jiang L, Huang A, et al. Electrospun polycaprolactone/gelatin composites with enhanced cell–matrix interactions as blood vessel endothelial layer scaffolds. *Materials Science and Engineering: C*. 2017; 71:901-908.
422. Ren K, Wang Y, Sun T, Yue W, Zhang H. Electrospun PCL/gelatin composite nanofiber structures for effective guided bone regeneration membranes. *Materials Science and Engineering: C*. 2017; 78:324-332.
423. Mehrasa M, Asadollahi MA, Ghaedi K, Salehi H, Arpanaei A. Electrospun aligned PLGA and PLGA/gelatin nanofibers embedded with silica nanoparticles for tissue engineering. *Int. J. Biol. Macromol.* 2015; 79:687-695.
424. Hajiali H, Shahgasempour S, Naimi-Jamal MR, Peirovi H. Electrospun PGA/gelatin nanofibrous scaffolds and their potential application in vascular tissue engineering. *International journal of nanomedicine*. 2011; 6:2133-2141.
425. Kim SE, Heo DN, Lee JB, et al. Electrospun gelatin/polyurethane blended nanofibers for wound healing. *Biomedical Materials*. 2009; 4
426. Li M, Guo Y, Wei Y, MacDiarmid AG, Lelkes PI. Electrospinning polyaniline-contained gelatin nanofibers for tissue engineering applications. *Biomaterials*. 2006; 27:2705-2715.
427. Binulal NS, Natarajan A, Menon D, et al. PCL-gelatin composite nanofibers electrospun using diluted acetic acid-ethyl acetate solvent system for stem cell-based bone tissue engineering. *J. Biomater. Sci. Polym. Ed.* 2014; 25:325-340.
428. Jeong SI, Lee AY, Lee YM, Shin H. Electrospun gelatin/poly(L-lactide-co-ε-caprolactone) nanofibers for mechanically functional tissue-engineering scaffolds. *J. Biomater. Sci. Polym. Ed.* 2008; 19:339-357.
429. Wang S, Zhao G. Quantitative characterization of the electrospun gelatin-chitosan nanofibers by coupling scanning electron microscopy and atomic force microscopy. *Mater. Lett.* 2012; 79:14-17.
430. Deng L, Zhang X, Li Y, et al. Characterization of gelatin/zein nanofibers by hybrid electrospinning. *Food Hydrocolloids*. 2018; 75:72-80.
431. Tamimi E, Ardila DC, Haskett DG, et al. Biomechanical Comparison of Glutaraldehyde-Crosslinked Gelatin Fibrinogen Electrospun Scaffolds to Porcine Coronary Arteries. *J. Biomech. Eng.* 2016; 138
432. Li J, He A, Han CC, et al. Electrospinning of hyaluronic acid (HA) and HA/ gelatin blends. *Macromol. Rapid Commun.* 2006; 27:114-120.
433. Dadras Chomachayi M, Solouk A, Akbari S, et al. Electrospun nanofibers comprising of silk fibroin/gelatin for drug delivery applications: Thyme essential oil and doxycycline monohydrate release study. *Journal of Biomedical Materials Research - Part A*. 2018; 106:1092-1103.
434. Okhawilai M, Rangkupan R, Kanokpanont S, Damrongsakkul S. Preparation of Thai silk fibroin/gelatin electrospun fiber mats for controlled release applications. *Int. J. Biol. Macromol.* 2010; 46:544-550.
435. Sasithorn N, Martinová L Needleless Electrospinning of Silk Fibroin/Gelatin Blend Nanofibres. Applied Mechanics and Materials; 2015 Trans Tech Publ. 213-216 p.
436. Kook YM, Kim H, Kim S, et al. Promotion of vascular morphogenesis of endothelial cells co-cultured with human adipose-derived mesenchymal stem cells using polycaprolactone/gelatin nanofibrous scaffolds. *Nanomaterials*. 2018; 8

437. Salifu AA, Lekakou C, Labeed FH. Electrospun oriented gelatin-hydroxyapatite fiber scaffolds for bone tissue engineering. *Journal of Biomedical Materials Research - Part A*. 2017; 105:1911-1926.
438. Kim HW, Song JH, Kim HE. Nanofiber generation of gelatin-hydroxyapatite biomimetics for guided tissue regeneration. *Adv. Funct. Mater.* 2005; 15:1988-1994.
439. Ba Linh NT, Lee KH, Lee BT. Functional nanofiber mat of polyvinyl alcohol/gelatin containing nanoparticles of biphasic calcium phosphate for bone regeneration in rat calvaria defects. *Journal of Biomedical Materials Research - Part A*. 2013; 101 A:2412-2423.
440. Ghasemi-Mobarakeh L, Prabhakaran MP, Morshed M, Nasr-Esfahani MH, Ramakrishna S. Electrospun poly(ε-caprolactone)/gelatin nanofibrous scaffolds for nerve tissue engineering. *Biomaterials*. 2008; 29:4532-4539.
441. Gupta D, Venugopal J, Prabhakaran MP, et al. Aligned and random nanofibrous substrate for the in vitro culture of Schwann cells for neural tissue engineering. *Acta Biomater.* 2009; 5:2560-2569.
442. Binan L, Tendey C, De Crescenzo G, et al. LDifferentiation of neuronal stem cells into motor neurons using electrospun poly-l-lactic acid/gelatin scaffold. *Biomaterials*. 2014; 35:664-674.
443. Yazdanpanah A, Tahmasbi M, Amoabediny G, et al. Fabrication and characterization of electrospun poly-L-lactide/gelatin graded tubular scaffolds: Toward a new design for performance enhancement in vascular tissue engineering. *Progress in Natural Science: Materials International*. 2015; 25:405-413.
444. Wang H, Feng Y, Fang Z, et al. Fabrication and characterization of electrospun gelatin-heparin nanofibers as vascular tissue engineering. *Macromolecular Research*. 2013; 21:860-869.
445. Gluck JM, Rahgozar P, Ingle NP, et al. Hybrid coaxial electrospun nanofibrous scaffolds with limited immunological response created for tissue engineering. *Journal of Biomedical Materials Research - Part B Applied Biomaterials*. 2011; 99 B:180-190.
446. Coimbra P, Santos P, Alves P, et al. Coaxial electrospun PCL/Gelatin-MA fibers as scaffolds for vascular tissue engineering. *Colloids Surf. B. Biointerfaces*. 2017; 159:7-15.
447. Joy J, Pereira J, Aid-Launais R, et al. Gelatin — Oxidized carboxymethyl cellulose blend based tubular electrospun scaffold for vascular tissue engineering. *Int. J. Biol. Macromol.* 2018; 107:1922-1935.
448. Tonsomboon K, Oyen ML. Composite electrospun gelatin fiber-alginate gel scaffolds for mechanically robust tissue engineered cornea. *Journal of the Mechanical Behavior of Biomedical Materials*. 2013; 21:185-194.
449. Gao Y, Yan J, Cui XJ, Wang HY, Wang Q. Aligned fibrous scaffold induced aligned growth of corneal stroma cells in vitro culture. *Chem. Res. Chin. Univ.* 2012; 28:1022-1025.
450. Powell HM, Boyce ST. Fiber density of electrospun gelatin scaffolds regulates morphogenesis of dermal-epidermal skin substitutes. *Journal of Biomedical Materials Research - Part A*. 2008; 84:1078-1086.
451. Rujitanaroj Po, Pimpha N, Supaphol P. Wound-dressing materials with antibacterial activity from electrospun gelatin fiber mats containing silver nanoparticles. *Polymer*. 2008; 49:4723-4732.
452. Li H, Wang M, Williams GR, et al. Electrospun gelatin nanofibers loaded with vitamins A and e as antibacterial wound dressing materials. *RSC Advances*. 2016; 6:50267-50277.
453. Yao CH, Yeh JY, Chen YS, Li MH, Huang CH. Wound-healing effect of electrospun gelatin nanofibres containing Centella asiatica extract in a rat model. *J. Tissue Eng. Regen. Med.* 2017; 11:905-915.
454. Han X, Xing Z, Si S, Yao Y, Zhang Q. Electrospun grape seed polyphenols/gelatin composite fibers contained silver nanoparticles as biomaterials. *Fibers and Polymers*. 2014; 15:2572-2580.
455. Vakilian S, Norouzi M, Soufi-Zomorrod M, et al. L. inermis-loaded nanofibrous scaffolds for wound dressing applications. *Tissue Cell*. 2018; 51:32-38.

456. Safdari M, Shakiba E, Kiaie SH, Fattahi A. Preparation and characterization of Ceftazidime loaded electrospun silk fibroin/gelatin mat for wound dressing. *Fibers and Polymers*. 2016; 17:744-750.
457. Chen J, Liu Z, Chen M, Zhang H, Li X. Electrospun Gelatin Fibers with a Multiple Release of Antibiotics Accelerate Dermal Regeneration in Infected Deep Burns. *Macromol. Biosci.* 2016:1368-1380.
458. Vatankhah E, Prabhakaran MP, Jin G, Mobarakeh LG, Ramakrishna S. Development of nanofibrous cellulose acetate/gelatin skin substitutes for variety wound treatment applications. *J. Biomater. Appl.* 2014; 28:909-921.
459. Gu SY, Wang ZM, Ren J, Zhang CY. Electrospinning of gelatin and gelatin/poly(l-lactide) blend and its characteristics for wound dressing. *Mater. Sci. Eng., C*. 2009; 29:1822-1828.
460. Kim SE, Heo DN, Lee JB, et al. Electrospun gelatin/polyurethane blended nanofibers for wound healing. *Biomedical Materials*. 2009; 4
461. Chong EJ, Phan TT, Lim IJ, et al. Evaluation of electrospun PCL/gelatin nanofibrous scaffold for wound healing and layered dermal reconstitution. *Acta Biomater.* 2007; 3:321-330.
462. Duan H, Feng B, Guo X, et al. Engineering of epidermis skin grafts using electrospun nanofibrous gelatin/polycaprolactone membranes. *International Journal of Nanomedicine*. 2013; 8:2077-2084.
463. Jin G, Li Y, Prabhakaran MP, Tian W, Ramakrishna S. In vitro and in vivo evaluation of the wound healing capability of electrospun gelatin/PLLCL nanofibers. *Bioact. Compatible Polym.* 2014:1-18.
464. Norouzi M, Shabani I, Ahvaz HH, Soleimani M. PLGA/gelatin hybrid nanofibrous scaffolds encapsulating EGF for skin regeneration. *Journal of Biomedical Materials Research - Part A*. 2015; 103:2225-2235.
465. Tan L, Hu J, Huang H, Han J, Hu H. Study of multi-functional electrospun composite nanofibrous mats for smart wound healing. *Int. J. Biol. Macromol.* 2015; 79:469-476.
466. Dhandayuthapani B, Krishnan UM, Sethuraman S. Fabrication and characterization of chitosan-gelatin blend nanofibers for skin tissue engineering. *Journal of Biomedical Materials Research - Part B Applied Biomaterials*. 2010; 94:264-272.
467. Avila Rodríguez MI, Rodríguez Barroso LG, Sánchez ML. Collagen: A review on its sources and potential cosmetic applications. *J. Cosmet. Dermatol.* 2018; 17:20-26.
468. Dong C, Lv Y. Application of collagen scaffold in tissue engineering: Recent advances and new perspectives. *Polymers*. 2016; 8
469. Prockop DJ, Kivirikko KI. Collagens: Molecular biology, diseases, and potentials for therapy. *Annu. Rev. Biochem.* 1995; 64:403-434.
470. Ricard-Blum S. The Collagen Family. *Cold Spring Harbor Perspectives in Biology*. 2011; 3:1-19.
471. Gordon MK, Hahn RA. Collagens. *Cell Tissue Res.* 2010; 339:247-257.
472. Kumar VA, Taylor NL, Jalan AA, et al. A nanostructured synthetic collagen mimic for hemostasis. *Biomacromolecules*. 2014; 15:1484-1490.
473. Yu Z, An B, Ramshaw JAM, Brodsky B. Bacterial collagen-like proteins that form triple-helical structures. *J. Struct. Biol.* 2014; 186:451-461.
474. Uitto J, Booth BA, Polak KL. Collagen biosynthesis by human skin fibroblasts II. Isolation and further characterization of type I and type III procollagens synthesized in culture. *Biochimica et Biophysica Acta (BBA) - Protein Structure*. 1980; 624:545-561.
475. Chevallay B, Herbage D. Collagen-based biomaterials as 3D scaffold for cell cultures: Applications for tissue engineering and gene therapy. *Med. Biol. Eng. Comput.* 2000; 38:211-218.
476. Cen L, Liu W, Cui L, Zhang W, Cao Y. Collagen tissue engineering: Development of novel biomaterials and applications. *Pediatr. Res.* 2008; 63:492-496.
477. Zuber M, Zia F, Zia KM, et al. Collagen based polyurethanes—A review of recent advances and perspective. *Int. J. Biol. Macromol.* 2015; 80:366-374.

478. Matthews JA, Wnek GE, Simpson DG, Bowlin GL. Electrospinning of Collagen Nanofibers. *Biomacromolecules*. 2002; 3:232-238.
479. Simpson DG, Jha BS, Ayres CE, et al. Electrospun collagen: A tissue engineering scaffold with unique functional properties in a wide variety of applications. *Journal of Nanomaterials*. 2011; 2011
480. Offeddu GS, Ashworth JC, Cameron RE, Oyen ML. Multi-scale mechanical response of freeze-dried collagen scaffolds for tissue engineering applications. *Journal of the Mechanical Behavior of Biomedical Materials*. 2015; 42:19-25.
481. Rýglová Š, Braun M, Suchý T. Collagen and Its Modifications—Crucial Aspects with Concern to Its Processing and Analysis. *Macromolecular Materials and Engineering*. 2017; 302
482. Mahmoud AA, Salama AH. Norfloxacin-loaded collagen/chitosan scaffolds for skin reconstruction: Preparation, evaluation and in-vivo wound healing assessment. *Eur. J. Pharm. Sci.* 2016; 83:155-165.
483. Zheng L, Jiang X, Chen X, Fan H, Zhang X. Evaluation of novel in situ synthesized nano-hydroxyapatite/collagen/alginate hydrogels for osteochondral tissue engineering. *Biomedical Materials (Bristol)*. 2014; 9
484. Cui M, Liu L, Guo N, Su R, Ma F. Preparation, Cell Compatibility and Degradability of Collagen-Modified Poly(lactic acid). *Molecules*. 2015; 20
485. Sadeghi-Avalshahr A, Nokhasteh S, Molavi AM, Khorsand-Ghayeni M, Mahdavi-Shahri M. Synthesis and characterization of collagen/PLGA biodegradable skin scaffold fibers. *Regen Biomater*. 2017; 4:309-314.
486. Abedi G, Sotoudeh A, Soleymani M, et al. A collagen-poly(Vinyl Alcohol) nanofiber scaffold for cartilage repair. *J. Biomater. Sci. Polym. Ed.* 2011; 22:2445-2455.
487. Zhu B, Li W, Lewis RV, Segre CU, Wang R. E-Spun Composite Fibers of Collagen and Dragline Silk Protein: Fiber Mechanics, Biocompatibility, and Application in Stem Cell Differentiation. *Biomacromolecules*. 2015; 16:202-213.
488. Sionkowska A, Kaczmarek B, Lewandowska K, et al. 3D composites based on the blends of chitosan and collagen with the addition of hyaluronic acid. *Int. J. Biol. Macromol.* 2016; 89:442-448.
489. Wang J, Wu D, Zhang Z, et al. Biomimetically Ornamented Rapid Prototyping Fabrication of an Apatite-Collagen-Polycaprolactone Composite Construct with Nano-Micro-Macro Hierarchical Structure for Large Bone Defect Treatment. *ACS Applied Materials and Interfaces*. 2015; 7:26244-26256.
490. Baylan N, Bhat S, Ditto M, et al. Polycaprolactone nanofiber interspersed collagen type-I scaffold for bone regeneration: A unique injectable osteogenic scaffold. *Biomedical Materials (Bristol)*. 2013; 8
491. Mozdzen LC, Vucetic A, Harley BAC. Modifying the strength and strain concentration profile within collagen scaffolds using customizable arrays of poly-lactic acid fibers. *Journal of the Mechanical Behavior of Biomedical Materials*. 2017; 66:28-36.
492. Sionkowska A, Kozłowska J. Properties and modification of porous 3-D collagen/hydroxyapatite composites. *Int. J. Biol. Macromol.* 2013; 52:250-259.
493. Pasqui D, Torricelli P, De Cagna M, Fini M, Barbucci R. Carboxymethyl cellulose - Hydroxyapatite hybrid hydrogel as a composite material for bone tissue engineering applications. *Journal of Biomedical Materials Research - Part A*. 2014; 102:1568-1579.
494. Calabrese G, Giuffrida R, Fabbi C, et al. Collagen-Hydroxyapatite scaffolds induce human adipose derived stem cells osteogenic differentiation in Vitro. *PLoS One*. 2016; 11
495. Kim T, Sridharan I, Zhu B, Orgel J, Wang R. Effect of CNT on collagen fiber structure, stiffness assembly kinetics and stem cell differentiation. *Mater. Sci. Eng., C*. 2015; 49:281-289.
496. Alhag M, Farrell E, Toner M, et al. Evaluation of the ability of collagen-glycosaminoglycan scaffolds with or without mesenchymal stem cells to heal bone defects in Wistar rats. *Oral Maxillofac. Surg.* 2012; 16:47-55.

497. Phipps MC, Clem WC, Catledge SA, et al. Mesenchymal stem cell responses to bone-mimetic electrospun matrices composed of polycaprolactone, collagen I and nanoparticulate hydroxyapatite. *PLoS One*. 2011; 6
498. Cao Z, Dou C, Dong S. Scaffolding Biomaterials for Cartilage Regeneration. *Journal of Nanomaterials*. 2014; 2014:8.
499. Griffin DJ, Bonnevie ED, Lachowsky DJ, et al. Mechanical characterization of matrix-induced autologous chondrocyte implantation (MACI®) grafts in an equine model at 53 weeks. *J. Biomech.*; 48:1944-1949.
500. Monaco G, Cholas R, Salvatore L, Madaghiele M, Sannino A. Sterilization of collagen scaffolds designed for peripheral nerve regeneration: Effect on microstructure, degradation and cellular colonization. *Materials Science and Engineering: C*. 2017; 71:335-344.
501. Liu T, Houle JD, Xu J, Chan BP, Chew SY. Nanofibrous collagen nerve conduits for spinal cord repair. *Tissue Engineering - Part A*. 2012; 18:1057-1066.
502. Cui Y, Lu C, Meng D, et al. Collagen scaffolds modified with CNTF and bFGF promote facial nerve regeneration in minipigs. *Biomaterials*. 2014; 35:7819-7827.
503. Schnell E, Klinkhammer K, Balzer S, et al. Guidance of glial cell migration and axonal growth on electrospun nanofibers of poly-ε-caprolactone and a collagen/poly-ε-caprolactone blend. *Biomaterials*. 2007; 28:3012-3025.
504. Weinberg CB, Bell E. A blood vessel model constructed from collagen and cultured vascular cells. *Science*. 1986; 231:397-400.
505. Lee SJ, Liu J, Oh SH, et al. Development of a composite vascular scaffolding system that withstands physiological vascular conditions. *Biomaterials*. 2008; 29:2891-2898.
506. Cen L, Liu W, Cui L, Zhang W, Cao Y. Collagen Tissue Engineering: Development of Novel Biomaterials and Applications. *Pediatr. Res.* 2008; 63:492.
507. Yannas IV, Burke JF, Orgill DP, Skrabut EM. Wound tissue can utilize a polymeric template to synthesize a functional extension of skin. *Science*. 1982; 215:174-176.
508. Chattopadhyay S, Raines RT. Collagen-Based Biomaterials for Wound Healing. *Biopolymers*. 2014; 101:821-833.
509. Zhong SP, Zhang YZ, Lim CT. Tissue scaffolds for skin wound healing and dermal reconstruction. *Wiley Interdisciplinary Reviews: Nanomedicine and Nanobiotechnology*. 2010; 2:510-525.
510. Rho KS, Jeong L, Lee G, et al. Electrospinning of collagen nanofibers: Effects on the behavior of normal human keratinocytes and early-stage wound healing. *Biomaterials*. 2006; 27:1452-1461.
511. Berthod F, Germain L, Li H, et al. Collagen fibril network and elastic system remodeling in a reconstructed skin transplanted on nude mice. *Matrix Biol.* 2001; 20:463-473.
512. Ti D, Hao H, Xia L, et al. Controlled release of thymosin beta 4 using a collagen-chitosan sponge scaffold augments cutaneous wound healing and increases angiogenesis in diabetic rats with hindlimb ischemia. *Tissue Engineering - Part A*. 2015; 21:541-549.
513. Rnjak-Kovacina J, Wise SG, Li Z, et al. Electrospun synthetic human elastin:collagen composite scaffolds for dermal tissue engineering. *Acta Biomater.* 2012; 8:3714-3722.
514. Alarcon EI, Udekwu KI, Noel CW, et al. Safety and efficacy of composite collagen-silver nanoparticle hydrogels as tissue engineering scaffolds. *Nanoscale*. 2015; 7:18789-18798.
515. Rath G, Hussain T, Chauhan G, Garg T, Goyal AK. Collagen nanofiber containing silver nanoparticles for improved wound-healing applications. *J. Drug Targeting*. 2016; 24:520-529.
516. Gümüşderelioglu M, Dalkiranoğlu S, Aydin RST, Çakmak S. A novel dermal substitute based on biofunctionalized electrospun PCL nanofibrous matrix. *Journal of Biomedical Materials Research - Part A*. 2011; 98 A:461-472.
517. Ananta M, Brown RA, Mudera V. A rapid fabricated living dermal equivalent for skin tissue engineering: An in vivo evaluation in an acute wound model. *Tissue Engineering - Part A*. 2012; 18:353-361.
518. Moroni L, Boland T, Burdick JA, et al. Biofabrication: A Guide to Technology and Terminology. *Trends Biotechnol.* 2018; 36:384-402.

519. Zhang X, Reagan MR, Kaplan DL. Electrospun silk biomaterial scaffolds for regenerative medicine. *Adv. Drug Del. Rev.* 2009; 61:988-1006.
520. Goyal R, Guvendiren M, Freeman O, Mao Y, Kohn J. Optimization of Polymer-ECM Composite Scaffolds for Tissue Engineering: Effect of Cells and Culture Conditions on Polymeric Nanofiber Mats. *Journal of Functional Biomaterials*. 2017; 8:1.
521. Rutledge K, Cheng Q, Pryzhkova M, Harris GM, Jabbarzadeh E. Enhanced Differentiation of Human Embryonic Stem Cells on Extracellular Matrix-Containing Osteomimetic Scaffolds for Bone Tissue Engineering. *Tissue Engineering. Part C, Methods*. 2014; 20:865-874.
522. Shamsi MH, Luqman M, Basarir F, et al. Plasma-modified halloysite nanocomposites: effect of plasma modification on the structure and dynamic mechanical properties of halloysite–polystyrene nanocomposites. *Polym. Int.* 2010; 59:1492-1498.
523. Carli LN, Crespo JS, Mauler RS. PHBV nanocomposites based on organomodified montmorillonite and halloysite: The effect of clay type on the morphology and thermal and mechanical properties. *Composites Part A: Applied Science and Manufacturing*. 2011; 42:1601-1608.
524. Chittur KK. FTIR/ATR for protein adsorption to biomaterial surfaces. *Biomaterials*. 1998; 19:357-69.
525. Zhan J, Morsi Y, Ei-Hamshary H, Al-Deyab SS, Mo X. Preparation and characterization of electrospun in-situ cross-linked gelatin-graphite oxide nanofibers. *J. Biomater. Sci. Polym. Ed.* 2016; 27:385-402.
526. Andiappan M, Sundaramoorthy S, Panda N, et al. Electrospun eri silk fibroin scaffold coated with hydroxyapatite for bone tissue engineering applications. *Progress in Biomaterials*. 2013; 2:6.
527. Bubnis WA, Ofner CM. The determination of ϵ-amino groups in soluble and poorly soluble proteinaceous materials by a spectrophotometrie method using trinitrobenzenesulfonic acid. *Anal. Biochem.* 1992; 207:129-133.
528. Chen Z, Wei B, Mo X, et al. Mechanical properties of electrospun collagen-chitosan complex single fibers and membrane. *Mater. Sci. Eng., C*. 2009; 29:2428-2435.
529. Muschler GF, Nakamoto C, Griffith LG. Engineering principles of clinical cell-based tissue engineering. *Journal of Bone and Joint Surgery - Series A*. 2004; 86:1541-1558.
530. Kidoaki S, Kwon IK, Matsuda T. Mesoscopic spatial designs of nano- and microfiber meshes for tissue-engineering matrix and scaffold based on newly devised multilayering and mixing electrospinning techniques. *Biomaterials*. 2005; 26:37-46.
531. Goldberg M, Langer R, Jia X. Nanostructured materials for applications in drug delivery and tissue engineering. *J. Biomater. Sci. Polym. Ed.* 2007; 18:241-268.
532. Kishan AP, Cosgriff-Hernandez EM. Recent advancements in electrospinning design for tissue engineering applications: A review. *Journal of Biomedical Materials Research - Part A*. 2017; 105:2892-2905.
533. Li ZH, Ji SC, Wang YZ, Shen XC, Liang H. Silk fibroin-based scaffolds for tissue engineering. *Frontiers of Materials Science*. 2013; 7:237-247.
534. Bhattacharjee P, Kundu B, Naskar D, et al. Silk scaffolds in bone tissue engineering: An overview. *Acta Biomater.* 2017; 63:1-17.
535. Zhang K, Mo X, Huang C, He C, Wang H. Electrospun scaffolds from silk fibroin and their cellular compatibility. *Journal of Biomedical Materials Research - Part A*. 2010; 93:976-983.
536. Cattaneo I, Figliuzzi M, Azzollini N, et al. In vivo regeneration of elastic lamina on fibroin biodegradable vascular scaffold. *Int. J. Artif. Organs*. 2013; 36:166-174.
537. Pan H, Zhang Y, Hang Y, et al. Significantly reinforced composite fibers electrospun from silk fibroin/carbon nanotube aqueous solutions. *Biomacromolecules*. 2012; 13:2859-2867.
538. Zhang K, Wang H, Huang C, et al. Fabrication of silk fibroin blended P(LLA-CL) nanofibrous scaffolds for tissue engineering. *Journal of Biomedical Materials Research - Part A*. 2010; 93:984-993.

539. Sheikh FA, Ju HW, Moon BM, et al. A comparative mechanical and biocompatibility study of poly(ε-caprolactone), hybrid poly(ε-caprolactone)-silk, and silk nanofibers by colloidal electrospinning technique for tissue engineering. *J. Bioact. Compatible Polym.* 2014; 29:500-514.
540. Lei C, Zhu H, Li J, et al. Preparation and characterization of polyhydroxybutyrate-co-hydroxyvalerate/silk fibroin nanofibrous scaffolds for skin tissue engineering. *Polym. Eng. Sci.* 2015; 55:907-916.
541. Marelli B, Achilli M, Alessandrino A, et al. Collagen-Reinforced Electrospun Silk Fibroin Tubular Construct as Small Calibre Vascular Graft. *Macromol. Biosci.* 2012; 12:1566-1574.
542. Taddei P, Tozzi S, Zuccheri G, et al. ntermolecular interactions between B. mori silk fibroin and poly(L-lactic acid) in electrospun composite nanofibrous scaffolds. *Mater. Sci. Eng., C*. 2017; 70:777-787.
543. Chouhan D, Chakraborty B, Nandi SK, Mandal BB. Role of non-mulberry silk fibroin in deposition and regulation of extracellular matrix towards accelerated wound healing. *Acta Biomater.* 2017; 48:157-174.
544. Huang B, Liu M, Long Z, Shen Y, Zhou C. Effects of halloysite nanotubes on physical properties and cytocompatibility of alginate composite hydrogels. *Materials Science and Engineering: C*. 2017; 70:303-310.
545. Zhou WY, Guo B, Liu M, et al. Poly(vinyl alcohol)/Halloysite nanotubes bionanocomposite films: Properties and in vitro osteoblasts and fibroblasts response. *Journal of Biomedical Materials Research - Part A*. 2010; 93:1574-1587.
546. Cai Q, Xu Q, Feng Q, et al. Biomineralization of electrospun poly(L-lactic acid)/gelatin composite fibrous scaffold by using a supersaturated simulated body fluid with continuous CO2 bubbling. *Appl. Surf. Sci.* 2011; 257:10109-10118.
547. Švachová V, Khunová V, Pavliňák D, Fohlerová Z, Vojtová L. The Effect of halloysite on structure and properties of polycaprolactone/gelatin nanofibers. *Polym. Eng. Sci.* 2017; 57:506-512.
548. Yoo HS, Kim TG, Park TG. Surface-functionalized electrospun nanofibers for tissue engineering and drug delivery. *Adv. Drug Del. Rev.* 2009; 61:1033-1042.
549. Murphy CM, O'Brien FJ. Understanding the effect of mean pore size on cell activity in collagen-glycosaminoglycan scaffolds. *Cell Adhesion and Migration*. 2010; 4:377-381.
550. Karageorgiou V, Kaplan D. Porosity of 3D biomaterial scaffolds and osteogenesis. *Biomaterials*. 2005; 26:5474-5491.
551. Stachewicz U, Szewczyk PK, Kruk A, Barber AH, Czyrska-Filemonowicz A. Pore shape and size dependence on cell growth into electrospun fiber scaffolds for tissue engineering: 2D and 3D analyses using SEM and FIB-SEM tomography. *Materials Science and Engineering: C*. 2017;
552. Lowery JL, Datta N, Rutledge GC. ffect of fiber diameter, pore size and seeding method on growth of human dermal fibroblasts in electrospun poly(ε-caprolactone) fibrous mats. *Biomaterials*. 2010; 31:491-504.
553. Murphy CM, Haugh MG, O'Brien FJ. The effect of mean pore size on cell attachment, proliferation and migration in collagen–glycosaminoglycan scaffolds for bone tissue engineering. *Biomaterials*. 2010; 31:461-466.
554. Makaremi M, De Silva RT, Pasbakhsh P. Electrospun Nanofibrous Membranes of Polyacrylonitrile/Halloysite with Superior Water Filtration Ability. *The Journal of Physical Chemistry C*. 2015; 119:7949-7958.
555. Prabhakaran MP, Venugopal JR, Chyan TT, et al. Electrospun biocomposite nanofibrous scaffolds for neural tissue engineering. *Tissue Engineering - Part A*. 2008; 14:1787-1797.
556. Altankov G, Groth T. Reorganization of substratum-bound fibronectin on hydrophilic and hydrophobic materials is related to biocompatibility. *J. Mater. Sci. Mater. Med.* 1994; 5:732-737.

557. Lee JH, Lee SJ, Khang G, Lee HB. The Effect of Fluid Shear Stress on Endothelial Cell Adhesiveness to Polymer Surfaces with Wettability Gradient. *J. Colloid Interface Sci.* 2000; 230:84-90.
558. Webb K, Hlady V, Tresco PA. Relative importance of surface wettability and charged functional groups on NIH 3T3 fibroblast attachment, spreading, and cytoskeletal organization. *J. Biomed. Mater. Res.* 1998; 41:422-430.
559. Fu SZ, Wang XH, Guo G, et al. Preparation and properties of nano-hydroxyapatite/PCL-PEG-PCL composite membranes for tissue engineering applications. *Journal of Biomedical Materials Research - Part B Applied Biomaterials*. 2011; 97 B:74-83.
560. Abdullayev E, Lvov Y. Halloysite clay nanotubes for controlled release of protective agents. *Journal of Nanoscience and Nanotechnology*. 2011; 11:10007-10026.
561. Liu M, Jia Z, Liu F, Jia D, Guo B. Tailoring the wettability of polypropylene surfaces with halloysite nanotubes. *J. Colloid Interface Sci.* 2010; 350:186-193.
562. Huang F, Wei Q, Cai Y, Wu N. Surface structures and contact angles of electrospun poly(vinylidene fluoride) nanofiber membranes. *Int. J. Polym. Anal. Charact.* 2008; 13:292-301.
563. Jin C, Yan R, Huang J. Cellulose substance with reversible photo-responsive wettability by surface modification. *J. Mater. Chem.* 2011; 21:17519-17525.
564. Cavallaro G, Lazzara G, Milioto S, Parisi F. Halloysite nanotubes as sustainable nanofiller for paper consolidation and protection. *J. Therm. Anal. Calorim.* 2014;
565. Cavallaro G, Donato DI, Lazzara G, Milioto S. Films of halloysite nanotubes sandwiched between two layers of biopolymer: From the morphology to the dielectric, thermal, transparency, and wettability properties. *Journal of Physical Chemistry C*. 2011; 115:20491-20498.
566. Marmur A. From hygrophilic to superhygrophobic: Theoretical conditions for making high-contact-angle surfaces from low-contact-angle materials. *Langmuir*. 2008; 24:7573-7579.
567. De Silva RT, Pasbakhsh P, Goh KL, Chai SP, Chen J. Synthesis and characterisation of poly (lactic acid)/halloysite bionanocomposite films. *J. Compos. Mater.* 2013; 48:3705-3717.
568. Ahn SH, Lee HJ, Kim GH. Polycaprolactone scaffolds fabricated with an advanced electrohydrodynamic direct-printing method for bone tissue regeneration. *Biomacromolecules*. 2011; 12:4256-4263.
569. Lins LC, Wianny F, Livi S, et al. Development of Bioresorbable Hydrophilic-Hydrophobic Electrospun Scaffolds for Neural Tissue Engineering. *Biomacromolecules*. 2016; 17:3172-3187.
570. Sultana N, Khan TH. Water Absorption and Diffusion Characteristics of Nanohydroxyapatite (nHA) and Poly(hydroxybutyrate-co-hydroxyvalerate-) Based Composite Tissue Engineering Scaffolds and Nonporous Thin Films. *Journal of Nanomaterials*. 2013; 2013:8.
571. Pinho ED, Martins A, Araújo JV, Reis RL, Neves NM. Degradable particulate composite reinforced with nanofibres for biomedical applications. *Acta Biomater.* 2009; 5:1104-1114.
572. Zhou T, Li G, Lin S, et al. Electrospun Poly(3-hydroxybutyrate-co-4-hydroxybutyrate)/Graphene Oxide Scaffold: Enhanced Properties and Promoted in Vivo Bone Repair in Rats. *ACS Applied Materials and Interfaces*. 2017; 9:42589-42600.
573. Lu Q, Zhang B, Li M, et al. Degradation mechanism and control of silk fibroin. *Biomacromolecules*. 2011; 12:1080-1086.
574. Li C, Vepari C, Jin H-J, Kim HJ, Kaplan DL. Electrospun silk-BMP-2 scaffolds for bone tissue engineering. *Biomaterials*. 2006; 27:3115-3124.
575. Zhang H, Li LL, Dai FY, et al. Preparation and characterization of silk fibroin as a biomaterial with potential for drug delivery. *J. Transl. Med.* 2012; 10
576. Motta A, Fambri L, Migliaresi C. Regenerated silk fibroin films: Thermal and dynamic mechanical analysis. *Macromol. Chem. Phys.* 2002; 203:1658-1665.

577. Tsukada M, Gotoh Y, Nagura M, et al. Structural changes of silk fibroin membranes induced by immersion in methanol aqueous solutions. *J. Polym. Sci., Part B: Polym. Phys.* 1994; 32:961-968.
578. Min G, Liqian L, Xiaoyue W, Houke L, Qingsong Z. Preparation of a novel breviscapine-loaded halloysite nanotubes complex for controlled release of breviscapine. *IOP Conference Series: Materials Science and Engineering*. 2017; 265:012011.
579. Moroni L, Elisseeff JH. Biomaterials engineered for integration. *Mater. Today*. 2008; 11:44-51.
580. Ramakrishna S, Lim TC, Inai R, Fujihara K. Modified Halpin-Tsai equation for Clay-Reinforced polymer nanofiber. *Mechanics of Advanced Materials and Structures*. 2006; 13:77-81.
581. Abdullah ZW, Dong Y. Preparation and characterisation of poly(vinyl) alcohol (PVA)/starch (ST)/halloysite nanotube (HNT) nanocomposite films as renewable materials. *Journal of Materials Science*. 2018; 53:3455-3469.
582. Zhang X, Tsukada M, Morikawa H, et al. Production of silk sericin/silk fibroin blend nanofibers. *Nanoscale Research Letters*. 2011; 6:1-8.
583. Lecouvet B, Gutierrez JG, Sclavons M, Bailly C. Structure–property relationships in polyamide 12/halloysite nanotube nanocomposites. *Polym. Degradation Stab.* 2011; 96:226-235.
584. Wu W, Cao X, Zhang Y, He G. Polylactide/halloysite nanotube nanocomposites: Thermal, mechanical properties, and foam processing. *J. Appl. Polym. Sci.* 2013; 130:443-452.
585. Christopherson GT, Song H, Mao H-Q. The influence of fiber diameter of electrospun substrates on neural stem cell differentiation and proliferation. *Biomaterials*. 2009; 30:556-564.
586. Fee T, Surianarayanan S, Downs C, Zhou Y, Berry J. Nanofiber alignment regulates NIH3T3 cell orientation and cytoskeletal gene expression on electrospun PCL+gelatin nanofibers. *PLoS One*. 2016; 11
587. Kim CH, Khil MS, Kim HY, Lee HU, Jahng KY. An improved hydrophilicity via electrospinning for enhanced cell attachment and proliferation. *Journal of Biomedical Materials Research - Part B Applied Biomaterials*. 2006; 78:283-290.
588. Liu HY, Du L, Zhao YT, Tian WQ. In vitro hemocompatibility and cytotoxicity evaluation of halloysite nanotubes for biomedical application. *Journal of Nanomaterials*. 2015; 2015
589. Ren K, Crouzier T, Roy C, Picart C. Polyelectrolyte multilayer films of controlled stiffness modulate myoblast cell differentiation. *Adv. Funct. Mater.* 2008; 18:1378-1389.
590. Ostrovidov S, Shi X, Zhang L, et al. Myotube formation on gelatin nanofibers – Multi-walled carbon nanotubes hybrid scaffolds. *Biomaterials*. 2014; 35:6268-6277.
591. Sirivisoot S, Harrison BS. Skeletal myotube formation enhanced by electrospun polyurethane carbon nanotube scaffolds. *International journal of nanomedicine*. 2011; 6:2483-2497.
592. Ricotti L, Polini A, Genchi GG, et al. Proliferation and skeletal myotube formation capability of C2C12 and H9c2 cells on isotropic and anisotropic electrospun nanofibrous PHB scaffolds. *Biomedical Materials*. 2012; 7
593. Hu X, Park S-H, Gil ES, et al. The influence of elasticity and surface roughness on myogenic and osteogenic-differentiation of cells on silk-elastin biomaterials. *Biomaterials*. 2011; 32:8979-8989.
594. Yang F, Murugan R, Wang S, Ramakrishna S. Electrospinning of nano/micro scale poly(l-lactic acid) aligned fibers and their potential in neural tissue engineering. *Biomaterials*. 2005; 26:2603-2610.
595. Shin YC, Lee JH, Jin L, et al. Stimulated myoblast differentiation on graphene oxide-impregnated PLGA-collagen hybrid fibre matrices matrices. *Journal of Nanobiotechnology*. 2015; 13

596. Khorasani MT, Mirzadeh H, Irani S. Plasma surface modification of poly (l-lactic acid) and poly (lactic-co-glycolic acid) films for improvement of nerve cells adhesion. *Radiat. Phys. Chem.* 2008; 77:280-287.
597. Shen Z, Guo S, Ye D, et al. Skeletal muscle regeneration on protein-grafted and microchannel-patterned scaffold for hypopharyngeal tissue engineering. *BioMed Research International*. 2013; 2013
598. Engler AJ, Griffin MA, Sen S, et al. Myotubes differentiate optimally on substrates with tissue-like stiffness: Pathological implications for soft or stiff microenvironments. *J. Cell Biol.* 2004; 166:877-887.
599. Chaturvedi V, Naskar D, Kinnear BF, et al. Silk fibroin scaffolds with muscle-like elasticity support in vitro differentiation of human skeletal muscle cells. *J. Tissue Eng. Regen. Med.* 2017; 11:3178-3192.
600. Levy-Mishali M, Zoldan J, Levenberg S. Effect of scaffold stiffness on myoblast differentiation. *Tissue Engineering - Part A*. 2009; 15:935-944.
601. Evrova O, Hosseini V, Milleret V, et al. Hybrid randomly electrospun poly(lactic-co-glycolic acid):poly(ethylene oxide) (PLGA:PEO) fibrous scaffolds enhancing myoblast differentiation and alignment. *ACS Applied Materials and Interfaces*. 2016; 8:31574-31586.
602. Ren K, Crouzier T, Roy C, Picart C. Polyelectrolyte multilayer films of controlled stiffness modulate myoblast cell differentiation. *Adv. Funct. Mater.* 2008; 18:1378-1389.
603. Gilmore KJ, Kita M, Han Y, et al. Skeletal muscle cell proliferation and differentiation on polypyrrole substrates doped with extracellular matrix components. *Biomaterials*. 2009; 30:5292-5304.
604. Benders KEM, Weeren PRv, Badylak SF, et al. Extracellular matrix scaffolds for cartilage and bone regeneration. *Trends Biotechnol.* 2013; 31:169-176.
605. Aamodt JM, Grainger DW. Extracellular matrix-based biomaterial scaffolds and the host response. *Biomaterials*. 2016; 86:68-82.
606. Taylor DA, Sampaio LC, Ferdous Z, Gobin AS, Taite LJ. Decellularized matrices in regenerative medicine. *Acta Biomater.* 2018; 74:74-89.
607. Mahmut P, Arin D, Sedat O, Elçin AE, Elçin YM. Clinical applications of decellularized extracellular matrices for tissue engineering and regenerative medicine. *Biomedical Materials*. 2016; 11:022003.
608. Elmashhady Hady H, Kraemer Bruce A, Patel Krishna H, Sell Scott A, Garg K. Decellularized extracellular matrices for tissue engineering applications 2017.
609. Goyal R, Vega ME, Pastino AK, et al. Development of hybrid scaffolds with natural extracellular matrix deposited within synthetic polymeric fibers. *J. Biomed. Mater. Res. A*. 2017; 105:2162-2170.
610. Tang X, Thankappan SK, Lee P, et al. Chapter 21 - Polymeric Biomaterials in Tissue Engineering and Regenerative Medicine. In: Kumbar SG, Laurencin CT, Deng M, editors. Natural and Synthetic Biomedical Polymers. Oxford: Elsevier; 2014. p. 351-371.
611. Kohane DS, Langer R. Polymeric Biomaterials in Tissue Engineering. *Pediatr. Res.* 2008; 63:487.
612. Hutmacher DW, Schantz JT, Lam CXF, Tan KC, Lim TC. State of the art and future directions of scaffold-based bone engineering from a biomaterials perspective. *J. Tissue Eng. Regen. Med.* 2007; 1:245-260.
613. Chan G, Mooney DJ. New materials for tissue engineering: towards greater control over the biological response. *Trends Biotechnol.* 2008; 26:382-392.
614. Shekaran A, García AJ. Extracellular matrix-mimetic adhesive biomaterials for bone repair. *Journal of Biomedical Materials Research - Part A*. 2011; 96 A:261-272.
615. Goyal R, Guvendiren M, Freeman O, Mao Y, Kohn J. Optimization of Polymer-ECM Composite Scaffolds for Tissue Engineering: Effect of Cells and Culture Conditions on Polymeric Nanofiber Mats. *Journal of Functional Biomaterials*. 2017; 8:1.
616. Taddei P, Chiono V, Anghileri A, et al. Silk fibroin/gelatin blend films crosslinked with enzymes for biomedical applications. *Macromol. Biosci.* 2013; 13:1492-1510.
617. Wongputtaraksa T, Ratanavaraporn J, Pichyangkura R, Damrongsakkul S. Surface modification of Thai silk fibroin scaffolds with gelatin and chitooligosaccharide for enhanced

osteogenic differentiation of bone marrow-derived mesenchymal stem cells. *J. Biomed. Mater. Res. B Appl. Biomater.* 2012; 100:2307-15.
618. Poursamar SA, Lehner AN, Azami M, et al. The effects of crosslinkers on physical, mechanical, and cytotoxic properties of gelatin sponge prepared via in-situ gas foaming method as a tissue engineering scaffold. *Materials Science and Engineering: C*. 2016; 63:1-9.
619. Bao W, Zhang Y, Yin G, Wu J. The structure and property of the electrospinning silk fibroin/gelatin blend nanofibers. *E-Polymers*. 2008;
620. Somvipart S, Kanokpanont S, Rangkupan R, Ratanavaraporn J, Damrongsakkul S. Development of electrospun beaded fibers from Thai silk fibroin and gelatin for controlled release application. *Int. J. Biol. Macromol.* 2013; 55:176-184.
621. Zhu B, Li W, Chi N, et al. Optimization of Glutaraldehyde Vapor Treatment for Electrospun Collagen/Silk Tissue Engineering Scaffolds. *ACS Omega*. 2017; 2:2439-2450.
622. Amariei N, Manea LR, Bertea AP, Bertea A, Popa A The Influence of Polymer Solution on the Properties of Electrospun 3D Nanostructures. IOP Conference Series: Materials Science and Engineering; 2017; p.
623. Kim HJ, Um IC. Relationship between rheology and electro-spinning performance of regenerated silk fibroin prepared using different degumming methods. *Korea Australia Rheology Journal*. 2014; 26:119-125.
624. Gomes SR, Rodrigues G, Martins GG, Henriques CMR, Silva JC. In vitro evaluation of crosslinked electrospun fish gelatin scaffolds. *Materials Science and Engineering: C*. 2013; 33:1219-1227.
625. Amadori S, Torricelli P, Rubini K, et al. Effect of sterilization and crosslinking on gelatin films. *Journal of materials science. Materials in medicine*. 2015; 26:69.
626. Silva SS, Maniglio D, Motta A, et al. Genipin-modified silk-fibroin nanometric nets. *Macromol. Biosci.* 2008; 8:766-774.
627. Gil ES, Frankowski DJ, Bowman MK, et al. Mixed protein blends composed of gelatin and Bombyx mori silk fibroin: Effects of solvent-induded crystallization and composition. *Biomacromolecules*. 2006; 7:728-735.
628. Tao W, Li M, Zhao C. Structure and properties of regenerated Antheraea pernyi silk fibroin in aqueous solution. *Int. J. Biol. Macromol.* 2007; 40:472-478.
629. Malay Ö, Yalçin D, BatIgün A, Bayraktar O. Characterization of silk fibroin/hyaluronic acid polyelectrolyte complex (PEC) films. *J. Therm. Anal. Calorim.* 2008; 94:749-755.
630. de Moraes MA, Nogueira GM, Weska RF, Beppu MM. Preparation and characterization of insoluble silk fibroin/chitosan blend films. *Polymers*. 2010; 2:719-727.
631. Cheung DT, Nimni ME. Mechanism of Crosslinking of Proteins by Glutaraldehyde II. Reaction with Monomeric and Polymeric Collagen. *Connect. Tissue Res.* 1982; 10:201-216.
632. Olde Damink LHH, Dijkstra PJ, Van Luyn MJA, et al. Glutaraldehyde as a crosslinking agent for collagen-based biomaterials. *J. Mater. Sci. Mater. Med.* 1995; 6:460-472.
633. Xiao W, Liu W, Sun J, et al. Ultrasonication and genipin cross-linking to prepare novel silk fibroin-gelatin composite hydrogel. *J. Bioact. Compatible Polym.* 2012; 27:327-341.
634. Soliman S, Sant S, Nichol JW, et al. Controlling the porosity of fibrous scaffolds by modulating the fiber diameter and packing density. *Journal of Biomedical Materials Research - Part A*. 2011; 96 A:566-574.
635. Sasithorn N, Martinová L. Needleless Electrospinning of Silk Fibroin/Gelatin Blend Nanofibres. *Applied Mechanics and Materials*. 2015; 804:213-216.
636. Zhou Z, Yang Z, Huang T, et al. Effect of Chemical Cross-linking on Properties of Gelatin/Hyaluronic Acid Composite Hydrogels. *Polym. Plast. Technol. Eng.* 2013; 52:45-50.
637. Zhu J, Yang F, He F, et al. A tubular gelatin scaffold capable of the time-dependent controlled release of epidermal growth factor and mitomycin C. *Colloids Surf. B. Biointerfaces*. 2015; 135:416-424.

638. Simonet M, Stingelin N, Wismans JGF, et al. Tailoring the void space and mechanical properties in electrospun scaffolds towards physiological ranges. *Journal of Materials Chemistry B*. 2014; 2:305-313.
639. Yin Y, Pu D, Xiong J. Analysis of the comprehensive tensile relationship in electrospun silk fibroin/polycaprolactone nanofiber membranes. *Membranes*. 2017; 7
640. Wu SC, Chang WH, Dong GC, et al. Cell adhesion and proliferation enhancement by gelatin nanofiber scaffolds. *J. Bioact. Compatible Polym.* 2011; 26:565-577.
641. Telemeco TA, Ayres C, Bowlin GL, et al. Regulation of cellular infiltration into tissue engineering scaffolds composed of submicron diameter fibrils produced by electrospinning. *Acta Biomater.* 2005; 1:377-385.
642. Ghasemi-Mobarakeh L, Prabhakaran MP, Morshed M, Nasr-Esfahani M-H, Ramakrishna S. Electrospun poly(ε-caprolactone)/gelatin nanofibrous scaffolds for nerve tissue engineering. *Biomaterials*. 2008; 29:4532-4539.
643. Grover CN, Gwynne JH, Pugh N, et al. Crosslinking and composition influence the surface properties, mechanical stiffness and cell reactivity of collagen-based films. *Acta Biomater.* 2012; 8:3080-3090.
644. Yao R, He J, Meng G, Jiang B, Wu F. Electrospun PCL/Gelatin composite fibrous scaffolds: Mechanical properties and cellular responses. *J. Biomater. Sci. Polym. Ed.* 2016; 27:824-838.
645. Singh BN, Panda NN, Mund R, Pramanik K. Carboxymethyl cellulose enables silk fibroin nanofibrous scaffold with enhanced biomimetic potential for bone tissue engineering application. *Carbohydr. Polym.* 2016; 151:335-347.
646. Watt SM, Pleat JM. Stem cells, niches and scaffolds: Applications to burns and wound care. *Adv. Drug Del. Rev.* 2018; 123:82-106.
647. Shevchenko RV, James SL, James SE. A review of tissue-engineered skin bioconstructs available for skin reconstruction. *Journal of the Royal Society Interface*. 2010; 7:229-258.
648. Pilehvar-Soltanahmadi Y, Akbarzadeh A, Moazzez-Lalaklo N, Zarghami N. An update on clinical applications of electrospun nanofibers for skin bioengineering. *Artificial Cells, Nanomedicine and Biotechnology*. 2016; 44:1350-1364.
649. Priya SG, Jungvid H, Kumar A. Skin tissue engineering for tissue repair and regeneration. *Tissue Eng Part B Rev*. 2008; 14:105-18.
650. Rheinwald JG, Green H. Serial cultivation of strains of human epidermal keratinocytes: the formation of keratinizing colonies from single cells. *Cell*. 1975; 6:331-43.
651. Bi H, Jin Y. Current progress of skin tissue engineering: Seed cells, bioscaffolds, and construction strategies. *Burns & Trauma*. 2013; 1:63-72.
652. Mogoşanu GD, Grumezescu AM. Natural and synthetic polymers for wounds and burns dressing. *Int. J. Pharm.* 2014; 463:127-136.
653. Reimers K, Liebsch C, Radtke C, Kuhbier JW, Vogt PM. Silks as scaffolds for skin reconstruction. *Biotechnol. Bioeng.* 2015; 112:2201-2205.
654. Min BM, Jeong L, Nam YS, et al. Formation of silk fibroin matrices with different texture and its cellular response to normal human keratinocytes. *Int. J. Biol. Macromol.* 2004; 34:281-288.
655. Min BM, Lee G, Kim SH, et al. Electrospinning of silk fibroin nanofibers and its effect on the adhesion and spreading of normal human keratinocytes and fibroblasts in vitro. *Biomaterials*. 2004; 25:1289-97.
656. Zhang W, Chen L, Chen J, et al. Silk Fibroin Biomaterial Shows Safe and Effective Wound Healing in Animal Models and a Randomized Controlled Clinical Trial. *Adv Healthc Mater*. 2017; 6
657. Navone SE, Pascucci L, Dossena M, et al. Decellularized silk fibroin scaffold primed with adipose mesenchymal stromal cells improves wound healing in diabetic mice. *Stem Cell. Res. Ther.* 2014; 5:7-7.
658. Yan S, Zhang Q, Wang J, et al. Silk fibroin/chondroitin sulfate/hyaluronic acid ternary scaffolds for dermal tissue reconstruction. *Acta Biomater.* 2013; 9:6771-6782.

659. Zhu C, Wang C, Chen R, Ru C Eskola H, Väisänen O, Viik J, Hyttinen J, editors. A Novel Composite and Suspended Nanofibrous Scaffold for Skin Tissue Engineering. EMBEC & NBC 2017; 2018 2018//; Singapore. Springer Singapore. 1-4 p.
660. Vasconcelos A, Pêgo AP, Henriques L, Lamghari M, Cavaco-Paulo A. Protein Matrices for Improved Wound Healing: Elastase Inhibition by a Synthetic Peptide Model. *Biomacromolecules*. 2010; 11:2213-2220.
661. Bhardwaj N, Sow WT, Devi D, et al. Silk fibroin-keratin based 3D scaffolds as a dermal substitute for skin tissue engineering. *Integr. Biol. (Camb.)*. 2015; 7:53-63.
662. Brett D. A Review of Collagen and Collagen-based Wound Dressings. *Wounds*. 2008; 20:347-56.
663. Gaspar A, Moldovan L, Constantin D, et al. Collagen–based scaffolds for skin tissue engineering. *J. Med. Life*. 2011; 4:172-177.
664. Kim EY, Tripathy N, Cho SA, et al. Bioengineered neo-corneal endothelium using collagen type-I coated silk fibroin film. *Colloids Surf. B. Biointerfaces*. 2015; 136:394-401.
665. Kim EY, Tripathy N, Cho SA, et al. Bioengineered neo-corneal endothelium using collagen type-I coated silk fibroin film. *Colloids Surf. B. Biointerfaces*. 2015; 136:394-401.
666. Kandhasamy S, Perumal S, Madhan B, et al. Synthesis and Fabrication of Collagen-Coated Ostholamide Electrospun Nanofiber Scaffold for Wound Healing. *ACS Appl Mater Interfaces*. 2017; 9:8556-8568.
667. Maghdouri-White Y, Bowlin GL, Lemmon CA, Dréau D. Mammary epithelial cell adhesion, viability, and infiltration on blended or coated silk fibroin–collagen type I electrospun scaffolds. *Materials Science and Engineering: C*. 2014; 43:37-44.
668. Xu Y, Zhang Z, Chen X, et al. A Silk Fibroin/Collagen Nerve Scaffold Seeded with a Co-Culture of Schwann Cells and Adipose-Derived Stem Cells for Sciatic Nerve Regeneration. *PLoS One*. 2016; 11:e0147184.
669. Kornmuller A, Brown CFC, Yu C, Flynn LE. Fabrication of Extracellular Matrix-derived Foams and Microcarriers as Tissue-specific Cell Culture and Delivery Platforms. *J Vis Exp*. 2017;
670. Robb KP, Shridhar A, Flynn LE. Decellularized Matrices As Cell-Instructive Scaffolds to Guide Tissue-Specific Regeneration. *ACS Biomaterials Science & Engineering*. 2017;
671. Livesey SA, Herndon DN, Hollyoak MA, Atkinson YH, Nag A. Transplanted acellular allograft dermal matrix: Potential as a template for the reconstruction of viable dermis. *Transplantation*. 1995; 60:1-9.
672. Reyzelman AM, Bazarov I. Human acellular dermal wound matrix for treatment of DFU: literature review and analysis. *J. Wound Care*. 2015; 24:128; 129-34.
673. Coolen NA, Verkerk M, Reijnen L, et al. Culture of keratinocytes for transplantation without the need of feeder layer cells. *Cell Transplant.* 2007; 16:649-661.
674. Fiorani A, Gualandi C, Panseri S, et al. Comparative performance of collagen nanofibers electrospun from different solvents and stabilized by different crosslinkers. *J. Mater. Sci. Mater. Med.* 2014; 25:2313-2321.
675. Belbachir K, Noreen R, Gouspillou G, Petibois C. Collagen types analysis and differentiation by FTIR spectroscopy. *Anal. Bioanal. Chem.* 2009; 395:829-837.
676. Sionkowska A, Michalska M, Walczak M, Śmiechowski K, Grabska S. Preparation and characterization of silk fibroin/collagen sponge modified by chemical cross-linking. *Mol. Cryst. Liq. Cryst.* 2016; 640:180-190.
677. Sadeghi AR, Nokhasteh S, Molavi AM, et al. Surface modification of electrospun PLGA scaffold with collagen for bioengineered skin substitutes. *Materials Science and Engineering: C*. 2016; 66:130-137.
678. Abreu EL, Palmer MP, Murray MM. Collagen density significantly affects the functional properties of an engineered provisional scaffold. *Journal of biomedical materials research. Part A*. 2010; 93:150-157.
679. Antoine EE, Vlachos PP, Rylander MN. Review of Collagen I Hydrogels for Bioengineered Tissue Microenvironments: Characterization of Mechanics, Structure, and Transport. *Tissue Engineering. Part B, Reviews*. 2014; 20:683-696.

680. Erikson A, Andersen HN, Naess SN, Sikorski P, Davies Cde L. Physical and chemical modifications of collagen gels: impact on diffusion. *Biopolymers*. 2008; 89:135-43.
681. Ramanujan S, Pluen A, McKee TD, et al. Diffusion and convection in collagen gels: implications for transport in the tumor interstitium. *Biophys. J.* 2002; 83:1650-60.
682. Xie J, Bao M, Bruekers SMC, Huck WTS. Collagen Gels with Different Fibrillar Microarchitectures Elicit Different Cellular Responses. *ACS Applied Materials & Interfaces*. 2017; 9:19630-19637.
683. Davenport EA, Nettesheim P. Type I Collagen Gel Modulates Extracellular Matrix Synthesis and Deposition by Tracheal Epithelial Cells. *Exp. Cell Res.* 1996; 223:155-162.
684. Brotchie H, Wakefield D. FIBRONECTIN: STRUCTURE, FUNCTION AND SIGNIFICANCE IN WOUND HEALING. *Australas. J. Dermatol.* 1990; 31:47-56.
685. Schultz GS, Ladwig G, Wysocki A. Extracellular matrix: Review of its roles in acute and chronic wounds. *World Wide Wounds*. 2005; 2005
686. Watt FM, Kubler MD, Hotchin NA, Nicholson LJ, Adams JC. Regulation of keratinocyte terminal differentiation by integrin-extracellular matrix interactions. *J. Cell Sci.* 1993; 106:175-182.
687. Adams JC, Watt FM. Changes in keratinocyte adhesion during terminal differentiation: reduction in fibronectin binding precedes alpha 5 beta 1 integrin loss from the cell surface. *Cell*. 1990; 63:425-35.
688. Peng Y, Bocker MT, Holm J, et al. Human fibroblast matrices bio-assembled under macromolecular crowding support stable propagation of human embryonic stem cells. *J. Tissue Eng. Regen. Med.* 2012; 6:e74-86.
689. Jiang D, Xu B, Yang M, et al. Efficacy of tendon stem cells in fibroblast-derived matrix for tendon tissue engineering. *Cytotherapy*. 2014; 16:662-73.
690. Zhou Y, Zimber M, Yuan H, et al. Effects of Human Fibroblast-Derived Extracellular Matrix on Mesenchymal Stem Cells. *Stem Cell Rev*. 2016; 12:560-572.
691. Lai Y, Sun Y, Skinner CM, et al. Reconstitution of marrow-derived extracellular matrix ex vivo: A robust culture system for expanding large-scale highly functional human mesenchymal stem cells. *Stem Cells and Development*. 2010; 19:1095-1107.
692. Marinkovic M, Block TJ, Rakian R, et al. One size does not fit all: developing a cell-specific niche for in vitro study of cell behavior. *Matrix Biol.* 2016; 52-54:426-441.
693. Sellaro TL, Ravindra AK, Stolz DB, Badylak SF. Maintenance of hepatic sinusoidal endothelial cell phenotype in vitro using organ-specific extracellular matrix scaffolds. *Tissue Eng.* 2007; 13:2301-10.
694. Asran A, Razghandi K, Aggarwal N, Michler GH, Groth T. Nanofibers from blends of polyvinyl alcohol and polyhydroxy butyrate as potential scaffold material for tissue engineering of skin. *Biomacromolecules*. 2010; 11:3413-21.
695. Pelipenko J, Kocbek P, Govedarica B, et al. The topography of electrospun nanofibers and its impact on the growth and mobility of keratinocytes. *Eur. J. Pharm. Biopharm.* 2013; 84:401-11.
696. Min BM, Lee G, Kim SH, et al. Electrospinning of silk fibroin nanofibers and its effect on the adhesion and spreading of normal human keratinocytes and fibroblasts in vitro. *Biomaterials*. 2004; 25:1289-1297.
697. Wilke MS, Furcht LT. Human keratinocytes adhere to a unique heparin-binding peptide sequence within the triple helical region of type IV collagen. *J. Invest. Dermatol.* 1990; 95:264-70.
698. Fujisaki H, Adachi E, Hattori S. Keratinocyte differentiation and proliferation are regulated by adhesion to the three-dimensional meshwork structure of type IV collagen. *Connect. Tissue Res.* 2008; 49:426-36.
699. Woodley DT, Bachmann PM, O'Keefe EJ. Laminin inhibits human keratinocyte migration. *J. Cell. Physiol.* 1988; 136:140-6.
700. O'Toole EA. Extracellular matrix and keratinocyte migration. *Clin. Exp. Dermatol.* 2001; 26:525-30.

701. Yang C, Wu X, Zhao Y, Xu L, Wei S. Nanofibrous scaffold prepared by electrospinning of poly(vinyl alcohol)/gelatin aqueous solutions. *J. Appl. Polym. Sci.* 2011; 121:3047-3055.
702. Menon NV, Chuah YJ, Phey S, et al. Microfluidic Assay To Study the Combinatorial Impact of Substrate Properties on Mesenchymal Stem Cell Migration. *ACS Appl Mater Interfaces*. 2015; 7:17095-103.
703. Chen P, Cescon M, Bonaldo P. Lack of Collagen VI Promotes Wound-Induced Hair Growth. *J. Invest. Dermatol.* 2015; 135:2358-2367.
704. Chermnykh E, Kalabusheva E, Vorotelyak E. Extracellular Matrix as a Regulator of Epidermal Stem Cell Fate. *Int. J. Mol. Sci.* 2018; 19
705. Morgner J, Ghatak S, Jakobi T, et al. Integrin-linked kinase regulates the niche of quiescent epidermal stem cells. *Nat Commun*. 2015; 6:8198.
706. Ahmed M, ffrench-Constant C. Extracellular Matrix Regulation of Stem Cell Behavior. *Current Stem Cell Reports*. 2016; 2:197-206.
707. Timpl R. Macromolecular organization of basement membranes. *Curr. Opin. Cell Biol.* 1996; 8:618-624.
708. Bisson F, Rochefort É, Lavoie A, et al. Irradiated Human Dermal Fibroblasts Are as Efficient as Mouse Fibroblasts as a Feeder Layer to Improve Human Epidermal Cell Culture Lifespan. *Int. J. Mol. Sci.* 2013; 14:4684-4704.
709. Ng CP, Sharif AR, Heath DE, et al. Enhanced ex vivo expansion of adult mesenchymal stem cells by fetal mesenchymal stem cell ECM. *Biomaterials*. 2014; 35:4046-57.
710. Altman GH, Diaz F, Jakuba C, et al. Silk-based biomaterials. *Biomaterials*. 2003; 24:401-416.
711. Zhang H, Zhou L, Zhang W. Control of Scaffold Degradation in Tissue Engineering: A Review. *Tissue Engineering Part B: Reviews*. 2014; 20:492-502.
712. Park S-H, Gil ES, Shi H, et al. Relationships Between Degradability of Silk Scaffolds and Osteogenesis. *Biomaterials*. 2010; 31:6162-6172.
713. Spagnuolo M, Liu L. Fabrication and degradation of electrospun scaffolds from l-tyrosine-based polyurethane blends for tissue engineering applications. *ISRN Nanotechnology*. 2012; 2012
714. Cui W, Li X, Zhu X, et al. Investigation of drug release and matrix degradation of electrospun poly (DL-lactide) fibers with paracetanol inoculation. *Biomacromolecules*. 2006; 7:1623-1629.
715. Liu H, Wang S, Qi N. Controllable structure, properties, and degradation of the electrospun PLGA/PLA-blended nanofibrous scaffolds. *J. Appl. Polym. Sci.* 2012; 125:E468-E476.
716. Sun L, Mills DK. Halloysite nanotube-based drug delivery system for treating osteosarcoma. *Conf. Proc. IEEE Eng. Med. Biol. Soc.* 2014; 2014:2920-3.
717. Veerabadran NG, Price RR, Lvov YM. Clay nanotubes for encapsulation and sustained release of drugs. *Nano*. 2007; 2:115-120.
718. Abdullayev E, Lvov Y. Halloysite clay nanotubes as a ceramic "skeleton" for functional biopolymer composites with sustained drug release. *Journal of Materials Chemistry B*. 2013; 1:2894-2903.
719. Tan D, Yuan P, Annabi-Bergaya F, et al. Loading and in vitro release of ibuprofen in tubular halloysite. *Applied Clay Science*. 2014; 96:50-55.
720. Trappmann B, Gautrot JE, Connelly JT, et al. Extracellular-matrix tethering regulates stem-cell fate. *Nat Mater*. 2012; 11:642-9.
721. Huang TY, Wu CH, Wang MH, et al. Cooperative regulation of substrate stiffness and extracellular matrix proteins in skin wound healing of axolotls. *Biomed Res Int*. 2015; 2015:712546.
722. Gupta P, Hari Narayana S. N G, Kasiviswanathan U, et al. Substrate stiffness does affect the fate of human keratinocytes. *RSC Advances*. 2016; 6:3539-3551.

"Every reasonable effort has been made to acknowledge the owners of copyright material. I would be pleased to hear from any copyright owner who has been omitted or incorrectly acknowledged."

Appendix A

Table A.1 Primary Antibody

Antibody Name	Clone	Species, Isotype	Manufacturer or Provided By/ Catalogue No.
Fibronectin	Polyclonal	Rabbit IgG	Abcam (ab2413)
Involucrin	Mouse, (SY5)	Mouse IgG1	Sigma (I9018)
K10	Monoclonal, (LH2)	Mouse IgG1	Prof. Birgit Lane, A*STAR Institute of Medical Biology
K14	Monoclonal, (LL001)	Mouse IgG2a	Prof. Birgit Lane, A*STAR Institute of Medical Biology
Myosin (slow muscle)	Monoclonal, NOQ7.4.D	Mouse IgG	Millipore(MAB1628)
Type I Collagen	Polyclonal	Rabbit IgG	Abcam (ab34710)
Type IV Collagen	Polyclonal	Rabbit IgG	Abcam (ab6586)

Table A.2 Secondary Antibody

Antibody Name	React Against	Conjugated	Manufacturer or Provided By/ Catalogue No.
Goat anti-mouse IgG	Mouse IgG	Alexa-488	ThermoFisher Scientific (A11001)
Goat anti-Rabbit IgG	Rabbit IgG	Alexa-647	Invitrogen (A32733)

Table A.3 Isotype Antibody

Antibody Name	Manufacturer or Provided By/ Catalogue No.
Mouse IgG2a	Dako (X0943)
Mouse IgG1	Dako (X0931)
Rabbit IgG	Invitrogen (02-6102)

Antibody isotype controls

Antibody isotype controls were utilized for respective antibodies to verify for the absence of non-specific staining.

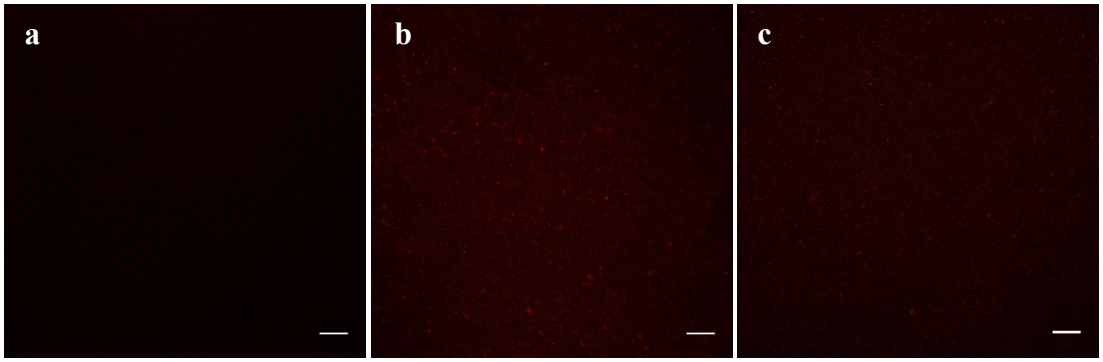

Figure A.1 Immunofluorescence labelling of ECM derived from 3T3 fibroblasts on GTA treated SF/ gelatin scaffolds.

ECM was fixed and stained antibody against isotype control rabbit IgG: (a) SF, (b) SF/gelatin 90/10 (c) SF/gelatin 70/30. Secondary antibody was anti-rabbit Alexa Fluor® 647. Scale bar = 100 µm.

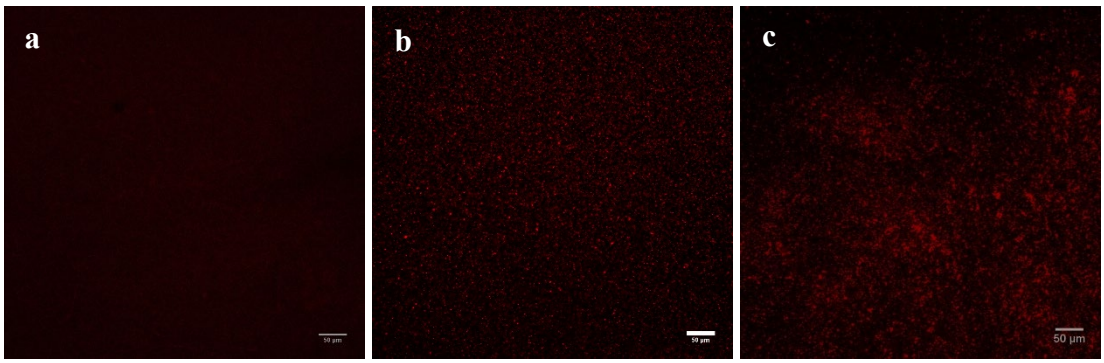

Figure A.2 Immunofluorescence labelling of ECM derived from 3T3 fibroblasts on (a) SF, (b) SF/Col I, (c) Col I hydrogel.

ECM was fixed and stained antibody against isotype control rabbit IgG. Secondary antibody was: anti-rabbit Alexa Fluor® 647. Scale bar = 50 µm.

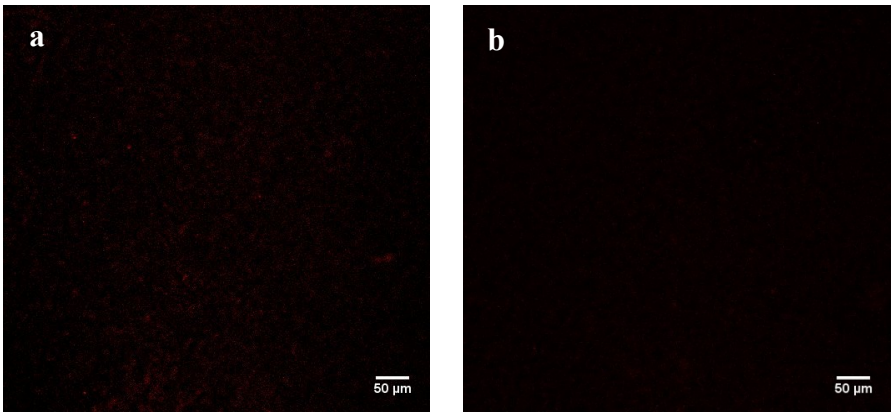

Figure A.3 Immunofluorescence labelling of ECM derived from 3T3 fibroblasts on (a) SF and (b) SF/HNT 1 wt% scaffolds.

ECM was fixed and stained antibody against isotype control rabbit IgG. Secondary antibody was: anti-rabbit Alexa Fluor® 647. Scale bar = 50 µm.

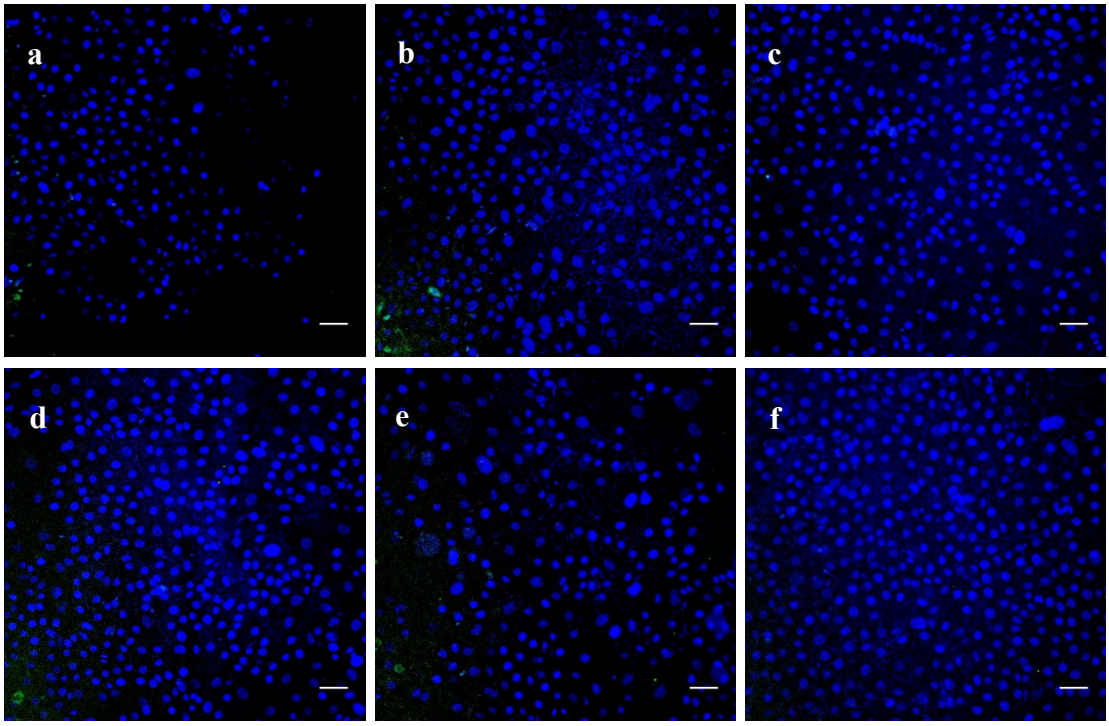

Figure A.4 Immunofluorescence labelling of keratinocytes on a) SF, b) SF-3T3 ECM, c) SF-HDF ECM, d) SF/HNT 1 wt%, e) SF/HNT 1wt%-3T3 ECM, f) SF/HNT 1wt%- HDF ECM.

Keratinocytes were cultured on scaffolds for 8 days, fixed and stained with antibody against isotype control mouse IgG1. The secondary antibody was an anti-mouse IgG Alexa Fluor® 488-conjugated antibody. Nuclei were stained using DAPI (Blue). Scales bars are 50 µm.

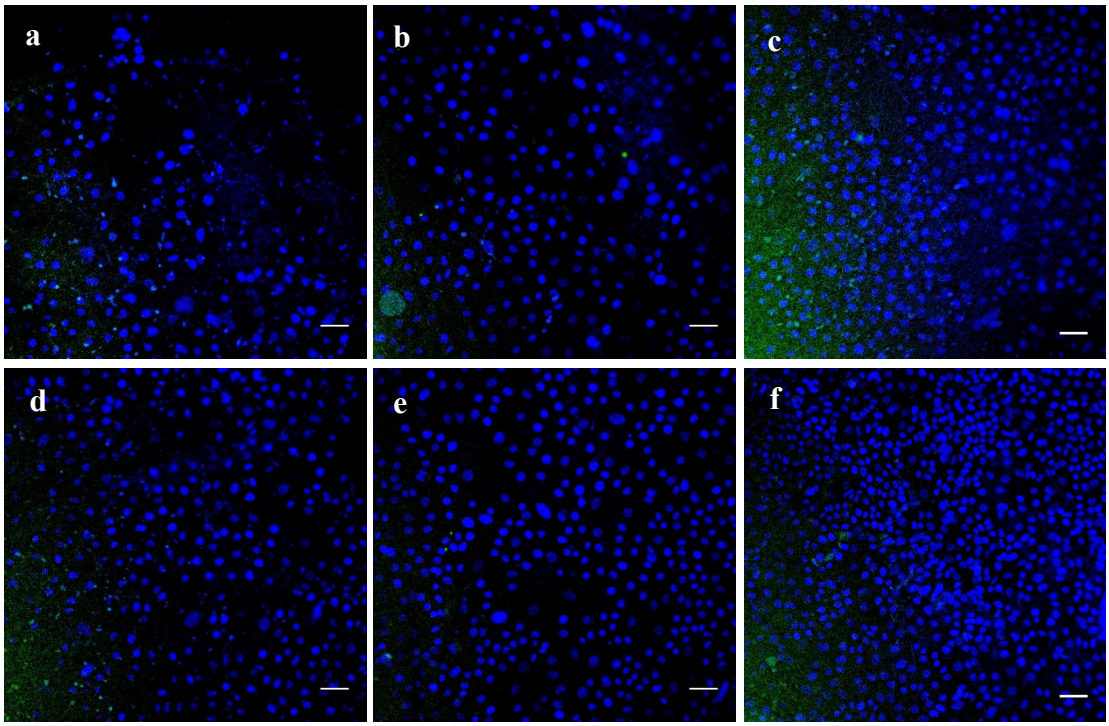

Figure A.5 Immunofluorescence labelling of keratinocytes on a) SF, b) SF-3T3 ECM, c) SF-HDF ECM, d) SF/HNT 1wt%, e) SF/HNT 1 wt%-3T3 ECM, f) SF/HNT 1wt%- HDF ECM.

Keratinocytes were cultured on scaffolds for 8 days, fixed and stained with antibody against isotype control mouse IgG 2a. The secondary antibody was an anti-mouse IgG Alexa Fluor® 488-conjugated. Nuclei were stained using DAPI (Blue). Scales bars are 50 μm.

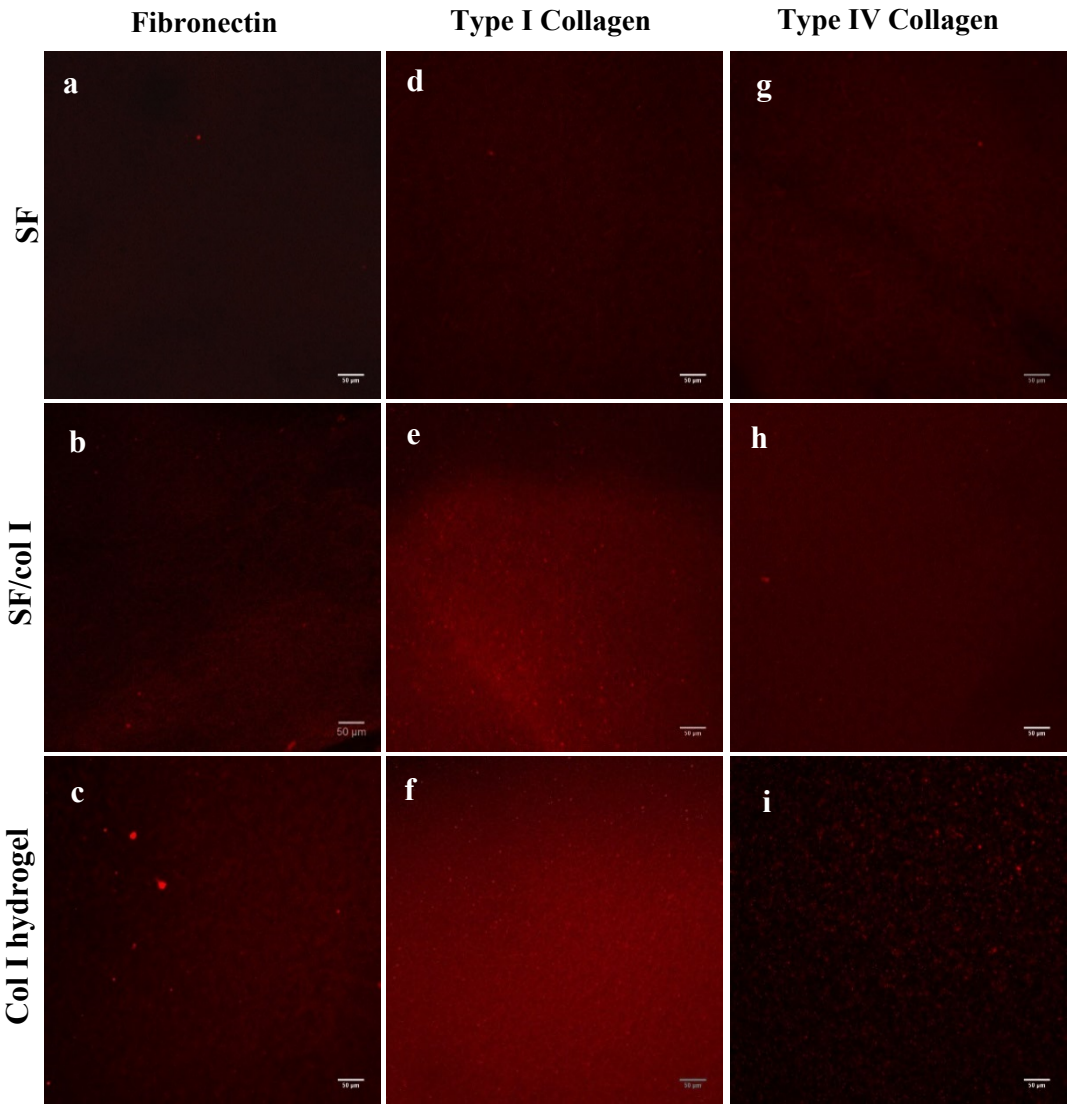

Figure A.6 Immunofluorescence labelling of SF (a,d,g), SF/col I (b,e,h) and col I hydrogel (c,f,i).

Scaffolds were incubated in MMC media for 24 h at 37 °C followed by fixation with 4% paraformaldehyde and stained with antibodies recognising fibronectin (a-c), type I collagen (d-f) and type IV collagen (g-i). Secondary antibody was: anti-rabbit Alexa Fluor® 647. Images were taken using Nikon A1+ confocal microscope. Scale bar = 50 µm.

Appendix B

Copyright Permission of the Figures

Figure 2.1

SPRINGER NATURE LICENSE TERMS AND CONDITIONS

Nov 25, 2018

This Agreement between soheila mohamadzadehmoghadam ("You") and Springer Nature ("Springer Nature") consists of your license details and the terms and conditions provided by Springer Nature and Copyright Clearance Center.

License Number	4476251197355
License date	Nov 25, 2018
Licensed Content Publisher	Springer Nature
Licensed Content Publication	Tissue Engineering and Regenerative Medicine
Licensed Content Title	Electrospun Collagen Nanofibers and Their Applications in Skin Tissue Engineering
Licensed Content Author	Jia Xian Law, Ling Ling Liau, Aminuddin Saim et al
Licensed Content Date	Jan 1, 2017
Licensed Content Volume	14
Licensed Content Issue	6
Type of Use	Thesis/Dissertation
Requestor type	academic/university or research institute
Format	print and electronic
Portion	figures/tables/illustrations
Number of figures/tables/illustrations	1
Will you be translating?	no
Circulation/distribution	501 to 1000
Author of this Springer Nature content	no
Title	Electrospun Silk Nanofibre Mats and Their Potential as Tissue Scaffolds
Institution name	Curtin University
Expected presentation date	Jan 2019
Portions	Figure. 1
Requestor Location	soheila mohamadzadehmoghadam 64 walpole street saint james perth, 6102 Australia Attn: soheila mohamadzadehmoghadam
Billing Type	Invoice
Billing Address	soheila mohamadzadehmoghadam 64 walpole street saint james perth, Australia 6102 Attn: soheila mohamadzadehmoghadam
Total	0.00 USD
Terms and Conditions	

Figure 2.2

SPRINGER NATURE LICENSE TERMS AND CONDITIONS

Nov 25, 2018

This Agreement between soheila mohamadzadehmoghadam ("You") and Springer Nature ("Springer Nature") consists of your license details and the terms and conditions provided by Springer Nature and Copyright Clearance Center.

License Number	4476260091125
License date	Nov 25, 2018
Licensed Content Publisher	Springer Nature
Licensed Content Publication	European Spine Journal
Licensed Content Title	Scaffolding in tissue engineering: general approaches and tissue-specific considerations
Licensed Content Author	B. P. Chan, K. W. Leong
Licensed Content Date	Jan 1, 2008
Licensed Content Volume	17
Licensed Content Issue	4
Type of Use	Thesis/Dissertation
Requestor type	academic/university or research institute
Format	print and electronic
Portion	figures/tables/illustrations
Number of figures/tables/illustrations	1
Will you be translating?	no
Circulation/distribution	501 to 1000
Author of this Springer Nature content	no
Title	Electrospun Silk Nanofibre Mats and Their Potential as Tissue Scaffolds
Institution name	Curtin University
Expected presentation date	Jan 2019
Portions	Figure 1
Requestor Location	soheila mohamadzadehmoghadam 64 walpole street saint james perth, 6102 Australia Attn: soheila mohamadzadehmoghadam
Billing Type	Invoice
Billing Address	soheila mohamadzadehmoghadam 64 walpole street saint james perth, Australia 6102 Attn: soheila mohamadzadehmoghadam

Figure 2.4

JOHN WILEY AND SONS LICENSE TERMS AND CONDITIONS

Nov 26, 2018

This Agreement between soheila mohamadzadehmoghadam ("You") and John Wiley and Sons ("John Wiley and Sons") consists of your license details and the terms and conditions provided by John Wiley and Sons and Copyright Clearance Center.

License Number	4476290917067
License date	Nov 26, 2018
Licensed Content Publisher	John Wiley and Sons
Licensed Content Publication	Journal of Polymer Science Part B: Polymer Physics
Licensed Content Title	Recent progress in electrospun nanofibers: Reinforcement effect and mechanical performance
Licensed Content Author	Soheila Mohammadzadehmoghadam, Yu Dong, Ian Jeffery Davies
Licensed Content Date	Jun 23, 2015
Licensed Content Volume	53
Licensed Content Issue	17
Licensed Content Pages	42
Type of use	Dissertation/Thesis
Requestor type	Author of this Wiley article
Format	Print and electronic
Portion	Figure/table
Number of figures/tables	1
Original Wiley figure/table number(s)	Figure 3
Will you be translating?	No
Title of your thesis / dissertation	Electrospun Silk Nanofibre Mats and Their Potential as Tissue Scaffolds
Expected completion date	Jan 2019
Expected size (number of pages)	1
Requestor Location	soheila mohamadzadehmoghadam 64 walpole street saint james perth, 6102 Australia Attn: soheila mohamadzadehmoghadam
Publisher Tax ID	EU826007151
Total	0.00 USD
Terms and Conditions	

TERMS AND CONDITIONS

This copyrighted material is owned by or exclusively licensed to John Wiley & Sons, Inc. or one of its group companies (each a"Wiley Company") or handled on behalf of a society with which a Wiley Company has exclusive publishing rights in relation to a particular work

Figure 2.5

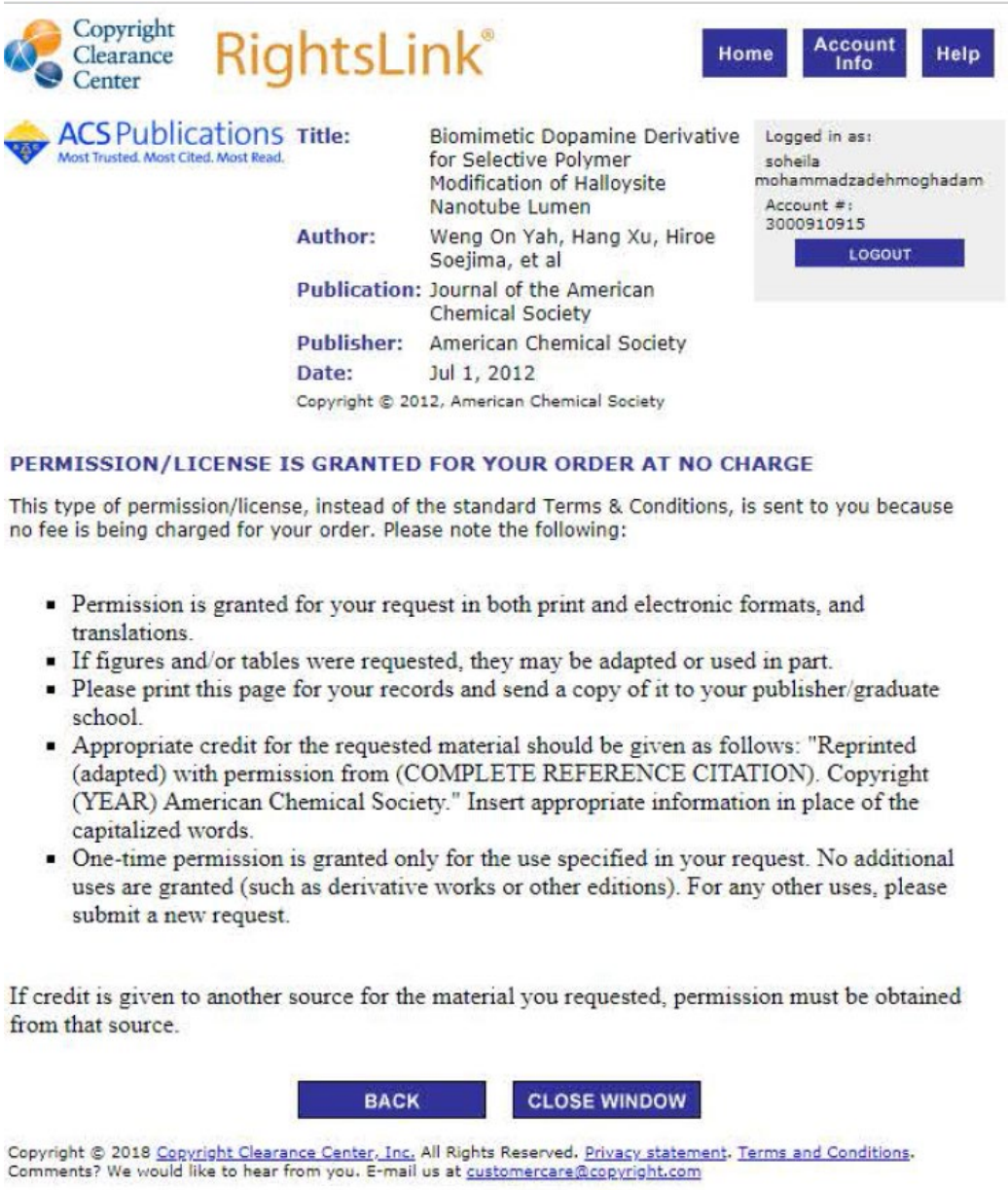

Copyright Clearance Center RightsLink®

Home | Account Info | Help

ACS Publications
Most Trusted. Most Cited. Most Read.

Title:	Biomimetic Dopamine Derivative for Selective Polymer Modification of Halloysite Nanotube Lumen
Author:	Weng On Yah, Hang Xu, Hiroe Soejima, et al
Publication:	Journal of the American Chemical Society
Publisher:	American Chemical Society
Date:	Jul 1, 2012

Copyright © 2012, American Chemical Society

Logged in as:
soheila mohammadzadehmoghadam
Account #: 3000910915
LOGOUT

PERMISSION/LICENSE IS GRANTED FOR YOUR ORDER AT NO CHARGE

This type of permission/license, instead of the standard Terms & Conditions, is sent to you because no fee is being charged for your order. Please note the following:

- Permission is granted for your request in both print and electronic formats, and translations.
- If figures and/or tables were requested, they may be adapted or used in part.
- Please print this page for your records and send a copy of it to your publisher/graduate school.
- Appropriate credit for the requested material should be given as follows: "Reprinted (adapted) with permission from (COMPLETE REFERENCE CITATION). Copyright (YEAR) American Chemical Society." Insert appropriate information in place of the capitalized words.
- One-time permission is granted only for the use specified in your request. No additional uses are granted (such as derivative works or other editions). For any other uses, please submit a new request.

If credit is given to another source for the material you requested, permission must be obtained from that source.

BACK | CLOSE WINDOW

Copyright © 2018 Copyright Clearance Center, Inc. All Rights Reserved. Privacy statement. Terms and Conditions.
Comments? We would like to hear from you. E-mail us at customercare@copyright.com

Figure 3.5

ELSEVIER LICENSE
TERMS AND CONDITIONS

Nov 26, 2018

This Agreement between soheila mohamadzadehmoghadam ("You") and Elsevier ("Elsevier") consists of your license details and the terms and conditions provided by Elsevier and Copyright Clearance Center.

License Number	4476300656578
License date	Nov 26, 2018
Licensed Content Publisher	Elsevier
Licensed Content Publication	Polymer
Licensed Content Title	Electrospinning and mechanical characterization of gelatin nanofibers
Licensed Content Author	Zheng-Ming Huang,Y.Z Zhang,S Ramakrishna,C.T Lim
Licensed Content Date	Jul 12, 2004
Licensed Content Volume	45
Licensed Content Issue	15
Licensed Content Pages	8
Start Page	5361
End Page	5368
Type of Use	reuse in a thesis/dissertation
Intended publisher of new work	other
Portion	figures/tables/illustrations
Number of figures/tables/illustrations	1
Format	both print and electronic
Are you the author of this Elsevier article?	No
Will you be translating?	No
Original figure numbers	Figure 8
Title of your thesis/dissertation	Electrospun Silk Nanofibre Mats and Their Potential as Tissue Scaffolds
Publisher of new work	Curtin University
Expected completion date	Jan 2019
Estimated size (number of pages)	1
Requestor Location	soheila mohamadzadehmoghadam 64 walpole street saint james perth, 6102 Australia Attn: soheila mohamadzadehmoghadam
Publisher Tax ID	GB 494 6272 12

Appendix C

Co-authors' Attribution statements

In this appendix, the signed co-authors' attribution statements are given and signed by the co-authors.

Curtin University
School of civil and Mechanical Engineering
Level 4, Building 204
GPO Box U1987
Perth, Australia

Co-author Attribution Approval Statement

Hereby, I, Dr Ian Jeffery Davies, confirm that the following papers are my joint papers with Soheila Mohammadzadehmoghadam. I, as a co-author, endorse that the level of all authors' contribution is accurately and appropriately addressed in the following tables. I also consent these papers to be used in the thesis "Electrospun Silk Nanofibre Mats and Their Potential as Tissue Scaffolds", submitted for the Degree of PhD in Mechanical Engineering of Curtin University.

Paper: Soheila Mohammadzadehmoghadam, Yu Dong, Ian Jeffery Davies, "Recent Progress in Electrospun Nanofibers: Reinforcement Effect and Mechanical Performance", Journal of Polymer Science, Part B: Polymer Physics, 2015, 53, 1171-1212.
Author's affiliation:

1- Soheila Mohammadzadehmoghadam, Faculty of Science and Engineering, School of Civil and Mechanical Engineering, Curtin University, Perth, Australia.
2- Yu Dong, Faculty of Science and Engineering, School of Civil and Mechanical Engineering, Curtin University, Perth, Australia.
3- Ian Jeffery Davies, Faculty of Science and Engineering, School of Civil and Mechanical Engineering, Curtin University, Perth, Australia.

		Attributions			
		Conception	Paper drafting	Paper revising	Final approval
Authors	Soheila Mohammadzadehmoghadam	×	×	×	×
	Yu Dong	×		×	×
	Ian Jeffery Davies	×		×	
	I acknowledge that these represent my contribution to the above research output. Signed…… Date……				

Paper: Soheila Mohammadzadehmoghadam, Yu Dong, Ian Jeffery Davies, "Modeling Electrospun Nanofibers: An Overview from Theoretical, Empirical, and Numerical Approaches" International Journal of Polymeric Materials and Polymeric Biomaterials, 2016, 65, 901-915.
Author's affiliation:

1- Soheila Mohammadzadehmoghadam, Faculty of Science and Engineering, School of Civil and Mechanical Engineering, Curtin University, Perth, Australia.
2- Yu Dong, Faculty of Science and Engineering, School of Civil and Mechanical Engineering, Curtin University, Perth, Australia.
3- Ian Jeffery Davies, Faculty of Science and Engineering, School of Civil and Mechanical Engineering, Curtin University, Perth, Australia.

		Attributions			
		Conception	Paper drafting	Paper revising	Final approval
Authors	Soheila Mohammadzadehmoghadam	×	×	×	×
	Yu Dong	×		×	×
	Ian Jeffery Davies			×	
	I acknowledge that these represent my contribution to the above research output. Signed…… Date……				

Curtin University
School of Civil and Mechanical Engineering
Level 4, Building 204
GPO Box U1987
Perth, Australia

Co-author Attribution Approval Statement

Hereby, I, Dr Yu Dong, confirm that the following papers are my joint papers with Soheila Mohammadzadehmoghadam. I, as a co-author, endorse that the level of all authors' contribution is accurately and appropriately addressed in the following tables. I also consent these papers to be used in the thesis "Electrospun Silk Nanofibre Mats and Their Potential as Tissue Scaffolds", submitted for the Degree of PhD in Mechanical Engineering of Curtin University.

Paper: Soheila Mohammadzadehmoghadam, Yu Dong, "Fabrication and characterisation of electrospun silk fibroin/gelatin scaffolds crosslinked with glutaraldehyde vapour" Frontiers in Materials, 2019, 6, 91.

Author's affiliation:

1- Soheila Mohammadzadehmoghadam, Faculty of Science and Engineering, School of Civil and Mechanical Engineering, Curtin University, Perth, Australia.
2- Yu Dong, Faculty of Science and Engineering, School of Civil and Mechanical Engineering, Curtin University, Perth, Australia.

		Attributions						
		Design	Acquisition of method	Data manipulation	Interpretation & discussion	Paper drafting	Paper revising	Final approval
Authors	Soheila Mohammadzadehmoghadam	×	×	×	×	×	×	×
	Yu Dong				×		×	×
	Yu Dong	I acknowledge that these represent my contribution to the above research output. Signed…… Date……						

Paper: Soheila Mohammadzadehmoghadam, Yu Dong, Ian Jeffery Davies, "Modeling Electrospun Nanofibers: An Overview from Theoretical, Empirical, and Numerical Approaches" International Journal of Polymeric Materials and Polymeric Biomaterials, 2016, 65, 901-915.
Author's affiliation:

1- Soheila Mohammadzadehmoghadam, Faculty of Science and Engineering, School of Civil and Mechanical Engineering, Curtin University, Perth, Australia.
2- Yu Dong, Faculty of Science and Engineering, School of Civil and Mechanical Engineering, Curtin University, Perth, Australia.
3- Ian Jeffery Davies, Faculty of Science and Engineering, School of Civil and Mechanical Engineering, Curtin University, Perth, Australia.

		Attributions			
		Conception	Paper drafting	Paper revising	Final approval
Authors	Soheila Mohammadzadehmoghadam	×	×	×	×
	Ian Jeffery Davies			×	
	Yu Dong	×		×	×
	Yu Dong	I acknowledge that these represent my contribution to the above research output. Signed…… Date……			

Paper: Soheila Mohammadzadehmoghadam, Yu Dong, Ian Jeffery Davies, "Recent Progress in Electrospun Nanofibers: Reinforcement Effect and Mechanical Performance", Journal of Polymer Science, Part B: Polymer P hysics, 2015, 53, 1171-1212.

Author's affiliation:

1- Soheila Mohammadzadehmoghadam, Faculty of Science and Engineering, School of Civil and Mechanical Engineering, Curtin University, Perth, Australia.
2- Yu Dong, Faculty of Science and Engineering, School of Civil and Mechanical Engineering, Curtin University, Perth, Australia.
3- Ian Jeffery Davies, Faculty of Science and Engineering, School of Civil and Mechanical Engineering, Curtin University, Perth, Australia.

		Attributions			
		Conception	Paper drafting	Paper revising	Final approval
Authors	Soheila Mohammadzadehmoghadam	×	×	×	×
	Ian Jeffery Davies	×		×	
	Yu Dong	×		×	×
		I acknowledge that these represent my contribution to the above research output. Signed…… Date……			

Conference Paper: Soheila Mohammadzadehmoghadam, Yu Dong, "Electrospinning and Characterization of Silk fibroin/Gelatin Nanofibre Mats" ICFNNNM 2018, Rome, Italy.

Author's affiliation:

1- Soheila Mohammadzadehmoghadam, Faculty of Science and Engineering, School of Civil and Mechanical Engineering, Curtin University, Perth, Australia.
2- Yu Dong, Faculty of Science and Engineering, School of Civil and Mechanical Engineering, Curtin University, Perth, Australia.

		Attributions						
		Design	Acquisition of method	Data manipulation	Interpretation & discussion	Paper drafting	Paper revising	Final approval
Authors	Soheila Mohammadzadehmoghadam	×	×	×	×	×	×	×
	Yu Dong				×		×	×
		I acknowledge that these represent my contribution to the above research output. Signed…… Date……						